Charles University in Prague
Faculty of Science

Developmental and Cell Biology

Mgr. Markéta Černohorská

NEW REGULATORY MECHANISMS OF MICROTUBULE NUCLEATION

Ph.D. Thesis

Supervisor: Assoc. Prof. Pavel Dráber, Ph.D.

Department of Biology of Cytoskeleton
Institute of Molecular Genetics of the AS CR

Prague 2015

Prohlášení:

Prohlašuji, že jsem závěrečnou práci vypracovala samostatně a že jsem uvedla všechny použité informační zdroje a literaturu. Tato práce ani její podstatná část nebyla předložena k získání jiného nebo stejného akademického titulu.

V Praze, 2. září 2015

Mgr. Markéta Černohorská

Prohlášení:

Jménem ostatních spoluautorů publikací, které tvoří základ disertační práce Mgr. Markéty Černohorské, potvrzuji, že podíl autora na jejich přípravě je popsaný v komentářích k jednotlivým publikacím pravdivě.

V Praze, 2. září 2015

Doc. RNDr. Pavel Dráber, CSc.

TABLE OF CONTENTS

ABBREVIATIONS

+TIP	Microtubule plus-end tracking proteins
2-ME	2-methoxyestradiol
AKAP450	A-kinase anchor protein 450
BMMC	Bone marrow mast cell
Cdc42	Cell division control protein 42 homolog
EB1	End-binding protein 1
ER	Endoplasmic reticulum
FA	Focal adhesion
FcεRI	High-affinity IgE receptor
Fyn	Src/Yes-related novel
GAP	GTPase-activating proteins
GBD	GIT-binding domain
CDK5RAP2	Cyclin-dependent kinase 5 regulatory subunit associated protein 2
GCP	γ-tubulin complex protein
GCP-WD	γ-tubulin complex protein with tryptophan-aspartic acid (W-D) dipeptide
GDP	Guanosine-diphosphate
GEF	Guanine nucleotide exchange factors
GIT	G-protein-coupled receptor kinase interacting protein
GTP	Guanosine-5'-triphosphate
γ-TuSC	γ-Tubulin small complex
γ-TuRC	γ-Tubulin ring complex
IgE	Immunoglobulin E
MAPs	microtubules associated proteins
MT(s)	Microtubule(s)
MTOC	Microtubule-organizing center
NEDD1	Neural precursor cell expressed, developmentally down-regulated 1
PAK	p21-activated kinase 1
PBD	Paxilin binding domain
PCM	Pericentriolar matrix
P-gp	P-glycoprotein
PI3K	Phosphoinositide 3-kinase
PIP2, 3	Phosphatidylinositol (4,5)-bisphosphate; (3,4,5)-trisphosphate
PIX/Cool	p21-activated kinase -interacting exchange factor/Cloned-out of library
PLCγ	phospholipase Cγ
PM	Plasma membrane
POPX1, 2	Partner of PIX-1 and PIX-2
PTK	Protein tyrosine kinase
Rac1	Ras-related C3 botulinum toxin substrate 1
Rho	Ras-homology
SHD	Src-homology 2 domain
Src	Proto-oncogene tyrosine-protein kinase Src
STIM1	Stromal interaction molecule 1
TBA	Tubulin-binding agent

ABSTRACT

Microtubules (MT) are dynamic cytoskeletal polymers indispensable for vital cellular activities such as maintenance of cell shape, division, spatial distribution of organelles, migration and ordered vesicle transport. Although microtubule nucleation from γ-tubulin complexes is an essential step in the formation of microtubule cytoskeleton, signaling pathways that regulate nucleation from centrosomes of interphase cells are largely unknown. In presented studies we concentrated on regulatory mechanisms of microtubule nucleation.

In mammalian cells, γ-tubulins are encoded by two genes. We demonstrated that γ-tubulin 2 is able to nucleate MTs and substitute for γ-tubulin 1 in cultured cells. Furthermore, we showed that γ-tubulins are differentially expressed during mouse early embryogenesis and in adult tissues. Based on these findings we propose that mammalian γ-tubulins are functionally equivalent with respect to their MT nucleation activity.

Activation of mast cells leads to generation of Ca^{2+}-depended protrusions containing MT. We identified βPIX and GIT1 as signaling proteins that interact with γ-tubulin and associate with centrosomes. GIT1 is phosphorylated on tyrosine in activated mast cells and interacts with γ-tubulin in a Ca^{2+}-dependent manner. Our data suggested a novel signaling pathway for microtubule rearrangement in mast cells, where tyrosine kinase-activated GIT1 and βPIX work in concert with Ca^{2+} signaling to regulate microtubule organization. Through this pathway Ag-induced signaling pathways leading to chemotaxis and degranulation could be regulated.

We found out that GIT1/βPIX signaling proteins together with PAK1 kinase regulate microtubule nucleation in different cell types. The GIT1 with PAK1 represent positive and βPIX negative regulators of this process. We also demonstrated that regulation is due to changes in γ-tubulin accumulation at centrosome. GIT1/βPIX signaling proteins are phosphorylated by PAK1 and directly interact with γ-tubulin. We propose that GIT1/βPIX signaling proteins with PAK1 kinase represent novel regulatory mechanism of microtubule nucleation in interphase cells.

We showed that newly synthesized cytotoxic steroidal compound, estradiol dimer, inhibits tubulin polymerization in vitro, reversibly disrupt microtubules in cells and affects microtubule dynamics at nanomolar concentrations. Estradiol dimer thus represents first steroid compound causing microtubule destabilization associated with cell death.

SOUHRN

Mikrotubuly jsou dynamické cytoskeletální polymery, které jsou nepostradatelné pro základní buněčné aktivity, jako je udržení buněčného tvaru, dělení, prostorová distribuce organel, migrace a transport váčků. Přestože je nukleace mikrotubulů z komplexů γ-tubulinu základním krokem ve formaci mikrotubulárního cytoskeletu, signální dráhy regulující nukleaci z centrosomů, jsou u interfázních buněk neznámé. V odborných studiích jsem se koncentrovali na tyto regulační mechanismy.

V savčích buňkách je γ-tubulin kódován dvěma geny. Ukázali jsme, že γ-tubulin 2 je schopen zastoupit γ-tubulin 1 v nukleaci mikrotubulů. Navíc jsme zjistili, že γ-tubuliny jsou různě exprimovány během časné embryogeneze a v dospělých tkáních u myší. Na základě těchto nálezů navrhujeme, že savčí γ-tubuliny jsou v otázce nukleace mikrotubulů funkčně rovnocenné.

Aktivace žírných buněk vede k formaci protruzí, které jsou tvořeny mikrotubuly v závilosti na vápníku. Objevili jsme dva signální proteiny, βPIX a GIT1, které interagují s γ-tubulinem a lokalizují se na centrozomu. GIT1 je fosforylován na tyrosinu u aktivovaných žírných buněk a interaguje s γ-tubulinem v závilosti na vápníku. Navrhujeme novou signální dráhu pro reorganizaci mikrotubulů u žírných buněk, ve které na tyrozinech-aktivované GIT1 a βPIX spolupracují s vápníkovou signalizací v regulaci organizace mikrotubulů. Skrze tyto dráhy také může být regulována indukce chemotaxe a degranulace.

Zjistili jsme, že GIT1 a βPIX spolu s kinázou PAK1 regulují mikrotubulární nukleaci také u jiných typů buněk. GIT1 a PAK1 reprezentují pozitivní regulátory a βPIX negativní regulátor nukleace. Nukleace je regulována prostřednictvím změn v akumulaci γ-tubulinu na centrozomu. Navrhujeme, že proteiny GIT1/βPIX spoli s PAK1 kinázou tvoří nové regulátory nukleace mikrotubulů u interfázních buněk.

Také jsem ukázali, že nově syntetizovaná cytotoxická steroidní látka, dimer estradiolu, inhibuje polymeraci tubulinu *in vitro*, reverzibilně narušuje mikrotubuly v buňkách a ovlivňuje jejih dynamiku v nanomolárních koncentraci. Estradiolový dimer takto reprezentuje první steroidní látku, která vyvolává destabilizaci mikrotubulů vedoucí k buněčné smrti.

I. INTRODUCTION

Cytoskeleton of eukaryotic cells is the intricate system of cellular filaments that reorganize in response to intracellular and extracellular stimuli. There are three types of cytoskeletal structures: microtubules, microfilaments and intermediate filaments. They differ in protein composition, structure, mechanical properties, dynamics and biological roles. All filaments form complex three-dimensional network. Cytoskeleton ensures numerous essential functions such as movement of the cell, intracellular transport of proteins, vesicles and organelles, maintenance of cell shape, protection from the mechanic stress, segregation of the chromosomes, and cytokinesis during cell division.

As the main focus of this thesis is on microtubules and their nucleation, they will be discussed further in more detail. First chapters focus on microtubules and their building proteins. The next chapters focus on γ-tubulin as key regulatory protein in microtubule nucleation, GIT/PIX/PAK regulatory proteins, and the role of calcium in regulation of microtubules. Tubulin-binding agents as tools for study of microtubules are described in last chapter.

I.1.   MICROTUBULES

I.1.1. Microtubule organization and function

In eukaryotes, microtubules (MTs) form many different specialized structures as radial cytoplasmic networks, mitotic/meiotic spindles, midbodies in cytokinesis, axonemes and centrioles. The main differences between those structures are in their composition, posttranslational modifications and stability. While MTs forming the axonemes in cilia and flagella are stable, cytoplasmic MTs turn over rapidly. MTs in radial cytoplasmic arrays are important for positioning of organelles such as endoplasmic reticulum (ER) or mitochondria. They also serve as tracks for transport of membranous vesicles, protein complexes and RNA as well as bacteria and viruses [1]. MTs participate in nuclear envelope break-down in prophase [2]. The stability of MT network is dependent on a large number of associated and interacting proteins.

MTs of radial arrays in the interphase animal cell emanate primarily from centrosome, the microtubule-organizing center (MTOC) localized near the nucleus. MTs explore

cytoplasm with their free ends and reach the cell periphery. After the onset of cell division, they radically reorganize to form spindle, dynamic and distinct structure necessary for precise separation and delivery of sister chromatids or homologous chromosomes to future daughter cells.

MTs and microfilaments cooperation is required for establishment and maintenance of cellular polarity in migrating cells. During migration MTs are selectively stabilized in different parts of cytoplasm, whereas at the other parts they are highly dynamic. This selective stabilization is necessary for directional MT-based vesicular transport contributing to maintenance of cellular polarity [3]. Destabilization of MTs support changes in migration. This is common in several types of invasive cancers. MTs are important targets for cancer chemotherapy.

I.1.2. Structure of dynamic microtubules

The basic building blocks of MTs are heterodimers of globular α- and β-tubulin subunits with molecular weight approximately 55 KDa. Each monomer of αβ-tubulin dimer is formed by three sequential and functionally distinctive domains: the nucleotide-binding N-terminal domain, intermediate domain and C-terminal domain, whose C-terminal tail is exposed on MT surface [4]. Each tubulin monomer binds one molecule of GTP (guanosine-5'-triphosphate) to nonechangeable N-site of α-tubulin and to exchangeable E-site of β-tubulin that is exposed on the surface of dimer [5]. Tubulin dimers also bind divalent cations and anti-mitotic drugs.

Polymerization process involves two types of contacts between tubulin subunits: head-to-tail covalent binding of dimers results in generation of protofilament that run along the length of the microtubule, and lateral interactions between parallel protofilaments complete the MT wall. Adjacent protofilaments are offset axially, resulting in a helical lattice of monomers that is interrupted by a "seam" where the lateral interface between protofilaments involves heterologous contacts (*α-β*) between the monomers. The cylindrical and left-handed helical MT wall typically comprises 13 protofilaments *in vivo* [5] (Fig. 1a, 1b).

MT has an outer diameter around 25 nm and two different ends. MT are inherently polar and contain two structurally distinct ends: a slow growing (-) end, exposing α-tubulin subunits, and fast growing (+) end, exposing β-tubulin subunits [5]. Typically in mammalian cells, MT (-) end is stably anchored in MTOC, whereas (+) ends are highly dynamic and switch between phases of growth and shrinkage.

7

This behavior is known as dynamic instability of MTs [6,7]. This phenomenon includes additional phases: catastrophe (transition from growth to shrinkage) and rescue (transition from shortening to growth) (Fig. 1c) [8]. Dynamic instability of MTs is fundamental process linked to the nucleotide state of tubulin. MTs grow by tubulin polymerization in the presence of GTP.

Tubulin dimers with bound GTP are added to protofilament. GTP is hydrolyzed to GDP (guanosine-diphosphate) after polymerization, yielding GDP-tubulin, which forms the majority in the MT lattice. When addition of new GTP-tubulin dimers is faster than hydrolysis, MT grows with "GTP cap" on its (+) end. GTP attracts different proteins for (+) end stabilization. When cytosolic concentration of free tubulin dimers is low, addition of new GTP-bound tubulin dimers is slow, and GDP-tubulins are exposed at (+) ends. This leads to shrinkage of MTs [6]. GTP hydrolysis is not required for MT polymerization *per se*, but for the destabilization of a MT lattice [9].

The longitudinal contacts between protofilaments are much stronger than those between adjacent protofilaments, based on the fact that depolymerization involves the peeling of protofilaments from MT ends [10]. GTP hydrolysis changes the conformation of protofilament from a slightly curved tubulin-GTP to a more profoundly fountain-like tubulin-GDP structures (e.g. rings, spirals, sheets or ribbons) [11]. MT growth rate fluctuates at a sub-second time-scale both *in vitro* and *in vivo* [12]. To allow rapid remodeling of the MTs, many microtubule associated proteins (MAPs) are capable of modulating MT dynamics [13,14]. Closure of terminal sheet structure of growing (+) end generates a metastable, blunt-ended microtubule intermediate. This state is termed pause. From pause MTs undergo further growth or switch to depolymerization phase. Phases of dynamic instability are shown in Figure 1c.
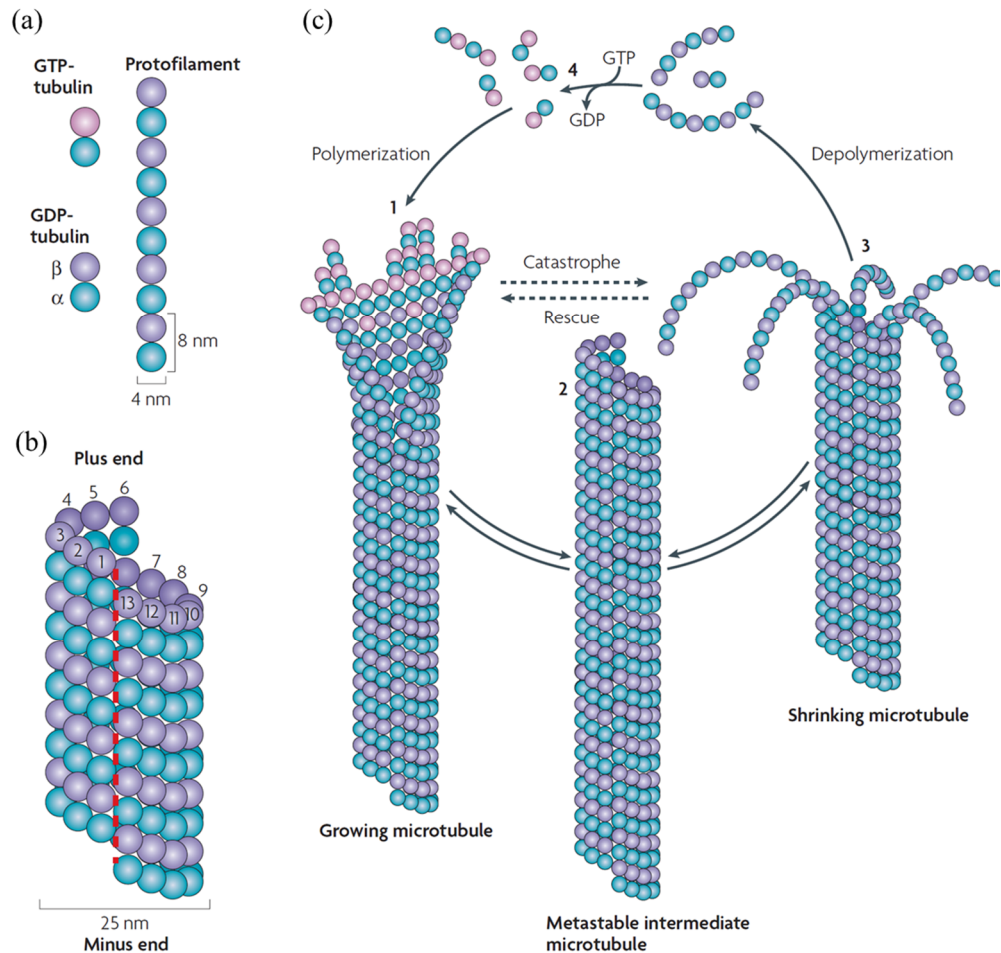
FIGURE 1. *MT structure and dynamic instability.* ***a)*** *MTs are composed of stable α/β-tubulin heterodimers that are aligned in a polar head-to-tail fashion to form protofilaments.* ***b)*** *The cylindrical and helical MT wall typically comprises 13 protofilaments in vivo. A discontinuity in the structure of the MT wall (lattice seam) is marked by red dashed line.* ***c)*** *Dynamic instability of MTs. Polymerization of MTs is initiated from a pool of GTP-loaded tubulin subunits. GTP hydrolysis changes the conformation of a protofilament from a slightly curved tubulin-GTP to a more intensely curved tubulin-GDP structure. The curved tubulin-GDP is forced to remain straight when it is part of the MT wall. Growing MT sheets presumably maintain the "cap" of tubulin-GTP subunits to stabilize the straight tubulin conformation within the MT lattice* ***(1)***. *Closure of the terminal sheet structure generates a metastable, blunt-ended MT intermediate* ***(2)***, *which might pause, undergo further growth or switch to the depolymerization phase. A shrinking MT is characterized by fountain-like arrays of ring and spiral protofilament structures* ***(3)***. *The polymerization–depolymerization cycle is completed by exchanging GDP of the disassembly products with GTP* ***(4)***. *Adapted from* [15].

9

Dynamics, stability, and spatial organization and functional diversity of MTs are regulated by many factors including expression of different tubulin isotypes, tubulin posttranslational modifications, and MT regulatory proteins.

I.1.3. Microtubule regulatory proteins

A wide variety of MT regulatory proteins provide the functional diversity of MTs. Regulation can occur on many levels, including regulation of tubulin monomer folding through the action of tubulin-folding factors, biding along the lattice of MT, to (+) or to (-) ends of MTs. [13]. The mechanical ATPases kinesines and dyneins (MT motor proteins) not discussed in detail, use MT as pathways for intracellular transport. Moreover, they create forces needed for mitotic spindle assembly and function.

I.1.3.1. Microtubule-stabilizing structural MAPs

The MT surface displays a large number of binding sites [16]. Structural MT-associated proteins (MAPs) bind along MT due to a highly positive net charge facilitating their interaction with negatively charged tubulin. Moreover, they possess conserved repeats of MT-binding domain in their C-terminal parts allowing each MAP to interact with more than one tubulin dimer. N-terminal domains of these MAPs have various lengths. They are exposed of the MT out to the cytoplasm and interact with various proteins. As a result, structural MAPs can cross-link individual MTs creating stabilized MT bundles or connect MTs to membranes, microfilaments or intermediate filaments. MAPs binding to MTs can attract signaling molecules, alter the MT binding sites for motor protein and protect MTs from severing. Binding of structural MAPs to MTs is controlled by kinases and phosphatases and dramatically decreases dynamic instability of MTs [17].

One of the best known structural MAPs are proteins from MAP2/tau family MAP2(A,B,C), MAP4, and tau. Generally, structural MAPs are important for normal development and function of the nervous system. While MAP2 is located mainly in dendrites, tau is concentrated in axons. The ability of MAP2 to interact with both MTs and microfilaments is crucial for neuromorphogenic processes. By contrast, MAP4 is almost absent in neurons and is found in other tissues. Tau hyperphosphorylation leading to formation of large Tau aggregates has been linked to Alzheimer disease [18]. MAP1A, MAP1B and MAP1S constitute the MAP1 family. These proteins are also neuronal and

stabilize MTs. There are also other structural MAPs with different mechanisms of MT binding and impact on MT dynamics such as doublecortin [19], ensconsin [20], stable tubulin only proteins (STOPs) [21] or tektins [22].

I.1.3.2. Microtubule severing proteins

Large family of AAA (ATPases associated with various cellular activities) proteins contain Katanin, spastin, fidgetin and vacuolar protein sorting-associated protein 4 (VPS4) that use energy from ATP hydrolysis to sever MT lattice. Both katanin and spastin form hexameric ring complexes with a hole in the center and specifically interacts with C-terminal tails of tubulin [23]. MT severing activities of spastin and katanin are crutial in neuronal development because they induce growth and branching of neurites [24]. In non-neuronal cells, katanin regulates cortical MT (+) end and cell migration. During mitosis, katanin controls mitotic and meiotic spindle length. It has been shown that tubulin glutamylation, particularly long polyglutamate chains, attracts spastin and promotes MT severing [25]. Interestingly, spastin is probably not required for MT severing within intercellular bridge during abscission of daughter cells, instead it regulates MT organization and endosome trafficking [26]. Since MTs influence ER remodeling, either by ER-sliding on existing MTs or by attachment to growing MT (+) ends, spastin might influence ER morphogenesis by severing MTs connected to the ER [27].

I.1.3.3. Microtubule-disassembly promoters

Apart from severing, MT depolymerization causing shrinkage is mediated by various strategies including the activity of MT depolymerases and/or sequestration of tubulin dimers. Stathmin/Oncoprotein18 binds to tubulin dimers and lowers the pool of free tubulin available for polymerization. It results in decreasing of MT growth, and increasing the frequency of spontaneous depolymerization. Each stathmin binds two tubulins and forms ternary tubulin-stathmin T_2S complex [28]. Moreover, stathmin can destabilize MTs by increasing catastrophe frequency by binding directly to MTs [29]. The activity of stathmin is down-regulated by multiple phosphorylation in response to a number of cellular signals. Inhibition of stathmin by mitotic kinases promotes the assembly of mitotic spindle. Stathmin overexpression correlates with its oncogenic activity represented by abnormal cell motility and invasivity in many malignant cells [30].

Two classes of kinesins, kinesin-13 (kinesin with internal motor domain; Mitotic centromere-associated kinesin; MCAK) and kinesin-8 (Kinesin-like protein KIF18A; KIF18A) bind directly to MT ends and use ATP hydrolysis to catalytically depolymerize MTs [31]. They represent MT depolymerizes which bind to and stabilize the bent protofilament conformation, a structural intermediate during depolymerization. MCAK, though it is a kinesin, does not move in a directed manner on the MT lattice. On the other hand, KIF18A is the most processive motor protein discovered so far; it moves on average 12 microns before falling off [32].

I.1.3.4. Microtubule assembly promoters

The XMAP215/Dis1 (*Xenopus* microtubule-associated protein 215/Dis1) family of proteins associate with MT (+) ends and accelerate growth, perhaps by reducing the dissociation of incoming tubulin dimers and stabilizing the GTP cap [32]. The N-termini of proteins contain 250 residue sequence repeats, termed tumor overexpressed gene (TOG) domains capable of direct binding to tubulin. XMAP215/ch-TOG (colonic and hepatic TOG) is a MT polymerase attached to the MT (+) end catalyzing addition of tubulin dimers [33].

I.1.3.5. Microtubule (+) end tracking proteins

The largest group of MAPs represent (+) end tracking proteins (+TIPs) typically binding and affecting MT (+) end. +TIPs are usually multidomain and/or multisubunit proteins that range in size from a few hundred up to thousands of residues [34]. +TIPs have a common ability to track growing MTs *in vivo*. +TIPs can be classified into several classes according to their sequence homologies and the domains and/or mechanisms involved in MT tracking [35]. MCAK and TOG proteins, discussed in the previous section, also belong to +TIPs.

Among the +TIPs, proteins from EB (End-binding) family directly bind to GTP-tubulin and stabilize MT growing (+) ends. They serve as scaffolds for other +TIPs together forming the highly complex (+) end–tracking protein machinery [36]. The EB family proteins include EB1, EB2, and EB3. They have highly conserved N-terminal calponin homology (CH) domain, which is used for tubulin-binding. The C-terminus of EB proteins harbors α-helical coiled-coil domain that mediates parallel dimerization of EB monomers. It further comprises the EB homology (EBH) domain and acidic tail with C-terminal EEY/F motif.

Both motives enable the EB proteins to interact with the other +TIPs and recruit them to (+) ends of MTs. The MT tracking property depends on this dimerization [15,37].

Many +TIPs contain SxIP motif which is specifically recognized by the EBH domain of EB proteins. Among proteins containing this motif belong cytoplasmic linker protein (CLIP-170), CLIP-170-associated protein (CLASP), adenomatous polyposis coli (APC), microtubule-actin crosslinking factor (MACF), cyclin-dependent kinase 5 regulatory subunit associated protein 2 (CDK5RAP2) and stromal interaction molecule 1 (STIM1). They promote growth and suppress catastrophes *in vivo.* Many +TIPs accumulate at centrosome where they might take part in MT nucleation and anchoring [31].

I.2.   MICROTUBULE ORGANIZING CENTER

Although MTs can self-assemble *in vitro* from highly concentrated purified tubulin [38], within cell MTs are formed at much lower tubulin concentrations with help of MTOC. There are two types of MTOCs: discrete and dispersed. Discrete MTOCs are locally restricted and include centrosomes (Fig. 2a), spindle pole bodies in yeasts, and basal bodies [39]. Dispersed MTOCs are localized in cytoplasm, scattered on membranes, pre-existing MTs, or kinetochores. Dispersed MTOCs are present in higher plants, in oocytes, in some differentiated animal cells as muscle, neuronal and epithelial cells, as well as in fission yeast, which has interphase MTOCs besides spindle pole bodies [40]. MTOCs vary greatly in shape, size and occurrence, both within one cell and also between species. In the most types of animal cells, MTOC is small spherical structure called centrosome.

Mammalian centrosome is non-membrane organelle that consists of two principal components, centrioles and the pericentriolar matrix (PCM). Centrioles are located in the core of the centrosome and provide structural platform for PCM. Electron microscopy has revealed that they consist of a pair of short barrel-shaped arrays, each containing nine sets of triplet MTs arranged as a pinwheel along the central MT doublet (Fig. 2b) [41,42]. Being composed of MTs, the centriole is also the inherently polar structure with MT (-) ends positioned at the proximal end of the centriole.

Within the centriole´s center is a luminal density composed of unrecognized proteins termed as MT inner proteins [43,44] (Fig. 2b). The proximal end is also the site from which the new centriole is built during centriole duplication. The centrioles within each centrosome are non-identical. We recognize mother and daughter centrioles. On the exterior of the centriole scaffold are filaments termed distal and subdistal appendages found exclusively on the mother centriole [45]. These appendages are docking sites for MTs once they have been nucleated [46,47] (Fig. 2c).
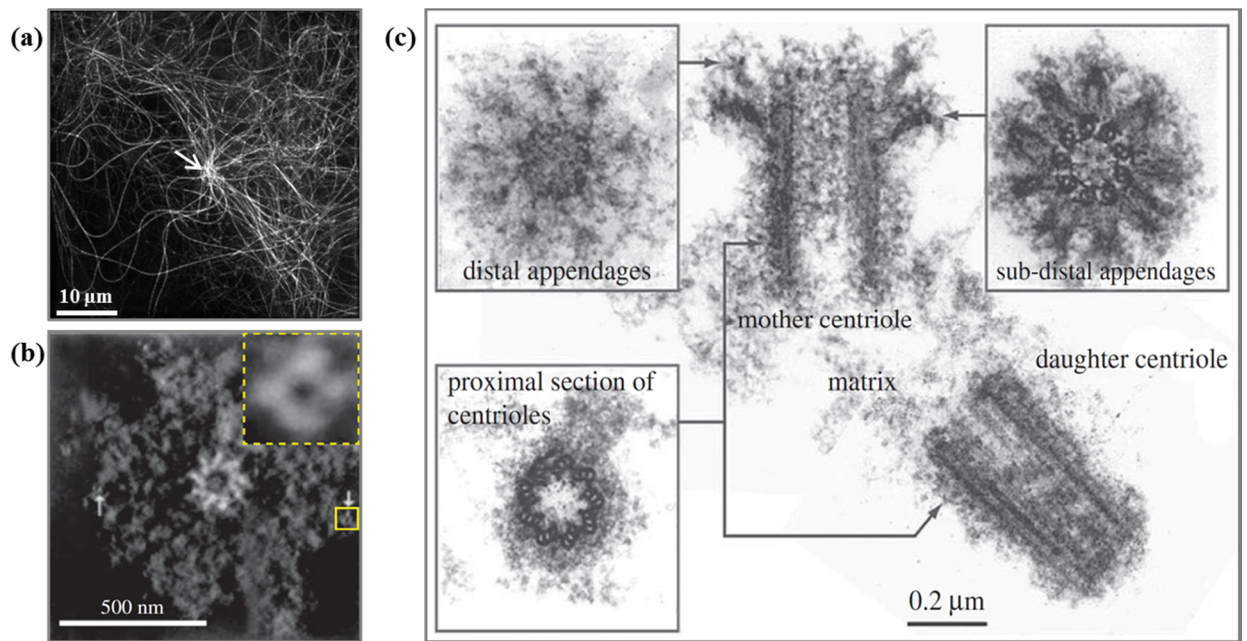
FIGURE 2. *Structural organization of centrosome and centrioles. (a) 3D-SIM super-resolution micrograph of MTs decorated by GFP-tubulin that emanate from the centrosome (Novotný I, 2015). (b) Structure of a purified Drosophila centrosome as revealed by electron tomography. A ninefold radially symmetric centriole can be seen at the center surrounded by PCM. The insert shows a magnified view of ring-like complexes found within the PCM (adapted from [48]). (c) Electron micrographs of centrioles in isolated centrosome show a longitudinal section and informative cross sections highlighting the distal and subdistal appendages (adapted from [49]).*

Although, centrioles are capable of self-assembly [50], their number is under tight regulation in dividing cells [51]. A newly born cell in the G1 phase contains two disengaged centrioles, both competent to organize PCM and form a new procentriole [52]. Two centrioles within a G1 centrosome are connected through a proteinous linker, which is often referred to as centrosome cohesion [53]. A pair of centrioles is duplicated once during one cell cycle in S-phase simultaneously with replication of DNA [54]. This centriole duplication drives duplication of whole centrosome in preparation of proper bipolar spindle assembly. In G2 phase, cell contains two centrosomes, each with two centrioles that are still tightly linked to each other [55,56]. At the beginning of mitosis, the primary centriole pair divides to form two pairs of centrioles forming the poles of mitotic spindle [57]. These two centrioles become primed for the next round of duplication by early G1 [58]. Although, centrioles serve as a

15

recruitment and assembly scaffold for the proteins and protein complexes of the PCM, it is mainly the PCM that nucleates MTs and enables centrosomes to function as MTOCs.

PCM is composed of over a hundred different proteins usually and it is described as lacking any discernable symmetry [59]. Using super-resolution microscopy on human centrosomes, it was recently revealed that PCM is organized into distinct domains, each populated by a specific set of proteins [60–63]. PCM proteins are organized into layers that enclose the cylinder of the mother centriole in a toroid-like arrangement. Therefore, PCM proteins are newly classified according to their distance from the centriole wall (Fig. 3).
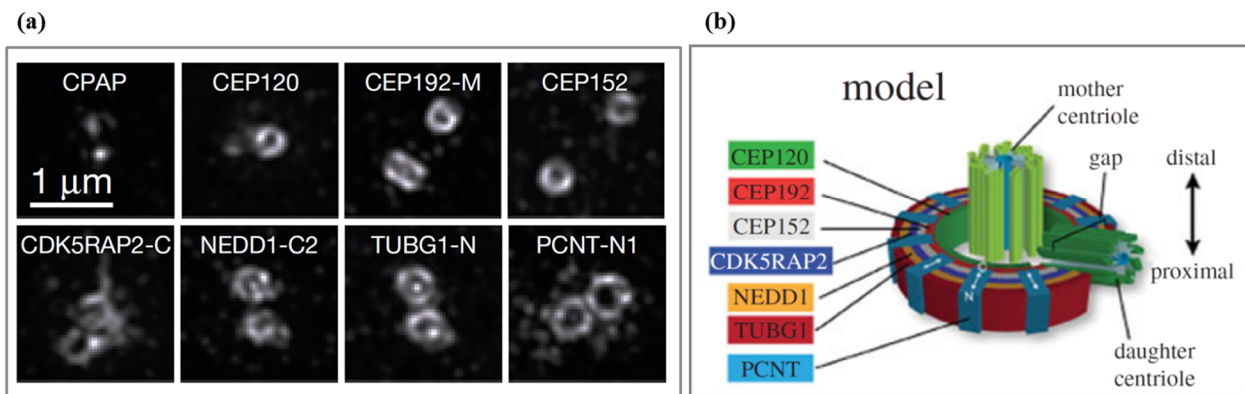
FIGURE 3. *Toroid structure of PCM. (a) Examples of 3D-SIM micrographs of interphase centrosome labelled for the indicated PCM proteins to show different toroid localization and position at the centrosome. (b) Scheme of concentric organization of the human interphase centrosome. Centrosome components (CEP120, CEP192, CEP152, CDK5RAP2, NEDD1 and γ-tubulin) adopt a toroidal pattern with progressively larger, overlapping diameters around the proximal end of the mother centriole. Adapted from [60].*

Analysis of centrosome by electron microscopy has identified MT nucleation cores within the PCM [29,64,65]. From many protein components of PCM only some participate in MT nucleation. The most important is γ-tubulin and its nucleating complexes [66].

I.3. γ-TUBULIN

γ-Tubulin, was first discovered in 1989 [67]. Later on, it was described as a member of tubulin superfamily which is highly evolutionarily conserved across a phylogenetically diverse group of organisms including all eukaryotes so far examined [68,69]. It exhibits more than 71% gene sequence identity between fission yeast (Tug1) and human (TUBG1) [70]. Among vertebrates, γ-tubulin is even more conserved, as human and *Xenopus laevis* γ-tubulins, for example, share 98% identity [71]. In the contrary, the most distant orthologs of human TUBG1 are those from budding yeast (Tub4p) and *Caenorhabditis elegans* (TBG-1) with identity ~43% [72].

Gene encoding γ-tubulin duplicated during evolution [73–75]. In yeast, *Aspergillus*, *Caenorhabditis* and *Xenopus* there is one gene. On the other hand, *Arabidopsis* [76], *Zea* [77], *Paramecium* [78], *Drosophila* [79] and mammals possess two genes. Mammalian genes TUBG1 and TUBG2 are located on the same chromosome in tandem and their genes as well as protein products are structurally almost identical.

γ-Tubulin is concentrated at various MTOCs in cells, but its majority is soluble in the cytoplasm [80]. At centrosome, γ-tubulin is associated with the PCM [81,82] and also with the core of centrioles [30,32,80]. γ-Tubulin was detected at many other MTOCs including Golgi apparatus (GA), apical and basal membranes of epithelial cells, midbody, basal body, along MTs in mitotic and meiotic spindles, on condensed mitotic chromosomes and on nuclear membranes in myotubes [59]. MT nucleation from GA is important for directional mesenchymal migration [83]. MT nucleation from spindle MTs [34,35,84,85] and condensed chromosomes [86–88] is needed for establishment and maintenance of proper spindle architecture and subsequent normal progression of cell division. Noticeably, various patterns of γ-tubulin distribution along interphase MTs were observed in *Drosophila* [89] and in human cancer cells [90]. In addition, we and others described γ-tubulin localization in the nucleus and nucleolus [90–93].

Surprisingly, although TUBG1 and TUBG2 seem to be functionally equivalent [74] differences in their expression and potentially in function have been reported [73]. In mouse, TUBG1 is expressed ubiquitously, whereas TUBG2 is primarily expressed in the brain. The differences were revealed also in knockout studies. TUBG1$^{-/-}$ embryo stopped its development at the stage of morula/blastocyst due to mitotic defects, TUBG2$^{-/-}$ mouse developed normally, but with slight behavioral changes in fertile adults. These defects include the abnormalities in circadian rhythm and reaction to painful stimulations. It was

suggested that TUBG1 is conventional γ-tubulin, whereas TUBG2 was not able to substitute for TUBG1 and therefore, it might have some other functions in the brain [73].

I.3.1. γ-Tubulin nucleation complexes

A ring shaped γ-tubulin complex (γ-TuC) denoted as γ-tubulin ring complex (γ-TuRC) was first purified from *Xenopus* egg extracts [81,94]. Two molecules of γ-tubulin (sometimes referred as GCP1) together with γ-tubulin complex proteins GCP2 and GCP3 form a small tetrameric complex called γ-tubulin small complex (γ-TuSC). Fully assembled γ-TuRC is composed from 5-7 copies of γ-TuSCs, and GCP4, GCP5 and GCP6 as linking proteins for closing of the nucleation ring [95]. Resulting γ-TuRC has a 13-fold symmetry with 13 exposed γ-tubulins for longitudinal interaction with α-tubulins (Fig. 4) [48,96].

While γ-TuRC is capable to nucleate MTs *in vitro*, γ-TuSC as well as γ-tubulin alone are very poor nucleators [81,95–98]. γ-TuSC has Y shape, where two γ-tubulin molecules are located on arms of GCPs. Conformation change in GCP3 allows reposition of γ-tubulins closer to each other thus permitting binding of α-tubulin to start MT nucleation [97,99,100].

Alanine substitution of five amino acids in γ-tubulin (R339, R341, E342, R343 and K344) disrupted of binding between two γ-tubulins and inhibited in fission yeast their growth [101]. This suggests direct link between γ-tubulin in γ-TuSC. γ-TuRC can also stabilize free MTs by capping their (-) ends, thereby preventing depolymerization [48,81,98,102,103].
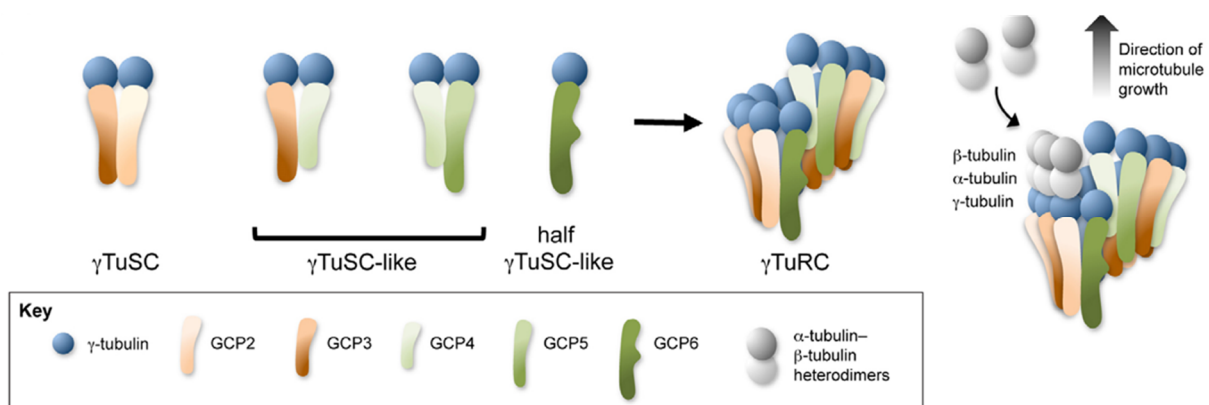
Figure 4: *Model of γ-TuRC assembly. γ-TuSCs are composed of GCP2 and GCP3 (shades of orange) and two molecules of γ-tubulin (blue). γ-TuSC-like complexes are assembled by replacement of GCP2 and/or GCP3 with GCP4, GCP5 and/or GCP6 (shades of green). Half complexes are composed of a single molecule of GCP4, GCP5 or GCP6 interacting with*

γ-tubulin. All complexes participate in the formation of the γ-TuRC. Nucleation of MT involves longitudinal interactions of α/β-tubulin heterodimers with γ-tubulin in the γ-TuRC (template nucleation model; adapted from [104]).

Hundreds of γ-TuRC can be found in PCM, and their number correlate with the ability of centrosome to nucleate MTs [105]. The regulation of γ-TuRCs is either on the level of their composition, recruitment, stabilization or activation at the MTOC. Moreover, it is also dependent on cell cycle phases. γ-TuRC is affected by different factors in mitosis or in G1 and S-phase of cell cycle [106].

Depletion of γ-tubulin in *Drosophila* resulted in a dramatic reduction of GCP2 and GCP3 protein level, but the γTuRC-specific components (GCP4-GCP6 analogs) were affected only slightly. On the other hand, depletion of any γTuRC-specific components did not change the protein levels of γ-TuSC-specific components. Moreover, it did not prevent centrosomal targeting of γ-TuSC and MT nucleation [107,108]. It suggests that (1) co-regulation and stabilization of γTuSC proteins is independent on γTuRC assembly, (2) proteins incorporated into γTuRC are stabilized and protected from degradation [89]. It was shown that except GCP2 and GCP3, also GCP4 directly binds γ-tubulin [100]. This indicates that γ-tubulin complexes can have different composition. Components of γ-TuRC are phylogenetically conserved (Table 1).

Table I. *Comparison of γ-TuRC proteins in different species (adapted from [109]).*

H. sapiens[a]	X. laevis	D. melanogaster	A. thaliana	A. nidulans	S. pombe	S. cerevisiae
GCP1	TUBG1, 2	γTub23C, CD	TUBG1, 2	MIPA	Gtb1/Tug1	Tub4
GCP2	Xgrip110	Dgrip84	GCP2	GCPB	Alp4	Spc97
GCP3	Xgrip109	Dgrip91	GCP3	GCPC	Alp6	Spc98
GCP4	Xgrip75	Dgrip75	GCP4	GCPD	Gfh1	
GCP5	Xgrip133	Dgrip128	GCP5	GCPE	Mod21	
GCP6	Xgrip210	Dgrip163	GCP6	GCPF	Alp16	

To proteins interacting with γ-TuRC belongs NEDD1 (neural precursor cell expressed, developmentally down-regulated 1; also known as GCP-WD; γ-tubulin complex protein with tryptophan-aspartic acid (W-D) dipeptide). NEDD1 is important attachment factor of γ-TuRC [110,111]. Its conserved C-terminal part binds γ-tubulin. N-terminal part harbors WD-40 domain necessary for binding to centrosome [111]. The other important proteins interacting

with γ-TuRC are GCP7 (known as Mozart1; mitotic-spindle organizing protein associated with a ring of γ-tubulin 1) [112], and GCP8 (known as Mozart2) [113]. GCP7 directly binds to N-terminus of GCP3 facilitating MT nucleation in fission yeast [114]. The GCP8 contributes to γ-tubulin recruitment but its localization depends on NEDD1 [113].

MT nucleation activity is promoted by transformic acidic coiled coil (TACC) family protein, +TIPs [115], as well as by RanGTP-activated factors, such as targeting protein for Xklp2 (TPX2) [116].

Among the most studied PCM components are pericentrin, kendrin, ninein, ninein-like proteins (Nlps), AKAP450 (A-kinase anchor protein 450), PCM-1 (pericentriolar material protein 1) and CDK5RAP2. Pericentrin, ninein and Nlp are important for cell cycle-dependent recruitment of γ-tubulin complexes to MTOC. Whereas pericentrin recruits increased amounts of γ-TuRC to the mitotic centrosome, ninein and Nlp anchor γ-TuRC preferably during the interphase [117].

Activation of PCM-1 by cyclin-dependent kinase 1 (CDK1), which promotes binding of CDK5RAP2 and other proteins, is important step in maturation of centrosome before mitosis. To facilitate MT nucleation in mitosis, ninein directly binds to C-terminal part of longer pericentrin variant known as kendrin [118] which interacts with PCM-1 protein. Both kendrin and PCM-1, localize to small 70-100 nm granules in the cytoplasm of interphase cells [118]. These granules move along MTs in a dynein-dependent manner [119] and often concentrate near the centrosome [120]. N-terminal part of kendrin indirectly binds GCP2/GCP3 via PCM-1. Moreover, kendrin binds AKAP450 which tethers GCP2/GCP3 [121]. AKAP450 and kendrin thus function as docking sites for γ-TuRC [122]. AKAP450 associates with a number of protein kinases and phosphatases, including Rho-activated protein kinases N, A, C (PKN, PKA, PKC), and the protein phosphatases 1 and 2A (PP1, PP2A) [123,124]. Kendrin binds calmodulin and PKA [118,125]. It was proposed that AKAP450 and kendrin direct the regulatory enzymes to their substrates at the centrosome [126].

I.3.1.1. Posttranslational modifications of γ-TuRC

γ-TuRC function is regulated by posttranslational modifications (PTMs) of its components. Hyperphosphorylation of γ-tubulin ortholog in fission yeast resulted in altered MT dynamics and changes in nuclear positioning [127]. Mass spectrometry analysis of budding yeast γ-tubulin, GCP2 and GCP3, revealed 4 serine phosphorylation (pS) sites in γ-tubulin, 20 pS sites in GCP2 and 12 pS sites in GCP3 [128]. Constitutive hyperphosphorylation of

γ-tubulin on S74 and S100 caused yeast death. CDK1 triggers degradation of free γ-tubulin by phosphorylation on S360. On the other hand, hyper- or hypophosphorylation in other CDK1 sites, namely T63, S262 and T273 did not show any changes in growth [128]. In mammalian cells, SADB kinase (S/T-protein kinase SAD-B) phosphorylates γ-tubulin on S131 which is necessary for centriole duplication during S-phase [129]. According to γ-tubulin tertiary structure, S74, S100 and S415 are located at the putative interface between γ-tubulin and αβ-tubulin heterodimer. The other three sites (S42, S346 and S360) face binding of GCP2 and GCP3 [130]. Wee1 (mitosis inhibitor protein kinase) is S/T kinase that phosphorylates γ-tubulin in *Drosophila* indirectly [131].

In budding yeast, phosphorylation of γ-tubulin on Y445 increases assembly of MTs, dynamic instability and influences MT organization [132]. Corresponding kinase is still unknown. Many kinases as PI3K (phosphoinositide 3-kinase) [133], Lyn (Lck/Yes novel tyrosine kinase) [134], Syk (spleen tyrosine kinase) [135], and Fyn (Src/Yes-related novel) [136] form complexes containing γ-tubulin. Fyn kinase was described at the centrosome in human T-lymphocytes [137]. Syk is actively transported to the centrosome via dynein/dynactin motors. Syk can target the centrosome only if it is catalytically active [138] by autophosphorylation on Y130 [139].

Src (proto-oncogene tyrosine-protein kinase Src) family kinases are primarily involved in regulation of receptor tyrosine kinases on plasma membrane (PM). However, it was reported that Src kinases stimulate MT nucleation and accumulation of γ-tubulin at the centrosome [140,141]. Src phosphorylates γ-tubulin or associated proteins and, in this way, modulate γ-tubulin functions [132,136,142]. Previously our laboratory reported association of Src family kinases with γ-tubulin complexes in differentiating P19 embryonic carcinoma cells [133,143], activated rat basophils (RBL-2H3) [134], and in activated bone-marrow mast cells (BMMCs) [136]. Src kinase is involved in the regulation of PI3K-dependent signaling pathways [144]. Direct association of γ-tubulin with regulatory subunit p85α of PI3K was described [133], but the physiological relevance of this interaction is still unknown.

The ubiquitination is important for γ-tubulin degradation It was reported that BRCA/BARD1 (breast cancer/BRCA1-associated RING domain protein 1) complex catalyzes γ-tubulin ubiquitination on K40 *in vitro* [145]. Deregulation of this ubiquitination causes abnormal nucleation from MTOC *in vivo.*

Posttranslational modification of γ-tubulin is not the only way how to tune γ-TuRC function. As noted above, γ-tubulin interactions with GCPs and recruitment factors are

essential for MT nucleation. Phosphorylation of GCP5 by GSK3-β (glycogen synthase kinase 3β) prevents over-accumulation of γ-TuRC on spindle poles during mitosis [146]. In NEDD1 there are phosphorylation sites controlled by CDK1 (T550) and Plk1 (S460), at the onset of mitosis to increase number of γ-TuRC in spindle poles [110,111,147,148]. On the other hand, hypophosphorylation of GCP2 and lower expression of γ-tubulin was found in aberrantly motile sperms in comparison to sperms from healthy donors [144].

I.4. GIT/PIX/PAK REGULATORY PROTEINS

I.4.1. GIT protein

GITs (G-protein-coupled receptor kinase interacting proteins) are multidomain proteins that form scaffold for many interacting partners. GITs were identified several times independently by two-hybrid screening using GRK5 (G protein-coupled receptor kinase 5) as bait [149] and by pull-downs using the paxilin LD4 domain [150] or N-terminus of PAK1 (p21-activated kinase 1) kinase [151]. GIT protein family contains two orthologs, GIT1 and GIT2. They have 65% sequence identity. Both members are stimulated by GTPase-activating proteins (GAPs) for activation of proteins from ADP ribosylation factor (Arf) subfamily [149,150]. Arf GTPase subfamily belongs to a large Ras-GTPases (Rat sarcoma-GTPase) family playing indispensable role in regulation of both, actin as well as MT cytoskeleton. GIT proteins have N-terminal GAP domain for activation of Arf proteins. Activation of Arf GTPases modulates cell polarity, motility, adhesion, growth, membrane transport and also gene transcription and translation [152].

GIT function and localization are most likely mediated through its interaction with various signaling molecules, including paxilin, p21-activated kinase interacting exchange factor (PIX), focal adhesion kinase (FAK), phospholipase Cγ (PLCγ) and mitogen-activated protein kinase kinase Erk 1 (MEK1) [150,151,153]. In fibroblasts and epithelial cells, GIT1 regulates migration and protrusive activity by assembling and targeting multi-protein signaling complexes that contain actin regulators, such as PIX and the Rac/Cdc42 (Ras-related C3 botulinum toxin substrate 1/cell division control protein 42 homolog) effector p21-activated kinase (PAK), to adhesions and the leading edge of a protrusion [154,155].

Among direct binding partners of GITs belong PIX and paxilin. GITs bind PIX protein through Src-homology 2 domain (SHD) and to paxilin through C-terminal paxilin binding site (PBS) [149] (Fig. 5). GITs use SHD and PBS for its recruitment to focal adhesion (FA) complexes and leading edge of migrating cells [151]. GITs use SHD for interaction with MEK1 that phosphorylates ERK1/2 (extracellular signal-regulated kinase 1/2). This activation of MEK1 is dependent on conformational change promoted by binding to GIT [153].

N-terminal ankyrin repeats (ANK) has unknown role, however first repetition is responsible for GIT-binding to endosomes [154,156]. In GITs, there are three coiled coil (CC) domains in SHD, in PBS and in C-terminus independently on any domain. CC domains are necessary for homo- and hetero-dimerization of GITs triggering its proper function [152,156].

Despite the dimerization, GITs are regulated by phosphorylations. GIT1 is rapidly phosphorylated in response to cellular adhesion to fibronectin [157]. GIT1 is phosphorylated on S709 in PBS domain that is necessary for protrusive activity [158]. GIT1 becomes tyrosine phosphorylated by Src kinase when cells are stimulated with growth factors [153,159]. Phosphorylation on Y246 and 293 is necessary for intramolecular conformational changes in GIT1 to release its autoinhibition for association to FAK (Y321) and PLCγ (Y392) in FA [160]. However, phosphorylations cause distinct effect in GIT1 and GIT2.
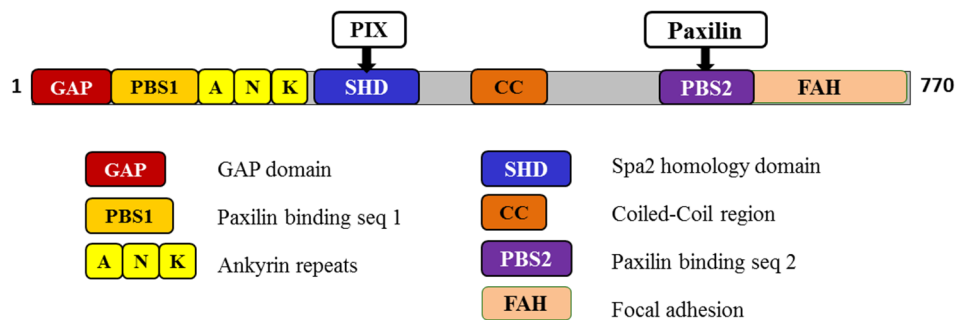
Figure 5. *Illustration of GIT1 with its domains. GIT1 contains N-terminal Arf-GAP domain (GAP; 3-124 base pairs, bps), Paxilin binding sequence 1 (PBS1) overlapping with ankyrin repeats (ANK; 137-254 bps), Spa2 homology domain 1 (SHD; 337-367 bps), coiled-coil domain (CC; 450-482 bps), C-terminal paxilin-binding domain (PBS2) overlapping with focal adhesion domain (FAH; 641-765 bps) (adapted from [161]).*

I.4.2. PIX protein

PIX/Cool (Pak-interacting exchange factor/Cloned-out of library) proteins were originally identified according to its Src homology 3 (SH3) domain as direct binding partners of PAK1 [162–164]. PIX family contains two orthologs, αPIX and βPIX. Both proteins are multidomain and play the important roles in regulation of actin cytoskeleton. PIXs regulate small Rho (Ras-homology) GTPases subfamily that belongs to Ras GTPases. Rho GTPases function as molecular switches [165]. They are converted from the GDP-bound inactive form to a GTP-bound active form by a reaction catalyzed by guanine nucleotide exchange factors (GEFs) (Fig. 6). This subfamily contains three members that are important for regulation of cytoskeleton, RhoA, Rac and Cdc42. Rac1 and Cdc42 are activated by GTP hydrolysis via PIX [163]. αPIX activate only Rac1 [164].
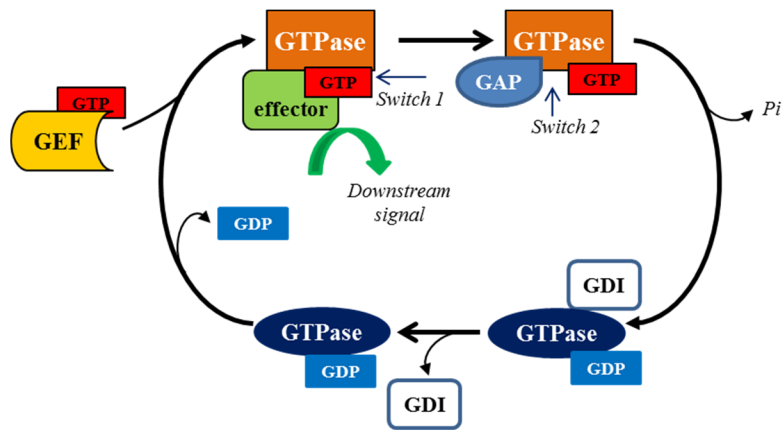
FIGURE 6. *Scheme of Rho GTPase activation/deactivation cycle. Activation of Rho GTPase occurs by stimulation with GEF that causes the release of GDP and the binding of GTP. In the GTP-bound form, Rho protein undergoes conformational change in its switch 1 domain. Thus it interacts with effector molecules and initiates downstream response. GTPase activating protein (GAP), by hydrolyzing GTP into GDP at the switch 2 domain, turns back GTPase to its GDP-bound state, to complete the cycle and terminate the signal transduction. Besides GEF and GAP proteins, a third factor that regulates Rho GTPase activity is the guanine dissociation inhibitor (GDI), which maintains Rho in the cytoplasm in the inactive form (linked to GDP) (adapted from [166]).*

While αPIX is predominantly expressed in hematopoietic cell lines and muscles, βPIX is expressed ubiquitously [163]. The main difference between both proteins is presence of calponin-homology (CH) domain in αPIX. βPIX is composed from diffuse B cell lymphoma homology (DH) domain and flanking pleckstrin homology (PH) domain, which are conserved in all of the GEFs for Rho GTPases. DH and PH domains are responsible for activation of Rho GTPases. PH domain also binds phosphatidylinositol, PKC and G-proteins [167]. PIX protein binds directly to GIT via GBD (GIT-binding domain) (Fig. 7). Both proteins can oligomerize, thus forming GIT-PIX signaling cassette [161]. The coiled-coil (CC) domain is necessary for dimerization causing changes in subcellular localization [168,169]. The dimerization of PIX is similarly to GIT dimerization important for its function. PDZ domain is characteristic only for βPIX as binding domain for three proteins forming the PDZ abbreviation (Post synaptic density protein, *Drosophila* disc large tumor suppressor a *Zonula*

occludens-1 protein) [170]. βPIX also contains T1 insert for inhibition of GEF activity, which has Y442. Phoshorylation of this site by Src kinase induces GEF activity [171].

SH3 domain binds to proteins containing PXXXPR motif, such has PAK1 kinase [162,163], Cbl (casitas B-lineage lymphoma) ubiquitin ligase [172] and Rac1 GTPase [173]. Although αPIX induce PAK1 activation [171], βPIX inhibits Rac1/Cdc42-stimulated PAK activity [162,171]. Moreover, PIX contain proline-rich motif (PXXP) for interaction with POPX1 and POPX2 (partner of PIX-1 and PIX-2) phosphatases for inactivation of PAK kinase [174]. PAK1 is effector of GTP-Rac and GTP-Cdc42 GTPases.
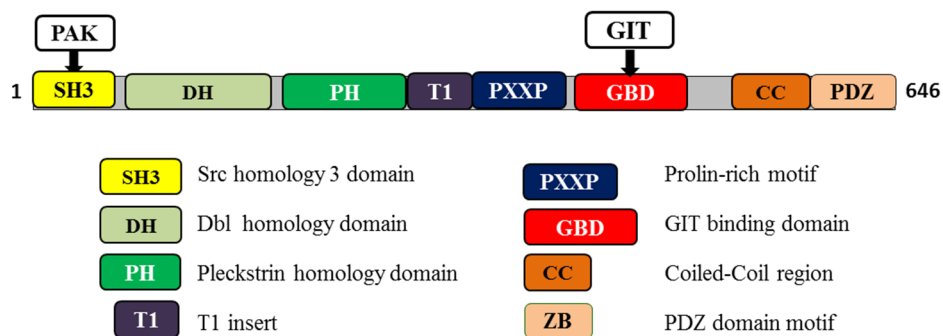
FIGURE 7. *Illustration of βPIX with its domains. βPIX contains N-terminal Src-homology (SH3; 10-63 bps) domain, diffuse B cell lymphoma homology (DH; 94-292 bps) domain, a flanking pleckstrin homology (PH; 302-400 bps) domain, T1 insert, Proline-rich motif (PXXP), GIT-binding domain (GBD), coiled-coil (CC) domain, C-terminal PDZ motif (ZB) (adapted from [161]).*

I.4.3. PAK kinase

The family of PAK kinases includes PAK1-PAK6. All are activated by phosphorylation and deactivated by phosphatases. Except their role in cytoskeleton organization, they are implicated also in cell cycle regulation [175]. The members of this family fall into two groups according to presence of activation domains. Group I contains PAK1-3 and Group II contains PAK3-PAK6 without activation domain. First group is directly regulated by Rho GTPases.

PAK1 kinase can form inactive homodimer by antiparallel dimerization [176]. Upon activation by GTPase binding to N-terminal autoinhibitory domain (AID), the trans-inhibitory conformation is released and PAK autophosphorylates at T423 and S144 [177]. In

open conformation, PAK1 can phosphorylate substrates and thus resides in an 'intermediate-active' state [176]. In the 'active state', trans-phosphorylation is crucial for maintaining the full catalytic activity of PAK1 [178].

The domain structure of PAK1 includes N-terminal conserved proline-rich motifs. The first motif selectively binds SH3 domain of Nck (non-catalytic region of tyrosine kinase adaptor protein 1) [179], Grb2 (Growth factor receptor-bound protein 2) [180], and PIX [163]. The C-terminus of PAK1 contains a conserved heterodimeric G-protein complex binding site for the G_β subunit [181] (Fig. 8).

The primary autophosphorylation sites that control the enzymatic activity of PAK1 are T423 and S144 [176,177]. The other phosphorylation sites contribute to kinase activation and/or maintenance of kinase activity (S21, S57, S149, S199, S204) [182,183]. These sites interfere with the proteins bound via SH3–PXXP domains [168].

Active PAK is localized in nucleus to induce gene expression and also in FA to regulate cell motility. PAK is at the centrosome for control of centrosome duplication and separation [184] in AuroraA kinase-dependent manner prior to mitosis [185]. Phosphorylation at T212 by CDK1 causes accumulation PAK1 at MTOC of mitotic cells and along spindles in fibroblast [184,186]. PAK1 is important in modulation of MT dynamics via stathmin. Phosphorylation of stathmin at S16 by PAK1 inhibits its binding to MTs and prevents destabilizing activity interphase cells [187].

Among the other proteins interacting with PAK1 are PKC, PI3K, CDK5RPA2, Cdc2 (cell division control protein 2), PP2A, sphingolipids, $G_{\beta\gamma}$, PIX/COOL and GIT via PIX [150,157]. PAK1 downstream proteins are MLCK (myosin light-chain kinase), BAD (Bcl2/Bcl-Xl antagonist carrying cell death), RAF (rapidly accelerated fibrosarcoma), MAPK/Erk1 (mitogen activated protein kinase), or Merlin protein.
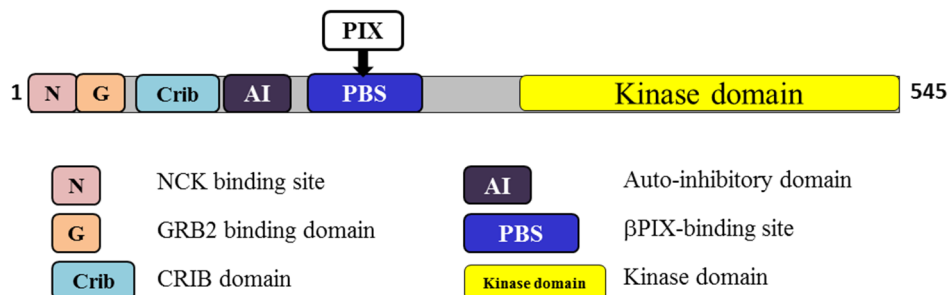
FIGURE 8. *Illustration of PAK1 with its domains. PAK1 contains N-terminal PXXP motifs for binding to Nck (N) and to Grb2 (G) proteins, a CDC42 and RAC1 interactive binding*

(CRIB) domain (73-118 bps), autoinhibitory (AI) domain, βPIX-binding site (PBS), and C-terminal kinase domain (262-517 bps) (adapted from [188]).

I.4.4. GIT/PIX/PAK signaling complex

GIT and PIX form signaling complex that *in vitro* has heteropentameric conformation [152]. PAK1 kinase is direct interacting partner of this cassette via βPIX thus forming GIT/PIX/PAK signaling complex. GIT/PIX/PAK complex provides a platform for cross-linking of Arf and Rho GTPase signaling pathways. Moreover, all proteins are in large complexes (1-2 MDa) that are composed from 10-20 other proteins [189]. Many of them can influence function as well as localization of this complex [151,190,191]. Among the most important belongs paxilin that mediates GIT/PIX/PAK complex formation in FA.

The role of GIT/PIX/PAK complex in FA was already revealed. Paxilin bind GIT1 and this binding is promoted by βPIX-binding [151]. GIT1 targets also PAK to FA and the leading edge of cells. All proteins modulate the assembly and disassembly of FA and protrusive activity of the cell [192]. Regarding regulation GIT/PIX/PAK activity in FA, βPIX tyrosine phosphorylation weakens its ability to bind GIT1 thus destabilizing FA [193]. Phosphorylation of PAK1 on S517 destabilizes PAK-PIX association [194]. Although MT (+) ends do not reach FA, it was suggested that GIT/PIX/PAK can affect FA also via MTs. GIT role in MTs regulation can be passed by regulation of centrosome function [195]. However, direct effect of GIT/PIX/PAK complex in MT regulation has not been evidenced yet.

First hint of the regulatory role of GIT, PIX, and PAK proteins in MT organization provided Zhao and coworkers. They have shown that GIT-PIX complex is localized at the centrosomes in mouse fibroblasts both in the interphase and mitosis [196]. They also reported that PAK1 can be activated by centrosome targeting and the basis for this activation involves a GTPase-independent mechanism requiring centrosome integrity. As cells pass through S-phase the centrosome duplicates and the PCM is enlarged, correlating with PAK activation [186]. One role of active PAK at this site is to participate in the activation of centrosomal kinase AuroraA by phosphorylation on S342 and T288 [196] that is required for spindle formation [197]. Like GIT1, AuroraA is localized to the PCM in a MT-independent manner [198]. Thus, GIT/PIX/PAK complex originally described for cell adhesion can provide a link between FA and centrosome function.

I.5. CALCIUM SIGNALING

I.5.1. Mast cells

Mast cells are one of the first cells activated during inflammation to initiate response against invading pathogens, environmental antigens (Ag) or environmentally derived toxins. In pathologic conditions they are responsible for early type of hypersensitivity termed as the allergy reaction.

Allergy reaction starts through receptor-antigen interaction. It causes release of proinflammatory mediators to extracellular space. These mediators are stored in granules in cytoplasm and contain hydrolytic enzymes, histamine, serotonin, proteases, chemokines, cytokines and prostaglandins. Released mediators help to defense the allergic antigens by vasodilatation and bronchoconstriction [199]. In resting cells granules are prepared for signal to start fusion with PM.

I.5.2. Regulation of mast cell activation

Mast cells can be physiologically activated through antigen by IgE-dependent (immunoglobulin E) aggregation of the high-affinity IgE receptor (FcεRI) that is expressed on PM [200]. The aggregation of FcεRI by antigen-IgE complex triggers a series of biochemical events leading to Ca^{2+} efflux from ER stores, changes in cell morphology and finally fusion of granules with the PM [201].

FcεRI is a tetrameric complex formed by an IgE-binding α-subunit, a signal amplifying β-subunit, and a homodimer of γ-subunits. Each FcεRI β- and γ-subunit contains one immunoreceptor tyrosine-based activation motif (ITAM) which must be activated by tyrosine kinases to complete receptor activation and promote downstream signaling. Among the protein tyrosine kinases (PTKs) necessary for receptor activation belong the Src family kinases containing 8 members [199]. However, there have been described three different models of receptor activation, all have in common the activation of Lyn or Fyn tyrosine kinases [202].

First pathway of mast cell activation requires Lyn. It leads to the activation of Syk that phosphorylates LAT (linker for activation of T cells) protein. It serves as an anchor for activation of PLCγ. The activation of PLCγ culminates in the formation of inositol triphosphate (IP_3) and diacyglycerol (DAG). The former binds IP_3 receptors located on the ER membrane, thereby directly releasing Ca^{2+} to cytoplasm by opening Ca^{2+} channels [203].

The second proximal pathway of mast cell activation utilizes Fyn kinase (Src/Yes-related novel), an enzyme essential for phosphorylation of Gab2 (Grb2-associated linker). This signaling pathway represents slower enhancement of intracellular Ca^{2+}. Gab2 activation leads to increased activation of PI3K that supports release of internal Ca^{2+} via synthesis of PIP2 (phosphatidylinositol 4,5-bisphosphate) and PIP3 (phosphatidylinositol (3,4,5)-trisphosphate) [204].

Ca^{2+} release from ER to cytoplasm represents activation of signaling cascades linking ER with PM receptors. It promotes opening of PM channels to pump extracellular Ca^{2+} inside the cell. The extracellular Ca^{2+} influx is essential for mast cell degranulation [200].

I.5.3. Calcium signaling and microtubule reorganization in mast cells

In various cell types Ca^{2+} signaling must be tightly regulated as it is critical for control of basic cellular function from cell cycle control and division, secretion, cell migration, to gene transcription and apoptosis. In cytoplasm Ca^{2+} concentration is maintained at low level via the constant action of Ca^{2+} pumps on membranes of ER and mitochondria. These organelles also serve as reservoirs from which Ca^{2+} is readily released to increase the cytoplasmic Ca^{2+} concentration [205]. Cell can draw on extracellular Ca^{2+} to maintain signaling or refill ER Ca^{2+} stores by opening channels on PM [206]. This Ca^{2+} entry stimulated by depletion of internal Ca^{2+} stores is known as store-operated Ca^{2+} entry (SOCE) [207].

Unlike excitable cell such as neurons or muscle cells which replenish their Ca^{2+} through voltage-gated Ca^{2+} channels, non-excitable cells such as epithelial cell, fibroblast or mast cell depend on non-voltage-gated channels. Calcium in cytoplasm participates in various signaling pathways where Ca^{2+} binding proteins are involved. Calmodulin and STIM1 are typical Ca^{2+}-dependent proteins in local intracellular signaling.

Proteins directly regulated by Ca^{2+} cations are characterized by specific structure motif termed EF-hand domain. This motif is formed by N-terminal helix (E helix) followed by central loop sensitive to Ca^{2+}, and C-terminal helix (F helix). Proteins with EF-hand domain can either be buffered or can transport Ca^{2+}. Calmodulin is the best studied and prototypical example of the EF-hand family of Ca^{2+}-sensing proteins. Changes in intracellular Ca^{2+} concentration regulate calmodulin in two distinct ways: (1) at the cellular level, by directing its subcellular distribution; (2) at the molecular level, by promoting different modes of

association with many target proteins [208]. Calmodulin was reported at the centrosome during Plk1 activation. It also controls assembly of PCM components [209].

STIM1 is transmembrane protein located in ER membrane. The main role of STIM1 is sensing intraluminal Ca^{2+} concentration and enabling SOCE. The intraluminal part of STIM1 has a low affinity EF-hand domain. When Ca^{2+} in ER is under subcritical concentration, the EF-hand is vacant and induces STIM1 conformational changes leading to STIM1 aggregation. Aggregates of STIM1 still bound to ER membrane become to close proximity with PM. There STIM1 physically associate with CRAC channels and induce influx of external calcium [210].

STIM1 represents a special type of a +TIPs. It binds to growing MT (+) ends via EB1. In cells it facilitates changes I ER associated with growing MTs. ER generates also a steric hindrance for interaction between STIM1 and Ca^{2+} channels on PM [211].

I.5.3.1.   Artificial activation of mast cell

Mast cell activation under *in vitro* conditions can be reached also artificially by pervanadate, thapsigargin, ionomycin, ATP (adenosine 5′ tripshophate), or histamine. Pervanadate (sodium orthovanadate, VO_4^{3-}) is a compound that inhibits protein tyrosine phosphatases (PTPases) causing tyrosine hyperphosphorylation. This activation leads to Ca^{2+} release and degranulation [212].

Maximal depletion of internal Ca^{2+} stores causes the openers of ER Ca^{2+} pump, such as Thapsigargin or ionomycin. Thapsigargin is natural agent synthetized by plant *Thapsia garganica*. It passively raises Ca^{2+} by blocking the sarco-endoplasmic reticulum ATPase pump (SERCA) on ER membrane [213]. Ionomycin is an ionophore produced by the bacterium *Streptomyces conglobatus*. It also passively stimulates Ca^{2+} influx by activating SOCE and not by direct action at the PM [214].

I.5.4.   The Role of microtubules in mast cell activation

The mast activation induces changes in cell morphology trigged by rapid changes in actin and MT cytoskeleton. It results in formation of protrusions to enlarge cell surface. Our laboratory proposed model, that MT protrusions might be involved in sensing external chemotactic gradients of antigen or other signals reaching mast cells at inflammatory sites [215].

The intact MTs are necessary for degranulation as was described by treatment with anti-tubulin drugs [216]. It is consistent with the fact, that MTs are necessary for transport of intracellular organelles. Calcium is important regulator of MTs in mast cells as depletion of STIM1 resulted in the inhibition of MT reorganization in activated mast cells. Calcium is also essential for generation of MT protrusions [215]. It was suggested that STIM1 is able to bind to different +TIPs. Interestingly, STIM1-deficient mast cells exhibit defects in chemotaxis toward antigen [217]. Although MTs are important in these processes, molecular mechanisms that control changes in MT organisation during mast cell activation are unknown. Both modulation of MT nucleation and dynamics can be involved in rearrangements of MTs in mast cells.

Besides Ca^{2+}, PTK might modulate γ-tubulin functions [132,134,136]. Previously, we have shown that during mast cell activation through FcεRI or treatment with pervanadate, γ-tubulin form complexes with phosphotyrosine proteins and tyrosine kinases [134]. The significance of Src kinases for MT nucleation from centrosome was ascertained by MT regrowth experiments [140,141]. Thus, identification of tyrosine kinase substrates that regulate γ-tubulin functions at the centrosome should help to elucidate the mechanisms involved in the regulation of MT nucleation during activation of mast cell.

I.6. TUBULIN-BINDING AGENTS AS TOOL FOR STUDY OF MTS

The importance of MTs in mitosis and cell motility makes them useful target for anticancer drugs. Knowledge of the mechanistic differences among the chemically diverse anti-tubulin drugs is vital to understanding their tissue and cell specificity and multi-drug resistance. A large number of small molecule inhibitors, termed tubulin-binding agents (TBAs) have been discovered, and some have entered clinical trials. Even though most of these agents stabilize or destabilize tubulin via binding to their binding sites, a few compounds bind to tubulin on undefined sites or disrupt MTs in diverse ways. TBAs are also essential tools for study MT nucleation, organization and their interactions with other cellular components [218].

TBAs can be classified based on their effect on MT structure or dynamics. These classes include MT stabilizing drugs such as the taxanes and epothilones, and MT depolymerizing drugs such as nocodazole, the later are further subdivided into vinca-domain binding agents (vinca alkaloids and dolostatins) and colchicine-domain binding agents

(colchicine, its analogues and estradiol-derived agents). The third subgroup encompasses other MT depolymerizing compounds such as estramustine, noscapine, certain psychoactive drugs (phenytoin), herbicides [219].

TBAs are commonly referred to as anti-mitotic drugs because they dominantly cause mitotic arrest and produce cell death. The mitotic arrest is caused via spindle defects or induction of G2/M or intra-M checkpoints. Drugs at low concentrations are insufficient to cause overall alteration in the net polymer mass [220–222]. TBA-induced tumoricidal action occurs either at the G1-phase of the cell cycle and/or after mitotic arrest; however, such action may escape by virtue of "mitotic slippage" [223].

Disadvantages in using of these agents for cancer treatment include side-effects on non-malignant cells, and development of multi-drug resistance (MDR). In this case cancer cells exposed to one anticancer drug show resistance to various anti-cancer drugs, although they are structurally and functionally different from the initial drug.

Generally, the most investigated mechanisms of MDR with known clinical significance are: a) point mutations of β-tubulin at the paclitaxel-binding site, polymorphisms or selective overexpression of β-tubulin isotypes; b) activation of transmembrane proteins effluxing the chemical substances from the cells; c) activation of the enzymes of the glutathione detoxification system; d) alterations of the genes and the proteins involved into the control of apoptosis (especially p53 and Bcl-2) [219,224–226]. The most typical efflux pump is P-glycoprotein (P-gp) ATPase, generated by gene amplification of *MDR1*, producing MRP1 protein [227].

Specific binding sites were described for colchicine, vinblastine, taxol and laulimalide [228]. Other anti-tubulin drugs usually bind to one of these prototype binding sites. It was described that nocodazole at low concentration is able to stop cell movement. Except above mentioned drugs, other chemical compounds can also affect MT dynamics [229,230].

There is a strong need to design and develop new analogues of antimitotic agents that interact with tubulin at sites different from those of TBAs, or that rather cause damage of MTs by another mechanism. Changes in posttranslational modifications of tubulins can result in attraction of MT-severing proteins.

I.6.1. Steroid compounds

One of possible agents exhibiting antitumor biological activity are steroid compounds that can be either natural or synthetic. Typical representatives are estradiol [231], testosterone

[232] and pregnenolone [233]. Steroids are used as anti-inflammatory, anti-cancer, anabolic, anti-androgenic, progestational and contraceptive agents.

Most natural estrogens are short-lived, do not accumulate in tissue and are easily broken down in the liver. In contrast to natural estrogens, estrogenic drugs such as ethynylestradiol diethylstilbestrol, synthetic environmental estrogens, polychlorinated biphenyls, and phytoestrogens such as isoflavones (genistein) or lignans, are more stable and remain in the body longer than natural estrogens. Because most of these compounds are lipophilic, they tend to accumulate within the fat and tissue of animals and humans [234].

All types of estrogens bind and activate the hormone receptors, which triggers specific cellular processes. As ligand inducible transcription factors they turns on specific genes to promote proliferation. Therefore, the estrogen-signaling pathways are implicated in development of cancer [235]. The binding of ligand to a steroid receptor can either induce (agonistic activity) or repress (antagonistic activity) the transcription from promoters of target genes. The steroid receptor family contains seven subfamilies: estrogen receptors (ERα, ERβ), estrogen-related receptors, and 3-ketosteroid receptors, which include the androgen receptor (AR) and others [236].

There are evidences that some estrogenic compounds, originally being the receptor antagonists, act directly on MTs by interacting with tubulin. Seegers et al., found that 2-methoxyestradiol (2-ME), a naturally occurring metabolite of estradiol and 17-ethynylestradiol, was more potent than estradiol in producing mitotic perturbations [237]. Basically, 2-methoxyestrogenes are extremely weak in binding to cytosolic ERα and β, thus its anti-proliferative activity is independent on the interaction with those receptors [238]. 2-ME works via its ability to bind to the colchicine-binding site in tubulin and its high concentrations have been shown to depolymerize MTs [239]. Moreover, 2-ME is known to interfere with the dynamics of tubulin polymerization [240]. Other estradiol metabolites were also described as competitive inhibitors of colchicine-binding to tubulin [241].

Advantages of 2-ME over classic TBAs include a better tolerated side-effects, prefential sparing of non-malignant cells and lipophilic properties. Among the disadvantages belongs rapid metabolism resulting in poor pharmacokinetic characteristics. 2-ME is also a substrate for P-gp efflux pumps that rapidly blow the drug out of the cell [242].

To date, there have been synthesized and studied number of 2-ME analogues and other steroidal dimers and ribbons to improve cancer treatment. The pharmacological effect of modified steroids heavily depends upon structural features of the steroid molecule and side

chains. For instance, modification the parental 2-ME compound in the A ring led to generation of more potent inhibitor of tubulin [243]. Analogues with modifications on the B ring or D ring are more effective anti-tubulin agents than the parental molecule [242]. The conjugated estrone derivatives were even 10-fold more potent than monomeric 2-ME and caused mitotic arrest and initiation of apoptosis [244]. Analogues cause mitotic spindle disruption, mitotic arrest, MT depolymerization, and inhibition of the assembly of purified tubulin similar to the effects of parental 2-ME. The new analogues and their biological properties with respect to the natural estrogen metabolite 2-ME show that specific substitutions of the A ring, either alone or in combination with specific changes in the B ring, lead to compounds with better biological potency. Although steroid derivatives are not as potent as classical anti-mitotic agents, they act in substoichiometric concentrations.

II. AIMS OF THE STUDY

The long-term research program of the Laboratory of Biology of Cytoskeleton has been focused on studying the structure-function relationships of MT proteins, their interactions with other cytoskeletal elements and MT regulation in cells under normal and pathological conditions. Recently we have focused on the role of signaling proteins in MT nucleation from centrosomes. In particular, we have been studying γ-tubulins, the essential proteins in this process. A panel of monoclonal antibodies against various MT building proteins including α-, β- and γ-tubulins as well as MT-associated proteins has been prepared in our laboratory and these antibodies represent powerful tools in studying MT organization. Newly introduced microscopic techniques for analysis of living cells provided new insights into the subcellular localization, dynamics and function of proteins involved in MT regulation.

Partial aims of this Ph.D. thesis were following:

1) Development of new tools for quantification of MT nucleation, polymerization and dynamics.
2) Analysis of novel functions of mammalian γ-tubulins.

3) Understandings of signaling pathways for MT reorganization during mast cell activation.

4) Functional analysis of GIT/PIX/PAK signaling complex in MT nucleation.

III. COMMENTS ON PRESENTED PUBLICATIONS

III.1. γ-TUBULIN 2 NUCLEATES MICROTUBULES AND IS DOWNREGULATED IN MOUSE EARLY EMBRYOGENESIS.

Vinopal S., **Černohorská M.**, Sulimenko V., Sulimenko T., Vosecká V., Flemr M., Dráberová E. & Dráber, P. γ-Tubulin 2 nucleates microtubules and is downregulated in mouse early embryogenesis. *Plos ONE*, **7**: e29919, (2012)

TUBG1 and TUBG2 were initially assumed to be functionally equivalent [74]. Gene knock-out analysis of *Tubg1* and *Tubg2* in mice suggesting that they might have different functions [73]. We proposed that TUBG1 is a conventional γ-tubulin, whereas TUBG2, which was not able to substitute for TUBG1 in *Tubg1*^{-/-} blastocysts, might have some unknown function(s) in the brain. However, the molecular basis of the suggested functional difference is unknown.

At this work, we identified and characterized molecular mechanisms underlying functional differences between TUBG1 and TUBG2. At first, we prepared FLAG-tagged human and mouse TUBG1 and TUBG2, because specific antibodies distinguishing between TUBG1 and TUBG2 were not available. We examined their subcellular localization and interactions with GCP2 and GCP4. All recombinant proteins localized properly to MTOCs and formed immunocomplexes with GCP2 and GCP4.

Next, we tested whether TUBG2 can substitute for TUBG1 *in vivo*. We depleted endogenous TUBG1 in U2OS cells using siRNA and performed phenotypic rescue experiments by expressing siRNA-resistant mouse TUBG1-FLAG, mouse TUBG2-FLAG or human TUBG2-FLAG in these cells. Although the used siRNA was TUBG1-specific, immunobloting with anti-γ-tubulin antibody recognizing both TUBG1 and TUBG2 revealed that TUBG1 is a predominant γ-tubulin in U2OS cells. Depletion of TUBG1 resulted in severe mitotic spindle defects including monopolar and collapsed spindles, very similar to those observed in *Tubg1*^{-/-} blastocysts [73], and induced accumulation of TUBG1-depleted cells in metaphase. As expected, mouse TUBG1-FLAG rescued wild-type phenotype and normal mitotic progression. Importantly, the same was true for both mouse and human TUBG2-FLAG indicating that TUBG2 is capable to replace TUBG1 *in vivo*.

We also examined MT nucleating capability of TUBG2 in MT regrowth experiments. We focused on mitotic cells, because γ-tubulin is enriched on prophase and metaphase centrosomes [245] and we could expect a prominent effect on MT nucleation. In accordance with our previous results, mouse TUBG1-FLAG as a positive control, mouse TUBG2-FLAG and human TUBG2-FLAG rescued MT aster formation in TUBG1-depleted cells. These findings suggested that mammalian TUBG2 is capable of centrosomal MT nucleation in mitotic cells.

To strengthen the evidence of MT nucleation capability of TUBG2, we quantified MT formation *in vivo* by the tracking of MT (+) ends marked by EB1-GFP in interphase U2OS cells (U2OS-EB1). For live cell imaging we prepared mouse TUBG1 and human TUBG2 tagged with a red fluorescent protein TagRFP and switched to shRNA-based system. MT formation was quantified in negative control cells, TUBG1-depleted cells and in TUBG1-depleted cells expressing either mouse TUBG1-TagRFP or human TUBG2-TagRFP. We observed

a significant reduction in the number of MT (+) end tracks in TUBG1-depleted cells. Both exogenous TUBG1 and TUBG2 rescued MT formation indicating that TUBG2 can take the place of TUBG1 also in interphase cells.

We showed that TUBG2 was able to nucleate MTs and substitute for TUBG1 in cultured cells. The inability of TUBG2 to do so in TUBG1-deficient blastocyst, where TUBG2 should have been present [73], was intriguing. Therefore we analyzed the expression of TUBG2 in wild-type mouse blastocysts in more detail. Using RT-qPCR, we quantified mRNA levels of *Tubg1*, *Tubg2*, *Tubgcp2* and *Tubgcp5* in mouse oocytes, 2-cell stage embryos, 8-cell stage embryos and blastocysts. Surprisingly, *Tubg2* mRNA level decreased dramatically in the course of mouse preimplantation development, unlike mRNA levels of *Tubg1*, *Tubgcp2* and *Tubgcp5,* resulting in a very low amount of *Tubg2* transcript in the blastocyst.

We established 2D-PAGE system for separation of TUBG1 and TUBG2. By this approach, we found out that while TUBG1 was abundant, there was a very low level of TUBG2 protein in the wild-type blastocyst, which was in a good agreement with our RT-qPCR data.

Based on our data, we proposed an alternative interpretation of *Tubg1*^{-/-} and *Tubg2*^{-/-} phenotypes previously described in mice [73]. Endogenous TUBG2 could not replace missing TUBG1 in Tubg1^{-/-} blastocyst, even though it can nucleate MTs, because it was not present in a sufficient amount. Nonetheless, our data did not directly exclude the possibility that

TUBG2 expression was up-regulated in *Tubg1*^{-/-} blastocysts in response to TUBG1 deficiency as it was observed for several other duplicate gene pairs [246]. It that case, TUBG2 would not be functionally equivalent to TUBG1 in mouse blastocysts. However, we consider this possibility unlikely for several reasons. First, although upregulation of a duplicate gene by transcriptional reprogramming occurs after its paralog deletion, it is not a genome-wide phenomenon [247]. Second, such paralog responsiveness occurred with almost no exceptions only when the duplicate genes were synthetic lethal [246], which is not the case of gamma-tubulin genes. Third, Yuba-Kubo *et al.* speculated that TUBG2 is not able to be recruited to centrosomes in the absence TUBG1, because they were not able to detect γ-tubulin signal on centrosomes in Tubg1^{-/-} blastocysts [73]. Our alternative and simpler interpretation of their observation is that TUBG2 is expressed neither in wild type nor in Tubg1^{-/-} blastocysts as well.

Behavioral abnormalities of *Tubg2*^{-/-} mice did not necessarily imply just unknown function of TUBG2. They might also reflect the reduction of total γ-tubulin in the brain of *Tubg2*^{-/-} mice, as TUBG2 is highly expressed in the brain [73,75]. Yet, we could not directly exclude the possibility that TUBG2 has some additional still unknown function(s). Results from running project in the laboratory indicate that human TUBG2 could play important role in neuritogenesis.

In conclusion, we have demonstrated that TUBG2 is able to nucleate MTs and substitute for TUBG1 *in vivo*. Further, we have shown at both mRNA and protein level that TUBG2 expression is dramatically reduced in blastocysts in contrast to TUBG1. Our data indicate that TUBG2 cannot rescue TUBG1 deficiency in *Tubg1*^{-/-} blastocysts, because it is not present in a sufficient amount. We propose that mammalian γ-tubulins are functionally redundant with respect to their MT nucleation activity.

In this project, I established method for preparation of double transfected U2Os cells for phenotypic rescue experiments and participated in quantification of MT (+) end dynamics. I participated in designing experiments, formulation of hypothesis and in preparation of images for publication. I was involved in preparation of manuscript and in response to review comments.

III.2. MICROTUBULE NUCLEATION IN MOUSE BONE MARROW-DERIVED MAST CELLS IS REGULATED BY THE CONCERTED ACTION OF GIT1/βPIX PROTEINS AND CALCIUM.

Although MT rearrangement during mast cell activation has been described, molecular mechanisms that control their remodeling are largely unknown. We have previously shown that in FcεRI- or pervanadate-activated bone marrow-derived mast cells (BMMCs), γ-tubulin interacts with a similar set of tyrosine-phosphorylated proteins [136]. In this work we wanted to identify these proteins and evaluate their potential role in MT nucleation.

For this we applied large scale immunoprecipitation coupled with mass spectrometry. Lysates from pervanadate-activated cells were immunoprecipitated with anti-peptide mAb to γ-tubulin and the bound proteins were eluted with peptide used for immunization. Eluted proteins were then concentrated on SH2 domain for tyrosine-phosphorylated proteins [248] and subjected to MALDI/MS fingerprint analysis. Out of the three independent experiments, βPIX was identified three times. In cells, the βPIX forms complexes with GIT1. Such complexes might serve as scaffolds to bring together signaling molecules affecting various cellular processes, including cytoskeletal organization [161].

To ascertain whether βPIX and GIT1 associates with γ-tubulin in BMMCs, immunoprecipitation experiments were performed with Abs to γ-tubulin, βPIX and GIT1. Immunoblot analysis confirmed an interaction of both βPIX and GIT1 with γ-tubulin. Multiple phosphorylation sites were identified on human GIT1 [249]. To determine whether tyrosine-phosphorylated GIT1 interacts with γ-tubulin, pervanadate-activated cells were precipitated with Abs to γ-tubulin and GIT1. Tyrosine-phosphorylated GIT1 from pervanadate activated cells is thus capable of interacting with γ-tubulin. In order to decide whether γ-tubulin and βPIX or GIT1 proteins appear in the form of complexes, BMMCs extracts were subjected to gel filtration chromatography on the Superose 6 column. γ-Tubulin was distributed through a large zone in complexes of various sizes. Large

complexes of ~2 MD could represent γTuRCs. Importantly, βPIX and GIT1 were also presented in the complexes and their distribution partially overlapped with γ-tubulin. Localization studies in live BMMCs revealed the association of βPIX and GIT1 with centrosomes of interphase cells.

As βPIX and GIT1 interact with γ-tubulin, we have compared MT regrowth from centrosomes in BMMCs with a reduced level of βPIX or GIT1 in nocodazole washout experiments. The βPIX and GIT1-deficient cells were produced using lentiviral vectors. The βPIX depletion resulted in an increase of MT regrowth, while depletion of GIT1 depletion resulted in a decrease of MT regrowth. These findings were confirmed by phenotypic rescue experiments. These experiments indicate that GIT1 and βPIX represent positive and negative regulators of MT nucleation from the centrosomes in BMMCs.

Next, we measured the role of GIT1 and βPIX in antigen (Ag)-induced chemotaxis and degranulation. Cells with reduced GIT1 exhibited significantly stronger Ag-mediated chemotactic response than the control cells. On the other hand βPIX-depleted cells showed less efficient chemotactic response. In contrast to chemotaxis, cells with depleted GIT1 exhibited reduced degranulation, whereas βPIX-deficient cells showed significantly higher degranulation when compared to control cells. This could reflect increased MT nucleation in βPIX-depleted cells and decreased nucleation GIT1-depleted cells. Although MTs have long been implicated in cell motility, the role of MTs in this process varies with cell types. The mechanism of their involvement in cell motility is poorly understood. It has been suggested that MTs normally act to restrain cell motility [250]. This could explain the observed opposite effects in degranulation and chemotaxis after depletion of GIT1 and βPIX proteins.

Finally, we have found that Ca^{2+} modulates the interaction of γ-tubulin with GIT1, βPIXs and GCPs, and that the C-terminal region of γ-tubulin (aa 423-451) is essential for Ca^{2+}-dependent changes in γ-tubulin electrophoretic mobility in the presence of BMMCs extracts. Nucleation of MTs in BMMCs is also affected by Ca^{2+}.

In conclusion, our data suggest a novel signaling pathway for MT rearrangement in mast cells, where tyrosine kinase-activated GIT1 and βPIX, in concert with Ca^{2+} signaling, regulate MT nucleation. Enhanced levels of Ca^{2+} affect γ-tubulin properties, resulting in higher binding of GCPs to γ-tubulin. Presumably, through this action GIT1 and βPIX are involved in regulation of such important processes in mast cells physiology as is Ag-induced degranulation and chemotaxis. Interference with the MT network via specific regulators of MT nucleation in mast cells could open up new rational approaches to the treatment of inflammatory and allergic diseases.

In this project, I established BMMCs stably expressing RFPtagged-γ-tubulin, which was used for localization studies. I quantified MT nucleation by measuring of α-tubulin fluorescence. For this I developed a method for semi-automatic analysis of large number of cell. I analyzed all data from RNAi and phenotypic rescue experiments, prepared documentation and participated on writing of the manuscript.

III.3. GIT1/BPIX SIGNALING PROTEINS AND PAK1 KINASE REGULATE MICROTUBULE NUCLEATION

Černohorská, M., Sulimenko, V., Hájková, Z., Sulimenko, T., Sládková, V., Vinopal, S., Dráberová, E. & Dráber, P. GIT1/βPIX signaling proteins and PAK1 kinase regulate microtubule nucleation. Submitted 2015

We have previously identified βPIX and GIT1 as proteins interacting with γ-tubulin in mouse bone marrow-derived mast cells (BMMCs), and regulating MT nucleation in these cells [251]. In this work, we wanted to identify and characterize molecular mechanisms underlying regulation of MT nucleation in well-adherent cells during interphase.

To evaluate whether GIT1/βPIX proteins form complexes with γ-tubulin in the other cell types, we combined large scale immunoprecipitation with anti-peptide antibody to γ-tubulin with MALDI/MS fingerprint analysis as described [251]. Using this approach we confirmed association of γ-tubulin with GIT1. In cells, the GIT1/βPIX proteins can form scaffold to bring together signaling molecules affecting various cellular processes, including cytoskeletal organization [161]. It is well established that PAK1 is part of such complexes. Precipitation and reprecipitation experiments revealed interaction of γ-tubulin with GIT1, βPIX and PAK1 in U2OS cells. Precipitation experiments also confirmed interactions between γ-tubulin and GIT1, βPIX and PAK1 in nontransformed immortalized human retinal pigment epithelial cells RPE1, proving that the association of γ-tubulin with these proteins is not restricted to transformed cells.

Next we prepared cell lines stably expressing phGIT1(tv1)-TagRFP, phβPIX(tv1)-TagRFP or phPAK1(tv1)-TagRFP to evaluate localization of these proteins in U2OS cells. In interphase and mitotic cells both GIT1-TagRFP and βPIX-TagRFP were present on centrosomes. On the other hand, PAK-TagRFP failed to show centrosome enrichment in interphase and mitotic cells. It is well established that increased PAK1 activity is associated with autophosphorylation of specific sites, including S144 and S199 [183]. Using antibody recognizing phospho-PAK1(pS144), clear association of autophosphorylated PAK1 with centrosomes both in interphase and mitotic cells was observed. When cells were stained with Ab to phospho-PAK1(pT423), that marks activated PAK1 [182], interphase and mitotic centrosomes were also clearly labelled. Activated PAK1 thus associated with interphase centrosomes. Localization of GIT1, βPIX and PAK1 in centrosomes was not affected when cells were treated with nocodazole. This indicated no requirement for intact MTs.

Because GIT1, βPIX and PAK1 interact with γ-tubulin, we compared MT regrowth from interphase centrosomes in U2OS cells with reduced levels of GIT1, βPIX or PAK1 in nocodazole-washout experiments. The GIT1 and PAK1 depletion resulted in a decrease of MT regrowth. On the other hand, βPIX depletion led to an increase of MT regrowth. Results for GIT1 and βPIX were confirmed by phenotypic rescue experiments as well as by double knockdown. As a second approach, we counted the numbers of new MTs emanating from centrosomes during MT regrowth using EB1 protein to label plus ends of growing MTs [15]. The number of EB1 comets leaving the centrosomes per unit time (nucleation rate) has been used to measure nucleation events in real time [140,252]. For these studies we used live-cell imaging in U2OS cells stably expressing low levels of EB1-GFP [253] to demonstrate that changes in MT regrowth in GIT1- and βPIX-depleted cells reflect altered nucleation rates. After depletion of GIT1, nucleation rate decreased when compared to control cells; depletion of βPIX resulted in the increase of nucleation rate. Importance of PAK1 for MT nucleation was confirmed by inhibition its kinase activity with IPA-3. Inhibition of PAK1 activity resulted in decrease of nucleation. These data supported the results obtained by measuring of α-tubulin signal. Collectively taken, these data indicate that GIT1 and PAK1 represent positive and βPIX negative regulators of MT nucleation from the interphase centrosomes in U2OS.

As GIT1 and βPIX differently affect MT nucleation, we have evaluated the possibility that regulatory role of these proteins in MT nucleation is due to different accumulation of γ-tubulin at the centrosome. After depletion of GIT1 and PAK1, the amount of γ-tubulin decreased, while after depletion of βPIX, the amount of γ-tubulin increased. These data

suggest that the regulatory roles of GIT1, βPIX and PAK1 proteins in MT nucleation from centrosomes are conveyed by the amount of γ-tubulin nucleation complexes (γTuRCs) at centrosomes. We also evaluated whether centrosomal localization of GIT1 and βPIX in interphase cells is dependent on presence of γ-tubulin. Previously, it has been shown that carboxy-terminal domain (CTD) of NEDD1 does not localize to the centrosome, but over-expression of this domain causes a loss of γ-tubulin from the centrosome by keeping it in cytoplasm [254]. We have, therefore, evaluate the presence of GIT1, βPIX and activated PAK1 at centrosomes in cells expressing EGFP-tagged CTD of NEDD1 (EGFP-NEDD1[CTD]). Results from these experiments showed that GIT1, βPIX and PAK1 are γ-tubulin independent and resemble thus the other proteins of pericentriolar matrix.

Next we attempted to identify the regions on GIT1 and βPIX molecules responsible for interaction with γ-tubulin. In pull-down experiments with GIT1 and βPIX fragments we localized γ-tubulin binding region into GAP (aa1-124) domain on GIT1 and into C-terminal half of βPIX (outside PAK1 binding site). Interestingly, GAP domain targets GIT1 to centrosome [196]. Pull-down experiments with purified proteins revealed direct binding of γ-tubulin to PAK1 and GIT1. Finally, *in vitro* kinase assays showed that GIT1 and βPIX, but not γ-tubulin, serve as substrates for PAK1.

In conclusion, we propose that GIT1/βPIX signaling proteins with PAK1 kinase represent novel regulatory mechanism of MT nucleation in interphase cells.

In this project, I did immunoprecipitation and immunofluorescence experiments, prepared RFP-tagged human GIT1 and established U2Os cell lines stable expressing GIT1-tagRFP and βPIX-tagRFP. I performed bioinformatics study and I tested and selected siRNAs and shRNAs for depletion of all transcription variants of GIT1, βPIX and PAK1.

I performed nocodazole washout experiments and quantified MT nucleation. For this I developed the image processing software for semi-automatic quantification of fluorescence intensity in large amount of cells. I used this approach for quantification of α- and γ-tubulin signals in cell with depleted levels of GIT1, βPIX or PAK1m in phenotypic rescue experiments double knock downs and after inhibition of PAK1 by IPA-3. I established new method for quantification of MT nucleation rate in living U2Os cells expressing EB1 in nocodazole washout experiments. I participate in conceiving and designing experiments, formulation of hypothesis, and preparation of manuscript draft and images for publication.

III.4. ESTRADIOL DIMER BLOCKS MICROTUBULE POLYMERIZATION.

Jurášek, M., Džubák, P., Sedlák, D., **Černohorská, M.**, Darmostuk, M., Ruml, T., Sulimenko, T., Dráberová, E., Dráber, P., Hajdůch, M., Bartůněk, P. & Drašar, P. Estradiol Dimer Blocks Microtubule Polymerization. Submitted 2015

In this research paper we present biological profiling of newly synthetized steroidal compounds based on 3-*O*-methyl estradiol, testosterone and pregnenolone. The prepared dimers possess a mirrored conformation of monomers. For preparation of dimers denoted in this paper as **1**, **2**, **3**, **4** were used following compounds: 17α-ethynylestradiol for dimer **1**; compound 3-*O*-methyl 17α-ethynylestradiol for dimer **2**, and compound 17α-ethynyltestosterone for dimer **3**. 24-Norchol-5-en-22-yn-3β-ol was synthesized from pregnenolone for dimer **4**.

The main question was whether these types of molecular conjugates are able to modulate activity of different steroid receptors better than parental monomers. Steroid receptor reporter cell lines were used in assays for ERα, ERβ and AR. The dimers **1** and **2** exhibited reduced potency on ERα. Dimer **2** simultaneously improved the effect on ERβ. The dimers **3** and **4** completely abolished this ability to activate both ER and AR. These results are consistent with the fact that methoxyestranes cannot effectively activate ER receptors [238].

To find out whether dimers have anti-proliferative effects, we tested cytotoxicity of compounds across cancer cell lines of different histogenic origin, multi-drug resistance profile and p53 protein status. Estradiol dimers **1** and **2,** as well as testosterone dimer **3,** exhibited

a high cytotoxic activity in low concentrations. The highest effect was induced by dimer **1**. We have also found that dimerization was not able to provide steric barrier for molecule efflux outside the cell within MDR. Moreover, by comparison of cell lines expressing only P-gp or those with P-gp and MRP1, we have found that the efflux of dimers **1**, **2** and **3** is dependent on MRP1 protein. The effect of dimer **1** was not dependent also on intact p53.

Next lymphoblasts without MDR were treated by dimers **1, 2** and **3** at $1\times$ and $5\times IC_{50}$ concentrations. Both dimers **1** and **2** were cytotoxic at high concentration. Dimer **1** arrested cells in G2/M and dimer **2** in G0/G1 phase of the cell cycle. Although, the arrest in G0/G1 demonstrated possible inhibition of key proteins responsible for G1/S transition, the arrest in G2/M could be caused by the tubulin-binding and inability to form mitotic spindle [255].

To shed more light on the mechanism of G2/M arrest, we performed *in vitro* tubulin assembly in the presence of dimer **1** and **3**, their monomers as well as taxol and nocodazole. Turbidimetric measurements revealed that although monomers had basically no effect on tubulin assembly, estradiol dimer **1** caused effect similar to nocodazole. In the contrast, estradiol dimer **1** inhibited tubulin polymerization. However, it was less effective than nocodazole.

Immunofluorescence microscopy confirmed that estradiol dimer **1** at concentration 2.5 µM, which is lower than $1\times IC_{50}$, reversibly depolymerized microtubules (MTs) in U2Os similarly to nocodazole. Estradiol monomer was without any effect and 2-ME induced MT bundling.

Since the interference of dimer **1** with MTs both *in vitro* and *in vivo*, we hypothesize that dimer **1** interacts directly with tubulin rather than with MTs associated proteins. In order to predict how dimer **1** binds to tubulin, we modulated the structure of α/β-tubulin dimer and its potential binding sites. Molecular modelling indicated that the most probable binding site is in colchicine-binding region between α- and β-tubulin monomers.

As nocodazole in subcritical concentrations inhibits MT dynamics [256,257], we examined the possibility that estradiol dimer **1** in subcritical concentration also affects MT (+) ends. We quantified MT dynamics *in vivo* in U2Os cells stably expressing EB1-GFP. We have found that percentages of the fast growing MTs as well as MT dynamicity were substantially reduced in estradiol dimer **1** or nocodazole-treated cells. Estradiol dimer **1** thus represents first steroid compounds causing MT depolymerization and cell death.

My contribution to this work was quantification of MT (+) end dynamics in cells treated by various steroid compounds. For this I introduce the use of program PlusTipsTracker for automated tracking of EB1 comets in U2Os. I processed all time-lapse sequences, analyzed corresponding datasets and prepared movie for publication. I also tested long-term treatment with these compounds and their effects to MT network.

IV.   CONCLUSIONS

We developed a new method for quantification of MT (+) end dynamics in living cells. It is based on semi-automatic tracking of MT (+) ends marked by a +TIP EB1-GFP. To quantify MT nucleation, we developed method for semi-automatic measuring of α-tubulin and γ-tubulin fluorescence signals in high number of cells, and method for counting of newly nucleated microtubules in living cells. These methods were successfully used in the presented publications and are now routinely used in our laboratory.

We demonstrated that mammalian γ-tubulin 2 is able to nucleate MTs and substitute for γ-tubulin 1 in cultured cells. Further, we demonstrated that almost identical mammalian γ-tubulins can be reliably discriminated according to their electrophoretic properties by 2D-PAGE. We showed that unlike TUBG1, TUBG2 expression is downregulated in mouse preimplantation development, which results in very low amount of γ-tubulin 2 in blastocysts. Based on our results we propose that mammalian γ-tubulins are functionally equivalent with respect to their MT nucleation activity.

We identified βPIX and GIT1 as signaling proteins that interact with γ-tubulin and associate with centrosomes. GIT1 is phosphorylated on tyrosine in activated cells and interacts with γ-tubulin in a Ca^{2+}-dependent manner. Our data suggested a novel signaling pathway for microtubule rearrangement in mast cells, where tyrosine kinase-activated GIT1 and βPIX work in concert with Ca^{2+} signaling to regulate MT organization. Through this pathway Ag-induced signaling pathways leading to chemotaxis and degranulation could be regulated.

We found out that GIT1/βPIX signaling proteins together with PAK1 kinase regulate MT nucleation in different cell types. The GIT1 with PAK1 represent positive and βPIX negative regulators of this process. We also demonstrated that regulation is due to changes in γ-tubulin accumulation at centrosome. GIT1/βPIX signaling proteins are phosphorylated by PAK1 and directly interact with γ-tubulin. Binding site for γ-tubulin on GIT1 was located in its N-terminal domain that targets GIT1 to centrosome. We propose that GIT1/βPIX signaling proteins with PAK1 kinase represent novel regulatory mechanism of MT nucleation in interphase cells.

We demonstrated that from panel of newly prepared steroidal dimers, estradiol dimer exerted cytotoxicity and cells were arrested in G2/M phase of the cell cycle. Estradiol dimer inhibited tubulin polymerization *in vitro*, reversibly disrupted MTs in cells and affected (+) end microtubule dynamics at nanomolar concentrations. Estradiol dimer thus represents first steroid compound causing microtubule destabilization associated with cell death.

V. REFERENCES

1. Li, R & Gundersen, G. Beyond polymer polarity: how the cytoskeleton builds a polarized cell. *Nat Rev Mol Cell Biol* **9,** 860–873 (2008).

2. Salina, D, Bodoor, K, Eckley, DM, Schroer, TA, Rattner, JB & Burke, B. Cytoplasmic Dynein as a Facilitator of Nuclear Envelope Breakdown. *Cell* **108,** 97–107 (2002).

3. Luxton, GW & Gundersen, GG Orientation and function of the nuclear – centrosomal axis during cell migration. *Curr. Opin. Cell Biol.* **23,** 579–588 (2011).

4. De Pereda, JM & Andreu, JM. Mapping Surface Sequences of the Tubulin Dimer and Taxol-Induced Microtubules with Limited Proteolysis. *Biochemistry* **35,** 14184–14202 (1996).

5. Nogales, E, Whittaker, M, Milligan, RA & Downing, KH. High-Resolution Model of the Microtubule. *Cell* **96,** 79–88 (1999).

6. Mitchinson T & Kirschner, M. Dynamic instability of microtubule growth. *Nature* **312,** 237–242 (1984).

7. Mitchinson T & Kirschner, M. Microtubule assembly nucleated by isolated centrosomes. *Nature* **312,** 232–237 (1984).

8. Walker RA, O'Brien ET, Pryer NK, Soboeiro MF, Voter WA, Erickson HP & Salmon, E. Dynamic instability of individual microtubules analyzed by video light microscopy: rate constants and transition frequencies. *J. Cell Biol.* **107,** 1437–1448 (1988).

9. Hyman AA, Salser S, Drechse, DN, Unwin N & Mitchison, T. Role of GTP hydrolysis in microtubule dynamics: information from a slowly hydrolyzable analogue, GMPCPP. *Mol. Biol. Cell* **23,** 3775–3775 (2012).

10. Mandelkow, E, Mandelkow, E & Milligan, RA. Microtubule dynamics and microtubule caps: a time-resolved cryo- electron microscopy study. *J. Cell Biol.* **114,** 977–991 (1991).

11. Wang, HW & Nogales, E. Nucleotide-dependent bending flexibility of tubulin regulates microtubule assembly. *Nature* **435,** 911–915 (2005).

12. Howard, J. & Hyman, A. A. Growth, fluctuation and switching at microtubule plus ends. *Nat. Rev. Mol. Cell Biol.* **10,** 569–574 (2009).

13. Desai, A & Mitchison, T. Microtubule polymerization dynamics. *Annu. rev cell dev biol* **13,** 83–117 (1997).

14. Howard, J & Hyman, AA. Dynamics and mechanics of the microtubule plus end. *Nature* **422,** 753–758 (2003).

15. Akhmanova A & Steinmetz, M. Tracking the ends: a dynamic protein network controls the fate of microtubule tips. *Nat Rev Mol Cell Biol* **9,** 309–322 (2008).

16. Downing, KH. Structural basis for the interaction of tubulin with proteins and drugs that affect microtubule dynamics. *Annu Rev Cell Dev Biol* **16,** 89–111 (2000).

17. Gardner, MK, Charlebois, BD, Jánosi, IM, Howard, J, Hunt, AJ & Odde, DJ. Rapid microtubule self-assembly kinetics. *Cell* **146,** 582–592 (2011).

18. Dehmelt L, Halpain S, Faire K, Waterman-Storer CM, Gruber D, Masson D, Salmon ED, Bulinski JC, Halpain S & Dehmelt, L. E-MAP-115 (ensconsin) associates dynamically with microtubules in vivo and is not a physiological modulator of microtubule dynamics. *Genome Biol.* **112,** 224 (2005).

19. Halpain, S & Dehmelt, L. The MAP1 family of microtubule-associated proteins. *Genome Biol.* **7,** 224 (2006).

20. Faire K, Waterman-Storer CM, Gruber D, Masson D, Salmon ED & Bulinski, J. E-MAP-115 (ensconsin) associates dynamically with microtubules in vivo and is not a physiological modulator of microtubule dynamics. *J Cell Sci.* **112,** 4243–4255 (1999).

21. Bosc C, Andrieux A & Job, D. STOP proteins. *Biochemistry* **42,** 12125–12132 (2003).

22. Amos, L. The tektin family of microtubule-stabilizing proteins. *Genome Biol.* **9,** 229 (2008).

23. Roll-Mecak, A & McNally, F. Microtubule-severing enzymes. *Curr. Opin. Cell Biol.* **22,** 96–103 (2010).

24. Stiess, M & Bradke, F. Neuronal polarization: the cytoskeleton leads the way. *Dev Neurobiol* **71,** 430–444 (2011).

25. Lacroix, B, van Dijk, J, Gold, ND, Guizetti, J, Aldrian-Herrada, G, Rogowski, K, Gerlich, DW & Janke, C. Tubulin polyglutamylation stimulates spastin-mediated microtubule severing. *J Cell Biol* **189,** 945–954 (2010).

26. Connell, JW, Lindon, C, Luzio, JP & Reid, E. Spastin couples microtubule severing to membrane traffic in completion of cytokinesis and secretion. *Traffic* **10,** 42–56 (2009).

27. Schiel, JA, Park, K, Morphew, MK, Reid, E, Hoenger, A & Prekeris, R. Endocytic membrane fusion and buckling-induced microtubule severing mediate cell abscission. *J Cell Sci.* **124,** 1411–1424 (2011).

28. Ringhoff, DN & Cassimeris, L. Stathmin regulates centrosomal nucleation of microtubules and tubulin dimer/polymer partitioning. *Methods Cell Biol.* **20,** 3451–3458 (2009).

29. Moritz, M, Braunfeld, M, Sedat, J, Alberts, B & Agard, D. Microtubule nucleation by g-tubulin-containing rings in the centrosome. *Nature* **378,** 638–640 (1995).

30. Fuller, SD, Gowen, BE, Reinsch, S, Sawyer, A, Buendia, B, Wepf, R & Karsenti, E. The core of the mammalian centriole contains gamma-tubulin. *Curr. Biol.* **5,** 1384–1393 (1995).

31. Galjart, N. Plus-end-tracking proteins and their interactions at microtubule ends. *Curr. Biol.* **20,** R528–537 (2010).

32. Guichard, P, Chrétien, D, Marco, S & Tassin, A. Procentriole assembly revealed by cryo-electron tomography. *EMBO J.* **29,** 1565–1572 (2010).

33. Widlund, PO, Stear, JH, Pozniakovsky, A, Zanic, M, Reber, S, Brouhard, GJ, Hyman, AA & Howard, J. XMAP215 polymerase activity is built by combining multiple tubulin-binding TOG domains and a basic lattice-binding region. *Proc. Natl. Acad. Sci.* **108,** 2741–2746 (2011).

34. Uehara, R, Nozawa, RS, Tomioka, A, Petry, S, Vale, RD, Obuse, C & Goshima, G. The augmin complex plays a critical role in spindle microtubule generation for mitotic progression and cytokinesis in human cells. *PNAS* **106,** 6998–7003 (2009).

35. Uehara, R & Goshima, G. Functional central spindle assembly requires de novo microtubule generation in the interchromosomal region during anaphase. *J Cell Biol* **191,** 259–267 (2010).

36. Vaughan, K. TIP maker and TIP marker; EB1 as a master controller of microtubule plus ends. *J Cell Biol* **171,** 197–200 (2005).

37. Komarova, Y. *et al.* Mammalian end binding proteins control persistent microtubule growth. *J Cell Biol* **184,** 691–706 (2009).

38. Olmsted, J.B., Borisy, G. G. Ionic and nucleotide requirements for microtubule polymerization in vitro. *Biochemistry* **14,** 2996–3005 (1975).

39. Wiese, C & Zheng, Y. Microtubule nucleation: gamma-tubulin and beyond. *J Cell Sci.* **119,** 4143–4153 (2006).

40. Bartolini, F & Gundersen, G. Generation of noncentrosomal microtubule arrays. *J Cell Sci.* **119,** 4155–4163 (2006).

41. Eddé, B. *et al.* Posttranslational glutamylation of alpha-tubulin. *Science* **247,** 83–85 (1990).

42. Kitagawa, D. *et al.* Structural basis of the 9-fold symmetry of centrioles. *Cell* **144,** 364–375 (2011).

43. Li, S, Fernandez, JJ, Marshall, WF & Agard, D. Three-dimensional structure of basal body triplet revealed by electron cryo-tomography. *EMBO J.* **31,** 552–562 (2012).

44. Guichard, P, Hachet, V, Majubu, N, Neves, A, Demurtas, D, *et al.* Native architecture of the centriole proximal region reveals features underlying its 9-fold radial symmetry. *Curr. Biol.* **23,** 1620–1628 (2013).

45. Vorobjev, IA & Chentsov, Y. Centrioles in the cell cycle. I. Epithelial cells. *J. Cell Biol.* **93,** 938–942 (1982).

46. Paintrand, M, Moudjou, M., Delacroix, H. & Bornens, M. Centrosome organization and centriole architecture: Their sensitivity to divalent cations. *J. Struct. Biol.* **108,** 107–128 (1992).

47. Piel, M, Meyer, P, Khodjakov, A, Rieder, CL & Bornens, M. The respective contributions of the mother and daughter centrioles to centrosome activity and behavior in vertebrate cells. *J. Cell Biol.* **149,** 317–329 (2000).

48. Moritz, M, Braunfeld, M. B, Guénebaut, V, Heuser, J & Agard, D. Structure of the gamma-tubulin ring complex: a template for microtubule nucleation. *Nat. Cell Biol.* **2,** 365–370 (2000).

49. Winey, M & O'Toole, E. Centriole structure. *Phil. Trans. R. Soc. B* **369,** 20130457 (2014).

50. Marshall, W. F., Vucica, Y. & Rosenbaum, J. L. Kinetics and regulation of de novo centriole assembly: Implications for the mechanism of centriole duplication. *Curr. Biol.* **11,** 308–317 (2001).

51. Song, MH, Miliaras, NB, Peel, N & O'Connell, K. F. Centrioles: some self-assembly required. *Curr. Opin. Cell Biol.* **20,** 688–693 (2008).

52. Nigg, E. Centrosome duplication: of rules and licenses. *Trends Cell Biol.* **17,** 215–221 (2007).

53. Barrera, JA *et al.* CDK5RAP2 regulates centriole engagement and cohesion in mice. *Dev. Cell* **18,** 913–926 (2010).

54. Tsou, MB & Stearns, T. Mechanism limiting centrosome duplication to once per cell cycle. *Nature* **422,** 947–951 (2006).

55. Sluder, G, Miller, FJ & Rieder, CL The reproduction of centrosomes: Nuclear versus cytoplasmic controls. *J. Cell Biol.* **103,** 1873–1881 (1986).

56. Nigg EA & Stearns, T. The centrosome cycle: Centriole biogenesis, duplication and inherent asymmetries. *Nat. Cell Biol.* **13,** 1154–1140 (2011).

57. Faragher, AJ & Fry, AM. Nek2A kinase stimulates centrosome disjunction and is required for formation of bipolar mitotic spindles. *Mol Biol Cell* **14,** 2876–2889 (2003).

58. Zyss, D & Gergely, F. Centrosome function in cancer: guilty or innocent? *Trends Cell Biol.* **19,** 334–346 (2009).

59. Lüders, J & Stearns, T. Microtubule-organizing centres: a re-evaluation. *Nat. Rev. Mol. Cell Biol.* **8,** 161–167 (2007).

60. Lawo, S, Hasegan, M, Gupta, GD & Pelletier, L. Subdiffraction imaging of centrosomes reveals higher-order organizational features of pericentriolar material. *Nat. Cell Biol.* **14,** 1148–1158 (2012).

61. Sonnen, KF, Schermelleh, L, Leonhardt, H & Nigg, E. 3D-structured illumination microscopy provides novel insight into architecture of human centrosomes. *Biol. Open* **1,** 965–976 (2012).

62. Mennella, V. *et al.* Subdiffraction-resolution fluorescence microscopy reveals a domain of the centrosome critical for pericentriolar material organization. *Nat. Cell Biol.* **14,** 1159–1168 (2012).

63. Fu, P & Glover, DM. Structured illumination of the interface between centriole and peri-centriolar material. *Open Biol.* **2,** 120104–120104 (2012).

64. Vogel, JM, Stearns, T, Rieder, CL & Palazzo, RE. Centrosomes Isolated from. *Cell* **137,** 193–202 (1997).

65. Schnackenberg, B, Khodjakov, A, Rieder, C & Palazzo, R. The disassembly and reassembly of functional centrosomes in vitro. *Proc. Natl. Acad. Sci.* **95,** 9295–9300 (1998).

66. Petry, S, Groen, AC, Ishihara, K, Mitchison, TJ & Vale, RD. Branching microtubule nucleation in xenopus egg extracts mediated by augmin and TPX2. *Cell* **152,** 768–777 (2013).

67. Oakley, CE & Oakley, B. Identification of gamma-tubulin, a new member of the tubulin superfamily encoded by mipA gene of Aspergillus nidulans. *Nature* **338,** 662–664 (1989).

68. Oakley BR, Oakley, CE Yoon, Y & Jung, JM. Gamma-tubulin is a component of the spindle pole body that is essential for microtubule function in Aspergillus nidulans. *Nature* **61,** 1289–1301 (1990).

69. Stearns, T, Evans, L & Kirschner, M. Gamma-tubulin is a highly conserved component of the centrosome. *Cell* **65,** 825–836 (1991).

70. Horio, T & Oakley, B. Human gamma-tubulin functions in fission yeast. *J. Cell Biol.* **126,** 1465–1473 (1994).

71. Oakley, BR. γ-Tubulin: the microtubule organizer? *Trends Cell Biol.* **2,** 1–5 (1992).

72. Spangm A, Geisslerm S, Greinm, K & Schiebel, E. gamma-Tubulin-like Tub4p of Saccharomyces cerevisiae is associated with the spindle pole body substructures that organize microtubules and is required for mitotic spindle formation. *J. Cell Biol.* **134,** 429–441 (1996).

73. Yuba-Kubo, A, Kubo, A, Hata, M & Tsukita, S. Gene knockout analysis of two y-tubulin isoforms in mice. *Dev. Biol.* **282,** 361–373 (2005).

74. Wise, DO, Krahe, R & Oakley, BR. The gamma-tubulin gene family in humans. *Genomics* **67,** 164–170 (2000).

75. Carson, AR & Scherer, SW. Identifying concerted evolution and gene conversion in mammalian gene pairs lasting over 100 million years. *BMC Evol. Biol.* **9,** 156 (2009).

76. Liu, B. *et al.* y-Tubulin in Arabidopsis: Gene Sequence, Immunoblot, and lmmunofluorescence Studies. *Plant Cell* **6,** 303–314 (1994).

77. Lopez, I, Khan, S, Sevik, M, Cande, WZ & Hussey, P. Isolation of a full-length cDNA encoding Zea mays gamma-tubulin. *Plant physiol* **107,** 309–310 (1995).

78. Ruiz, F, Beisson, J, Rossier, J & Dupuis-Williams, P. Basal body duplication in Paramecium requires γ-tubulin. *Curr. Biol.* **9,** 43–46 (1999).

79. Wilson, PG *et al.* Differential expression of two gamma-tubulin isoforms during gametogenesis and development in Drosophila. *Dev. Biol.* **184,** 207–221 (1997).

80. Moudjou, M, Bordes, N, Paintrand, M & Bornens, M. gamma-Tubulin in mammalian cells: the centrosomal and the cytosolic forms. *J Cell Sci.* **109,** 875–887 (1996).

81. Zheng, Y, Wong, ML, Alberts, B & Mitchinson, T. Nucleation of mikrotubule assembly by a g-tubulin-containing ring complex. *Nature* **378,** 578–583 (1995).

82. Moritz, M, Braunfeld, MB, Fung, JC, Sedat, JW, Alberts, BM & Agard, DA. Microtubule nucleation by gamma-tubulin-containing rings in the centrosome. *J. Cell Biol.* **130,** 1149–1159 (1995).

83. Efimov, A, Kharitonov, A, Efimova, N, Loncarek, J & Miller, PM, *et al.* Asymmetric CLASP-dependent nucleation of noncentrosomal microtubules at the trans-Golgi network. *Dev Cell* **12,** 917–930 (2007).

84. Goshima, G, Mayer, M, Zhang, N, Stuurman, N & Vale, R. Augmin: a protein complex required for centrosome-independent microtubule generation within the spindle. *J Cell Biol* **181,** 421–429 (2008).

85. Hughes, SE, Beeler, JS, Seat, A, Slaughter, BD, Unruh, JR, Bauerly, E, Matthies, HJ & Hawley, R. Gamma-tubulin is required for bipolar spindle assembly and for proper kinetochore microtubule attachments during prometaphase I in Drosophila oocytes. *PLoS Genet.* **7,** e1002209 (2011).

86. Carazo-Salas, RE, Guarguaglini, G, Gruss, OJ, Segref, A, Karsenti, E & Mattaj, I. Generation of GTP-bound Ran by RCC1 is required for chromatin-induced mitotic spindle formation. *Nature* **400,** 178–181 (1999).

87. Maiato, H & Sunkel, CE. Kinetochore-microtubule interaction during cell division. *Chromosom. Res* **12,** 585–597 (2004).

88. Mishra, RK, Chakraborty, P, Arnaoutov, A, Fontoura, BM & Dasso, M. The Nup107-160 complex and gamma-TuRC regulate microtubule polymerization at kinetochores. *Nat. Cell Biol.* **12,** 164–169 (2010).

89. Bouissou, A. *et al.* γ-Tubulin ring complexes regulate microtubule plus end dynamics. *J. Cell Biol.* **187,** 327–334 (2009).

90. Hubert, T, Vandekerckhove, J & Gettemans, J. Cdk1 and BRCA1 target γ-tubulin to microtubule domains. *Biochem Biophys Res Commun* **414,** 240–245 (2011).

91. Binarová, P, Cenklová, V, Hause, B, Kubátová, E, Lysák, M, Dolezel, J, Bögre, L & Dráber, P. Nuclear gamma-tubulin during acentriolar plant mitosis. *Plant Cell* **12,** 433–442 (2000).

92. Höög, G, Zarrizi, R, von Stedingk, K, Jonsson, K & Alvarado-Kristensson, M. Nuclear localization of γ-tubulin affects E2F transcriptional activity and S-phase progression. *FASEB J.* **25,** 3815–3827 (2011).

93. Hořejší, B, Vinopal, S, Sládková, V, Dráberová, E, Sulimenko, V, Sulimenko, T, Vosecká, V, Philimonenko, A, Hozák, P, Katsetos, CD & Dráber, P. Nuclear γ-tubulin associates with nucleoli and interacts with tumor suppressor protein C53. *J Cell Physiol* **227,** 367–382 (2012).

94. Zheng, Y, Alberts, B & Mitchinson, T. Purification and assay of gamma tubulin ring complex. *Methods Enzym.* **298,** 218–228 (1998).

95. Murphy, SM, Preble, AM, Patel, UK, O'Connell, KL, Dias, DP, Moritz, M, Agard, D, Stults, JT & Stearns, T. GCP5 and GCP6: two new members of the human gamma-tubulin complex. *Mol Biol Cell* **12,** 3340–3352 (2001).

96. Kollman, JM, Polka, JK, Zelter, A, Davis, TN & Agard, DA. Microtubule nucleating gamma-TuSC assembles structures with 13-fold microtubule-like symmetry. *Nature* **466,** 879–882 (2010).

97. Kollman, JM, Zelter, A, Muller, EG, Fox, B, Rice, LM, Davis, TN & Agard, D. The structure of the gamma-tubulin small complex: implications of its architecture and flexibility for microtubule nucleation. *Mol Biol Cell* **19,** 207–215 (2008).

98. Oegema, K. *et al.* Characterization of two related Drosophila y-tubulin complexes that differ in their ability to nucleate microtubules. *J. Cell Biol.* **144,** 721–733 (1999).

99. Kollman, JM, Merdes, A, Mourey, L & Agard, DA. Microtubule nucleation by γ-tubulin complexes. *Nat. Rev. Mol. Cell Biol.* **12,** 709–721 (2011).

100. Guillet, V. *et al.* Crystal structure of γ-tubulin complex protein GCP4 provides insight into microtubule nucleation. *Nat. Struct. Mol. Biol.* **18,** 915–919 (2011).

101. Suri, C, Hendrickson, TW, Joshi, HC, Naik, P. Molecular insight into γ-γ tubulin lateral interactions within the γ-tubulin ring complex (γ-TuRC). *J Comput Aided Mol Des* **28,** 961–972 (2014).

102. Höög, JL. *et al.* Organization of Interphase Microtubules in Fission Yeast Analyzed by Electron Tomography. *Dev. Cell* **12,** 349–361 (2007).

103. O'Toole, ET. *et al.* Morphologically distinct microtubule ends in the mitotic centrosome of Caenorhabditis elegans. *J. Cell Biol.* **163,** 451–456 (2003).

104. Teixidó-Travesa, N, Roig, J & Lüders, J. The where, when and how of microtubule nucleation - one ring to rule them all. *J Cell Sci.* **125,** 4445–4456 (2012).

105. Schnackenberg, BJ & Palazzo, R. Reconstitution of centrosome microtubule nucleation in Spisula. *methods cell biol* **67,** 149–165 (2001).

106. Fant, X, Gnadt, N, Haren, L & Merdes, A. Stability of the small gamma-tubulin complex requires HCA66, a protein of the centrosome and the nucleolus. *J. Cell Sci.* **122,** 1134–1144 (2009).

107. Vérollet, C. *et al.* Drosophila melanogaster γ-TuRC is dispensable for targeting γ-tubulin to the centrosome and microtubule nucleation. *J. Cell Biol.* **172,** 517–528 (2006).

108. Xiong, Y & Oakley, BR. In vivo analysis of the functions of gamma-tubulin-complex proteins. *J. Cell Sci.* **122,** 4218–4227 (2009).

109. Masuda, H, Mori, R, Yukawa, M & Toda, T. Fission yeast MOZART1/Mzt1 is an essential γ-tubulin complex component required for complex recruitment to the microtubule organizing center, but not its assembly. *Mol Biol Cell* **24,** 2894–2906 (2013).

110. Haren, L. *et al.* NEDD1-dependent recruitment of the γ-tubulin ring complex to the centrosome is necessary for centriole duplication and spindle assembly. *J. Cell Biol.* **172,** 505–515 (2006).

111. Lüders, J, Patel, U & Stearns, T. GCP-WD is a gamma-tubulin targeting factor required for centrosomal and chromatin-mediated microtubule nucleation. *Nat. Cell Biol.* **8,** 137–147 (2006).

112. Hutchins, JR. a *et al.* Systematic Analysis of Human Protein. **593,** 593–600 (2013).

113. Teixidó-Travesa, N, Villén, J, Lacasa, C, Bertran, MT, Archinti, M, Gygi, SP, Caelles, C, Roig J & Lüders J. The gammaTuRC revisited: a comparative analysis of interphase and mitotic human gammaTuRC redefines the set of core components and identifies the novel subunit GCP8. *Mol Biol Cell* **21,** 3963–3972 (2010).

114. Dhani, DK, Goult, BT, George, GM, Rogerson, DT, Bitton, DA, Miller, CJ, Schwabe, JW & Tanaka, K. Mzt1/Tam4, a fission yeast MOZART1 homologue, is an essential component of the γ-tubulin complex and directly interacts with GCP3(Alp6). *Mol Biol Cell* **24,** 3337–3349 (2013).

115. Rusan, NM & Rogers, GC. Centrosome function: Sometimes less is more. *Traffic* **10,** 472–481 (2009).

116. Gruss, OJ & Vernos, I. The mechanism of spindle assembly: Functions of Ran and its target TPX2. *J. Cell Biol.* **166,** 949–955 (2004).

117. Casenghi, M, Meraldi, P, Weinhart, U, Duncan, PI, Körner, R & Nigg, E. Polo-like kinase 1 regulates Nlp, a centrosome protein involved in microtubule nucleation. *Dev Cell* **5,** 113–125 (2003).

118. Li, Q, Hansen, D, Killilea, A, Joshi, HC, Palazzo, RE & Balczon, R. Kendrin/pericentrin-B, a centrosome protein with homology to pericentrin that complexes with PCM-1. *J Cell Sci.* **114,** 797–809 (2001).

119. Purohit, A, Tynan, SH, Valle, R & Doxsey, S. J. Direct interaction of pericentrin with cytoplasmic dynein light intermediate chain contributes to mitotic spindle organization. *J. Cell Biol.* **147,** 481–491 (1999).

120. Balczon, R, Bao, L & Zimmer, W. PCM-1, A 228-kD centrosome autoantigen with a distinct cell cycle distribution. *J Cell Biol* **124,** 783–793 (1994).

121. Takahashi, M, Yamagiwa, A, Nishimura, T, Mukai, H & Ono, Y. Centrosomal proteins CG-NAP and kendrin provide microtubule nucleation sites by anchoring gamma-tubulin ring complex. *Mol Biol Cell* **13,** 3235–3245 (2002).

122. Gillingham, K & Munro, S. The PACT domain, a conserved centrosomal targeting motif in the coiled-coil proteins AKAP450 and pericentrin. *EMBO Rep.* **1,** 524–529 (2000).

123. Takahashi, M. *et al.* Characterization of a novel giant scaffolding protein, CG-NAP, that anchors multiple signaling enzymes to centrosome and the Golgi apparatus. *J. Biol. Chem.* **274,** 17267–17274 (1999).

124. Takahashi, M, Mukai, H, Oishi, K, Isagawa, T & Ono, Y. Association of immature hypophosphorylated protein kinase Ce an Anchoring protein CG-NAP. *J. Biol. Chem.* **275,** 34592–34596 (2000).

125. Diviani, D, Langeberg, LK, Doxsey, SJ & Scott, J. D. Pericentrin anchors protein kinase A at the centrosome through a newly identified RII-binding domain. *Curr. Biol.* **10,** 417–420 (2000).

126. Sillibourne, JE, Milne, DM, Takahashi, M, Ono, Y & Meek, D. W. Centrosomal anchoring of the protein kinase CK1d mediated by attachment to the large, coiled-coil scaffolding protein CG-NAP/AKAP450. *J. Mol. Biol.* **322,** 785–797 (2002).

127. Masuda, H, Miyamoto, R, Haraguchi, T & Hiraoka, Y. The carboxy-terminus of Alp4 alters microtubule dynamics to induce oscillatory nuclear movement led by the spindle pole body in Schizosaccharomyces pombe. *Genes to Cells* **11,** 337–352 (2006).

128. Lin, TC. *et al.* Phosphorylation of the yeast y-tubulin tub4 regulates microtubule function. *PLoS One* **6,** (2011).

129. Alvarado-Kristensson, M, Rodríguez, MJ, Silió, V, Valpuesta, JM. & Carrera, AC. SADB phosphorylation of gamma-tubulin regulates centrosome duplication. *Nat. Cell Biol.* **11,** 1081–1092 (2009).

130. Santamaria, A. *et al.* The Plk1-dependent phosphoproteome of the early mitotic spindle. *Mol. Cell. Proteomics* **10,** M110.004457 (2011).

131. Stumpff, J, Kellogg, DR, Krohne, KA & Tin, TS. Drosophila Wee1 interacts with members of the yTURC and is required for proper mitotic-spindle morphogenesis and positioning. *Curr. Biol.* **15,** 1525–1534 (2005).

132. Vogel, J. *et al.* Phosphorylation of gamma-tubulin regulates microtubule organization in budding yeast. *Dev. Cell* **1,** 621–631 (2001).

133. Macurek, L. *et al.* Regulation of microtubule nucleation from membranes by complexes of membrane-bound gamma-tubulin with Fyn kinase and phosphoinositide 3-kinase. *Biochem. J.* **416,** 421–430 (2008).

134. Dráberová, L, Dráberová, E, Surviladze, Z, Dráber, P & Dráber, P. Protein tyrosine kinase p53/p56(lyn) forms complexes with gamma-tubulin in rat basophilic leukemia cells. *Int. Immunol.* **11,** 1829–1839 (1999).

135. Zyss, D. *et al.* The Syk tyrosine kinase localizes to the centrosomes and negatively affects mitotic progression. *Cancer Res.* **65,** 10872–10880 (2005).

136. Sulimenko, V. *et al.* Regulation of microtubule formation in activated mast cells by complexes of gamma-tubulin with Fyn and Syk kinases. *J. Immunol.* **176,** 7243–7253 (2006).

137. Ley, SC, Marsh, M, Bebbington, CR, Proudfoot, K & Jordan, P. Distinct intracellular localization of Lck and Fyn protein tyrosine kinases in human T lymphocytes. *J Cell Biol* **125,** 639–649 (1994).

138. Faruki, S, Geahlen, RL, Asai, D. Syk-dependent phosphorylation of microtubules in activated B-lymphocytes. *J Cell Sci.* **113,** 2557–2565 (2000).

139. Fargier, G, Favard, C, Parmeggiani, A, Sahuquet, A, Mérezègue, F, Morel, A, Denis, M, Molinari, N, Mangeat, PH, Coopman, PJ & Montcourrier, P. Centrosomal targeting of Syk kinase is controlled by its catalytic activity and depends on microtubules and the dynein motor. *FASEB J.* **27,** 109–122 (2013).

140. Colello, D. *et al.* Androgen and Src signaling regulate centrosome activity. *J. Cell Sci.* **123,** 2094–2102 (2010).

141. Colello, D, Mathew, S, Ward, R, Pumiglia, K & LaFlamme, S. E. Integrins regulate microtubule nucleating activity of centrosome through mitogen-activated protein kinase/extracellular signal-regulated kinase kinase/extracellular signal-regulated kinase (MEK/ERK) signaling. *J. Biol. Chem.* **287,** 2520–2530 (2012).

142. Keck JM, Jones MH, Wong CC, Binkley J, Chen D, Jaspersen SL, Holinger EP, Xu T, Niepel M, Rout MP, Vogel J, Sidow A, Yates JR 3rd, Winey, M. A cell cycle phosphoproteome of the yeast centrosome. *Science (80-.).* **332,** 1557–1561 (2011).

143. Kukharskyy, V, Sulimenko, V, Macůrek, L, Sulimenko, T, Dráberová, E & Dráber, P. Complexes of gamma-tubulin with nonreceptor protein tyrosine kinases Src and Fyn in differentiating P19 embryonal carcinoma cells. *Exp Cell Res* **298,** 218–228 (2004).

144. Chan, CC, Shui, HA, Wu, CH, Wang, CY, Sun, GH, Chen, HM & Wu, G. Motility and protein phosphorylation in healthy and asthenozoospermic sperm. *J Proteome Res* **8,** 5382–5386 (2009).

145. Starita, LM. *et al.* BRCA1-Dependent Ubiquitination of γ-Tubulin Regulates Centrosome Number. **24,** 8457–8466 (2004).

146. Izumi, N, Fumoto, K, Izumi, S & Kikuchi, A. GSK-3β regulates proper mitotic spindle formation in cooperation with a component of the γ-tubulin ring complex, GCP5. *J. Biol. Chem.* **283,** 12981–12991 (2008).

147. Johmura, Y. *et al.* Regulation of microtubule-based microtubule nucleation by mammalian polo-like kinase 1. *Proc. Natl. Acad. Sci.* **108,** 11446–11451 (2011).

148. Zhang, X. *et al.* Sequential phosphorylation of Nedd1 by Cdk1 and Plk1 is required for targeting of the gammaTuRC to the centrosome. *J. Cell Sci.* **122,** 2240–2251 (2009).

149. Premont, RT, Claing, A, Vitale, N, Freeman, JL, Pitcher, JA, Patton, WA, Moss, J, Vaughan, M & Lefkowitz, R. beta2-Adrenergic receptor regulation by GIT1, a G protein-coupled receptor kinase-associated ADP ribosylation factor GTPase-activating protein. *PNAS1* **95,** 14082–14087 (1998).

150. Turner CE, Brown MC, Perrotta JA, Riedy MC, Nikolopoulos SN, McDonald AR, Bagrodia S, Thomas S, Leventhal, P. Paxillin LD4 motif binds PAK and PIX through a novel 95-kD ankyrin repeat, ARF-GAP protein: A role in cytoskeletal remodeling. *J Cell Biol* **145,** 851–863 (1999).

151. Zhao ZS, Manser E, Loo TH, Lim, L. Coupling of PAK-interacting exchange factor PIX to GIT1 promotes focal complex disassembly. *Mol Biol Cell* **20,** 6354–6363 (2000).

152. Schlenker O, Rittinger, K. Structures of dimeric GIT1 and trimeric beta-PIX and implications for GIT-PIX complex assembly. *J Mol Biol* **386,** 280–289 (2009).

153. Yin G, Haendeler J, Yan C, Berk, B. GIT1 functions as a scaffold for MEK1-extracellular signal-regulated kinase 1 and 2 activation by angiotensin II and epidermal growth factor. *Mol Biol Cell* **24,** 875–885 (2004).

154. Di Cesare A, Paris S, Albertinazzi C, Dariozzi S, Andersen J, Mann M, Longhi R, de Curtis, I. p95-APP1 links membrane transport to Rac-mediated reorganization of actin. *Nat Cell Biol* **2,** 521–530 (2000).

155. Manabe R, Kovalenko M, Webb DJ, Horwitz, A. GIT1 functions in a motile, multi-molecular signaling complex that regulates protrusive activity and cell migration. *J Cell Sci.* **115,** 1497–1510 (2002).

156. Paris S, Longhi R, Santambrogio P, de Curtis, I. Leucine-zipper-mediated homo- and hetero-dimerization of GIT family p95-ARF GTPase-activating protein, PIX-, paxillin-interacting proteins 1 and 2. *Biochem J* **372,** 391–398 (2003).

157. Bagrodia, S. *et al.* A tyrosine-phosphorylated protein that binds to an important regulatory region on the cool family of p21-activated kinase-binding proteins. *J. Biol. Chem.* **274,** 22393–22400 (1999).

158. Webb DJ, Kovalenko M, Whitmore L, Horwitz, A. Phosphorylation of serine 709 in GIT1 regulates protrusive activity in cells. *Biochem Biophys Res Commun* **346,** 1284–1288 (2006).

159. Haendeler J, Yin G, Hojo Y, Saito Y, Melaragno M, Yan C, Sharma VK, Heller M, Aebersold R, Berk, B. GIT1 mediates Src-dependent activation of phospholipase Cgamma by angiotensin II and epidermal growth factor. *J Biol Chem* **278,** 49936–49944 (2003).

160. Totaro, A, Astro, V, Tonoli, D & De Curtis, I. Identification of two tyrosine residues required for the intramolecular mechanism implicated in GIT1 activation. *PLoS One* **9,** 1–12 (2014).

161. Frank SR, Hansen, S. The PIX-GIT complex: a G protein signaling cassette in control of cell shape. *Semin Cell Dev Biol.* **19,** 234–244 (2008).

162. Bagrodia, S, Taylor, S J., Jordon, KA, Aelst, L Van & Cerione, RA. A Novel Regulator of p21-activated Kinases. 23633–23636 (1998).

163. Manser, E. *et al.* PAK kinases are directly coupled to the PIX family of nucleotide exchange factors. *Mol. Cell* **1,** 183–192 (1998).

164. Koh, CG, Manser, E, Zhao, ZS, Ng, CP & Lim, L. Beta1PIX, the PAK-interacting exchange factor, requires localization via a coiled-coil region to promote microvillus-like structures and membrane ruffles. *J. Cell Sci.* **114,** 4239–4251 (2001).

165. Aspenström, P. The Rho GTPases have multiple effects on the actin cytoskeleton. *Exp. Cell Res.* **246,** 20–25 (1999).

166. Fiorentini, C, Falzano, L, Travaglione, S. & Fabbri, A. Hijacking Rho GTPases by protein toxins and apoptosis: molecular strategies of pathogenic bacteria. *Cell Death Differ.* **10,** 147–152 (2003).

167. Yao, L, Kawakami, Y & Kawakami, T. The pleckstrin homology domain of Bruton tyrosine kinase interacts with protein kinase C. *Proc. Natl. Acad. Sci. U. S. A.* **91,** 9175–9179 (1994).

168. Zhao, ZS, Manser, E, Loo, TH & Lim, L. Coupling of PAK-interacting exchange factor PIX to GIT1 promotes focal complex disassembly. *Mol. Cell. Biol.* **20,** 6354–6363 (2000).

169. Chahdi, A, Miller, B & Sorokin, A. Endothelin 1 induces beta1Pix translocation and Cdc42 activation via protein kinase A-dependent pathway. *J. Biol. Chem.* **280,** 578–584 (2005).

170. Park, E. *et al.* The Shank family of postsynaptic density proteins interacts with and promotes synaptic accumulation of the βPIX guanine nucleotide exchange factor for Rac1 and Cdc42. *J. Biol. Chem.* **278,** 19220–19229 (2003).

171. Feng, Q, Albeck, JG, Cerione, RA. & Yang, W. Regulation of the Cool/Pix proteins. Key binding partners of the Cdc42/Rac targets, the p21-activated kinases. *J. Biol. Chem.* **277,** 5644–5650 (2002).

172. Flanders, J. A. *et al.* The Cbl proteins are binding partners for the Cool/Pix family of p21-activated kinase-binding proteins. *FEBS Lett.* **550,** 119–123 (2003).

173. Ten Klooster, JP, Jaffer, ZM, Chernoff, J & Hordijk, P. L. Targeting and activation of Rac1 are mediated by the exchange factor bPix. *J. Cell Biol.* **172,** 759–769 (2006).

174. Koh, CG, Tan, EJ, Manser, E & Lim, L. The p21-activated kinase PAK is negatively regulated by POPX1 and POPX2, a pair of serine/threonine phosphatases of the PP2C family. *Curr. Biol.* **12,** 317–321 (2002).

175. Bagrodia, S, De, B, Davis, RJ & Cerione, RA. Signaling Leads to Jun Kinase Protein Kinase Activation. *Biochemistry* 27995–27998 (1995).

176. Lei, M. *et al.* Structure of PAK1 in an autoinhibited conformation reveals a multistage activation switch. *Cell* **102,** 387–397 (2000).

177. King, CC. *et al.* p21-activated kinase (PAK1) is phosphorylated and activated by 3-phosphoinositide-dependent kinase-1 (PDK1). *J. Biol. Chem.* **275,** 41201–41209 (2000).

178. Zenke, FT, King, CC, Bohl, BP & Bokoch, GM. Identification of a central phosphorylation site in p21-activated kinase regulating autoinhibition and kinase activity. *J. Biol. Chem.* **274,** 32565–32573 (1999).

179. Bokoch, GM. *et al.* Interaction of the Nck adapter protein with p21-activated kinase (PAK1). *J. Biol. Chem.* **271,** 25746–25749 (1996).

180. Puto, LA, Pestonjamasp, K, King, CC & Bokoch, GM. p21-activated kinase 1 (PAK1) interacts with the Grb2 adapter protein to couple to growth factor signaling. *J. Biol. Chem.* **278,** 9388–9393 (2003).

181. Wu, C, Leeuw, T, Leberer, E, Thomas, DY & Whiteway, M. Cell cycle- and Cln2p-Cdc28p-dependent phosphorylation of the yeast Ste20p protein kinase. *J. Biol. Chem.* **273,** 28107–28115 (1998).

182. Gatti, A, Huang, Z, Tuazon, PT & Traugh, JA. Multisite autophosphorylation of p21-activated protein kinase a-PAK as a function of activation. *J. Biol. Chem.* **274,** 8022–8028 (1999).

183. Chong, C, Tan, L, Lim, L & Manser, E. The mechanism of PAK activation. Autophosphorylation events in both regulatory and kinase domains control activity. *J. Biol. Chem.* **276,** 17347–17353 (2001).

184. Li, Z. Y. *et al.* Genomic structure of the human beta-PIX gene and its alteration in gastric cancer. *Cancer Lett.* **177,** 203–208 (2002).

185. Cotteret, S. & Chernoff, J. Pak GITs to Aurora-A. *Dev. Cell* **9,** 573–574 (2005).

186. Banerjee, M, Worth, D, Prowse, DM. & Nikolic, M. Pak1 phosphorylation on T212 affects microtubules in cells undergoing mitosis. *Curr. Biol.* **12,** 1233–1239 (2002).

187. Daub, H, Gevaert, K, Vandekerckhove, J, Sobel, A. & Hall, A. Rac/Cdc42 and p65PAK regulate the microtubule-destabilizing protein stathmin through phosphorylation at serine 16. *J. Biol. Chem.* **276,** 1677–1680 (2001).

188. Mayhew, M. W. *et al.* Identification of phosphorylation sites in betaPIX and PAK1. *J. Cell Sci.* **120,** 3911–3918 (2007).

189. Premont, RT. *et al.* The GIT/PIX complex: An oligomeric assembly of GIT family ARF GTPase-activating proteins and PIX family Rac1/Cdc42 guanine nucleotide exchange factors. *Cell. Signal.* **16,** 1001–1011 (2004).

190. Manabe, R, Kovalenko, M, Webb, DJ & Horwitz, AR. GIT1 functions in a motile, multi-molecular signaling complex that regulates protrusive activity and cell migration. *J. Cell Sci.* **115,** 1497–1510 (2002).

191. Saneyoshi T, Wayman G, Fortin D, Davare M, Hoshi N, Nozaki N, Natsume T, Soderling, T. Activity-dependent synaptogenesis: regulation by a CaM-kinase kinase/CaM-kinase I/betaPIX signaling complex. *Neuron* **57,** 94–107 (2008).

192. Webb, DJ, Kovalenko, M, Whitmore, L & Horwitz, AF. Phosphorylation of serine 709 in GIT1 regulates protrusive activity in cells. *Biochem. Biophys. Res. Commun.* **346,** 1284–1288 (2006).

193. Feng, Q, Baird, D, Yoo, S, Antonyak, M & Cerione, RA. Phosphorylation of the cool-1/b-pix protein serves as a regulatory signal for the migration and invasive activity of Src-transformed cells. *J. Biol. Chem.* **285,** 18806–18816 (2010).

194. Manser, E. *et al.* Expression of constitutively active alpha-PAK reveals effects of the kinase on actin and focal complexes. *Mol. Cell. Biol.* **17,** 1129–1143 (1997).

195. Manser E, Lim, L. Roles of PAK family kinases. *Prog Mol Subcell Biol* **22,** 115–133 (1999).

196. Zhao, Z, Lim, JP, Ng, YW, Lim, L & Manser, E. The GIT-Associated Kinase PAK Targets to the Centrosome and Regulates Aurora-A. *Mol. Cell* **20,** 237–249 (2005).

197. Dutertre, S, Descamps, S. & Prigent, C. On the role of aurora-A in centrosome function. *Oncogene* **21,** 6175–6183 (2002).

198. Giet, R. & Prigent, C. The non-catalytic domain of the Xenopus laevis auroraA kinase localises the protein to the centrosome. *J. Cell Sci.* **114,** 2095–2104 (2001).

199. Gilfillan, AM. & Rivera, J. The tyrosine kinase network regulating mast cell activation. *Immunol. Rev.* **228,** 149–169 (2009).

200. Kalesnikoff, J & Galli, S. New developments in mast cell biology. *Nat Immunol* **9,** 1215–1223 (2008).

201. Kawakami, T & Galli, S. Regulation of mast-cell and basophil function and survival by IgE. *Nat Rev Immunol* **2,** 773–786 (2002).

202. Bugajev, V, Bambousková, M, Dráberová, L & Dráber, P. What precedes the initial tyrosine phosphorylation of the high affinity IgE receptor in antigen-activated mast cell? *FEBS Lett.* **584,** 4949–4955 (2010).

203. Rosado, JA & Sage, S. Phosphoinositides are required for store-mediated calcium entry in human platelets. *J Biol Chem* **275,** 9110–9113 (2000).

204. Vaca, L. SOCIC: The store-operated calcium influx complex. *Cell Calcium* **47,** 199–209 (2010).

205. Petersen, OH, Tepikin, A & Park, M. The endoplasmic reticulum: one continuous or several separate Ca(2+) stores? *Trends Neurosci* **24,** 271–276 (2001).

206. Rizzuto, R & Pozzan, T. Microdomains of Intracellular Ca 2 ℰ: Molecular Determinants and Functional Consequences. *Physiol. Rev.* **86,** 369–408 (2006).

207. Venkatachalam, K & Montell, C. TRP channels. *Annu. Rev. Biochem.* **76,** 387–417 (2007).

208. Chin, D & Means, A. R. Calmodulin: A prototypical calcium sensor. *Trends Cell Biol.* **10,** 322–328 (2000).

209. Dai G, Qian Y, Chen J, Meng FL, Pan FY, Shen WG, Zhang SZ, Xue B, L. C. Calmodulin activation of polo-like kinase 1 is required during mitotic entry. *Biochem cell biol* **91,** 287–294 (2013).

210. Zhang, SL. *et al.* STIM1 is a Ca2+ sensor that activates CRAC channels and migrates from the Ca2+ store to the plasma membrane. *Nature* **437,** 902–905 (2005).

211. Smith, A. J. *et al.* Microtubule-dependent transport of secretory vesicles in RBL-2H3 cells. *Traffic* **4,** 302–312 (2003).

212. Atkinson, TP & Lee, C. Orthovanadate Induces Translocation of Phospholipase C-γ'll and. **151,** 1448–1455 (1993).

213. Ali, H, Maeyama, K, Sagi-Eisenberg, R & Beaven, M. Antigen and thapsigargin promote influx of Ca2+ in rat basophilic RBL-2H3 cells by ostensibly similar mechanisms that allow filling of inositol 1,4,5-trisphosphate-sensitive and mitochondrial Ca2+ stores. *Biochem J* **304,** 431–440 (1994).

214. Morgan, AJ. & Jacob, R. Ionomycin enhances Ca2+ influx by stimulating store-regulated cation entry and not by a direct action at the plasma membrane. *Biochem. J.* **300 (Pt 3,** 665–672 (1994).

215. Hájková, Z. *et al.* STIM1-directed reorganization of microtubules in activated mast cells. *J. Immunol.* **186,** 913–923 (2011).

216. Cruse, G. *et al.* A Truncated Splice-Variant of the FcεRIβ Receptor Subunit Is Critical for Microtubule Formation and Degranulation in Mast Cells. *Immunity* **38,** 906–917 (2013).

217. Hartmann, K, Henz, BM, Krüger-Krasagakes, S, Köhl, J, Burger, R, Guhl, S, Haase, I, Lippert, U, Zuberbier, T. C3a and C5a stimulate chemotaxis of human mast cells. *Blood* **89,** 2863–2870 (1997).

218. Jordan, M. A. & Wilson, L. MIicrotubules as a Target for Anticancer Drugs. **4,** 253–265 (2004).

219. Dumontet, C, J. M. Microtubule-binding agents: a dynamic field of cancer therapeutics. *nat rev drug discov* **9,** 790–803 (2010).

220. Derry, WB, Wilson, L & Jordan. MA. Substoichiometric binding of taxol suppresses microtubule dynamics. *Biochemistry* **34,** 2203–2211 (1995).

221. Dhamodharan, R, Jordan, MA, Thrower, D, Wilson, L & Wadsworth. P. Vinblastine suppresses dynamics of individual microtubules in living interphase cells. *Mol Biol Cell* **6,** 1215–1229 (1995).

222. Liao, G, Nagasaki, T & Gundersen, GG. Low concentrations of nocodazole interfere with fibroblast locomotion without significantly affecting microtubule level : implications for the role of dynamic microtubules in cell locomotion. **3483,** 3473–3483 (1995).

223. Jordan, MA. Microtubles and actin filaments: dynamic targets for cancer chemotherapy. *Curr. Opin. Cell Bio.* **10,** 123–130 (1998).

224. Buey, RM. *et al.* Emerging Microtubule Targets in Glioma Therapy. *J. Cell Biol.* **22,** 94–101 (2011).

225. Kavallaris, M. Microtubules and resistance to tubulin-binding agents. *Nat. Rev. Cancer* **10,** 194–204 (2010).

226. Jordan MA, KK. How do microtubule-targeted drugs work? An overview. *Curr Cancer Drug Targets* **7,** 730–742 (2007).

227. Di Pietro, A, Dayan, G, Conseil, G, Steinfels, E, Krell, T, Trompier, D, Baubichon-Cortay, H & Jault, J. P-glycoprotein-mediated resistance to chemotherapy in cancer cells: using recombinant cytosolic domains to establish structure-function relationships. *Braz J Med Biol Res.* **32,** 925–939 (1999).

228. Katsetos, CD, Reginato, MJ, Baas, PW, D'Agostino, L, Legido, A, Tuszynski, JA, Dráberová, E & Dráber, P. Emerging microtubule targets in glioma therapy. *Semin Pediatr Neurol.* **22,** 49–72 (2015).

229. Dhamodharan, R. & Wadsworth, P. Modulation of microtubule dynamic instability in vivo by brain microtubule associated proteins. *J. Cell Sci.* **108,** 1679–1689 (1995).

230. Landen, JW, Lang, R, McMahon, SJ, Rusan, NM, Yvon, AM, Adams, AW, Sorcinelli, MD, Campbell, R, Bonaccorsi, P, Ansel, JC, Archer, DR, Wadsworth, P, Armstrong CA, Joshi. HC. Noscapine alters microtubule dynamics in living cells and inhibits the progression of melanoma. *Cancer Res.* **62,** 4109–4114 (2002).

231. Fournier, D & Poirier, D. Estradiol dimers as a new class of steroid sulfatase reversible inhibitors. *Bioorg Med Chem Lett.* **19,** 693–696 (2009).

232. Bastien, D, Leblanc, V, Asselin, E & Bérubé, G. First synthesis of separable isomeric testosterone dimers showing differential activities on prostate cancer cells. *Bioorg Med Chem Lett.* **20,** 2078–2081 (2010).

233. Liu S, Tam D, Chen X & Pang, K. P-glycoprotein and an unstirred water layer barring digoxin absorption in the vascularly perfused rat small intestine preparation: induction studies with pregnenolone-16alpha-carbonitrile. *Drug Metab Dispos.* **34,** 1468–1479 (2006).

234. Tapiero H, Ba GN & Tew, K. Estrogens and environmental estrogens. *Biomed Pharmacother* **56,** 34–44 (2002).

235. Bonkhoff, H & Berges, R. The evolving role of oestrogens and their receptors in the development and progression of prostate cancer. *Eur Urol* **55,** 533–542 (2009).

236. Dalal K, Roshan-Moniri M, Sharma A, Li H, Ban F, Hassona MD, Hsing M, Singh K, LeBlanc E, Dehm S, Tomlinson Guns ES, Cherkasov A & Rennie, P. Selectively targeting the DNA-binding domain of the androgen receptor as a prospective therapy for prostate cancer. *J Biol Chem.* **289,** 26417–26429 (2014).

237. Seegers JC, Aveling ML, Van Aswegen CH, Cross M, Koch F & Joubert, W. The cytotoxic effects of estradiol-17 beta, catecholestradiols and methoxyestradiols on dividing MCF-7 and HeLa cells. *J Steroid Biochem.* **32,** 797–809 (1989).

238. Merriam, GR, MacLusky, NJ, Johnson, LA & Naftolin, F. 2-hydroxyestradiol-17 alpha and 4-hydroxyestradiol-17 alpha, catechol estrogen analogs with reduced estrogen receptor affinity. *Steroids* **36,** 13–20 (1980).

239. D'Amato, RJ, Lin, CM, Flynn, E, Folkman, J & Hamel, E. 2-Methoxyestradiol, an endogenous mammalian metabolite, inhibits tubulin polymerization by interacting at the colchicine site. *Proc. Natl. Acad. Sci.* **91,** 3964–3968 (1994).

240. Salama, SA. *et al.* Catechol-O-methyltransferase expression and 2-methoxyestradiol affect microtubule dynamics and modify steroid receptor signaling in leiomyoma cells. *PLoS One* **4,** 1–8 (2009).

241. Prota AE, Bargsten K, Diaz JF, Marsh M, Cuevas C, Liniger M, Neuhaus C, Andreu JM, Altmann KH & Steinmetz, M. A new tubulin-binding site and pharmacophore for microtubule-destabilizing anticancer drugs. *Proc. Natl. Acad. Sci. U. S. A.* **111,** 13817–13821 (2014).

242. Tinley, TL. *et al.* Novel 2-Methoxyestradiol Analogues with Antitumor Activity Novel 2-Methoxyestradiol Analogues with Antitumor Activity 1. *Cancer Res.* **63,** 1538–1549 (2003).

243. Cushman M, He HM, Katzenellenbogen JA, Lin CM & Hamel, E. Synthesis, antitubulin and antimitotic activity, and cytotoxicity of analogs of 2-methoxyestradiol, an endogenous mammalian metabolite of estradiol that inhibits tubulin polymerization by binding to the colchicine binding site. *J Med Chem* **38,** 2041–2049 (1995).

244. MacCarthy-Morrogh, L, Townsend, PA, Purohit, A, Hejaz, HAM, Potter, BVL, Reed, MJ & Packham, G. Differential effects of estrone and estrone-3-O-sulfamate derivatives on mitotic. Arrest, apoptosis, and microtubule assembly in human breast cancer cells. *Cancer Res.* **60,** 5441–5450 (2000).

245. Janke, C & Chloë Bulinski, J. Post-translational regulation of the microtubule cytoskeleton: mechanisms and functions. *Nat. Rev. Mol. Cell Biol.* **12,** 773–786 (2011).

246. DeLuna A, Springer M, Kirschner MW & Kishony, R. Need-based up-regulation of protein levels in response to deletion of their duplicate genes. *Plos Biol* **8,** e1000347 (2010).

247. He, X & Zhang, J. Transcriptional reprogramming and backup between duplicate genes: is it a genomewide phenomenon? *Genetics* **172,** 1363–1367 (2006).

248. Kukharskyy, V. *et al.* Complexes of γ-tubulin with nonreceptor protein tyrosine kinases Src and Fyn in differentiating P19 embryonal carcinoma cells. *Exp. Cell Res.* **298,** 218–228 (2004).

249. Webb, D. J. *et al.* Identification of phosphorylation sites in GIT1. *J. Cell Sci.* **119,** 2847–2850 (2006).

250. Ganguly, A, Yang, H, Sharma, R, Patel, KD & Cabral, F. The role of microtubules and their dynamics in cell migration. *J. Biol. Chem.* **287,** 43359–43369 (2012).

251. Sulimenko, V. *et al.* Microtubule Nucleation in Mouse Bone Marrow-Derived Mast Cells Is Regulated by the Concerted Action of GIT1/ PIX Proteins and Calcium. *J. Immunol.* (2015).

252. Piehl, M, Tulu, US, Wadsworth, P & Cassimeris, L. Centrosome maturation: measurement of microtubule nucleation throughout the cell cycle by using GFP-tagged EB1. *Proc. Natl. Acad. Sci. U. S. A.* **101,** 1584–1588 (2004).

253. Vinopal, S. *et al.* γ-Tubulin 2 Nucleates Microtubules and Is Downregulated in Mouse Early Embryogenesis. *PLoS One* **7,** (2012).

254. Manning, JA, Shalini, S, Risk, JM, Day, CL & Kumar, S. A direct interaction with NEDD1 regulates gamma-tubulin recruitment to the centrosome. *PLoS One* **5,** e9618 (2010).

255. Lanni, JS & Jacks, T. Characterization of the p53-dependent postmitotic checkpoint following spindle disruption. *Mol Biol Cell* **18,** 1055–1064 (1998).

256. Vasquez, RJ, Howell, B, Yvon, AM, Wadsworth, P & Cassimeris. L. Nanomolar concentrations of nocodazole alter microtubule dynamic instability in vivo and in vitro. *Mol Biol Cell* **8,** 973–985 (1997).

257. Mikhailov, A. & Gundersen, GG. Relationship between microtubule dynamics and lamellipodium formation revealed by direct imaging of microtubules in cells treated with nocodazole or taxol. *Cell Motil. Cytoskeleton* **41,** 325–340 (1998).

VI. PRESENTED PUBLICATIONS

VI.1.

Vinopal S., <u>Černohorská M.</u>, Sulimenko V., Sulimenko T., Vosecká V., Flemr M., Dráberová E. & Dráber, P. γ-Tubulin 2 nucleates microtubules and is downregulated in mouse early embryogenesis. *PloS One*, 7: e29919, 2012

PLoS one

γ-Tubulin 2 Nucleates Microtubules and Is Downregulated in Mouse Early Embryogenesis

Stanislav Vinopal[1], Markéta Černohorská[1], Vadym Sulimenko[1], Tetyana Sulimenko[1], Věra Vosecká[1], Matyáš Flemr[2], Eduarda Dráberová[1], Pavel Dráber[1]*

1 Department of Biology of Cytoskeleton, Institute of Molecular Genetics, Academy of Sciences of the Czech Republic, Prague, Czech Republic, 2 Department of Epigenetic Regulations, Institute of Molecular Genetics, Academy of Sciences of the Czech Republic, Prague, Czech Republic

Abstract

γ-Tubulin is the key protein for microtubule nucleation. Duplication of the γ-tubulin gene occurred several times during evolution, and in mammals γ-tubulin genes encode proteins which share ~97% sequence identity. Previous analysis of *Tubg1* and *Tubg2* knock-out mice has suggested that γ-tubulins are not functionally equivalent. *Tubg1* knock-out mice died at the blastocyst stage, whereas *Tubg2* knock-out mice developed normally and were fertile. It was proposed that γ-tubulin 1 represents ubiquitous γ-tubulin, while γ-tubulin 2 may have some specific functions and cannot substitute for γ-tubulin 1 deficiency in blastocysts. The molecular basis of the suggested functional difference between γ-tubulins remains unknown. Here we show that exogenous γ-tubulin 2 is targeted to centrosomes and interacts with γ-tubulin complex proteins 2 and 4. Depletion of γ-tubulin 1 by RNAi in U2OS cells causes impaired microtubule nucleation and metaphase arrest. Wild-type phenotype in γ-tubulin 1-depleted cells is restored by expression of exogenous mouse or human γ-tubulin 2. Further, we show at both mRNA and protein levels using RT-qPCR and 2D-PAGE, respectively, that in contrast to *Tubg1*, the *Tubg2* expression is dramatically reduced in mouse blastocysts. This indicates that γ-tubulin 2 cannot rescue γ-tubulin 1 deficiency in knock-out blastocysts, owing to its very low amount. The combined data suggest that γ-tubulin 2 is able to nucleate microtubules and substitute for γ-tubulin 1. We propose that mammalian γ-tubulins are functionally redundant with respect to the nucleation activity.

Introduction

γ-Tubulin is a highly conserved member of the tubulin superfamily essential for microtubule nucleation in all eukaryotes [1–3]. It assembles together with other proteins, named Gamma-tubulin Complex Proteins (GCPs) in human, into two main γ-Tubulin Complexes (γTuCs): the γ-Tubulin Small Complex (γTuSC) and the γ-Tubulin Ring Complex (γTuRC). The γTuSC, a vital component of microtubule nucleation machinery in all eukaryotes, is composed of two molecules of γ-tubulin and one copy each of GCP2 and GCP3. The γTuRCs are found only in metazoa and consist of seven γTuSCs and additional GCPs, including GCP4-6 [4,5]. The γTuRC is a ring structure with an arrangement of γ-tubulin molecules that matches the 13-fold symmetry of a microtubule. It serves as a template for microtubule polymerization [6]. It has recently been shown that the budding yeast γTuSCs alone form *in vitro* ring structures similar to γTuRCs [7]; it supports the general template model of microtubule nucleation [6].

γTuCs are concentrated at Microtubule Organizing Centers (MTOCs) such as centrosomes and basal bodies in animals or spindle pole bodies in fungi. They are also found on nuclear membranes in acentrosomal plants and on Golgi membranes,

condensed mitotic chromosomes, midbodies and along microtubules in mitotic spindles [8]. We have recently reported nucleolar localization of γ-tubulin [9]. However, the majority of γTuCs exist in cytoplasm in soluble form [10]. In addition to its function in microtubule nucleation, γ-tubulin is also involved in centriole biogenesis [11,12], regulation of microtubule (+) end dynamics [13–15], regulation of the anaphase-promoting complex/cyclosome during interphase in *Aspergillus* [16] or regulation of bipolar spindle assembly in fission yeast [17].

Many organisms including *Arabidopsis* [18], *Paramecium* [19], *Euplotes* [20], *Drosophila* [21] and mammals [22–24] possess two genes encoding γ-tubulin. Nevertheless, phylogenetic analyses revealed that γ-tubulin gene duplication in mammals occurred independent of the others [23,24]. Mammalian γ-tubulin genes are located on the same chromosome in tandem, and their coding sequences share very high sequence similarity (>94% in human)[22]. Although it was initially assumed that γ-tubulin genes are functionally redundant [22], gene knock-out analysis of *Tubg1* and *Tubg2* in mice suggested that they might have different functions [23]. While *Tubg1* was expressed ubiquitously, *Tubg2* was primarily detected in brain and also in blastocysts. *Tubg1*^{-/-} embryos stopped their development at the morula/blastocyst stage because of severe mitotic defects. *Tubg2*^{-/-} mice developed
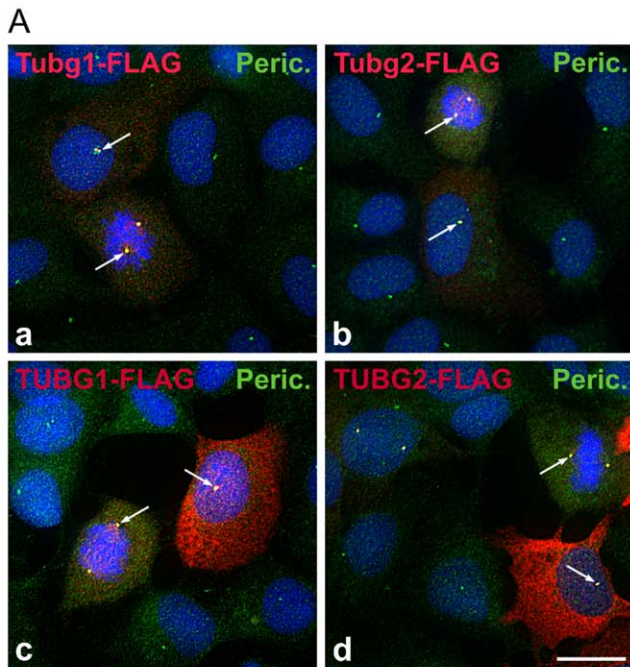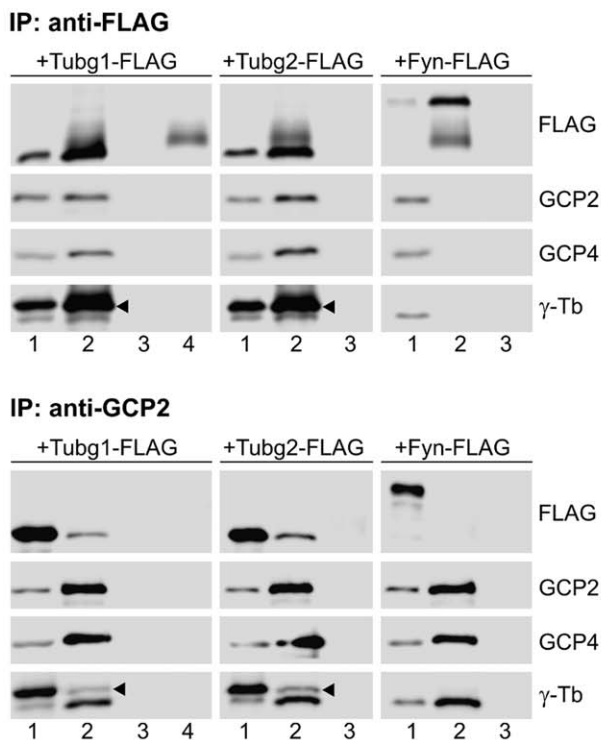
Figure 1. Exogenous γ-tubulin 2 locates to centrosomes and interacts with GCPs. (A) Localization of FLAG-tagged γ-tubulins. Human U2OS cells expressing mouse γ-tubulin 1 (a, Tubg1-FLAG), mouse γ-tubulin 2 (b, Tubg2-FLAG), human γ-tubulin 1 (c, TUBG1-FLAG) and human γ-tubulin 2 (d, TUBG2-FLAG) were stained for FLAG (red) and pericentrin (green). DNA was stained with DAPI (blue). Arrows denote positions of MTOCs where FLAG-tagged γ-tubulins co-localize with pericentrin. Final images were made by maximum intensity projection of 3 deconvolved z-sections spaced at 0.25 μm. Scale bar 10 μm. (B) Coimmunoprecipitation of mouse γ-tubulins with GCP2 and GCP4 proteins. Extracts from HEK cells expressing FLAG-tagged γ-

tubulin 1 (Tubg1-FLAG), γ-tubulin 2 (Tubg2-FLAG) or control mouse Fyn (Fyn-FLAG) were immunoprecipitated with antibodies to FLAG or GCP2, and blots were probed with antibodies to FLAG, GCP2, GCP4 and γ-tubulin (γ-Tb). Extracts (1), immunoprecipitated proteins (2), protein A without antibodies incubated with extracts (3), immobilized antibodies not incubated with extracts (4). Arrowheads indicate the positions of exogenous γ-tubulins.
doi:10.1371/journal.pone.0029919.g001

normally and produced fertile offspring. However, adults exhibited some behavioral changes including abnormalities in circadian rhythm and different reaction to painful stimulations. These findings led to a conclusion that γ-tubulin 1 is the conventional γ-tubulin, whereas γ-tubulin 2, which lacks the capability to rescue the consequences of γ-tubulin 1 deficiency, might have specific function(s) in the brain [23]. Nevertheless, the molecular basis of suggested functional differences between γ-tubulin 1 and γ-tubulin 2 is unknown.

To gain a deeper insight into the potential functional differences of mammalian γ-tubulins, we have examined subcellular distribution of γ-tubulin 2 in cultured cells, its interactions with GCPs, capability to nucleate microtubules and substitute for γ-tubulin 1. We have also analyzed γ-tubulin 2 expression in the course of mouse preimplantation development. Our results indicate that even though γ-tubulins are differentially expressed during mouse early embryogenesis and in adult tissues, they are functionally redundant with respect to their nucleation activity.

Results

γ-Tubulin 2 is indistinguishable from γ-tubulin 1 in subcellular localization and interactions with GCPs

To decide whether or not γ-tubulin 2 differs from γ-tubulin 1 in subcellular localization, we examined U2OS cells expressing FLAG-tagged mouse or human γ-tubulin 2 (Tubg2-FLAG, TUBG2-FLAG) by immunofluorescence microscopy with anti-FLAG antibody. Centrosomes were marked with antibody to pericentrin. U2OS cells expressing FLAG-tagged mouse and human γ-tubulin 1 (Tubg1-FLAG, TUBG1-FLAG) served as controls. As expected, exogenous mouse (Fig. 1A, a) and human (Fig. 1A, c) γ-tubulin 1 localized to the centrosomes in both interphase and mitotic cells. FLAG-tagged γ-tubulin 1 was also found along mitotic spindle and diffusely in cytoplasm. The same staining pattern was detected in cells expressing exogenous mouse (Fig. 1A, b) and human (Fig. 1A, d) γ-tubulin 2. Fully displayed immunofluorescence of Fig. 1A appears in Fig. S1.

Next we checked by coimmunoprecipitation the ability of γ-tubulin 2 to interact with GCP2 (γTuSC marker) and GCP4 (γTuRC marker). FLAG-tagged mouse γ-tubulin 1, γ-tubulin 2 or Fyn kinase (negative control) were immunoprecipitated from HEK 293FT cells with rabbit anti-FLAG antibody. Immunoblot analysis revealed that both FLAG-tagged γ-tubulins interacted with GCP2 and GCP4, yet no coimmunoprecipitation was observed in case of FLAG-tagged Fyn kinase (Fig. 1B, upper panel). Negative control rabbit antibody failed to coimmunoprecipitate GCP proteins (not shown). In addition, the reciprocal precipitation with antibody to GCP2 (IgG2b), confirmed the interaction of FLAG-tagged γ-tubulins with GCP2 (Fig. 1B, lower panel). Again, negative control antibody (IgG2b) did not coimmunoprecipitate FLAG-tagged γ-tubulins (not shown). We obtained the same results when lysates from HEK 293FT cells expressing FLAG-tagged human γ-tubulin 1 and γ-tubulin 2 were used for immunoprecipitation with anti-FLAG and anti-GCP2 antibodies (Fig. S2). Altogether the data indicate that mammalian γ-tubulin 2 is indiscernible from γ-tubulin 1 as far as the subcellular distribution and interactions

with components of small and large γ-tubulin complexes are concerned.

γ-Tubulin 2 rescues mitotic progression in γ-tubulin 1-depleted cells

To find out whether or not γ-tubulin 2 is able to take the place of γ-tubulin 1, we performed phenotypic rescue experiments in U2OS cells depleted of γ-tubulin 1 by RNAi. As demonstrated by immunoblotting, transfection of TUBG1-specific siRNAs (KD1 and KD2) led to a substantial reduction of total γ-tubulin content when compared to negative control cells (Fig. S3A). Noticeably, it means that γ-tubulin 1 is the dominant γ-tubulin in U2OS cells, because the specificity of both KD1 and KD2 siRNAs was verified *in silico* (NCBI BLAST) and by means of RT-qPCR (data not shown). Since KD2 siRNA proved to be more efficient, it was used in further experiments. Effective γ-tubulin depletion by KD2 siRNA was further confirmed by immunofluorescence microscopy (Fig. 2A). The most prominent phenotypic feature of γ-tubulin 1 depletion was mitotic arrest in metaphase (Fig. 2B), most likely induced by severe mitotic spindle defects (Fig 2C). Basically, cells in anaphase, telophase or cytokinesis were absent in the population of γ-tubulin 1-depleted cells.

FLAG-tagged mouse γ-tubulin 1, used as a positive control, restored the original phenotype in γ-tubulin 1-depleted U2OS. Cells expressing exogenous γ-tubulin 1 were able to pass the spindle assembly checkpoint, as demonstrated by the presence of cells in anaphase, whereas the untrasfected cells were not (Fig. 3, a–d). Interestingly, FLAG-tagged mouse γ-tubulin 2 (Fig. 3, e–h) and FLAG-tagged human γ-tubulin 2 (Fig. 3, i–l) also rescued the normal mitotic division similarly to mouse γ-tubulin 1. Detailed microscopic examination of rescued cells revealed that they regained the ability to build properly arranged metaphase (Fig. S4, a–c) and anaphase (Fig. S4, d–f) mitotic spindles. Importantly, we failed to detect any mitotic spindle defects in the rescued cells.
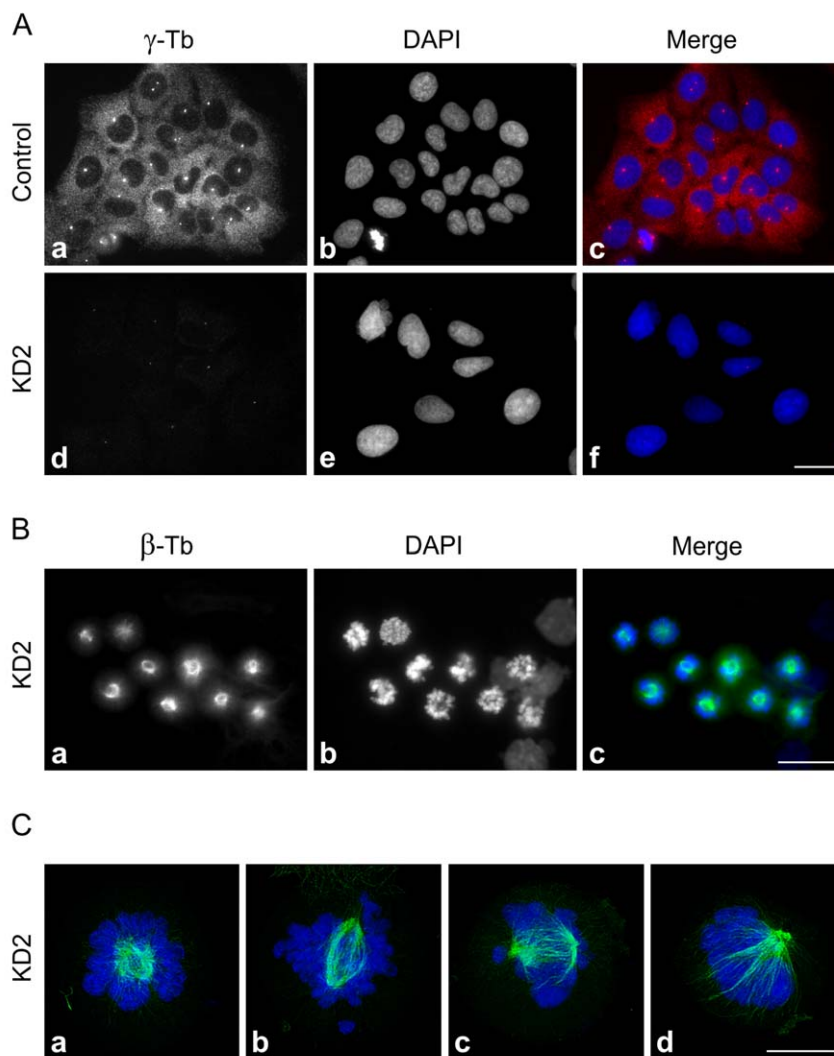
Figure 2. Depletion of human γ-tubulin 1 leads to mitotic spindle defects and metaphase arrest. (A) Interphase U2OS cells transfected with negative control siRNA (Control) or with γ-tubulin 1 specific siRNA (KD2). Cells were stained for γ-tubulin (a, d; red). DNA was stained with DAPI (b, e; blue). Images of cells stained for γ-tubulin were captured under identical conditions and processed in exactly the same way. Scale bar 20 μm. (B) Aberrant spindle formation and metaphase arrest in U2OS cells depleted of γ-tubulin 1 (KD2). Cells were stained for β-tubulin (a; green). DNA was stained with DAPI (b; blue). Scale bar 20 μm. (C) Detailed images of aberrant mitotic spindles. Cells were stained for β-tubulin (a–d; green). DNA was stained with DAPI (a–d; blue).Maximum intensity projections of 30–40 deconvolved confocal z-sections spaced at 0.125 μm. Scale bar 10 μm.
doi:10.1371/journal.pone.0029919.g002

Immunoblot tests in performed rescue experiments confirmed an effective expression of FLAG-tagged γ-tubulins in γ-tubulin 1-depleted cells (Fig. S3B). These findings suggest that γ-tubulin 2 is capable of replacing γ-tubulin 1 during mitosis.

γ-Tubulin 2 nucleates microtubules

Taking advantage of the above described phenotypic rescue experimental set-up, we further investigated the microtubule nucleating capability of γ-tubulin 2 in microtubule regrowth experiments. The amount of γ-tubulin on prophase/metaphase centrosomes is significantly higher than that in interphase due to the process called centrosome maturation [25,26]. We therefore first focused on mitotic centrosomes, where one could expect a prominent effect of γ-tubulin depletion on microtubule nucleation. Microtubules were depolymerized by nocodazole, washed by ice-cold PBS, and allowed to regrow before fixation and staining for β-tubulin. Mitotic cells became more abundant in the course of nocodazole treatment. While the regrowth of microtubules from centrosomes was easily observable in cells transfected with negative control siRNA (Fig. 4A, a–d), it was substantially delayed and/or impaired in γ-tubulin 1-depleted cells (Fig. 4A, e–h). Clearly recognizable microtubule asters were seen in 97% (n = 369) of negative control mitotic cells. In γ-tubulin 1-depleted cells, however, microtubule asters were indistinct and formed in only 18% (n = 274) of mitotic cells. As expected, FLAG-tagged mouse γ-tubulin 1 (positive control) rescued the microtubule aster formation in γ-tubulin 1-depleted cells (Fig. 4B, a–d). In accordance with our previous results, both FLAG-tagged mouse γ-tubulin 2 (Fig. 4B, e–h) and FLAG-tagged human γ-tubulin 2 (Fig. 4B, i–l) also rescued aster formation. Clear microtubule regrowth was observed in all γ-tubulin 1-depleted cells expressing exogenous γ-tubulin 2; it indicates that

γ-tubulin 2 is capable of centrosomal microtubule nucleation in mitotic cells.

In order to strengthen the evidence of microtubule nucleation capability of γ-tubulin 2, we quantified microtubule formation in vivo by the tracking microtubule (+) ends marked by EB1-GFP in interphase U2OS cells (U2OS-EB1). For live cell imaging we used the shRNA system based on pLKO.1 vectors. Puromycin selection for 6 days made it possible to analyze only γ-tubulin-depleted cells. We constructed TUBG1-specific shRNA expressing vectors based on siRNAs (KD1 and KD2), and tested their effectivity by immunoblotting (Fig S5A). Since KD2 shRNA was found more efficient, further experiments were limited to that. Substantial γ-tubulin depletion by KD2 shRNA was confirmed by immunofluorescence microscopy (Fig. S5B). Additionally, we prepared TagRFP-tagged mouse γ-tubulin 1 (pmTubg1-TagRFP) and TagRFP-tagged human γ-tubulin 2 (phTUBG2-TagRFP) for phenotypic rescue experiments. TagRFP (pCI-TagRFP) served as control.

Following puromycin selection, transfected U2OS-EB1 cells were subjected to live cell imaging; time-lapse sequences of EB1-GFP dynamics were acquired only from cells coexpressing TagRFP or TagRFP-tagged proteins. Immunoblotting confirmed an effective expression of tagged γ-tubulins in γ-tubulin 1-depleted cells (Fig. S6). Results of typical experiments are presented in Fig. 5, where single-frame (Fig. 5, a–d) as well as 60-frame projections (Fig. 5, e–h) of time-lapse sequences are shown. While TagRFP was found in both cytoplasm and nuclei (Fig 5, a–b), TagRFP-tagged γ-tubulins were concentrated to MTOC (Fig. 5, c–d). This is more distinctly demonstrated in Fig. S7, where green and red channels are depicted separately. The density of microtubule (+) end tracks, reconstructed by maximum intensity projection of time-lapse sequences, was markedly reduced in γ-
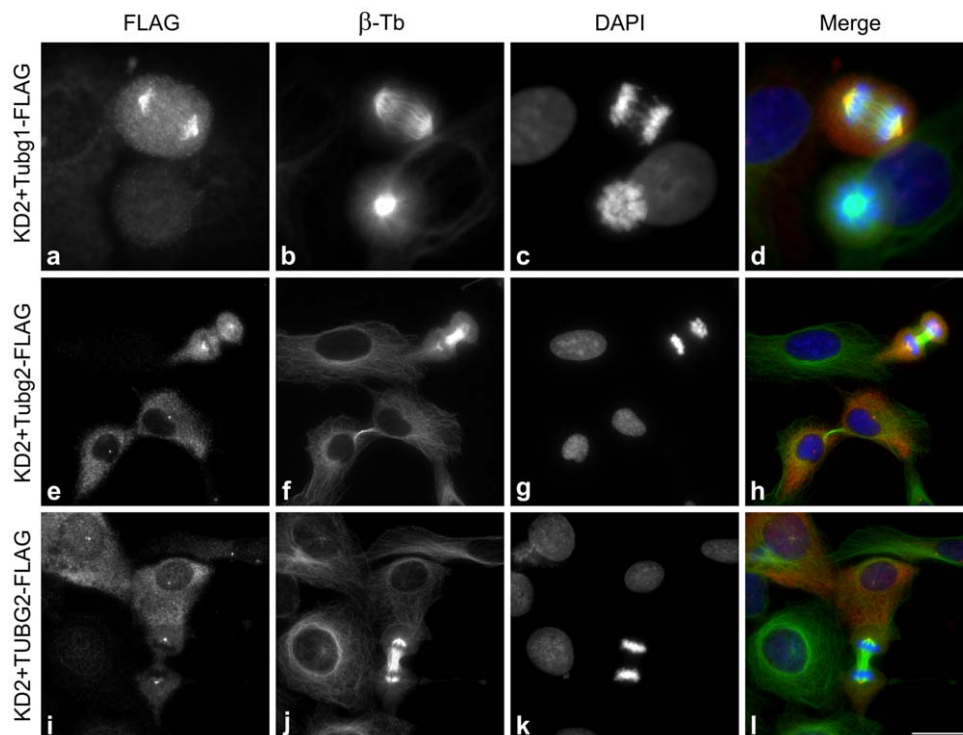
Figure 3. γ-Tubulin 2 restores normal mitotic spindle functioning in γ-tubulin 1-depleted cells. U2OS cells depleted of γ-tubulin 1 and expressing FLAG-tagged mouse γ-tubulin 1 (a-d, Tubg1-FLAG), mouse γ-tubulin 2 (e-h, Tubg2-FLAG) or human γ-tubulin 2 (i–l, TUBG2-FLAG) were stained for FLAG (a, e, i; red) and β-tubulin (b, f, j; green). DNA was stained with DAPI (c, g, k; blue). Scale bar 20 μm.
doi:10.1371/journal.pone.0029919.g003
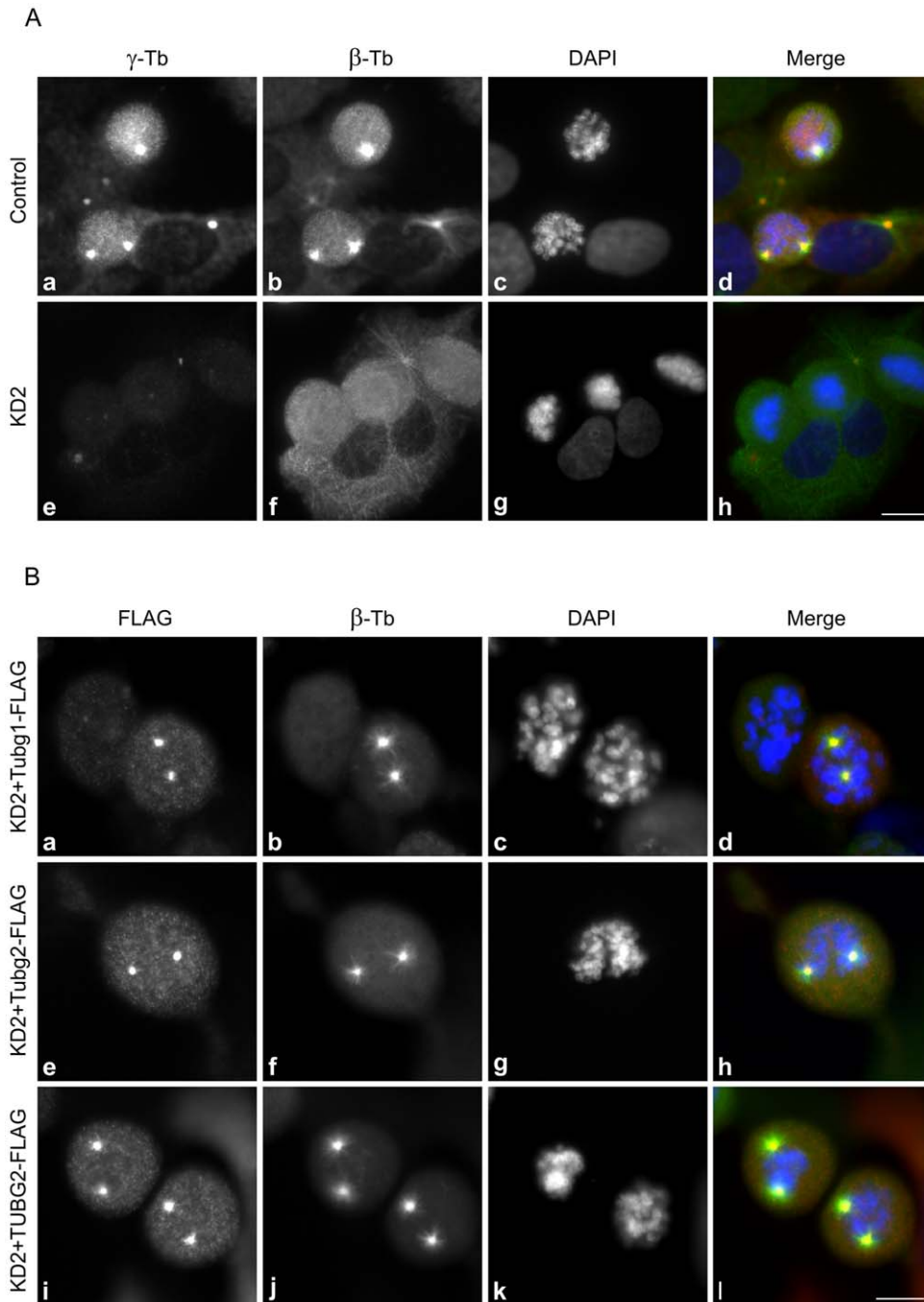
Figure 4. γ-Tubulin 2 rescues centrosomal microtubule nucleation in γ-tubulin 1-depleted mitotic cells. A) U2OS cells transfected with negative control siRNA (Control) or with γ-tubulin 1 specific siRNA (KD2) were treated with 10 µM nocodazole for 6 h and fixed after 3 min incubation in medium without nocodazole. Cells were stained for γ-tubulin (a, e; red) and β-tubulin (b, f; green). DNA was stained with DAPI (c, g; blue). Fluorescence images of cells stained for γ-tubulin were captured under identical conditions and processed in exactly the same way. Scale bar 10 µm. (B) U2OS cells depleted of γ-tubulin 1 and expressing FLAG-tagged mouse γ-tubulin 1 (a–d, Tubg1-FLAG), mouse γ-tubulin 2 (e–h, Tubg2-FLAG) or human γ-tubulin 2 (i–l, TUBG2-FLAG) were treated with 10 µM nocodazole for 6 h and fixed after 3 min incubation in medium without nocodazole. Cells were stained for FLAG (a, e, i; red) and β-tubulin (b, f, j; green). DNA was stained with DAPI (c, g, k; blue). Scale bar 10 µm.
doi:10.1371/journal.pone.0029919.g004

tubulin 1-depleted cells (Fig. 5, f) when compared with negative control cells (Fig. 5, e). This most likely reflects an impaired microtubule nucleation. In contrast, the density of EB1 tracks in cells rescued by exogenous mouse γ-tubulin 1 (Fig. 5, g) resembled that seen in negative controls cells (Fig. 5, e). Clear phenotypic rescue was also observed in cells expressing exogenous human

γ-tubulin 2 (Fig. 5, h). These findings were confirmed by evaluation of statistical data as documented in histograms of the microtubule growth rates, where the number of EB1 tracks was normalized by the cell area and tracking time (Fig. 6). To compare whole populations of EB1 tracks in analyzed cells, we applied Bonferroni correction of p-values to velocity histograms (Fig. 6).

Calculated p-values for differences among individual growth velocity groups were multiplied by the number of all growth velocity groups in the histogram (n = 13). Based on this correction, the number of EB1 tracks was significantly reduced in γ-tubulin 1-depleted cells when compared with negative control cells (p<0.0001, Fig. 6A). Conversely, the number of EB1 tracks was significantly higher in cells rescued by exogenous mouse γ-tubulin 1 (p<1.10^{-6}, Fig. 6B) or human γ-tubulin 2 (p<1.10^{-5}, Fig. 6C) than in γ-tubulin 1-depleted cells. Differences between negative control (blue columns in Fig. 6A) and γ-tubulin 2 expressing cells (blue columns in Fig. 6C) were statistically insignificant. Interestingly, the number of EB1 tracks in cells expressing exogenous mouse γ-tubulin 1 (blue columns in Fig. 6B) exceeded that seen in negative control (p<0.05; blue columns in Fig. 6A) or in cells expressing exogenous γ-tubulin 2 (p<0.05; blue columns in Fig. 6C). Taken collectively, our experimental data demonstrate that mammalian γ-tubulin 2 is able to nucleate microtubules and substitute for γ-tubulin 1 even in interphase cells.

## Tubg2 is downregulated in mouse preimplantation development

Since γ-tubulin 2 was capable to substitute for γ-tubulin 1 in cultured cells, its inability to do so in blastocysts [23] is intriguing. We therefore quantified by RT-qPCR the mRNA levels of Tubg1 and Tubg2 in mouse oocytes, 2-cell stage embryos, 8-cell stage embryos and blastocysts. Adult mouse liver and brain tissues served as controls, because Tubg2 expression is high in brain and low in liver [23,24]. Geometric mean of mouse peptidylprolyl isomerase A (Ppia) and mouse glyceraldehyde-3-phosphate dehydrogenase (Gapdh) mRNA levels were used for normalization. Tubg1 mRNA level decreased 17 times, when 2-cell stage embryos were compared with blastocysts, and was almost equal in liver and brain (Fig 7A). In contrast, Tubg2 mRNA level decreased dramatically by almost three orders of magnitude (815 times),

when these two developmental stages were compared. Tubg2 expression in blastocysts was comparable to that in liver and was 38 times lower than in brain (Fig. 7B). For comparison, mRNA levels were also ascertained for Tubgcp2 and Tubgcp5 that encode, respectively, GCP2 and GCP5 proteins. While Tubgcp2 mRNA level remained relatively stable (Fig. 7C), that of Tubgcp5 decreased 9 times when comparing the 2-cell stage embryos and blastocysts (Fig. 7D). Notably, the highest mRNA levels of tested genes were detected in oocytes, which probably reflects the high content of stored maternal mRNA [27]. Taken together, our data clearly show that Tubg2 mRNA level is appreciably decreasing during mouse preimplantation development.

RT-qPCR analysis disclosed that blastocyst contains a very low amount of Tubg2 mRNA. However, γ-tubulin 2 protein might still be present. To analyze the expression of Tubg2 at the protein level, we first identified the positions of mouse γ-tubulin 1 and γ-tubulin 2 in samples separated by 2D-PAGE. Different antibodies reacting with both γ-tubulins were used for immunoblotting. The exact positions of γ-tubulin 1 and γ-tubulin 2 were determined by overexpression of, respectively, untagged mouse γ-tubulin 1 and γ-tubulin 2 in P19 cells, where Tubg2 was undetectable by RT-qPCR (Fig. S8). Immunoblotting of untransfected and transfected cells with anti-γ-tubulin antibodies revealed that the signal of main γ-tubulin isoforms in P19 cells (Fig. 8, wt) was enhanced in cells overexpressing the γ-tubulin 1 (Fig. 8, +γ-Tb1). In cells overexpressing γ-tubulin 2, a new signal appeared in a more basic position compared to γ-tubulin1 isoforms (Fig. 8, +γ-Tb2). This was in agreement with theoretical isoelectric points for γ-tubulin 1 (5.66) and γ-tubulin 2 (5.80). These experiments demonstrate that mouse γ-tubulins can be easily discriminated on 2D-PAGE.

To rule out the possibility that the isoelectric point of exogenous γ-tubulin 2 expressed in P19 cells substantially differs from that in mouse tissues, we compared the expression of γ-tubulins in mouse
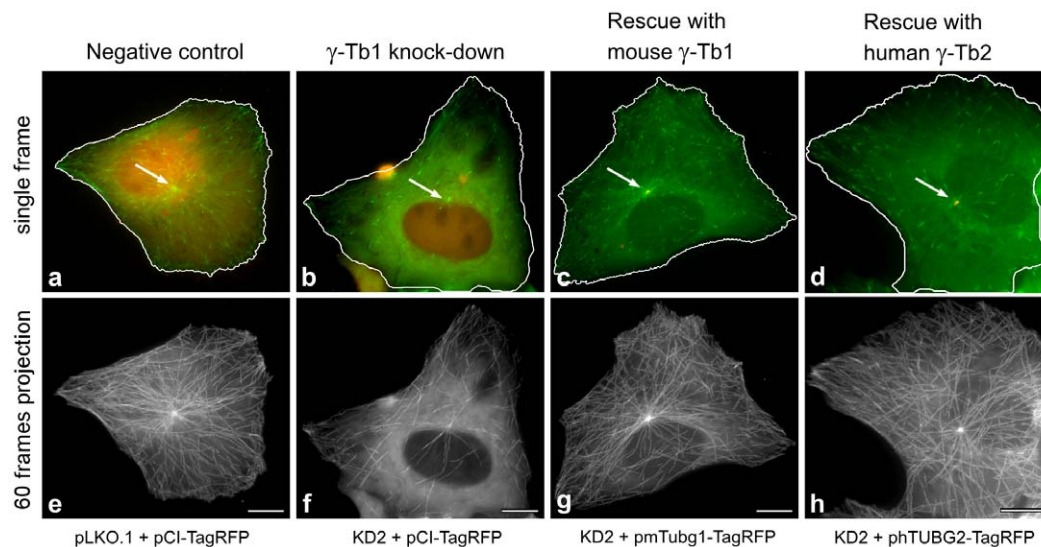
Figure 5. γ-Tubulin 2 rescues microtubule formation in γ-tubulin 1-depleted cells during interphase. Time-lapse imaging of U2OS-EB1 cells for quantitative evaluation of microtubule (+) end dynamics. Cells with depleted γ-tubulin 1 (KD2) expressing either TagRFP (pCI-TagRFP), mouse γ-tubulin 1 (pmTubg1-TagRFP) or human γ-tubulin 2 (phTUBG2-TagRFP). Cells with empty vector (pLKO.1) expressing TagRFP (pCI-TagRFP) served as negative control. (a–d) Still images of typical cells selected for evaluation. Only cells expressing both EB1-GFP (green) and TagRFP (red) or γ-tubulin-TagRFP fusions (red) were evaluated. In contrast to freely diffusible TagRFP (a, b), γ-tubulin-TagRFP fusions properly localized to MTOCs (c, d) marked by white arrows. (e–f) Maximum intensity projections of 60 consecutive time-frames from acquired time-lapse sequences. Note the markedly lower density of microtubule tracks in cell with depleted human γ-tubulin 1 (f). Microtubule track density is rescued in cells expressing exogenous mouse γ-tubulin 1 (g) or exogenous human γ-tubulin 2 (h). Scale bar 10 μm.
doi:10.1371/journal.pone.0029919.g005
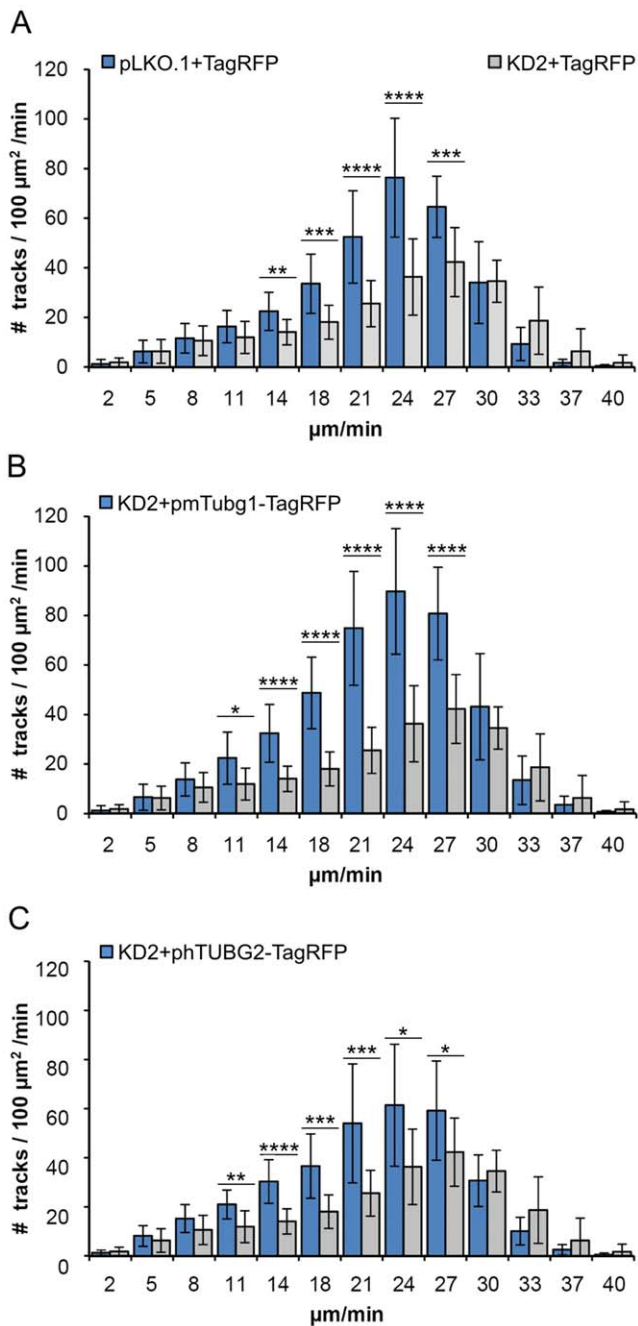
Figure 6. Quantitative evaluation of microtubule formation in phenotypic rescue experiments. Microtubule (+) end dynamics in U2OS-EB1 cells presented as velocity histograms. Cells with depleted γ-tubulin 1 (KD2) or negative control cells (pLKO.1), expressing either TagRFP (pCI-TagRFP), mouse γ-tubulin 1 (pmTubg1-TagRFP) or human γ-tubulin 2 (phTUBG2-TagRFP). (A) Comparison of negative control cells (pLKO.1+pCI-TagRFP; n = 19) with γ-tubulin 1 depleted cells (KD2+pCI-TagRFP; n = 15). (B) Comparison of cells rescued with mouse γ-tubulin 1 (positive control; KD2+pmTubg1-TagRFP; n = 18) with γ-tubulin 1 depleted cells. (C) Comparison of cells rescued with human γ-tubulin 2 (KD2+hTubg2-TagRFP; n = 19) with γ-tubulin 1 depleted cells. Data are from 3 independent experiments. Bars represent means±SD. Asterisks represent the p-values (p) of two-sided unpaired t-test (****, p< 0.00001; ***, p<0.0001; **, p<0.001; *, p<0.01).
doi:10.1371/journal.pone.0029919.g006

brain and mouse liver, where *Tubg2* expression is high and low, respectively [23,24]. For this, we used immunoblotting after 2D-PAGE separation of samples containing similar total protein amounts. γ-Tubulin 1 was clearly detectable in both brain and liver. In contrast, a strong signal in the position of γ-tubulin 2 was detected merely in brain, whereas it was undetectable in liver (Fig. 9A). Again, these results correlated with data obtained in RT-qPCR experiments (Fig. 7B). The performed experiments confirmed that γ-tubulin 2 can be discriminated by 2D-PAGE also in mouse tissues. Using the same approach, we compared the expression of γ-tubulin 1 and γ-tubulin 2 in mouse oocytes and blastocysts. Samples were prepared from 150 fully grown oocytes at the GV stage and from 197 early blastocysts to ensure that the total protein amount in blastocyst sample was not underestimated. A fully grown oocyte (from adult animals) at GV stage contains approximately 30 ng of protein. Zona pellucida contributes to this amount some 4–5 ng [28]. An early blastocyst contains approximately 25 ng of protein [29]. γ-Tubulin 1 was clearly detectable in both oocytes and blastocysts. On the other hand, while there was a strong signal detectable in the position of γ-tubulin 2 in oocytes, the relevant signal in this position was dramatically reduced in blastocysts (Fig. 9B). Expression of γ-tubulin 2 at the protein level in oocytes and blastocysts thus correlated with its mRNA level (Fig. 7B). Collectively taken, these data strongly indicate that a very low amount of γ-tubulin 2 is present in wild-type blastocysts due to its transcriptional downregulation.

Discussion

Mammalian γ-tubulins are encoded by two closely related genes [22,24], and specific functions have been attributed to them. [23]. The molecular basis of suggested functional differences between γ-tubulins is however unknown. In this study we document that mammalian γ-tubulin 2 is able to nucleate microtubules and substitute for γ-tubulin 1. In addition, we show that *Tubg1* and *Tubg2* are differentially transcribed during mouse early embryogenesis, with *Tubg2* transcription being progressively downregulated.

In general, γ-tubulins are highly conserved proteins in all eukaryotes. At the amino acid sequence level, human γ-tubulin 1 and γ-tubulin 2, respectively, show 98.9% and 97.6% identity with the corresponding mouse isoforms (Table S1) [23]. To study the subcellular localization and function of human and mouse γ-tubulin 2, we have chosen human osteosarcoma cells U2OS. Because of their flat shape, they are excellent for immunofluorescence analysis and are easily transfectable. Moreover, the the selection of U2OS made it possible to answer the question whether or not the mouse γ-tubulin 2 is capable of replacing human γ-tubulin 1. We have used exogenously expressed FLAG-tagged mouse and human γ-tubulins to evaluate the subcellular localization of γ-tubulin 2 proteins and their interactions with GCPs. It was reported previously that exogenous mouse γ-tubulin 2 located to interphase and mitotic centrosomes in mouse Eph4 epithelial cells [23]. Our data corroborate this finding by showing that both human and mouse γ-tubulin 2 are recruited to interphase and mitotic centrosomes in human U2OS cells. By immunoprecipitation experiments we found that γ-tubulin 2 interacted with GCP2, an integral component of γTuSCs. Reciprocal coimmunoprecipitations of γ-tubulin 2 and GCP4 (T. Sulimenko, unpublished data) indicated that γ-tubulin 2 normally also incorporated in γTuRCs. We found no differences between γ-tubulin 1 and γ-tubulin 2 with regard to their localization and interactions. Intriguingly, antibody to GCP2 coimmunoprecipitated more endogenous than exogenous γ-tubulins (Fig. 1B, Fig. S2). A similar result was obtained with
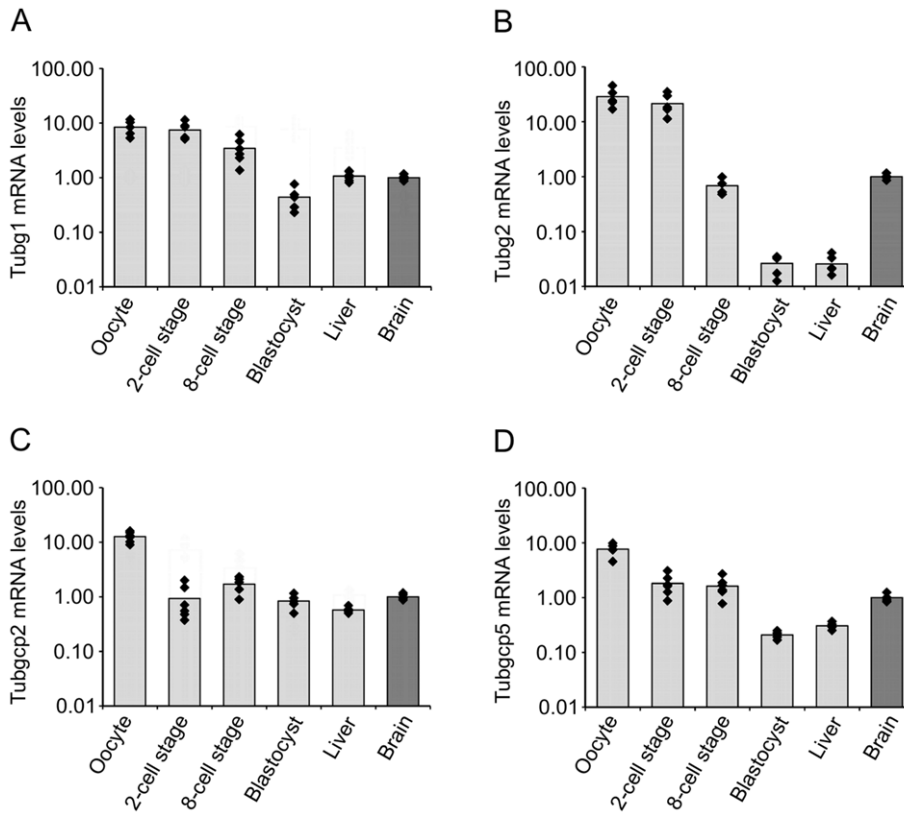
Figure 7. *Tubg2* mRNA level is decreasing during mouse preimplantation development. mRNA levels of *Tubg1* (A), *Tubg2* (B), *Tubgcp2* (C) and *Tubgcp5* (D) in mouse oocyte, 2-cell stage embryo, 8-cell stage embryo, blastocyst and liver relative to the level found in brain. Data are presented as mean fold change (columns) with individual samples displayed (diamonds). Three biological replicates were measured twice under identical conditions. Note that the Y-axis is in the logarithmic scale.
doi:10.1371/journal.pone.0029919.g007

antibody to GCP4 (T. Sulimenko, unpublished data). This fact might indicate a slow turnover of γTuCs, because precipitations were performed 48 hours after transfection. Alternatively, FLAG tags might interfere with interaction of γ-tubulin with GCPs. However, this seems unlikely as FLAG tags were fused to the C-termini of γ-tubulins, which probably is not involved in the interaction with GCP2 and GCP3 [30]. Moreover, FLAG-tagged γ-tubulins rescued normal mitotic progression in γ-tubulin 1-depleted cells (Fig. 3).

The most remarkable phenotypic sign of γ-tubulin 1-depleted U2OS cells was arrest in metaphase caused by mitotic spindle defects such as monopolar or collapsed spindles (Fig. 2C), previously described in mammalian cells depleted of γ-tubulin [11,23,31]. Similar defects were detected in cells in which γ-tubulin localization to centrosomes, mitotic spindle and mitotic chromatin was damaged by depletion of γTuRC recruitment factors like GCP-WD/NEDD1 [11,31] or components of augmin complex [32,33]. As expected, the observed phenotype was reverted by expression of mouse γ-tubulin 1. Both human and mouse γ-tubulin 2 likewise rescued the normal mitotic progression in γ-tubulin 1-depleted cells, indicating that mammalian γ-tubulin 2 is able to substitute for γ-tubulin 1 *in vivo* (Fig. 3). Consistent with these findings are the results of microtubule regrowth experiments on mitotic cells which reveal that γ-tubulin 2 does have microtubule nucleating capability (Fig. 4). We used only KD2 siRNA and corresponding shRNA for phenotypic rescue experiments, because it was more efficient than KD1 (Fig. S3A, Fig. S5A) and its specificity was verified in an independent study [34]. Rescue experiments also ruled out potential off-target RNAi effects.

When testing the microtubule (+) end dynamics in γ-tubulin 1-depleted cells, we observed a significant reduction in the number of EB1 tracks in interphase cells (Fig. 5, f; Fig. 6A), a sign of impaired microtubule nucleation. Alternatively, reduction in the EB1 track number might be explained by changes in microtubule dynamics; the nucleation is not affected but the fraction of growing microtubules relative to pausing or depolymerizing microtubules is diminished. Although one cannot exclude a potential contribution of impaired microtubule (+) ends dynamics to the observed phenotype, we consider this possibility much less probable because it has been previously demonstrated by regrowth experiments that microtubule nucleation is impaired and/or delayed in interphase cells depleted of γ-tubulin [31]. We therefore conclude that γ-tubulin 2 is able to nucleate microtubules also in interphase cells. Interestingly, a higher number of EB1 tracks was in γ-tubulin 1-depleted cells expressing exogenous γ-tubulin 1 than in cells expressing exogenous γ-tubulin 2 (Fig. 6). It might imply that for interphase cells γ-tubulin 1 is a more potent nucleator of microtubules than γ-tubulin 2. However, no corresponding differences in microtubule regrowth were observed in mitotic cells (Fig. 4), where centrosomes are highly enriched with γTuCs [25,26], and where consequently the potential differences in nucleation capability ought to be stronger. In addition, statistical significance ($p < 0.05$) of this difference is relatively low. We therefore do not think that γ-tubulin 1 and γ-tubulin 2 substantially differ in nucleation activity.

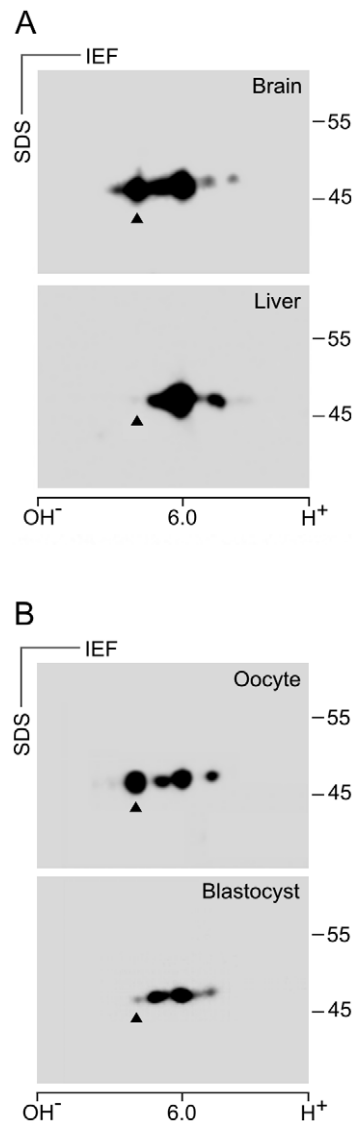Functional redundancy of mammalian γ-tubulins was expected because of their high sequence similarity [22]. Importantly, only 6
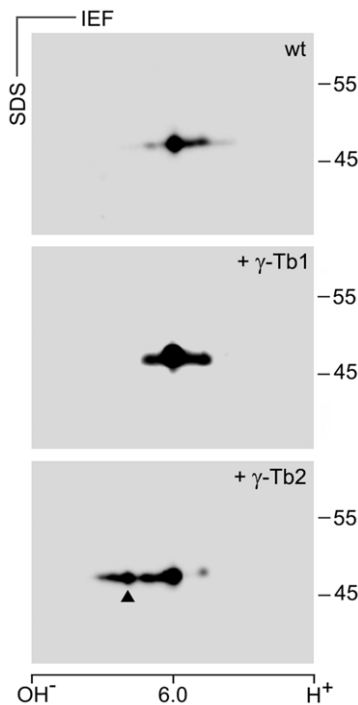
Figure 8. Electrophoretic distinction of mouse γ-tubulins on 2D-PAGE. Immunoblots of mouse P19 cell extracts separated by 2D-PAGE probed with antibody to γ-tubulin. Wild-type cells (wt), cells expressing exogenous untagged mouse γ-tubulin 1 (+γ-Tb1) or mouse γ-tubulin 2 (+γ-Tb2). Molecular mass markers (in kDa) are indicated on the right. The pI scale is shown along the bottom of the figure. IEF, isoelectric focusing. Arrowhead indicates the position of mouse γ-tubulin 2.
doi:10.1371/journal.pone.0029919.g008

Figure 9. Differences in the expression of mouse γ-tubulin 2 protein in oocytes and blastocysts. Immunoblot analysis of tissue and cell extracts separated by 2D-PAGE with antibody to γ-tubulin. (A) Comparison of control adult mouse brain and liver. (B) Comparison of mouse oocytes and blastocysts. Molecular mass markers (in kDa) are indicated on the right. The pI scale is shown along the bottom of the figure. IEF, isoelectric focusing. Arrowheads indicate the position of γ-tubulin 2 as defined in Fig. 8.
doi:10.1371/journal.pone.0029919.g009

amino acids specific for γ-tubulin 1- or γ-tubulin 2 are conserved in the majority of mammalian species. They are located in two clusters in helixes H11 (3 amino acids) and H12 (3 amino acids) of γ-tubulins (Table S2). These regions might be important for hypothetical divergent functions of mammalian γ-tubulins. However, when γ-tubulin in fission yeast was replaced by human γ-tubulin 1, with all three γ-tubulin 1-specific amino acids in helix H11 (R390, T391, R393) or one amino acid in helix H12 (I427) mutated to alanines, no deleterious effect on cell viability was observed [35]. It indicates that these regions are not essential for conserved γ-tubulin functions; this is in line with our data suggesting that γ-tubulin 2 is able to substitute for γ-tubulin 1.

Yuba-Kubo et al. reported that γ-tubulin 2 is expressed in the wild-type mouse blastocyst [23]. In contrast, our 2D-PAGE analysis indicates that there is very low level of γ-tubulin 2 protein in the wild-type blastocyst, whereas γ-tubulin 1 is abundant (Fig. 9). This is in a good agreement with our RT-qPCR data, indicating that *Tubg2* mRNA level is dramatically decreasing during preimplantation development unlike mRNA levels of *Tubg1*, *Tubgcp2* and *Tubgcp5* (Fig. 7). The reason for such discrepancy is unclear. Previously blastocysts were analyzed only by immunoblotting after one-dimensional PAGE. Anti-γ-tubulin antibody recognized two bands that were supposed to represent γ-tubulin 1 and γ-tubulin 2 [23]. However, reported separation of γ-tubulins in blastocysts by SDS-PAGE need not reflect only the presence of different genes, but proteolysis or posttranslational modification(s) as well.

A common fate of the members of duplicate-gene pairs is the partitioning of tissue-specific patterns of expression of the ancestral

gene [36]. Analyses of expression of mammalian γ-tubulin genes showed differential expression in many tissues [23,24]; the same holds also for this study. It suggests that an important mechanism acting on γ-tubulin gene pair is the subfunctionalization. It was reported that some gene segments of γ-tubulin genes had been evolving together in the process known as "concerted evolution" [24]. It was proposed that concerted evolution might have been operative to maintain perfect homology at essential binding sites. Indeed, exons 2–3 and 7–10 of the two γ-tubulin genes homogenized by concerted evolution [24] encode regions which are probably critical for interaction of γ-tubulin with GCP2 and GCP3 [30]. Thus, concerted evolution together with subfunctionalization foster the preservation of highly similar and functionally redundant γ-tubulin genes in mammalian genomes [24].

Our data allow an alternative interpretation of $Tubg1^{-/-}$ and $Tubg2^{-/-}$ phenotypes previously described in mice [23]. Endogenous γ-tubulin 2 cannot rescue γ-tubulin 1 deficiency in Tubg1$^{-/-}$ blastocyst, even though it can nucleate microtubules, because it is not present in a sufficient amount. It was previously reported that knock out of single gene resulted in overexpression of related genes [37–39]. Our data do not strictly exclude the possibility that γ-tubulin 2 expression could be up-regulated in $Tubg1^{-/-}$ blastocysts, however, γ-tubulin 2 may be insufficient to fully replacer the lacking γ-tubulin 1. On the other hand, whole-mount immunostaining with anti-γ-tubulin antibody in Tubg1$^{-/-}$ blastocyst cells did not identify any γ-tubulin 2-positive foci, even though one pericentrin-positive focus occurred in each cell [23]. It was suggested that γ-tubulin 1 was necessary for recruitment of γ-tubulin 2 to blastocyst centrosomes [23]. We propose that such observation can be alternatively explained by the absence of γ-tubulin 2 at the blastocyst stage both both in wild type and Tubg1$^{-/-}$ embryos. Behavioral abnormalities of Tubg2$^{-/-}$ mice do not necessarily imply unknown function(s) of γ-tubulin 2. They might also reflect a reduction of total γ-tubulin in brain of $Tubg2^{-/-}$ mice, since $Tubg2$ is highly expressed in the brain [23,24] as demonstrated also in this study. Yet, we cannot exclude the possibility that brain γ-tubulin 2 has some additional still unknown function(s). Thorough phenotype analysis of $Tubg2^{-/-}$ mice could shed more light on γ-tubulin 2 function(s) in brain and its development. Further, elucidation of transcriptional regulation of γ-tubulin genes would by very important not only from the developmental point of view but also with respect to tumorigenesis. Significantly higher expression of γ-tubulin was found in high-versus low-grade gliomas, common brain cancers [40,41].

In conclusion, the findings indicate that mammalian γ-tubulin 2 is able to nucleate microtubules and substitute for γ-tubulin 1. Although γ-tubulins are differentially expressed during mouse early embryogenesis and in adult tissues, they are functionally redundant with respect to their nucleation activity.

Materials and Methods

Ethics statement

All mice were maintained in accordance with the Institute of Molecular Genetics Guidelines. Experiments were approved by the Committee on the Ethics of Animal Experiments of the Institute of Molecular Genetics (permit number 18/2009).

Cell cultures and transfections

Human osteogenic sarcoma cells U2OS, human glioblastoma cell line T98G, mouse embryonal carcinoma cells P19, mouse neuroblastoma Neuro-2a and mouse embryonal fibroblasts NIH 3T3 were obtained from the American Type Culture Collection. Human kidney embryonal cells HEK293-FT (HEK) were from Promega Biotec. Mouse bone marrow-derived mast cell line (BMMC) was kindly provided by M. Hibbs (Ludwig Institute for Cancer Research, Melbourne, Australia). Cells were cultured in Dulbecco's modified Eagle's medium (DMEM) containing 10% fetal bovine serum, penicillin (100 units/ml), and streptomycin (0.1 mg/ml). Cells were grown at 37°C in 5% CO_2 in air, and passaged every 2 or 3 days using 0.25% trypsin/0.01% EDTA in PBS. BMMC were cultured in RPMI 1640 medium supplemented with serum, antibiotics and interleukin 3 (PeproTech) as described previously [42].

U2OS cells were transfected with 2.5 μg (single plasmid) or 4 μg (cotransfection of 2 plasmids) DNA/well in a 6-well plate using Lipofectamine LTX reagent (Invitrogen) (DNA[μg]: LTX [μl] ratio was 1:2.5) and Opti MEM medium (Gibco) according to the manufacturer's instruction. After 12 h, the transfection mixture was replaced with fresh complete medium, and cells were incubated for 48 h. HEK cells were transfected with 17 μg DNA per 9-cm tissue culture dish using 51 μg polyethylenimine (Polysciences) and serum-free DMEM. After 24 h, the transfection mixture was replaced with fresh medium supplemented with serum, and cells were incubated for additional 24 h.

Some of the U2OS cells, growing on coverslips, were treated with 10 μM nocodazole (Sigma) for 6 h. Afterwards, cells were washed 5 times in ice-cold PBS, transferred to new medium and incubated for 3 min at 28°C before fixation.

Mouse oocytes, embryos and tissues

Oocytes and embryos were obtained from 6–8 week old C57BL/6 mice. Fully grown germinal vesicle (GV) oocytes were liberated from ovaries by puncturing the antral follicles with syringe needle and collected in M2 medium (Sigma) containing 0.2 mM isobutylmethylxanthine (IBMX; Sigma). To obtain preimplantation embryos, mice were superovulated with 5 IU of Folligon (pregnant mare serum gonadotropin; PMSG) (Intervet) followed by stimulation with 5 IU of human chorionic gonadotrophin (hCG, Sigma) 47 hours post-PMSG. The stimulated mice were mated with 8–10 week old C57BL/6 males immediately after hCG injection. Two-cell and eight-cell stage embryos were collected 48 and 68 hours post-hCG, respectively, by flushing the oviducts with M2 medium. Blastocyst stage embryos were collected 96 hours post-hCG by flushing the uteri with M2 medium. Oocytes and embryos were washed 5 times in PBS prior to transfer into TRI reagent (Ambion) for RNA isolation or into buffer for 2D-PAGE. Liver and brain were dissected from 6–8 week old female C57BL/6 mice.

DNA constructs

Total RNA from BALB/c adult mouse brain or from human cell line T98G was isolated by the RNeasy Mini kit (QIAGEN) according to the manufacturer's directions. The purity and integrity of the RNA preparations were checked using Experion automated electrophoresis system for microfluidic chip-based analysis and RNA StdSens analysis kit (Bio-Rad Laboratories). The quantity of RNA was checked by Nanodrop spectrophotometer (NanoDrop Technologies). Reverse transcription was performed with oligo(dT) primers and SuperScript III Reverse Transcriptase kit (Invitrogen).

The full length human γ-tubulin 2 (TUBG2, Refseq ID: NM_016437) was amplified by PCR using forward 5′-GCCCACGTCTGAAGAGCGATGC-3′ and reverse 5′-CTG-GAGATGAACCAAGAAGGGTTG-3′ primers and T98G cell cDNA as template. The full length mouse γ-tubulin 1 (Tubg1, Refseq ID: NM_134024) and mouse γ-tubulin 2 (Tubg2, Refseq ID: NM_134028) were amplified by PCR using the following specific primers - Tubg1: forward 5′-GAGAGACTGCAACGCC-GATGTCTG-3′ and reverse 5′-TTGTGAGGTCCCTGATC-TGTGCTC-3′; Tubg2, forward 5′- GGCAGGAGTTCCTCT-CAGTCGTGAC-3′ and reverse 5′-TGTGAGGCGAAGTTGG-GTCAGAG-3′ - and mouse brain cDNA as template.

PCR products were ligated into pCR 3.1 vector (Invitrogen) by TA-cloning method. Sequencing revealed that the M413V variant of human γ-tubulin 2 was isolated (refSNP ID: rs1046097). The constructed vectors (pCR-hTUBG2, pCR-mTubg1, pCR-mTubg2) served as templates for additional PCRs with following specific forward and reverse primers carrying EcoRI/SalI restriction sites (underlined): human TUBG2, forward 5′-CTGAATTC-CACGTCTGAAGAGCGATGC-3′ and reverse 5′-TCAAGTC-GACCTGCTCCTGGGTGCC-3′; mouse Tubg1: forward

5′-ACGAATTCTGCCTGAGGAGCGATGC-3′ and reverse 5′-TCAAGTCGACCTGCTCCTGGGTGCC-3′; mouse *Tubg2*: forward 5′- CTGAATTCGGTCTGATCGGCGATGC-3′ and reverse 5′-TCAAGTCGACCTGCTCCTGGGTGCC-3′. PCR products without stop codon were digested with *Eco*RI/*Sal*I restriction enzymes and inserted into pFLAG-CMV5a vector (Sigma) resulting in C-terminally FLAG-tagged human γ-tubulin 2 (phTUBG2-FLAG), mouse γ-tubulin 1 (pmTubg1-FLAG) and mouse γ-tubulin 2 (pmTubg2-FLAG). Constructs encoding C-terminally FLAG-tagged human γ-tubulin 1 (phTUBG1-FLAG) or mouse Fyn (pFyn-FLAG) were described previously [9].

Complete coding sequences of mouse *Tubg1* and *Tubg2* were cut out from pCR-mTubg1 and pCR-mTubg2, respectively, by *Eco*RI and inserted into pCI-NEO (Promega) to create vectors expressing untagged mouse γ-tubulin 1 (pCI-mTubg1) and γ-tubulin 2 (pCI-mTubg2).

Coding sequence of monomeric red fluorescent protein TagRFP-T (GenBank: EU582019.1) was amplified from pcDNA3.1-TagRFP (kind gift of Dr. R.Y. Tsien, HHMI at the University of California, San Diego, USA) by PCR with the following specific forward and reverse primers carrying *Sal*I and *Not*I restriction sites (underlined): forward 5′-AGTCGACG-GAGGTGGTGGAGGTATGGTGTCTAAGGGCGAAGA-3′ (added 5x glycine coding motif in *italic*) and reverse 5′- TGC-GGCCGCTTACTTGTACAGCTCGTCCATGCCA -3′. PCR products were ligated into pCR 2.1 vector (Invitrogen) by TA-cloning method. TagRFP coding sequence was digested from this vector using *Sal*I/*Not*I restriction enzymes and inserted into pCI-Neo (Promega) resulting in a vector encoding TagRFP (pCI-TagRFP) and allowing construction of C-terminally TagRFP-tagged fusion proteins. Coding sequences of mouse *Tubg1* and human *TUBG2* without stop codon were cut out from pmTubg1-FLAG and phTUBG2-FLAG, respectively, by *Eco*RI/*Sal*I restriction enzymes and ligated into pCI-TagRFP resulting in vectors encoding TagRFP-tagged mouse γ-tubulin 1 (pmTubg1-TagRFP) and human γ-tubulin 2 (phTUBG2-TagRFP). All constructs were verified by sequencing.

U2OS cells stably expressing EB1-GFP (U2OS-EB1) were obtained by transfection of cells with pEB1-GFP, obtained from Dr. Y. Mimori-Kiyosue [43], and selection in 1.1 mg/ml geneticin (G418, Sigma) for 2 weeks. Cells were then diluted to one cell/well on 96-well plate and allowed to grow for 2 weeks. Homogeneous colonies expressing EB1-GFP were propagated.

Antibodies

The following anti-peptide antibodies prepared to human γ-tubulin were used: mouse monoclonal antibodies TU-30 (IgG1) and TU-32 (IgG1) to the sequence 434–449 [44]; monoclonal antibody GTU 88 (IgG1; Sigma, T6657) and rabbit antibody (Sigma, T5192) to the sequence 38–53. The anti-γ-tubulin antibodies react with both γ-tubulin 1 and γ-tubulin 2 in mouse and human. β-Tubulin was detected with monoclonal antibody TUB 2.1 conjugated with FITC (IgG1; Sigma F2043) and pericentrin with rabbit antibody (Covance PRB-432C). Rabbit antibodies to GAPDH (G9545) and FLAG peptide (F7425) as well as monoclonal antibody M2 (IgG1) to FLAG peptide (F1804) were from Sigma. Monoclonal antibodies to GCP2 protein, GCP2-01 (IgG2b) and GCP2-02 (IgG1), were described previously [9]. Monoclonal antibody to GCP4 (IgG1) was from Santa Cruz (sc-271876). Monoclonal antibody NF-09 (IgG2b) to neurofilament NF-M protein [45] and rabbit antibody to non-muscle myosin BT-561 (Biomed Techn. Inc) served as controls.

The Cy3-conjugated anti-mouse and anti-rabbit antibodies were from Jackson Immunoresearch Laboratories. Anti-rabbit antibody conjugated with Alexa 488 was from Invitrogen. Secondary horseradish peroxidase-conjugated antibodies were from Promega.

RNAi

U2OS cells in 6-well plates were transfected with siRNAs (final concentration 20 nM) using Lipofectamine RNAi MAX (Invitrogen) according to the manufacturer's instruction. Five siRNAs (Ambion/Applied Biosystems) that target the regions present in human γ-tubulin 1, namely, (5′-GGGAGAAAAGATCCAT-GAG-3′; siRNA ID #9227), (5′-CGCATCTCTTTCTCA-TATA-3′; siRNA ID #120194), (5′-GGACATTTTTGACAT-CATA -3′; siRNA ID #9317), (5′-GAACCTGTCGCC-AGTATGA-3′; siRNA ID #120784), (5′-GGTATCCTAA-GAAGCTGGT-3′; siRNA ID #9396) were tested. Maximal depletion was reached by transfecting the siRNA twice with a 72-h time interval and harvesting cells 72 h after the second transfection. Negative control siRNA was from Ambion/Applied Biosystems (Silencer Negative Control #1 siRNA).

Immunoblotting and immunofluorescence analyses revealed that the highest reduction of γ-tubulin was obtained with siRNA ID#9396 (KD1) and siRNA ID#120194 (KD2; results not shown). These siRNAs were used for some phenotypic rescue experiments. In that case siRNA was mixed with the plasmid of interest and transfected into cells which already underwent the first round of 72 h-long siRNA treatment, using Lipofectamine LTX. Cells were analyzed 72 h after the second transfection.

The selected siRNAs were also used for construction of shRNA vectors based on pLKO.1 (Addgene, #8453) that enabled puromycin selection. Corresponding sense and antisense oligonucleotides were synthetized by Sigma-Aldrich: 9396sh-sense 5′-CCGGGGTATCCTAAGAAGCTGGTTTCTCGAGACCAGC-TTCTTAGGATACCTGTTTTTG-3′, 9396-antisense 5′-AAT-TCAAAAACAGGTATCCTAAGAAGCTGGTCTCGAGAA-ACCAGCTTCTTAGGATACC-3′; 120194sh-sense 5′- CCGGC-GCATCTCTTTCTCATATATTCTCGAGTATATGAGAAAG-AGATGCGTGTTTTTG-3′, 120194sh-antisense 5′- AATT-CAAAAACACGCATCTCTTTCTCATATACTCGAGAATAT-ATGAGAAAGAGATGCG-3′. Sense and antisense oligonucleotides, at final concentration 45 μM of each, were annealed in 1x NEB 2 buffer (New England Biolabs) by initial warming up to 95°C followed by slow (3 h) cooling down to the room temperature. Annealed oligonucleotides were inserted into pLKO.1 previously linearized with *Age*I/*Eco*RI resulting in human TUBG1 shRNA expressing vectors p9396sh (KD1) and p120194sh (KD2). Correct sequences of all vectors were verified by sequencing.

shRNA vectors were transfected in the same way as other plasmids used in the study. To select shRNA expressing cells, the transfection mixture was replaced with fresh complete medium 12 h later. Puromycin (Sigma) at final concentration 2.5 μg/ml was added after 12 h incubation, and cells were selected in puromycin for 6 days before analysis.

Reverse transcription quantitative real-time PCR (RT-qPCR) analysis

Total cellular RNA was extracted in three independent isolations from 20 mouse oocytes and 5–10 embryos using TRI reagent (Ambion) according to manufacturer's instructions. Three independent isolations of total cellular RNA were also made from four mouse cell lines Neuro2a, P19, BMMC and 3T3 using RNeasy Mini kit (QIAGEN). In three independent experiments mouse livers and brains were frozen in liquid nitrogen, homogenized under liquid nitrogen using mortar and pestle, and total RNA was extracted from 10–15 mg of homogenized tissue

using RNeasy Minikit (QIAGEN). Concentration of the purified RNA was determined with spectrophotometer NanoDrop (Thermo Scientific). The quality of RNA was checked on Agilent 2100 Bioanalyzer. All RNA samples were of good qPCR quality (RNA integrity number [RIN] ≥7.6 for all tissue samples; RIN≥9.8 for all cell lines samples). Purified RNA was stored at −70°C. Purified RNAs from oocytes and embryos were converted to cDNA immediately after isolation. RNA from each sample was converted to cDNA using the ImProm-II RT kit (Promega). For tissues and cell lines, each reaction sample (20 µl) contained 1 µg RNA, random hexamer primers (25 ng/ µl), ImPROM-II reaction buffer, 5.6 mM $MgCl_2$, dNTP mix (0.5 mM each dNTP), 0.5 µl RNasin and 1 µl ImProm-II reverse transcriptase. For oocytes and embryos, all isolated RNA was used for reverse transcription.

Quantitative PCR was performed with gene-specific primers for mouse γ-tubulin 1 (*Tubg1*, NM_134024), mouse γ-tubulin 2 (*Tubg2*, NM_134028), mouse GCP2 (*Tubgcp2*, NM_133755), mouse GCP5 (*Tubgcp5*, NM_146190), mouse peptidylprolyl isomerase A (*Ppia*, NM_008907) and mouse glyceraldehyde-3-phosphate dehydrogenase (*Gapdh*, NM_008084). All primers were tested *in silico* by NCBI BLAST to amplify specific targets. Primer sequences are summarized in Table S3. Oligonucleotides were from East Port (Prague, Czech Republic).

Quantitative PCRs were carried out on LightCycler 480 System (Roche). Each reaction (5 µl) consisted of 2.5 µl LightCycler® 480 SYBR Green I Master (Roche), 0.5 µl mixed gene-specific forward and reverse primers (5 µM each) and 2 µl diluted cDNA. cDNA samples from brain, liver and cell lines were diluted 1:50. In case of oocyte and embryonal cDNA samples, the used amounts of cDNA per reaction corresponded to 1/4 of oocyte, 1/2 of 2-cell stage embryo, 1/10 of 8-cell stage embryo and 1/10 of blastocyst. Calibration curves for tested genes were made by serial dilutions (dilution factor 4) of brain cDNA. Each sample was run in duplicate. Thermocycling parametres are described in Text S1. Identity of PCR products was verified by sequencing.

Preparation of cell extracts

Whole-cell extracts for SDS-PAGE were prepared by rinsing the cells twice in Hepes buffer (50 mM Hepes adjusted to pH 7.6 with NaOH, 75 mM NaCl, 1 mM $MgCl_2$ and 1 mM EGTA), scraping them into Hepes buffer supplemented with protease (Roche; Complete EDTA-free protease mixture) and phosphatase (1 mM Na_3VO_4 and 1 mM NaF) inhibitors, and solubilizing in hot SDS-sample buffer [46] without bromphenol blue and boiling for 5 min.

When preparing the extracts for immunoprecipitation, cells were rinsed twice in cold Hepes buffer and extracted for 10 min at 4°C with Hepes buffer supplemented with protease and phosphatase inhibitors and 1% Nonidet P-40. The suspension was then spun down (20,000 *g*, 15 min, 4°C).

For preparation of samples for 2D-PAGE, oocytes and blastocysts were directly lysed in 2D-PAGE sample buffer [47]. Brain and liver were mixed with cold Hepes buffer supplemented with protease and phosphatase inhibitors in tissue/buffer ratio 1:10 and homogenized in teflon/glass grinder. The suspension was then spun down (20,000 *g*, 15 min, 4°C) and 10–15 µl aliquots of supernatant were mixed with 200 µl of sample buffer. Similarly, 20 µl aliquots of supernatants from 1% NP-40 extracts of P19 cells were mixed with 200 µl of sample buffer.

Protein quantifications in lysates and SDS-PAGE-samples were performed, respectively, with bicinchoninic acid assay and silver dot assay [48].

Immunoprecipitation, gel electrophoresis and immunoblotting

Immunoprecipitation from 1% NP-40 extracts was performed as described [49]. Cell extracts were incubated with beads of protein A (Pierce, Rockford, IL) saturated with: (I) rabbit antibody to FLAG, (II) monoclonal antibody GCP2-01 (IgG2b) to GCP2 (III) rabbit antibody to non-muscle myosin (negative control), (IV) monoclonal antibody NF-09 (IgG2a; negative control) or with (V) immobilized protein A alone. Gel electrophoresis and immunoblotting were performed using standard protocols. Two-dimensional electrophoresis (2D-PAGE) was performed as described [47] using for the first dimension 7 cm long Immobiline DryStrip gels with a linear pH 4-7 gradient (Amersham Biosciences). Comparable protein amounts were loaded in case of P19, liver and brain extracts (~25 µg).

For immunoblotting, rabbit antibodies to GAPDH, γ-tubulin (Sigma T5192) and FLAG peptide (Sigma F7425) were diluted 1:20,000, 1:5,000 and 1:2,000, respectively. Monoclonal antibodies to γ-tubulin (GTU88) and GCP4 were diluted 1:10,000 and 1:2,000, respectively. Monoclonal antibodies to γ-tubulin (TU-32) and GCP2 (GCP2-02), in the form of spent culture supernatants, were diluted 1:10. Peroxidase-conjugated secondary antibodies were diluted 1:10,000. Bound antibodies were detected by SuperSignal WestPico Chemiluminescent reagents (Pierce).

Immunofluorescence

Immunofluorescence staining was performed as previously described [50]. Samples were fixed in methanol at −20°C, air-dried and washed in PBS. Rabbit antibodies to FLAG peptide and pericentrin were diluted 1:1000 and 1:750, respectively. Monoclonal antibodies to FLAG peptide and β-tubulin were diluted 1:1,000 and 1:100, respectively. Monoclonal antibody TU-30 to γ-tubulin was used as spent culture medium diluted 1:50. Cy3-conjugated anti-mouse and ant-rabbit antibodies were diluted 1:1,000, Alexa 488-conjugated anti-rabbit antibody was diluted 1:200. For double-label immunofluorescence, coverslips were incubated separately with the primary antibodies, and simultaneously with the secondary conjugated antibodies. The preparations were mounted in MOWIOL 4–88 (Calbiochem) supplemented with 4,6-diamidino-2-phenylindole (DAPI, Sigma) to label nuclei, and examined on Delta Vision Core system (Applied Precision) equipped with 60x/1.42 NA oil-immersion objective. Optical z-sections were acquired in 0.25–0.30 µm steps. Z-stacks were deconvolved by a built-in deconvolution program (Softworx) using default parameters. Alternatively, some preparations were examined on Olympus AX-70 equipped with 40x/1.0 NA water objective. Some preparations were also examined on confocal microscope Leica SP5 with 60x/1.4 NA oil objective. Optical z-sections were acquired at 0.125 µm. Z-stacks were deconvolved by Huygens Professional software (SVI, The Netherlands). All presented Maximum Intensity Projections (MIP) of deconvolved z-stacks were prepared in ImageJ (NIH/USA). Conjugates alone gave no significant staining.

Time-lapse imaging

For time-lapse imaging, U2OS cells expressing EB1-GFP were grown on glass-bottom-dishes (MatTek) and transfected with different sets of plasmids, as specified in Result section. Before imaging, DMEM was replaced with medium for live cell imaging (DMEM without phenol red, riboflavin, folic acid, pyridoxal, $Fe[NO_3]_3$ and puromycin). Only cells expressing TagRFP or TagRPF-fusion proteins were selected for time-lapse imaging.

Time-lapse sequences of EB1-GFP dynamics were collected for 2 min at 1 sec intervals on Delta Vision Core system (Applied

Precision) equipped with 60x/1.42 NA oil-immersion objective. The focus plane was near the coverslip where the best resolution of EB1 comets was observed. Time-lapse sequences were adjusted in ImageJ (NIH, USA) by manual cropping of individual cells, enhancement of brightness and contrast, and converting sequences to a depth of 8 bits. Adjusted time-lapse sequences of individual cells were analyzed by in-house-written particle tracking plug-in implemented in Ellipse program version 2.07 (ViDiTo, Systems, Košice Slovakia; http://www.ellipse.sk) as described [42]. The particle speed was calculated as the ratio of particle trajectory length and trajectory duration. Statistical analysis was performed with the Student's two-tailed unpaired t-test using Microsoft Excel.

Supporting Information

Figure S1 Exogenous γ-tubulin 2 locates to centrosomes. Human U2OS cells expressing FLAG-tagged mouse γ-tubulin 1 (a–d, Tubg1-FLAG), mouse γ-tubulin 2 (e–h, Tubg2-FLAG), human γ-tubulin 1 (i–l, TUBG1-FLAG) and human γ-tubulin 2 (m–p, TUBG2-FLAG) were stained for FLAG (red) and pericentrin (green). DNA was stained with DAPI (blue). Final images were made by maximum intensity projection of 3 deconvolved z-sections spaced at 0.25 μm. Scale bar 10 μm.
(TIF)

Figure S2 Coimmunoprecipitation of human γ-tubulins with GCP2 and GCP4 proteins. Extracts from HEK cells expressing FLAG-tagged human γ-tubulin 1 (TUBG1-FLAG), human γ-tubulin 2 (TUBG2-FLAG) or control mouse Fyn (Fyn-FLAG) were immunoprecipitated with antibodies to FLAG or GCP2, and blots were probed with antibodies to FLAG, GCP2, GCP4 and γ-tubulin (γ-Tb). Extracts (1), immunoprecipitated proteins (2), protein A without antibodies incubated with extracts (3), immobilized antibodies not incubated with extracts (4). Arrowheads indicate the positions of exogenous γ-tubulins.
(TIF)

Figure S3 Immunoblot analysis of U2OS cells in phenotypic rescue experiments with FLAG-tagged γ-tubulins. (A) Immunoblot analysis of whole cell extracts from cells transfected with negative control (Control) or γ-tubulin specific siRNAs (KD1 and KD2). Staining with antibodies to γ-tubulin (γ-Tb) and GAPDH. (B) Cells with depleted γ-tubulin 1 (KD2), expressing FLAG-tagged mouse γ-tubulin 1 (Tubg1-FLAG), mouse γ-tubulin 2 (Tubg2-FLAG) or human γ-tubulin 2 (TUBG2-FLAG). Immunoblots of whole cell lysates probed with antibodies to γ-tubulin (γ-Tb), FLAG and GAPDH (loading control). Arrowhead indicates the position of endogenous γ-tubulin.
(TIF)

Figure S4 γ-Tubulin 2 rescues mitotic spindle organization and function in γ-tubulin 1-depleted cells. U2OS cells depleted of γ-tubulin 1 and expressing FLAG-tagged mouse γ-tubulin 1 (a, d; Tubg1-FLAG), mouse γ-tubulin 2 (b, e; Tubg2-FLAG) or human γ-tubulin 2 (c, f; TUBG2-FLAG). Cells were stained for FLAG (red) and β-tubulin (green). DNA was stained with DAPI (blue). Final images were made by maximum intensity projection of 30–40 deconvolved confocal z-sections spaced at 0.125 μm. Scale bars 5 μm.
(TIF)

Figure S5 Depletion of γ-tubulin 1 in U2OS cells by shRNA. Cells transfected with empty pLKO.1 vector (Control), TUBG1 shRNA expressing vectors p9396sh (KD1) or p120194sh (KD2). (A) Immunoblots of whole cell lysates probed with antibodies to γ-tubulin (γ-Tb) and GAPDH (loading control). (B)

Immunofluorescence staining with antibody to γ-tubulin (red) and with DAPI (blue). Fluorescence images of cells stained for γ-tubulin were captured under identical conditions and processed in exactly the same manner. Scale bar 20 μm.
(TIF)

Figure S6 Immunoblot analysis of U2OS cells in phenotypic rescue experiments with TagRFP-tagged γ-tubulins. U2OS-EB1 cells with depleted γ-tubulin 1 (KD2; shRNA) or negative control cells (NC; pLKO.1), expressing TagRFP, tagged mouse γ-tubulin 1 (Tubg1-TagRFP) or tagged human γ-tubulin 2 (TUBG2-TagRFP). Immunoblots of whole cell lysates probed with antibodies to γ-tubulin (γ-Tb) and GAPDH (loading control). Arrowhead indicates the position of endogenous γ-tubulin.
(TIF)

Figure S7 γ-Tubulin 2 rescues microtubule formation in γ-tubulin 1-depleted cells during interphase. Time-lapse imaging of U2OS-EB1 cells for quantitative evaluation of microtubule (+) end dynamics. Cells with depleted γ-tubulin 1 (KD2) expressing either mouse γ-tubulin 1 (pmTubg1-TagRFP) or human γ-tubulin 2 (phTUBG2-TagRFP). Single frame coloured images Fig 5c and Fig. 5d were separated to red and green channels for a better evaluation of γ-tubulin-TagRFP fusions (red) and EB1-GFP (green). White arrows mark MTOCs.
(TIF)

Figure S8 Comparison of γ-tubulin 2 expression in mouse brain and cell lines. Expression of gene for γ-tubulin 2 (Tubg2) in neuroblastoma (Neuro2a), bone marrow mast cells (BMMC), embryonal fibroblasts (3T3) and embryonic carcinoma cells (P19) relative to the level in brain. Data are presented as mean fold change (columns) with individual samples displayed (diamonds). Three biological replicates were quantified twice under identical conditions. *, undetectable level in P19 cells.
(TIF)

Table S1 Sequence alignments of human and mouse γ-tubulins.
(PDF)

Table S2 Multiple sequence alignment of carboxy-terminal domains of mammalian γ-tubulins.
(PDF)

Table S3 Sequences of primers used for RT-qPCR analysis of mouse genes.
(PDF)

Text S1 Thermocycling parameters at quantitative PCR.
(PDF)

Author Contributions

Conceived and designed the experiments: SV ED PD. Performed the experiments: SV MČ VS TS ED VV MF. Analyzed the data: SV VS TS ED PD. Wrote the paper: SV PD.

References

1. Oakley BR, Oakley CE, Yoon Y, Jung M (1990) γ-Tubulin is a component of the spindle pole body that is essential for microtubule function in *Aspergillus nidulans*. Cell 61: 1289–1301.

2. Stearns T, Evans L, Kirschner M (1991) γ-Tubulin is highly conserved component of the centrosome. Cell 65: 825–836.

3. Joshi HC, Palacios MJ, McNamara L, Cleveland DW (1992) γ-Tubulin is a centrosomal protein required for cell cycle-dependent microtubule nucleation. Nature 356: 80–83.

4. Wiese C, Zheng Y (2006) Microtubule nucleation: gamma-tubulin and beyond. J Cell Sci 119: 4143–4153.

5. Raynaud-Messina B, Merdes A (2007) γ-Tubulin complexes and microtubule organization. Curr Opin Cell Biol 19: 24–30.

6. Moritz M, Braunfeld MB, Guenebaut V, Heuser J, Agard DA (2000) Structure of the γ-tubulin ring complex: a template for microtubule nucleation. Nat Cell Biol 2: 365–370.

7. Kollman JM, Polka JK, Zelter A, Davis TN, Agard DA (2010) Microtubule nucleating γ-TuSC assembles structures with 13-fold microtubule-like symmetry. Nature 466: 879–882.

8. Lüders J, Stearns T (2007) Microtubule-organizing centres: a re-evaluation. Nat Rev Mol Cell Biol 8: 161–167.

9. Hořejší B, Vinopal S, Sládková V, Dráberová E, Sulimenko V, et al. (2011) Nuclear γ-tubulin associates with nucleoli and interacts with tumor suppressor protein C53. J Cell Physiol 227: 367–382.

10. Moudjou M, Bordes N, Paintrand M, Bornens M (1996) γ-Tubulin in mammalian cells: the centrosomal and the cytosolic forms. J Cell Sci 109: 875–887.

11. Haren L, Remy MH, Bazin I, Callebaut I, Wright M, et al. (2006) NEDD1-dependent recruitment of the γ-tubulin ring complex to the centrosome is necessary for centriole duplication and spindle assembly. J Cell Biol 172: 505–515.

12. Dammermann A, Maddox PS, Desai A, Oegema K (2008) SAS-4 is recruited to a dynamic structure in newly forming centrioles that is stabilized by the gamma-tubulin-mediated addition of centriolar microtubules. J Cell Biol 180: 771–785.

13. Zimmerman S, Chang F (2005) Effects of γ-tubulin complex proteins on microtubule nucleation and catastrophe in fission yeast. Mol Biol Cell 16: 2719–2733.

14. Cuschieri L, Miller R, Vogel J (2006) Gamma-tubulin is required for proper recruitment and assembly of Kar9-Bim1 complexes in budding yeast. Mol Biol Cell 17: 4420–4434.

15. Bouissou A, Verollet C, Sousa A, Sampaio P, Wright M, et al. (2009) γ-Tubulin ring complexes regulate microtubule plus end dynamics. J Cell Biol 187: 327–334.

16. Nayak T, Edgerton-Morgan H, Horio T, Xiong Y, De Souza CP, et al. (2010) Gamma-tubulin regulates the anaphase-promoting complex/cyclosome during interphase. J Cell Biol 190: 317–330.

17. Rodriguez AS, Batac J, Killilea AN, Filopei J, Simeonov DR, et al. (2008) Protein complexes at the microtubule organizing center regulate bipolar spindle assembly. Cell Cycle 7: 1246–1253.

18. Liu B, Joshi HC, Wilson TJ, Silflow CD, Palevitz BA, et al. (1994) γ-Tubulin in Arabidopsis: gene sequence, immunoblot, and immunofluorescence studies. Plant Cell 6: 303–314.

19. Ruiz F, Beisson J, Rossier J, Dupuis-Williams P (1999) Basal body duplication in Paramecium requires gamma-tubulin. Current Biology 9: 43–46.

20. Tan M, Heckmann K (1998) The two gamma-tubulin-encoding genes of the ciliate Euplotes crassus differ in their sequences, codon usage, transcription initiation sites and poly(A) addition sites. Gene 210: 53–60.

21. Wilson PG, Zheng Y, Oakley CE, Oakley BR, Borisy GG, et al. (1997) Differential expression of two γ-tubulin isoforms during gametogenesis and development in *Drosophila*. Dev Biol 184: 207–221.

22. Wise DO, Krahe R, Oakley BR (2000) The γ-tubulin gene family in humans. Genomics 67: 164–170.

23. Yuba-Kubo A, Kubo A, Hata M, Tsukita S (2005) Gene knockout analysis of two γ-tubulin isoforms in mice. Develop Biol 282: 361–373.

24. Carson AR, Scherer SW (2009) Identifying concerted evolution and gene conversion in mammalian gene pairs lasting over 100 million years. BMC Evol Biol 9: 156.

25. Khodjakov A, Rieder CL (1999) The sudden recruitment of γ-tubulin to the centrosome at the onset of mitosis and its dynamic exchange throughout the cell cycle, do not require microtubules. J Cell Biol 146: 585–596.

26. Piehl M, Tulu US, Wadsworth P, Cassimeris L (2004) Centrosome maturation: Measurement of microtubule nucleation throughout the cell cycle by using GFP-tagged EB1. Proc Natl Acad Sci USA 101: 1584–1588.

27. Piko L, Clegg KB (1982) Quantitative changes in total RNA, total poly(A), and ribosomes in early mouse embryos. Dev Biol 89: 362–378.

28. Schultz RM, Wassarman PM (1977) Biochemical studies of mammalian oogenesis: Protein synthesis during oocyte growth and meiotic maturation in the mouse. J Cell Sci 24: 167–194.

29. Sellens MH, Stein S, Sherman MI (1981) Protein and free amino acid content in preimplantation mouse embryos and in blastocysts under various culture conditions. J Reprod Fertil 61: 307–315.

30. Guillet V, Knibiehler M, Gregory-Pauron L, Remy MH, Chemin C, et al. (2011) Crystal structure of gamma-tubulin complex protein GCP4 provides insight into microtubule nucleation. Nat Struct Mol Biol 18: 915–919.

31. Lüders J, Patel UK, Stearns T (2006) GCP-WD is a γ-tubulin targeting factor required for centrosomal and chromatin mediated microtubule nucleation. Nature Cell Biol 8: 137–147.

32. Uehara R, Nozawa RS, Tomioka A, Petry S, Vale RD, et al. (2009) The augmin complex plays a critical role in spindle microtubule generation for mitotic progression and cytokinesis in human cells. Proc Natl Acad Sci U S A 106: 6998–7003.

33. Uehara R, Goshima G (2010) Functional central spindle assembly requires de novo microtubule generation in the interchromosomal region during anaphase. J Cell Biol 191: 259–267.

34. Hutchins JR, Toyoda Y, Hegemann B, Poser I, Heriche JK, et al. (2010) Systematic analysis of human protein complexes identifies chromosome segregation proteins. Science 328: 593–599.

35. Hendrickson TW, Yao J, Bhadury S, Corbett AH, Joshi HC (2001) Conditional mutations in gamma-tubulin reveal its involvement in chromosome segregation and cytokinesis. Mol Biol Cell 12: 2469–2481.

36. Lynch M, Force A (2000) The probability of duplicate gene preservation by subfunctionalization. Genetics 154: 459–473.

37. Lam EW, Glassford J, Banerji L, Thomas NS, Sicinski P, et al. (2000) Cyclin D3 compensates for loss of cyclin D2 in mouse B-lymphocytes activated via the antigen receptor and CD40. J Biol Chem 275: 3479–3484.

38. Kafri R, Levy M, Pilpel Y (2006) The regulatory utilization of genetic redundancy through responsive backup circuits. Proc Natl Acad Sci U S A 103: 11653–11658.

39. DeLuna A, Springer M, KIrschner MW, Kishony R (2010) Need-based up-regulation of protein levels in response to deletion of their duplicate genes. PLoS Biol 8: e1000347.

40. Katsetos CD, Reddy G, Dráberová E, Šmejkalová B, Del Valle L, et al. (2006) Altered cellular distribution and subcellular sorting of γ-tubulin in diffuse astrocytic gliomas and human glioblastoma cell lines. J Neuropathol Exp Neurol 65: 465–477.

41. Loh JK, Lieu AS, Chou CH, Lin FY, Wu CH, et al. (2010) Differential expression of centrosomal proteins at different stages of human glioma. Bmc Cancer 10: 268.

42. Hájková Z, Bugajev V, Dráberová E, Vinopal S, Dráberová L, et al. (2011) STIM1-directed reorganization of microtubules in activated cells. J Immunol 186: 913–923.

43. Mimori-Kiyosue Y, Shiina N, Tsukita S (2004) The dynamic behavior of the APC-binding protein EB1 on the distal ends of microtubules. Curr Biol 10: 865–868.

44. Nováková M, Dráberová E, Schürmann W, Czihak G, Viklický V, et al. (1996) γ-Tubulin redistribution in taxol-treated mitotic cells probed by monoclonal antibodies. Cell Motil Cytoskel 33: 38–51.

45. Dráberová E, Sulimenko V, Kukharskyy V, Dráber P (1999) Monoclonal antibody NF-09 specific for neurofilament protein NF-M. Folia Biol (Prague) 45: 163–165.

46. Laemmli UK (1970) Cleavage of structural proteins during the assembly of the head of bacteriophage T_4. Nature 227: 680–685.

47. Sulimenko V, Sulimenko T, Poznanovic S, Nechiporuk-Zloy V, Böhm JK, et al. (2002) Association of brain γ-tubulins with αβ-tubulin dimers. Biochem J 365: 889–895.

48. Dráber P (1991) Quantitation of proteins in sample buffer for sodium dodecyl sulfate-polyacrylamide gel electrophoresis using colloidal silver. Electrophoresis 12: 453–456.

49. Kukharskyy V, Sulimenko V, Macůrek L, Sulimenko T, Dráberová E, et al. (2004) Complexes of γ-tubulin with non-receptor protein tyrosine kinases Src and Fyn in differentiating P19 embryonal carcinoma cells. Exp Cell Res 298: 218–228.

50. Dráberová E, Dráber P (1993) A microtubule-interacting protein involved in coalignment of vimentin intermediate filaments with microtubules. J Cell Sci 106: 1263–1273.

Supplement

Vinopal S., <u>Černohorská M.</u>, Sulimenko V., Sulimenko T., Vosecká V., Flemr M., Dráberová E. & Dráber, P. γ-Tubulin 2 nucleates microtubule and is downregulated in mouse early embryogenesis. *PloS One*, 7: e29919, 2012

Table S1   Alignments of human and mouse γ-tubulins

γ-Tubulin 1

```
H.s.  MPREIITLQLGQCGNQIGFEFWKQLCAEHGISPEGIVEEFATEGTDRKDVFFYQADDEHYIPRAVLLDLEPRVIHSILNSPYAKLYNPENIYLSEHGGGAGNNWASGFSQGEKIHEDIFD 120
M.m.  MPREIITLQLGQCGNQIGFEFWKQLCAEHGISPEGIVEEFATEGTDRKDVFFYQADDEHYIPRAVLLDLEPRVIHSILNSSYAKLYNPENIYLSEHGGGAGNNWASGFSQGEKIHEDIFD 120
      ****************************************************************************** .**********************************************

H.s.  IIDREADGSDSLEGFVLCHSIAGGTGSGLGSYLLERLNDRYPKKLVQTYSVFPNQDEMSDVVVQPYNSLLTLKRLTQNADCVVVLDNTALNRIATDRLHIQNPSFSQINQLVSTIMSAST 240
M.m.  IIDREADGSDSLEGFVLCHSIAGGTGSGLGSYLLERLNDRYPKKLVQTYSVFPNQDEMSDVVVQPYNSLLTLKRLTQNADCVVVLDNTALNLIATDRLHIQNPSFSQINQLVSTIMSAST 240
      ********************************************************************************************** **********************************

H.s.  TTLRYPGYMNNDLIGLIASLIPTPRLHFLMTGYTPLTTDQSVASVRKTTVLDVMRRLLQPKNVMVSTGRDRQTNHCYIAILNIIQGEVDPTQVHKSLQRIRERKLANFIPWGPASIQVAL 360
M.m.  TTLRYPGYMNNDLIGLIASLIPTPRLHFLMTGYTPLTTDQSVASVRKTTVLDVMRRLLQPKNVMVSTGRDRQTNHCYIAILNIIQGEVDPTQVHKSLQRIRERKLANFIPWGPASIQVAL 360
      ****************************************************************************************************************************

H.s.  SRKSPYLPSAHRVSGLMMANHTSISSLFERTCRQYDKLRKREAFLEQFRKEDMFKDNFDEMDTSREIVQQLIDEYHAATRPDYISWGTQEQ 451
M.m.  SRKSPYLPSAHRVSGLMMANHTSISSLFERTCRQFDKLRKREAFMEQFRKEDIFKDNFDEMDTSREIVQQLIDEYHAATRPDYISWGTQEQ 451
      **********************************:*********:*******:**************************************
```

γ-Tubulin 2

```
H.s.  MPREIITLQLGQCGNQIGFEFWKQLCAEHGISPEGIVEEFATEGTDRKDVFFYQADDEHYIPRAVLLDLEPRVIHSILNSPYAKLYNPENIYLSEHGGGAGNNWASGFSQGEKIHEDIFD 120
M.m.  MPREIITLQLGQCGNQIGFEFWKQLCAEHGISPEGIVEEFATEGTDRKDVFFYQADDEHYIPRAVLLDLEPRVIHSILNSSYAKLYNPENIYLSEHGGGAGNNWGRGFSQGEKIHEDIFD 120
      ****************************************************************************** .*************************** .*************

H.s.  IIDREADGSDSLEGFVLCHSIAGGTGSGLGSYLLERLNDRYPKKLVQTYSVFPYQDEMSDVVVQPYNSLLTLKRLTQNADCVVVLDNTALNRIATDRLHIQNPSFSQINQLVSTIMSAST 240
M.m.  IIDREADGSDSLEGFVLCHSIAGGTGSGLGSYLLERLNDRYPKKLVQTYSVFPNQDEMSDVVVQPYNSLLTLKRLTQNADCVVVLDNTALNRIATDRLHIQNPSFSQINQLVSTIMSAST 240
      **************************************************** *******************************************************************

H.s.  TTLRYPGYMNNDLIGLIASLIPTPRLHFLMTGYTPLTTDQSVASVRKTTVLDVMRRLLQPKNVMVSTGRDRQTNHCYIAILNIIQGEVDPTQVHKSLQRIRERKLANFIPWGPASIQVAL 360
M.m.  TTLRYPGYMNNDLIGLIASLIPTPRLHFLMTGYTPLTTDQSVASVRKTTVLDVMRRLLQPKNVMVSTGRDRQTNHCYIAILNIIQGEVDPTQVHKSLQRIRERKLANFIPWGPASIQVAL 360
      ****************************************************************************************************************************

H.s.  SRKSPYLPSAHRVSGLMMANHTSISSLFESSCQQFDKLRKRDAFLEQFRKEDMFKDNFDEMDRSREVVQELIDEYHAATQPDYISWGTQEQ 451
M.m.  SRKSPYLPSAHRVSGLMMANHTSISSLFESSCQQYDKLWKRGAFLEQFRKEDIFKDNFEEMHRSREVVQELIDEYHAATRPDYISWGTQEQ 451
      *********************************:*** **.**********:*****:**.*******************:**********
```

Table S2. **Multiple sequence alignment of carboxy-terminal domains of mammalian γ-tubulins**

Species	Part of helix H11	Part of helix H12	Accesion number
γ-tubulin 2			
Human (*Homo sapiens*)	(386) SLFESSCQQFDK	(419) DEMDRSREVVQELIDE	NP_057521.1
Chimpanzee (*Pan troglodytes*)	(386) SLFESSCQQFDK	(419) DEMDRSREVVQELIDE	XP_003315538
Mouse (*Mus musculus*)	(386) SLFESSCQQYDK	(419) EEMHRSREVVQELIDE	NP_598789.1
Rat (*Rattus norvegicus*)	(411) SLFESSCQQYDK	(444) EEMDRSREVVQELIDE	NP_001178004.1
Horse (*Equus caballus*)	(386) SLFESSCQQYDK	(419) DELDRSREVVQELIDE	XP_001493749.1
Bat (*Myotis lucifugus*)	(386) SLFESSCQQYDK	(419) DELDRSREVVQELIDE	ENSMLUP00000007140 (Ensembl)
Bovine (*Bos taurus*)	(386) SLFESSCQQYDK	(419) DELDRSREVVQELIDE	NP_001032704.1
Dog (*Canis familiaris*)	(386) SLFESSCQQYDK	(419) DELDTSREVVQELIDE	XP_548085.2
γ-tubulin 1			
Human (*Homo sapiens*)	(386) SLFERTCRQYDK	(419) DEMDTSREIVQQLIDE	NP_001061.2
Chimpanzee (*Pan troglodytes*)	(386) SLFERTCRQYDK	(419) DEMDTSREIVQQLIDE	XP_001162243
Mouse (*Mus musculus*)	(386) SLFERTCRQFDK	(419) DEMDTSREIVQQLIDE	NP_598785.1
Rat (*Rattus norvegicus*)	(386) SLFERTCRQFDK	(419) DEMDTSREIVQQLIDE	NP_665721.1
Horse (*Equus caballus*)	(386) SLFERTCRQYDK	(419) DELDTSREIVQQLIDE	XP_001493897.2
Bat (*Myotis lucifugus*)	(386) SLFERTCRQYDK	(419) DELDTSREIVQQLIDE	ENSMLUP00000015217 (Ensembl)
Bovine (*Bos taurus*)	(386) SLFERTCRQYDK	(419) DELDTSREIVQQLIDE	NP_001069723.1
Dog (*Canis familiaris*)	(386) SLFERTCRQYDK	(419) DELDTSREVVHQLIDE	NP_001003105.1
	**** :*:*:**	:*:. ***:*::****	

Protein sequences of indicated mammalian γ-tubulins were aligned by online version of ClustalW2 (www.ebi.ac.uk/Tools/msa/clustalw2) using default parametres. Only clusters of conserved amino acids located on helix H11 and helix H12 of γ-tubulin are shown. Numbers in brackets indicate the position of the first amino acid in the whole polypeptide chain. Accesion numbers to NCBI or Ensembl databases are provided. An asterisk indicates positions which have one single, fully conserved residue. A colon indicates conservation among groups of strongly similar properties. A period indicates conservation among groups of weakly similar properties. Conserved γ-tubulin 2-specific amino acids are highlighted.

Table S3.   **Sequences of primers used for RT-qPCR analysis of mouse genes**

Name	Sequence	Amplicon length
Tubg1, fwd	5'-GCCACACGGCCAGACTATAT-3'	131 bp
Tubg1, rev	5'-TCCCTGATCTGTGCTCCGAG-3'	
Tubg2, fwd	5'-GAGGAGATGCACAGATCGAGG-3'	140 bp
Tubg2, rev	5'-GGACTGTGCTTCTTGTCCAGG-3'	
Tubgcp2, fwd	5'-CGGGCTTGAGCTCAGACACAGTTT-3'	220 bp
Tubgcp2, rev	5'-GGCGGCCACAGGGAGGATTC-3'	
Tubgcp5, fwd	5'-TGTCGTCCGGGCATCTCACCT-3'	185 bp
Tubgcp5, rev	5'-TCCCTTGCGCCGTCCCATAG-3'	
Ppia, fwd	5'-CGCGTCTCCTTCGAGCTGTTTG-3'	150 bp
Ppia, rev	5'-TGTAAAGTCACCACCCTGGCACAT-3'	
Gadph, fwd	5'-AACTTTGGCATTGTGGAAGG-3'	68 bp
Gapdh, rev	5'-ATCCACAGTCTTCTGGGTGG-3'	

Text S1   Thermocycling parameters at quantitative PCR

Data presented in Fig. 7 and Fig. S7 were obtained in the LightCycler® 480 (Roche) using the following thermocycling parameters: initial denaturation - 95°C/5 min; cycling - 45 cycles.

Target temperature	Fluorescence acquisition mode	Hold	Ramp Rate
95°C	None	10 s	4.8°C/s
60°C	None	20 s	2.5°C/s
72°C	Single	20 s	4.8°C/s

Melting curve

Target temperature	Fluorescence acquisition mode	Hold	Ramp Rate	Acquisitions #
95°C	None	10 s	4.8°C/s	X
60°C	None	20 s	2.5°C/s	X
72°C	Continuous	X	0.06°C/s	10/1°C
40°C	None	40 s	2.5°C/s	X

Cp values of all samples were determined in LightCycler® 480 Software, release 1.5.0, by the module "Abs quant/2nd Derivative Max". Melting curves were analyzed in the module "Melting curve genotyping". Only samples with the correct melting and amplification curves were further evaluated. PCR efficiencies (E) for probed genes were calculated from calibration curves by the LightCycler® 480 Software. Calculation of the normalized relative quantity (NRQ) of evaluated transcripts was based on the following formula [1]:

$$NRQ = \frac{E_{goi}^{\Delta Cp,goi}}{\sqrt[f]{\prod_{0}^{f} E_{ref_0}^{\Delta Cp,ref_0}}}$$

taking into account different PCR efficiencies of the gene of interest (goi) and multiple reference genes (ref) used for normalization.

Expression of mouse hypoxanthine guanine phosphoribosyl transferase (*Hprt*, NM_013556), mouse peptidylprolyl isomerase A (*Ppia*, NM_008907) and mouse glyceraldehyde-3-phosphate dehydrogenase (*Gapdh*, NM_008084) was determined and their average expression stability (M) calculated as described previously [2]. *Hprt* and *Ppia* are considered to be suitable house-keeping genes during mouse early embryogenesis [3]. However, *Hprt* was excluded from internal control gene set, because it was the least stable gene in the analyzed sample collection. Thus, geometric mean of *Ppia* and *Gapdh* expression was used for normalization.

References

1. Hellemans J, Mortier G, De Paepe A, Speleman F, Vandesompele J (2007) qBase relative quantification framework and software for management and automated analysis of real-time quantitative PCR data. Genome Biol 8: R19.

2. Vandesompele J, De Preter K, Pattyn F, Poppe B, Van Roy N et al. (2002) Accurate normalization of real-time quantitative RT-PCR data by geometric averaging of multiple internal control genes. Genome Biol 3: RESEARCH0034.

3. Mamo S, Gal AB, Bodo S, Dinnyes A (2007) Quantitative evaluation and selection of reference genes in mouse oocytes and embryos cultured in vivo and in vitro. BMC Dev Biol 7: 14.

Figure S1. Exogenous γ-tubulin 2 locates to centrosomes. Human U2OS cells expressing FLAG-tagged mouse γ-tubulin 1 (a-d, Tubg1-FLAG), mouse γ-tubulin 2 (e-h, Tubg2-FLAG), human γ-tubulin 1 (i-l, TUBG1-FLAG) and human γ-tubulin 2 (m-p, TUBG2-FLAG) were stained for FLAG (red) and pericentrin (green). DNA was stained with DAPI (blue). Final images were made by maximum intensity projection of 3 deconvolved z-sections spaced at 0.25 μm. Scale bar 10 μm.

Figure S2. Coimmunoprecipitation of human γ-tubulins with GCP2 and GCP4 proteins. Extracts from HEK cells expressing FLAG-tagged human γ-tubulin 1 (TUBG1-FLAG), human γ-tubulin 2 (TUBG2-FLAG) or control mouse Fyn (Fyn-FLAG) were immunoprecipitated with antibodies to FLAG or GCP2, and blots were probed with antibodies to FLAG, GCP2, GCP4 and γ-tubulin (c-Tb). Extracts (1), immunoprecipitated proteins (2), protein A without antibodies incubated with extracts (3), immobilized antibodies not incubated with extracts (4). Arrowheads indicate the positions of exogenous γ-tubulins.
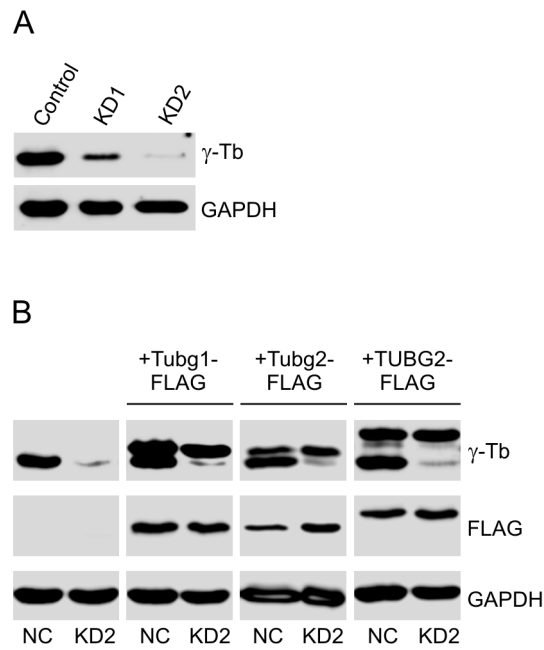
Figure S3. Immunoblot analysis of U2OS cells in phenotypic rescue experiments with FLAG-tagged γ-tubulins. (A) Immunoblot analysis of whole cell extracts from cells transfected with negative control (Control) or γ-tubulin specific siRNAs (KD1 and KD2). Staining with antibodies to γ-tubulin (γ-Tb) and GAPDH. (B) Cells with depleted c-tubulin 1 (KD2), expressing FLAG-tagged mouse γ-tubulin 1 (Tubg1-FLAG), mouse γ-tubulin 2 (Tubg2-FLAG) or human γ-tubulin 2 (TUBG2-FLAG). Immunoblots of whole cell lysates probed with antibodies to γ-tubulin (γ-Tb), FLAG and GAPDH (loading control). Arrowhead indicates the position of endogenous γ-tubulin.

Figure S4. γ-Tubulin 2 rescues mitotic spindle organization and function in γ-tubulin 1-depleted cells. U2OS cells depleted of γ-tubulin 1 and expressing FLAG-tagged mouse γ-tubulin 1 (a, d; Tubg1-FLAG), mouse γ-tubulin 2 (b, e; Tubg2-FLAG) or human γ-tubulin 2 (c, f; TUBG2-FLAG). Cells were stained for FLAG (red) and β-tubulin (green). DNA was stained with DAPI (blue). Final images were made by maximum intensity projection of 30–40 deconvolved confocal z-sections spaced at 0.125 μm. Scale bars 5 μm.

Figure S5. Depletion of γ-tubulin 1 in U2OS cells by shRNA. Cells transfected with empty pLKO.1 vector (Control), TUBG1 shRNA expressing vectors p9396sh (KD1) or p120194sh (KD2). (A) Immunoblots of whole cell lysates probed with antibodies to γ-tubulin (γ-Tb) and GAPDH (loading control). (B) Immunofluorescence staining with antibody to γ-tubulin (red) and with DAPI (blue). Fluorescence images of cells stained for γ-tubulin were captured under identical conditions and processed in exactly the same manner. Scale bar 20 μm.

Figure S6. Immunoblot analysis of U2OS cells in phenotypic rescue experiments with TagRFP-tagged γ-tubulins. U2OS-EB1 cells with depleted γ-tubulin 1 (KD2; shRNA) or negative control cells (NC; pLKO.1), expressing TagRFP, tagged mouse γ-tubulin 1 (Tubg1-TagRFP) or tagged human γ-tubulin 2 (TUBG2-TagRFP). Immunoblots of whole cell lysates probed with antibodies to γ-tubulin (γ-Tb) and GAPDH (loading control). Arrowhead indicates the position of endogenous γ-tubulin.

Figure S7. γ-Tubulin 2 rescues microtubule formation in γ-tubulin 1-depleted cells during interphase. Time-lapse imaging of U2OS-EB1 cells for quantitative evaluation of microtubule (+) end dynamics. Cells with depleted γ-tubulin 1 (KD2) expressing either mouse γ-tubulin 1 (pmTubg1-TagRFP) or human γ-tubulin 2 (phTUBG2-TagRFP). Single frame coloured images Fig 5c and Fig. 5d were separated to red and green channels for a better evaluation of c-tubulin-TagRFP fusions (red) and EB1-GFP (green). White arrows mark MTOC
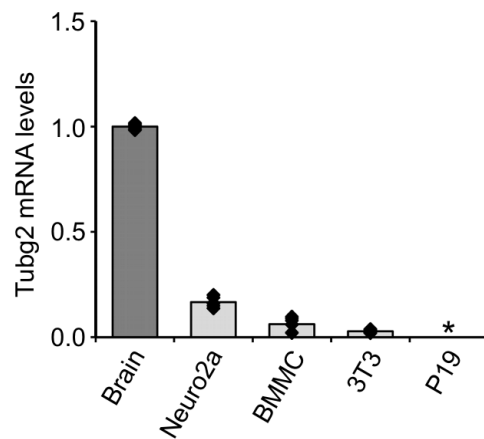
Figure S8. Comparison of γ-tubulin 2 expression in mouse brain and cell lines.
Expression of gene for γ-tubulin 2 (Tubg2) in neuroblastoma (Neuro2a), bone marrow mast cells (BMMC), embryonal fibroblasts (3T3) and embryonic carcinoma cells (P19) relative to the level in brain. Data are presented as mean fold change (columns) with individual samples displayed (diamonds). Three biological replicates were quantified twice under identical conditions. *, undetectable level in P19 cells.

VI.2.

Sulimenko V., Hájková Z., <u>Černohorská M.</u>, Sulimenko T., Sládková V., Dráberová L., Vinopal S., Dráberová E. & Dráber, P. Microtubule nucleation in mouse bone marrow-derived mast cells is regulated by the concerted action of GIT1/βPIX proteins and calcium. *J Immunol*, **194**: 4099-4011, 2015

Microtubule Nucleation in Mouse Bone Marrow–Derived Mast Cells Is Regulated by the Concerted Action of GIT1/βPIX Proteins and Calcium

Vadym Sulimenko,* Zuzana Hájková,*,† Markéta Černohorská,*,† Tetyana Sulimenko,* Vladimíra Sládková,* Lubica Dráberová,‡ Stanislav Vinopal,* Eduarda Dráberová,* and Pavel Dráber*

Ag-mediated activation of mast cells initiates signaling events leading to Ca²⁺ response, release of allergic mediators from cytoplasmic granules, and synthesis of cytokines and chemokines. Although microtubule rearrangement during activation has been described, the molecular mechanisms that control their remodeling are largely unknown. Microtubule nucleation is mediated by complexes that are formed by γ-tubulin and γ-tubulin complex proteins. In this study, we report that, in bone marrow–derived mast cells (BMMCs), γ-tubulin interacts with p21-activated kinase interacting exchange factor β (βPIX) and G protein–coupled receptor kinase-interacting protein (GIT)1. Microtubule regrowth experiments showed that the depletion of βPIX in BMMCs stimulated microtubule nucleation, whereas depletion of GIT1 led to the inhibition of nucleation compared with control cells. Phenotypic rescue experiments confirmed that βPIX and GIT1 represent negative and positive regulators of microtubule nucleation in BMMCs, respectively. Live-cell imaging disclosed that both proteins are associated with centrosomes. Immunoprecipitation and pull-down experiments revealed that an enhanced level of free cytosolic Ca²⁺ affects γ-tubulin properties and stimulates the association of GIT1 and γ-tubulin complex proteins with γ-tubulin. Microtubule nucleation also was affected by Ca²⁺ level. Moreover, in activated BMMCs, γ-tubulin formed complexes with tyrosine-phosphorylated GIT1. Further experiments showed that GIT1 and βPIX are involved in the regulation of such important physiological processes as Ag-induced chemotaxis and degranulation. Our study provides for the first time, to our knowledge, a possible mechanism for the concerted action of tyrosine kinases, GIT1/βPIX proteins, and Ca²⁺ in the propagation of signals leading to the regulation of microtubule nucleation in activated mast cells. *The Journal of Immunology*, 2015, 194: 4099–4111.

M ast cells play a crucial role in allergy, as well as in innate and adaptive immune responses. They express plasma membrane–associated high-affinity IgERs (FcεRIs), the

*Department of Biology of Cytoskeleton, Institute of Molecular Genetics, Academy of Sciences of the Czech Republic, CZ-142 20 Prague 4, Czech Republic; †Department of Cell Biology, Faculty of Science, Charles University Prague, CZ-128 43 Prague 2, Czech Republic; and ‡Department of Signal Transduction, Institute of Molecular Genetics, Academy of Sciences of the Czech Republic, CZ-142 20 Prague 4, Czech Republic

aggregation of which triggers mast cell activation, resulting in degranulation, the release of proinflammatory mediators, and the production of various cytokines. The first step in FcεRI signaling is tyrosine phosphorylation of the FcεRI β- and γ-subunits by the Src family nonreceptor kinase Lyn. This is followed by enhanced activity of tyrosine kinase Syk and the phosphorylation of transmembrane adaptors, which organize and coordinate further signals, resulting in a Ca²⁺ efflux from the endoplasmic reticulum (ER). Depletion of Ca²⁺ from the ER lumen induces Ca²⁺ influx across the plasma membrane, leading to enhancement of the free cytoplasmic Ca²⁺ concentration, a step that is important in further signaling events (1).

Microtubules, built up from αβ-tubulin heterodimers, are important for mast cell degranulation, because the movement of secretory granules depends on intact microtubules (2, 3), and compounds inhibiting tubulin polymerization suppress degranulation (4). It was reported that FcεRI aggregation leads to reorganization of microtubules (3, 5) and that the influx of Ca²⁺ plays a decisive role in microtubule remodeling (6, 7). An important role in Ca²⁺ influx was reported for stromal-interacting protein 1 (STIM1), the Ca²⁺ sensor in ER that associates with the end binding protein 1 located on the tips of growing microtubules (8). Depletion of STIM1 resulted in the inhibition of microtubule reorganization in stimulated cells (6). Although these data point to the necessity of the microtubule network for mast cell degranulation, the molecular mechanisms responsible for microtubule reorganization in activated mast cells are still largely unknown. The role of Ca²⁺ in this process is also unclear.

In cells, microtubules are dominantly nucleated from centrosomes or the other microtubule-organizing centers. One of the key

components for microtubule nucleation is γ-tubulin (9), a highly conserved member of the tubulin superfamily. In cytosol, γ-tubulin exists as a γ-tubulin ring complex (γTuRC; with size ∼2.2 MDa) comprising γ-tubulin small complexes (∼280 kDa), composed of two molecules of γ-tubulin, one molecule of γ-tubulin complex protein (GCP)2, one molecule of GCP3, and some other proteins (10). Cumulative data indicate that protein tyrosine kinases phosphorylate γ-tubulin or associated proteins and, in this way, modulate γ-tubulin functions (5, 11, 12). The significance of Src kinases for microtubule nucleation from centrosomes was ascertained by microtubule regrowth experiments (13). Identification of tyrosine kinase substrates that regulate γ-tubulin functions should help to elucidate the mechanisms involved in the regulation of microtubule nucleation.

In this study, we examined the hypothesis that phosphotyrosine (P-Tyr) proteins associated with γ-tubulin modulate microtubule nucleation in activated mast cells. We identified p21-activated kinase (PAK) interacting exchange factor β (βPIX) and G protein–coupled receptor kinase-interacting protein (GIT)1 as signaling proteins that interact with γ-tubulin and associate with centrosomes. GIT1 is phosphorylated on tyrosine in activated cells and interacts with γ-tubulin in a Ca^{2+}-dependent manner. Our data suggest a novel signaling pathway for microtubule rearrangement in mast cells, where tyrosine kinase–activated GIT1 and βPIX work in concert with Ca^{2+} signaling to regulate microtubule nucleation. Through this pathway, Ag-induced signaling pathways leading to chemotaxis and degranulation could be regulated.

Materials and Methods

Reagents

BAPTA-AM, fibronectin, nocodazole, puromycin, ionomycin, and Hygromycin B were from Sigma. IL-3 and stem cell factor were from PeproTech EC. Protein A immobilized on Trisacryl GF-2000 and SuperSignal West Pico Chemiluminescent reagents were bought from Pierce. Protease-inhibitor mixture tablets (Complete EDTA-free) were from Roche Molecular Biochemicals, GFP-trap_A was purchased from ChromoTek, and Ni-NTA-agarose was from QIAGEN. Restriction enzymes were from New England Biolabs, and Glutathione Sepharose 4 Fast Flow was from GE Healthcare Life Sciences. Oligonucleotides were synthesized by East Port.

Abs

The following anti-peptide Abs prepared to human γ-tubulin were used: mouse mAb TU-31 (IgG2b) and mAb TU-30 (IgG1) to the sequence 434–449 (14) and mAb GTU 88 (IgG1; Sigma, cat. no. T6657) to the sequence 38–53. α-Tubulin was detected with rabbit Ab from GeneTex (GTX15246). Rabbit Abs to βPIX (HPA004744), GFP (G1544), GAPDH (G9545), and actin (A2066) were from Sigma. Rabbit Ab to GIT1 (sc-13961) and mAb to GCP4 (IgG1; sc-271876) were from Santa Cruz. Rabbit mAb to GIT1 (ab156001) was from Abcam. Rabbit mAb D11B8 to GIT2 (8072) was from Cell Signaling, and rabbit Ab to tRFP (AB234) was from Evrogen. mAb 4G10 (IgG2b) to P-Tyr conjugated with HRP (16-184) was from Upstate Laboratories, and mAb to 6xHis was from BD Biosciences (San Jose, CA; IgG2b; 8916-1). mAb GCP2-02 (IgG1) to GCP2 protein was described previously (15). Rabbit Ab to nonmuscle myosin H chain (BT-561; Biomedical Technologies) and mAb NF-09 (IgG2a) to neurofilament NF-M protein (16) served as negative controls in the immunoprecipitation experiments. Rabbit Ab to GST was from Dr. Petr Dráber (Institute of Molecular Genetics). The DY488-conjugated anti-rabbit and the DY549-conjugated anti-mouse Abs were from Jackson ImmunoResearch. Secondary HRP-conjugated Abs were from Promega Biotech.

Cell cultures and transfection

Bone marrow–derived mast cells (BMMCs) were isolated from the femurs and tibias of 6–8-wk-old BALB/c mice. All mice were maintained and used in accordance with the Institute of Molecular Genetics guidelines (permit number 12135/2010-17210) and national guidelines (2048/2004-1020). The cells were differentiated in suspension cultures for 6–8 wk, as previously described (6).

Stable cell lines derived from mouse BMMCs and Lyn$^{-/-}$ BMMCs were donated by Dr. M. Hibbs (Ludwig Institute for Cancer Research, Melbourne,

Australia) (17). In this article, the cells are denoted as BMMC lines (BMMCLs) or Lyn$^{-/-}$ BMMCLs. Both the Ca^{2+} response (18) and Ag-induced degranulation (L. Dráberová and P. Dráber, unpublished observations) were decreased in Lyn$^{-/-}$ BMMCLs compared with BMMCLs. Cells were cultured in freshly prepared culture medium (RPMI 1640 supplemented with 20 mM HEPES [pH 7.5], 100 U/ml penicillin, 100 mg/ml streptomycin, 100 mM MEM nonessential amino acids, 1 mM sodium pyruvate, 10% FCS, and 10% WEHI-3 cell supernatant as a source of IL-3). In some cases, cells were cultivated for 30 min in serum-free and Ca^{2+}-free medium to which Ca^{2+} was freshly added to a final concentration of 1.8 mM. Alternatively, cells were incubated with 1 μM ionomycin in the presence or absence of Ca^{2+}. Cells were grown at 37°C in 5% CO_2 in air and passaged every 2 d.

HEK 293-FT (HEK) cells (Promega Biotech) were grown at 37°C in 5% CO_2 in DMEM supplemented with 10% FCS and antibiotics. The cells used for lentivirus production were at passage 4–15. HEK cells were transfected with 17 μg DNA/9-cm tissue culture dish using 51 μg polyethylenimine (Polysciences) and serum-free DMEM. After 24 h, the transfection mixture was replaced with fresh medium supplemented with serum, and cells were incubated for an additional 24 h.

Cell activation

Cells were sensitized with DNP-specific IgE and activated with Ag (DNP-BSA conjugate, 30–40 mol DNP/mol BSA), as described (6). Alternatively, cells were activated by pervanadate. Pervanadate solution was freshly prepared by mixing sodium orthovanadate solution with H_2O_2 to get a 10 mM final concentration of both components. The pervanadate solution was incubated for 15 min at room temperature and then diluted 1:100 in buffered saline solution (6).

DNA constructs

To prepare N-terminally EGFP-tagged human γ-tubulin (*TUBG1*; RefSeq ID: NM_001070.4), pH3-16 plasmid containing the full-length cDNA of human γ-tubulin (19) was digested with EcoRI/BglII restriction enzymes, and the fragment was inserted into pEGFP-C1 (Clontech), resulting in the plasmid pEGFP-hTUBG1_1-451. To prepare truncated forms of EGFP-tagged γ-tubulin, fragments encoding aa regions 1–440, 1–422, and 1–382 were amplified by PCR from the pH3-16 using forward primer 5′-AGTCAAGCTTATGCCGAGGGAAATCATC-3′ and the following reverse primers: 5′-CTAAGATCTCTACCGTGTGGCCGCATG-3′ (aa 1–440); 5′-GTCAGATCTCTAGTCCATCTCATCAAAGTTGTCC-3′ (aa 1–422), and 5′-CAAAGATCTCTAGGTGTGGTTGGCCATCAT-3′ (aa 1–382), respectively. Sites recognized by restriction endonucleases are underlined. PCR products were digested with HindIII/BglII and inserted into pEGFP-C3 (Clontech), resulting in the plasmids pEGFP-hTUBG1_1-440, pEGFP-hTUBG1_1-422, and pEGFP-hTUBG1_1-382, respectively. The C-terminal part of γ-tubulin (aa 362–451) was amplified from pH3-16 using forward 5′-TCGGATCCAGGAAGTCTCCCTACCT-3′ and reverse 5′-TTCTCGAGTCACTGCTCCTGGGTG-3′ primers. The PCR product was digested with BamHI/XhoI and ligated into pGEX-6P-1 (Amersham Biosciences), resulting in the plasmid pGST-hTUBG1_362-451. The shorter C-terminal part of γ-tubulin (aa 378–451) was amplified from pGST-hTUBG1_362-451 using forward 5′-GAATTCGGCCAACCACACCAGC-3′ and reverse 5′-GGATCCTCACTGCTCCTGGGTGC-3′ primers. The C-terminal part of α-tubulin (aa 378–451) was amplified from pGST-hTUBA1B_364-451 (V. Sulimenko, manuscript in preparation) using forward 5′-GAATTCGAGCAACACCACAGCC-3′ and reverse 5′-GGATCCTTAGTATTCCTCTCCTTCTTCC-3′ primers. PCR products were ligated into pCR2.1 (Invitrogen) by TA cloning, and fragments were excised with EcoRI/BamHI and ligated into pEGFP-C1, resulting in the plasmids pEGFP-hTUBG1_378-451 and pEGFP-hTUBA1B_378-451. To prepare N-terminally 6xHis-tagged γ-tubulin, the coding sequence was amplified from pH3-16 using forward 5′-AAGCATGCCGAGGGAAATCATCAC-3′ and reverse 5′-CTAAGCTTTCACTGCTCCTGGGTGC-3′ primers. The PCR product was digested with SphI/HindIII and ligated to pQE-82L (QIAGEN), resulting in the plasmid 6xHis-hTUBG1_1-451. γ-Tubulin fragment (aa 1–225) was amplified from pH3-16 using forward 5′-AAGCATGCCGAGGGAAATCATCAC-3′ and reverse 5′-AATAAGCTTTCAGGAGAAGGATGGGTTC-3′ primers. The PCR product was digested with SphI/HindIII and ligated to pQE-82L (QIAGEN), resulting in the plasmid 6xHis-hTUBG1_1-225. γ-Tubulin fragment (aa 223–451) was amplified from pH3-16 using forward 5′-AATGGTACCTCCTTCTCCCAGATCAAC-3′ and reverse 5′-GATTAAGCTTTCACTGCTCCTGGGTGC-3′ primers. The PCR product was digested with KpnI/HindIII and ligated to pQE-80 (QIAGEN), resulting in the plasmid 6xHis-hTUBG1_223-451. A cassette encoding mouse γ-tubulin fused to TagRFP was digested out from the pmTubg1-TagRFP construct (20) by EcoRI/NotI and ligated to pCDH-CMV-MCS-EF1-puro vector (System Biosciences), resulting in the lentiviral construct pmTubg1-TagRFP-puro.

A cassette encoding mouse GIT1 (mGIT1; *Git1*; RefSeq ID: NM_001004144.1) fused to GFP was amplified from the TurboGFP-tagged *Git1* cDNA ORF clone (MG210556; OriGene Technologies) using forward 5′-GTCTAGAGAGGAGATCTGCCGCCG-3′ and reverse 5′-GCCG-GGAATTCGTTTAAACTCTTTC-3′ primers. The PCR product was ligated into pCR 2.1 by TA cloning, and the fragment was excised with XbaI/EcoRI and ligated into pCDH-CMV-MCS-EF1-puro, resulting in the lentiviral construct pmGIT1-GFP-puro. The coding sequence of human GIT1 (hGIT1; *GIT1*, transcript variant [tv]1; RefSeq ID: NM_001085454.1) was excised from phGIT1(tv1)-neo (M. Černohorská, manuscript in preparation) with NheI/NotI and ligated into the pCDH-CMV-MCS-EF1-hygro vector (System Biosciences), resulting in the lentiviral construct phGIT1(tv1)-hygro.

A cassette encoding mouse βPIX (mβPIX; *Arhgef7*, tv3; RefSeq ID: NM_017402.4) fused to GFP was amplified from the TurboGFP-tagged *Arhgef7* cDNA ORF clone (MG223397; OriGene Technologies) using forward 5′-TATGCTAGCGTCGACTGGATCCGG-3′ and reverse 5′-GC-CGGGAATTCGTTTAAACTCTTTC-3′ primers. The PCR product was ligated into pCR 2.1 by TA cloning, and the fragment was excised with NheI/EcoRI and ligated into pCDH-CMV-MCS-EF1-puro, resulting in the lentiviral construct pmβPIX(tv3)-GFP-puro. The coding sequence of human βPIX (hβPIX; *ARHGEF7*, tv1; RefSeq ID: NM_003899.3) was excised from GST-hβPIX(tv1) (21) with BamHI/NotI and ligated into the pCDH-CMV-MCS-EF1-hygro vector. For a phenotypic rescue experiment, two silent point mutations (a1620g, t1623g) were generated in this construct by site-directed mutagenesis using the QuikChange II XL Site-Directed Mutagenesis Kit (Stratagene), according to the manufacturer's protocol. The resulting lentiviral construct was named phβPIX(tv1)mut-hygro.

All constructs were verified by sequencing. Plasmid pFYSH2 encoding the GST-tagged SH2 domain of mouse Fyn kinase was described previously (5). The lentiviral vector pCT-Mito-GFP containing cytochrome oxidase c subunit VIII (COX8) tag for visualization of mitochondria was obtained from System Biosciences (CYTO102-PB-1).

Lentiviral infection

Lentiviral infections were done as described previously (6), using HEK packaging cells for virus preparation. The transfection mixture was replaced after 3 d with fresh complete medium containing 5 μg/ml puromycin. Stable selection was achieved by culturing cells for 1–2 wk in the presence of puromycin. In phenotypic rescue experiments, medium containing puromycin was supplemented with 1 mg/ml Hygromycin B, and stable selection was achieved by culturing cells for 1–2 wk. BMMCL stably expressing TagRFP-tagged mouse γ-tubulin (BMMCL-γTb) was prepared by lentiviral transduction with pmTubg1-TagRFP-puro. To follow the distribution of GIT1 or βPIX in living cells, BMMCL-γTb was transduced with pmGIT1-GFP-puro or pmβPIX(tv3)-GFP-puro. After 3 d, cells expressing fluorescently tagged proteins were flow sorted using the BD Influx cell sorter (BD Biosciences). GFP and TagRFP emission was triggered by 488- and 561-nm lasers; fluorescence was detected with 525/50 and 585/20 band-pass filters. Only double-positive cells were used for subsequent live-cell imaging.

RNA interference

A set of five mouse Arhgef7 (National Center for Biotechnology Information RefSeq: NM_001113517.1, NM_001113518.1, NM_017402.4) short hairpin RNA (shRNA) constructs cloned into the lentiviral pLKO.1 vector (TRCN0000110025, TRCN0000110026, TRCN0000110027, TRCN0000110028, and TRCN0000110029) were purchased from Open Biosystems. With the exception of TRCN0000110025, the vectors target all transcript variants of Arhgef7. A set of five murine GIT1 (National Center for Biotechnology Information RefSeq: NM_001004144.1) shRNA constructs cloned into the pLKO.1 vector (TRCN0000106120, TRCN0000106121, TRCN0000106122, TRCN0000106123, and TRCN0000106124) were also purchased from Open Biosystems. Immunoblotting experiments revealed that cells with the greatest reduction in βPIX protein were obtained with TRCN0000110026 (βPIX-KD1) and TRCN0000110027 (βPIX-KD2). Similarly, cells with the greatest reduction in GIT1 protein were obtained with TRCN0000106122 (GIT1-KD1) and TRCN0000106121 (GIT1-KD2). The stable selected cells with the greatest reduction in βPIX or GIT1 were used for additional experiments. Cells transduced with empty lentiviral pLKO.1 vector (Addgene) or pLKO.1 vector containing nontarget shRNA (Sigma) were used as negative controls.

Preparation of cell extracts

Whole-cell extracts for SDS-PAGE were prepared by washing the cells in cold HEPES buffer (50 mM HEPES [pH 7.6], 75 mM NaCl, 1 mM MgCl₂, and 1 mM EGTA), solubilizing them in hot SDS sample buffer without bromophenol blue, and boiling for 5 min. When preparing extracts for immunoprecipitation and GST pull-down assays, cells were rinsed twice in

cold HEPES buffer and extracted at a concentration of 15×10^6 cells/ml for 10 min at 4°C with HEPES buffer supplemented with 1% Nonidet P-40 (extraction buffer), protease inhibitor mixture, and phosphatase inhibitors (1 mM Na₃VO₄, 1 mM NaF). The suspension was spun down ($20,000 \times g$, 15 min, 4°C), and supernatant was collected. In some cases, cell lysates were supplemented with CaCl₂ at concentrations ranging from 50 μM to 1.0 mM or with 10 mM EGTA. Alternatively, lysates were supplemented with MgCl₂ or ZnCl₂ at a concentration of 0.8 mM. When preparing extracts for gel-filtration chromatography, cells were extracted at a concentration of 14×10^7 cells/ml. Protein quantification in lysates and SDS-PAGE samples was assessed with a bicinchoninic acid assay and a silver dot assay, respectively (22).

Gel-filtration chromatography

Gel filtration was performed using fast protein liquid chromatography (AKTA-FPLC system; Amersham) on a Superose 6 10/300 GL column (Amersham). Column equilibration and chromatography were performed in an extraction buffer. The column was eluted at 30 ml/h, and 0.5-ml aliquots were collected. Samples for SDS-PAGE were prepared by mixing with 5× concentrated SDS sample buffer. The following molecular mass standards were used: IgM (900 kDa), thyroglobulin (669 kDa), ferritin (440 kDa), catalase (232 kDa), and BSA (66 kDa).

Immunoprecipitation, GST pull-down assay, gel electrophoresis, and immunoblotting

Immunoprecipitation was performed as previously described (23). Cell extracts were incubated with Protein A beads (Pierce, Rockford, IL) saturated with mAb TU-31 (IgG2b) to γ-tubulin, rabbit Ab to GIT1, rabbit Ab to βPIX, rabbit Ab to RFP, rabbit Ab to nonmuscle myosin (negative control), mAb NF-09 (IgG2a; negative control), or immobilized protein A alone. Abs to βPIX, GIT1, and tRFP were used at Ig concentrations of 2, 2, and 5 μg/ml, respectively. Ab to myosin was used at a dilution of 1:100. mAb TU-31 and mAb NF-09, in the form of hybridoma supernatants, were diluted 1:2. GFP-tagged proteins were immunoprecipitated using GFP-trap_A, according to the manufacturer's directions.

For large-scale immunoprecipitation experiments, Lyn⁻/⁻ BMMCLs (total 6×10^8 cells) were activated by pervanadate, as described (6), and resuspended in 15 ml cold extraction buffer supplemented with protease and phosphatase inhibitors. After 10 min of incubation at 4°C, the suspension was centrifuged at $28,000 \times g$ for 15 min at 4°C. Supernatant was incubated with anti-peptide mAb TU-31 to γ-tubulin immobilized on 5 ml Protein A beads overnight at 4°C. After extensive washing in TBST (10 mM Tris-HCl [pH 7.4] 150 mM NaCl, 0.05% Tween 20), immobilized protein A with bound proteins was loaded into a 10-ml (7 × 1.5 cm) column, washed with 70 ml TBST, and eluted with peptide used for immunization (14) at a concentration of 200 μg/ml in TBST. From the 0.5-ml fractions collected, 1-μl aliquots were spotted onto nitrocellulose and probed with anti–P-Tyr mAb conjugated with HRP (dilution 1:30,000), followed by chemiluminescent detection of bound Ab. Fractions containing tyrosine-phosphorylated proteins were collected (total 2 ml) and loaded onto 50 μl pelleted glutathione-Sepharose with bound GST-tagged mouse Fyn-SH2 domain to concentrate the tyrosine-phosphorylated proteins capable of binding this domain. After 3 h of incubation at 4°C and extensive washing, the proteins associated with the domain were dissolved in 50 μl 2× SDS sample buffer and boiled for 5 min.

Preparation and purification of GST-tagged fusion proteins were described previously, as were pull-down assays with whole-cell extracts (23). For comparison of immunoprecipitation and pull-down assays in the presence or absence of Ca²⁺, protein extracts were used at the same protein concentration. Gel electrophoresis and immunoblotting were performed using standard protocols. Preparation, purification, and immobilization of 6xHis-tagged proteins onto Ni-NTA agarose were performed according to the manufacturer's recommendations.

SDS-PAGE and immunoblotting were performed using standard protocols (24). For immunoblotting, mAbs to 6xHis, γ-tubulin (GTU-88), P-Tyr, and GCP4 were diluted 1:50,000, 1:10,000, 1:10,000, and 1:1,000, respectively. mAb to GCP2, in the form of spent culture supernatant, was diluted 1:10. Rabbit Abs to GAPDH, βPIX, GIT1, actin, and GIT2 were diluted 1:50,000, 1:4,000, 1:2,000, 1:2,000, and 1:500, respectively. Rabbit Abs to GST, GFP, and RFP were diluted 1:20,000, 1:5,000, and 1:5,000, respectively. Secondary anti-mouse and anti-rabbit Abs conjugated with HRP were diluted 1:10,000. Bound Abs were detected by SuperSignal West Pico Chemiluminescent reagents (Pierce).

Mass spectrometry

Following large-scale immunoprecipitation and concentration of peptide-eluted samples on the GST-Fyn-SH2 domain, proteins dissolved in SDS sample buffer were separated on preparative 7.5% SDS-PAGE using the

Multigel-Long electrophoretic system (Biometra). Gels were stained by Coomassie Brilliant Blue G-250. The bands of interest were excised from the gel, destained, and digested by trypsin. Extracted peptides were analyzed by a MALDI-FTICR mass spectrometer (APEX-Qe) equipped with a 9.4 tesla superconducting magnet (both from Bruker Daltonics, Billerica, MA) at the Core facility of the Institute of Microbiology, Academy of Sciences of the Czech Republic. The obtained data were processed by Data Analysis 4.0 software (Bruker Daltonics) and searched by the ProFound (PROWL) search engine against the nonredundant database of all known *Mus musculus* proteins.

Degranulation assay

The degree of degranulation was quantified as the release of β-glucuronidase from anti-TNP IgE-sensitized cells activated with Ag (TNP-BSA conjugate, 15–25 mol TNP/mol BSA), using 4-methylumbelliferyl β-D-glucuronide as substrate (25). The total content of the enzyme was evaluated in supernatants from cells lysed by 0.1% Triton X-100.

Chemotaxis assay

The chemotactic response of cells was examined using a 24-well Transwell system with 8-μm-diameter pore size polycarbonate filters (Corning), as described previously (26). TNP-BSA, at a concentration of 250 ng/ml in RPMI 1640, supplemented with 20 mM HEPES and 1% BSA (assay buffer), served as a chemoattractant.

Evaluation of cell proliferation and apoptosis

Cell proliferation was assessed by manual counting of stable cell lines with the greatest reduction in βPIX or GIT1. Cells transduced with empty lentiviral pLKO.1 vector or pLKO.1 vector containing nontarget shRNA (pLKO.1-NT) were used as negative controls. A total of 2×10^5 transfected cells was plated on a 6-cm-diameter petri dish. Cells were counted from 1 to 5 d. Samples were counted in doublets in a total of three independent experiments. Cell viability was evaluated by a trypan blue exclusion test.

One of the classic features of apoptosis is the cleavage of genomic DNA into oligonucleosomal fragments represented by multiples of 180–200 bp. Genomic DNA was isolated from BMMCLs by the QIAamp DNA Mini kit (QIAGEN), according to the manufacturer's directions, and prepared samples were incubated with RNase A (Fermentas) at a final concentration of 10 μg/ml for 1 h at 37°C. DNA integrity was evaluated by electrophoresis in 1.5% agarose gel in 40 mM Tris-acetate/1 mM EDTA buffer. For staining, we used GelRed Nucleic Acid Gel Stain (Biotium). GeneRuler 1 kb Plus DNA Ladder 75 to 20,000 bp (Thermo Scientific) was used for DNA sizing. Apoptosis was induced in control BMMCLs by treating cells with 10 μM 17-(allylamino)-17-demethoxygeldanamycin (Sigma) for 24 h.

Microtubule regrowth

Microtubule regrowth from centrosomes was followed in a nocodazole-washout experiment. BMMCLs in complete medium were overlaid on fibronectin-coated coverslips (6) and allowed to attach for 1 h at 37°C. Cells were then treated with nocodazole at a final concentration of 10 μM for 50 min at 37°C to depolymerize microtubules. Cells were washed with medium precooled to 4°C (3 × 5 min each) to remove the drug, and microtubule regrowth was allowed for 1–6 min at 26°C. To test the effect of pervanadate, cells treated with 10 μM nocodazole for 40 min at 37°C were transferred into medium containing 10 μM nocodazole and freshly prepared pervanadate. After 10 min of incubation at 37°C, cells were washed (2 × 2 min each) with precooled medium, and microtubule regrowth was allowed in the presence of pervanadate. Samples were fixed in cold methanol, air-dried, and washed in PBS before immunostaining (27). In some cases, nocodazole-washout experiments were performed in the absence of both extracellular and intracellular Ca^{2+}. Cells in complete medium were treated with nocodazole (10 μM, 40 min, at 37°C), transferred into Ca^{2+}- and serum-free medium supplemented with 5 μM BAPTA-AM and 10 μM nocodazole, and incubated for 10 min at 37°C to deplete intracellular Ca^{2+}. After washing in cold Ca^{2+}- and serum-free medium to remove the drug, microtubule regrowth was allowed for 1–6 min at 26°C in Ca^{2+}- and serum-free medium containing 5 μM BAPTA-AM. The nocodazole-washout experiment also was performed in the absence of extracellular Ca^{2+} only. In control experiments, Ca^{2+}- and serum-free medium was substituted for serum-free medium with 1.8 mM Ca^{2+}.

Immunofluorescence microscopy

Immunofluorescence staining was performed as described (27). To visualize centrosomes and microtubules in fixed cells, coverslips were incubated with mAb TU-30 (spent culture supernatant diluted 1:5) and rabbit Ab to α-tubulin (diluted 1:150). Anti-mouse DY549-conjugated Ab was diluted

1:800, and anti-rabbit DY488-conjugated Ab was diluted 1:300. The preparations were mounted in MOWIOL 4-88 (Calbiochem), supplemented with 4,6-diamidino-2-phenylindole (Sigma), and examined on an Olympus Scan^R system (Olympus) equipped with Acquisition Scan^R program and an oil-immersion objective 60×/1.4 NA. Huygens Deconvolution Software (Scientific Volume Imaging) was used for preparation of immunofluorescence figures.

Quantification of the microtubule regrowth assay was performed on a large number of cells that were selected automatically and compared with the quantification of cells selected manually to confirm the reliability of the automatic method. In the course of automatic quantification, 36 areas/sample were taken in both fluorescence channels, and optical z-sections were acquired at 0.3-μm steps. Maximum intensity projection of γ-tubulin staining was used to identify the position of centrosomes. The sum of α-tubulin immunofluorescence intensities was generated by Sum Slices projection in ImageJ software (National Institutes of Health). The α-tubulin fluorescent signal near the centrosome was measured in separate concentric circles centered at the centrosome with radii of 1, 1.5, and 2 μm (regions of interest; ROIs). Background fluorescence using circles of corresponding sizes was subtracted from each measurement. Measurements were made using ImageJ. In manually performed analyses, only images of cells with a homogeneous background around the centrosomes were selected. The sum of α-tubulin immunofluorescence intensities was obtained from 11 consecutive frames (0.2-μm steps), with the middle frame chosen with respect to the highest γ-tubulin intensity. For statistical analysis, the two-tailed, unpaired Student t test was used to compare samples and to obtain p values.

Live-cell imaging

BMMCL-γTb expressing mGIT1-GFP, mβPIX-GFP, or GFP-COX8 tags were plated on 35-mm glass-bottom culture dishes (MatTek; P35G-1.5-14-C) precoated with fibronectin (6), and cells were allowed to attach for 1 h at 37°C. Cells were washed and subsequently incubated in medium for live-cell imaging (RPMI 1640 without phenol red, riboflavin, folic acid, pyridoxal, $Fe[NO_3]_3$) supplemented with 20 mM HEPES. Cells were imaged on the Delta Vision Core system (Applied Precision) equipped with a 60×/1.42 NA oil-immersion objective. Optical z-sections were acquired in 0.3-μm steps.

Results

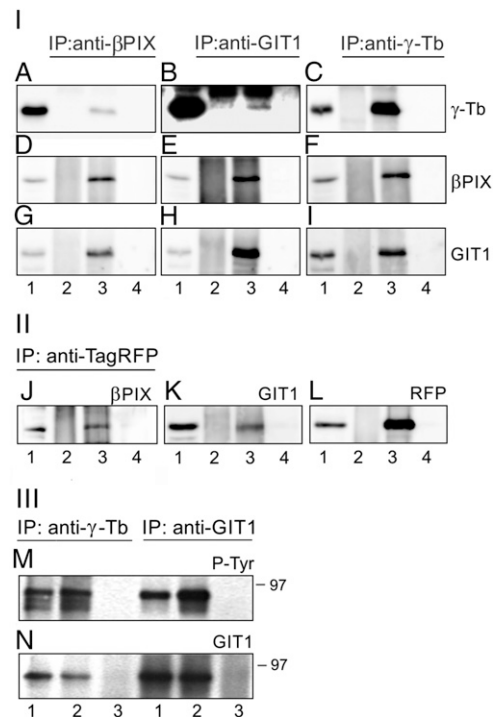### Proteins βPIX and GIT1 interact with γ-tubulin and associate with centrosomes in BMMCLs

We showed previously that, in FcεRI- or pervanadate-activated BMMCLs or Lyn$^{-/-}$ BMMCLs, γ-tubulin interacts with a similar set of tyrosine-phosphorylated proteins (5). In an attempt to identify these proteins, we applied large-scale immunoprecipitation coupled with mass spectrometry (MS). Lysates from pervanadate-activated cells were immunoprecipitated with anti-peptide mAb to γ-tubulin, and the bound proteins were eluted with peptide used for immunization. Eluted proteins were concentrated on the immobilized GST-SH2 domain of Fyn kinase, which effectively binds tyrosine-phosphorylated proteins (23). Bound proteins were separated on SDS-PAGE and subjected to MALDI/MS fingerprint analysis. Because slightly higher recovery of tyrosine-phosphorylated proteins associated with γ-tubulin was observed from activated Lyn$^{-/-}$ BMMCLs (5), we used these cells for MALDI/MS fingerprint analysis. Of the three independent experiments, βPIX (also known as Rho guanine nucleotide exchange factor 7, Arhgef7, β-Pix, COOL-1; gene name *Arhgef7*; Swiss-Prot identifier Q9ES28) was identified three times. A typical example of MS identification is shown in Supplemental Table I.

In cells, βPIX forms complexes with GITs, which are GTPase-activating proteins for the ADP-ribosylation factor family of small GTP-binding proteins (28). Such complexes might serve as scaffolds to bring together signaling molecules affecting various cellular processes, including cytoskeletal organization (29). To ascertain whether βPIX or GIT1 associates with γ-tubulin in Lyn$^{-/-}$ BMMCL cells, immunoprecipitation experiments were performed with Abs to βPIX and GIT1. Immunoblot analysis revealed the coprecipitation of γ-tubulin with both βPIX (Fig. 1A, *lane 3*) and GIT1 (Fig. 1B, *lane 3*). In addition, reciprocal precipitation with Ab to γ-tubulin confirmed an interaction between both βPIX (Fig. 1F, *lane 3*)

and GIT1 (Fig. 1I, *lane 3*) with γ-tubulin. As expected, Ab to βPIX coprecipitated GIT1 (Fig. 1G, *lane 3*), and Ab to GIT1 coprecipitated βPIX (Fig. 1E, *lane 3*). Immunoblot analysis revealed that GIT2 also interacted with γ-tubulin (Supplemental Fig. 1A, *lane 3*). Negative-control mAb of IgG2b class or rabbit polyclonal Ab did not precipitate GIT1, βPIX, or γ-tubulin (Supplemental Fig. 1D). No association of γ-tubulin with βPIX and GIT1 was detected when precipitation with anti-peptide Ab to γ-tubulin was performed in the presence of immunizing peptide (data not shown). Immunoprecipitation experiments also confirmed interactions between γ-tubulin and βPIX, GIT1, or GIT2 in BMMCLs, proving that the association of γ-tubulin with these proteins is not restricted to cells with depleted Lyn kinase (data not shown). To independently confirm the interaction of γ-tubulin with βPIX and GIT1, immunoprecipitation experiments were performed with BMMCL-γTb. Precipitation with anti-RFP Ab revealed the coprecipitation of endogenous βPIX (Fig. 1J, *lane 3*) and GIT1 (Fig. 1K, *lane 3*). Precipitation of γ-tubulin–TagRFP is shown in Fig. 1L (*lane 3*). Immunoblot analysis also revealed that GIT2 was coprecipitated by anti-RFP Ab (Supplemental Fig. 1B, *lane 3*). Multiple phosphorylation sites were identified on hGIT1 (30). To determine whether GIT1 can be phosphorylated on tyrosine in activated BMMCLs or Lyn$^{-/-}$ BMMCLs, as well as whether tyrosine-phosphorylated GIT1 interacts with γ-tubulin, pervanadate-activated cells were precipitated with Abs to γ-tubulin and GIT1. Blots were probed with Abs to P-Tyr and GIT1. Both Abs precipitated P-Tyr proteins from both cell lines (Fig. 1M, *lanes 1, 2*), which were stained with Ab to GIT1 (Fig. 1N, *lanes 1, 2*). Negative-control Abs did not precipitate tyrosine-phosphorylated GIT1 from activated cells (data not shown). Thus, tyrosine-phosphorylated GIT1 from pervanadate-activated cells is capable of interacting with γ-tubulin. Similar, but less profound, results were obtained after activation of the cells by aggregation of FcεRI (data not shown). To decide whether γ-tubulin and βPIX or GIT1 protein appear in the form of complexes, BMMCL extracts were subjected to gel-filtration chromatography on the Superose 6 column. γ-Tubulin was distributed through a large zone in complexes of various sizes. Large complexes of ∼2 MDa could represent γTuRCs. Importantly, βPIX and GIT1 also were present in the complexes, and their distribution partially overlapped with γ-tubulin. In contrast, control actin was only found in low molecular mass fractions (Supplemental Fig. 1C). Immunoprecipitation experiments with anti–γ-tubulin Ab from fractions containing GIT1 and PIX (fractions 24–26 in Supplemental Fig. 1C) revealed the formation of complexes between γ-tubulin and these proteins (data not shown). Isotype controls for immunoprecipitation experiments are shown in Supplemental Fig. 1D.

For the localization of centrosomes in live cells, BMMCL-γTb were used. The TagRFP-tagged γ-tubulin marked centrosomes and properly nucleated microtubules as documented by microtubule staining of mitotic cells (Fig. 2A–C). Because βPIX (tv3) is the most abundant variant in BMMCLs (V. Sládková, unpublished observations), GFP-tagged mβPIX (tv3) was expressed in BMMCL-γTb. Live-cell imaging revealed the association of βPIX with centrosomes of interphase BMMCLs. Moreover, diffuse staining of the cytoplasm was observed (Fig. 2D–F). Similarly, GFP-tagged GIT1 localized to centrosomes, and granular staining in cytoplasm was detected (Fig. 2G–I). Nocodazole treatment did not affect GIT1 localization on the centrosome, indicating no requirement for intact microtubules (data not shown). In control cells expressing GFP-tagged mitochondrial marker, no association of the expressed protein with the centrosome was detected (Fig. 2J–L). Collectively, the data suggest that βPIX and GITs form complexes with γ-tubulin and that βPIX and GIT1 associate with centrosomes in BMMCLs.

FIGURE 1. γ-Tubulin interacts with βPIX and GIT1 in mast cells. (**A–I**) γ-Tubulin coprecipitates with βPIX and GIT1 in Lyn$^{-/-}$ BMMCLs. Extracts were precipitated with Protein A–immobilized Abs specific to βPIX (A, D, and G), GIT1 (B, E, and H), or γ-tubulin (C, F, and I). Blots were probed with Abs to γ-tubulin (γ-Tb), βPIX, or GIT1. Load (*lane 1*), immobilized Abs not incubated with cell extract (*lane 2*), immunoprecipitated proteins (*lane 3*), and protein A without Abs, incubated with cell extracts (*lane 4*). (**J–L**) TagRFP-tagged γ-tubulin associates with βPIX and GIT1 in BMMCLs. Extracts from BMMCL-γTb were precipitated with Protein A–immobilized Abs specific to RFP (J–L). Blots were probed with Abs to βPIX (J), GIT1 (K), and RFP (L). Load (*lane 1*), immobilized Abs not incubated with cell extract (*lane 2*), immunoprecipitated proteins (*lane 3*), and protein A without Abs, incubated with cell extracts (*lane 4*). In (J), one quarter of the load was applied compared with (K) and (L). (**M** and **N**) GIT1 is a substrate for protein tyrosine kinases in activated Lyn$^{-/-}$ BMMCLs and BMMCLs. Extracts from pervanadate-activated Lyn$^{-/-}$ BMMCLs (*lane 1*) or BMMCLs (*lane 2*) were precipitated with Protein A–immobilized Abs specific to γ-tubulin or GIT1. Immobilized Abs not incubated with cell extracts (*lane 3*). Blots were probed with Abs to P-Tyr (M) and GIT1 (N). Lines on the *right* indicate the positions of molecular mass markers (in kDa).

Ca²⁺ level affects γ-tubulin properties and its interaction with GITs and GCPs in BMMCLs

During the immunoprecipitation experiments, we noticed that Ca^{2+} affects the association of γ-tubulin with GITs and GCPs. When BMMCLs were cultivated for 30 min in serum- and Ca^{2+}-free medium to which Ca^{2+} was freshly added to a final concentration of 1.8 mM, more GIT1 (Fig. 3A) or GIT2 (Fig. 3A) coprecipitated with γ-tubulin. Similarly, more GCP2 (Fig. 3A) or GCP4 (Fig. 3A) was associated with γ-tubulin in the presence of Ca^{2+}. No substantial changes in the amount of βPIX associated with γ-tubulin were observed in the presence or absence of Ca^{2+} (Fig. 3A, βPIX), and actin (negative control) did not coprecipitate with γ-tubulin (Fig. 3A, Actin). Interestingly, two protein bands with different electrophoretic mobilities were detected in γ-tubulin immunoprecipitates from extracts containing Ca^{2+}: an upper band with slow mobility and a lower band with fast mobility. Sometimes, three closely spaced γ-tubulin bands were detected in the presence of Ca^{2+}. This was an unexpected finding because no
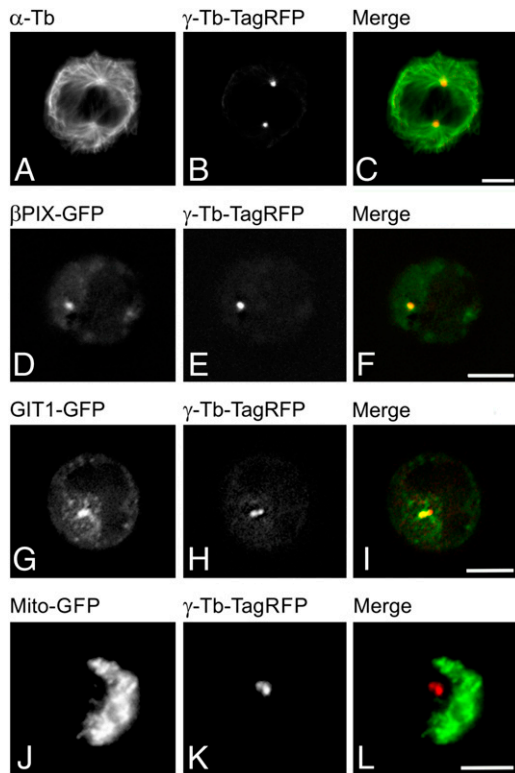
FIGURE 2. Subcellular localization of GFP-tagged βPIX and GIT1 in BMMCLs. Mitotic BMMCL-γTb stained for α-tubulin (**A**) to visualize localization of TagRFP-tagged γ-tubulin (**B**). (**C**) Superposition of images (α-tubulin, green; γ-tubulin, red), methanol-fixed cells. Localization of βPIX-GFP (**D**) and γ-tubulin–TagRFP (**E**) in live BMMCL-γTb cells. (**F**) Superposition of images (βPIX, green; γ-tubulin, red). Localization of GIT1-GFP (**G**) and γ-tubulin–TagRFP (**H**) in live BMMCL-γTb. (**I**) Superposition of images (GIT1, green; γ-tubulin, red). Localization of control mitochondrial Mito-GFP (**J**) and γ-tubulin-TagRFP (**K**) in live BMMCL-γTb. (**L**) Superposition of images (Mito-GFP, green; γ-tubulin, red). In (D)–(L), the best centrosomal plane is shown. Scale bars, 5 μm.

such split in γ-tubulin electrophoretic mobilities was observed in loads (Fig. 3A, γ-Tb). Comparable results from immunoprecipitation experiments were obtained when Ca²⁺ was added to cell extracts. Moreover, Ca²⁺ similarly affected the electrophoretic mobility of γ-tubulin immunoprecipitated from BMMCs (data not shown). Negative-control Abs did not precipitate βPIX, GIT1, GIT2, γ-Tb, GCP2, or GCP4 from lysates containing Ca²⁺ (data not shown).

Immunoprecipitation experiments with Ab to γ-tubulin also were performed with extracts obtained from cells incubated with ionomycin, an effective Ca²⁺ ionophore, in the presence or absence of Ca²⁺. In the absence of Ca²⁺, ionomycin did not affect the mobility of γ-tubulin and coprecipitation of GCP2 and GCP4 with γ-tubulin. However, in the presence of ionophore and Ca²⁺, large amounts of GCP4 coprecipitated with γ-tubulin. Under such conditions the amount of coprecipitated GCP2 increased only slightly, and the amount of modified γ-tubulin was basically unchanged (Supplemental Fig. 1E).

When TagRFP–γ-tubulin was precipitated in the presence of Ca²⁺, slow-migrating electrophoretic variants of tagged γ-tubulin were detected (Fig. 3B, *lane 3*). Together, these data suggest that Ca²⁺ modulates the interaction of γ-tubulin with GITs and GCPs in BMMCLs and that both endogenous and exogenous γ-tubulin concentrated by immunoprecipitation is affected by an increased concentration of Ca²⁺ in BMMCLs.

C-terminal region of γ-tubulin is essential for Ca²⁺-dependent changes in γ-tubulin

To obtain deeper insight into the γ-tubulin region that is sensitive to Ca²⁺, we performed experiments with truncated γ-tubulins. For this, we used human γ-tubulin 1, which shows 99% identity with mouse γ-tubulin 1 (20). First, we immobilized 6xHis-tagged whole-length γ-tubulin (aa 1–451) or its truncated constructs covering aa regions 1–225 and 223–451 on Ni-NTA agarose and incubated them with BMMCL extracts in the presence or absence of Ca²⁺. The shift in electrophoretic mobility of γ-tubulin was observed in the C-terminal part of the molecule (Fig. 4A). When γ-tubulin was incubated with Ca²⁺ in the absence of extract, no mobility shift was observed (Fig. 4A, Control). Next, we prepared EGFP-tagged versions of γ-tubulin truncated from the C-terminal end of molecules containing α-helixes H11 (aa 385–400) and H12 (aa 419–437), which are exposed on the surface of the molecule (Protein Data Bank ID: 3CB2). A schematic diagram of the used constructs is depicted in Fig. 4B. The EGFP-tagged proteins covering γ-tubulin aa regions 1–382, 1–422, 1–440, and 1–451
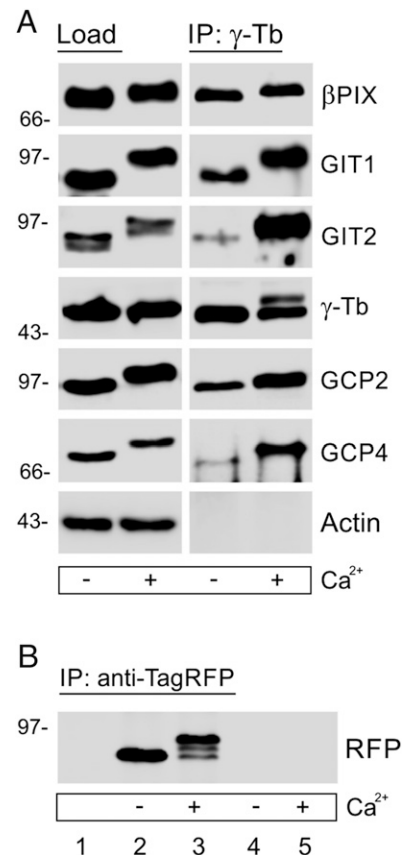
FIGURE 3. Effect of Ca²⁺ on coimmunoprecipitation of proteins with γ-tubulin. (**A**) Ca²⁺ stimulates coprecipitation of GITs and GCPs with γ-tubulin. BMMCLs were preincubated in the presence or absence of 1.8 mM Ca²⁺, and extracts were precipitated with Ab to γ-tubulin immobilized on Protein A. Blots were probed with Abs to βPIX, GIT1, GIT2, γ-tubulin (γ-Tb), GCP2, GCP4, or actin. Note the change in electrophoretic mobility of precipitated γ-tubulin and the higher amount of coprecipitated GIT1, GIT2, GCP2, and GCP4 in the presence of Ca²⁺. (**B**) Ca²⁺ affects the electrophoretic mobility of TagRFP-tagged γ-tubulin. Extracts from BMMCL-γTb were supplemented or not with 0.8 mM Ca²⁺ and precipitated with Ab to RFP immobilized on protein A. Blot was probed with Ab to RFP. Immobilized Ab not incubated with cell extract (*lane 1*), immunoprecipitated proteins (*lanes 2 and 3*), and protein A without Ab, incubated with cell extract (*lanes 4 and 5*). Lines on the *left* indicate the positions of the molecular mass markers (in kDa).

were precipitated from HEK-293 lysates using GFP-trap; after thorough washing, immobilized constructs were incubated with BMMCL extracts in the presence or absence of Ca^{2+}. Although electrophoretic mobilities were basically not affected in truncated γ-tubulins (aa 1–382 or 1–422), a Ca^{2+}-dependent shift in mobility was seen in whole-length γ-tubulin and in truncated γ-tubulin (aa 1–440) (Fig. 4C). When the EGFP-tagged γ-tubulin C-terminal region (aa 378–451) was used, a shift in electrophoretic mobility was detected, whereas the EGFP-tagged C-terminal region of α-tubulin (aa 378–451) was not affected (Fig. 4D). Mg^{2+} or Zn^{2+} ions were not capable of forming γ-tubulin variants; when EGTA was added to deplete Ca^{2+}, the generation of slow-migrating γ-tubulin forms was inhibited. Generation of γ-tubulin electrophoretic variants in the presence of Ca^{2+} also was observed when lysates from BMMCs were used in pull-down experiments (data not shown). Altogether, these findings indicate that the C-terminal region of γ-tubulin (aa 423–451) is essential for Ca^{2+}-dependent changes in γ-tubulin in the presence of BMMCL or BMMC extracts.

Ca^{2+} modulates the interaction of βPIX with the C-terminal region of γ-tubulin

In HEK cells expressing either GFP-tagged whole-length (aa 1–451) or truncated (aa 1–382) γ-tubulin, anti-βPIX and anti-GIT1 Abs coprecipitated GFP-tagged whole-length γ-tubulin. Coprecipitation of the truncated form of γ-tubulin was undetectable or it was substantially lower (Fig. 5A). This indicated that the C-terminal region of γ-tubulin is important for the interaction with βPIX and GIT1. Because Ca^{2+} affected the interactions of GIT1 with γ-tubulin and also generated changes in the C-terminal domain of γ-tubulin, we evaluated the possibility that Ca^{2+} might modulate the binding of GIT1 and βPIX to the γ-tubulin C-terminal region. The pull-down experiments were performed with the GST-tagged C-terminal part of γ-tubulin (aa 362–451) and BMMCL extracts in the presence or absence of Ca^{2+}. βPIX associated with the GST-tagged γ-tubulin domain, but its binding was inhibited in the presence of Ca^{2+}. In contrast, GIT1 bound to the GST-fusion protein both in the absence and presence of Ca^{2+}. Actin (negative control) did not bind to the GST-tagged γ-tubulin domain, and no binding of GIT1 or βPIX was observed when GST alone was used in the pull-down assay (Fig. 5B). These findings suggest that Ca^{2+} adversely affects the interaction of βPIX with the C-terminal region of the γ-tubulin molecule in BMMCLs.

Nucleation of microtubules in BMMCLs is affected by Ca^{2+} and cell activation

To evaluate the possibility that the Ca^{2+} level affects microtubule assembly from centrosomes, we performed the nocodazole-washout assay. Microtubules were depolymerized with nocodazole and allowed to grow in the absence of the drug. To perform microtubule regrowth in the absence of both intracellular and extracellular Ca^{2+}, cells were preincubated with BAPTA-AM, which depleted intracellular Ca^{2+}. Cells for analysis were selected either manually or automatically. The α-tubulin fluorescence of microtubule asters was measured in ROIs centered at centrosomes that were marked by staining for γ-tubulin immunofluorescence, as previously described (13). In control cells, a clearly visible microtubule array, originating from the centrosomes, appeared after 3 min (Fig. 6Aa), and a fully developed microtubule array was detected after 4 min. In the absence of both extracellular and intracellular Ca^{2+}, only small microtubule asters were formed after 3 min of microtubule regrowth (Fig. 6Ac), and a fully developed microtubule array was observed after 6 min. Statistical evaluation of α-tubulin fluorescence in ROIs with diameters of 1, 1.5, or 2 μm after manual selection documented clear differences between regrowth in control
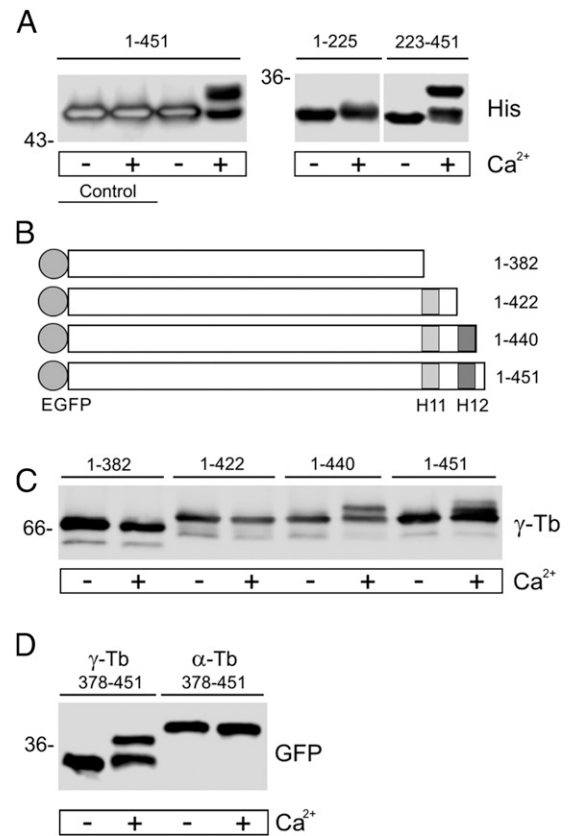

FIGURE 4. Ca^{2+}-dependent changes in electrophoretic mobility of γ-tubulin C-terminal domain. Immobilized tagged human γ-tubulin fragments were incubated with BMMCL extracts in the presence or absence of 0.8 mM Ca^{2+} for 30 min at 37°C before immunoblotting. (**A**) 6xHis-tagged human whole-length γ-tubulin or its fragments encoding aa regions 1–225 and 223–451 immobilized on Ni-NTA agarose and immunoblotted with Ab to 6xHis. Extracts were not added in the Control. (**B**) Schematic diagram of the constructs used. Positions of helixes H11 (gray) and H12 (dark gray) are highlighted. (**C**) EGFP-tagged truncated forms of human γ-tubulin encoding aa regions 1–382, 1–422, 1–440, and full-length γ-tubulin (1–451) immobilized on GFP-trap and immunoblotted with Ab to γ-tubulin (γ-Tb). (**D**) EGFP-tagged human γ-tubulin or α-tubulin fragments encoding aa regions 378–451 immobilized on GFP-trap and immunoblotted with Ab to GFP. Lines on the *left* indicate the positions of molecular mass markers (in kDa).

and Ca^{2+}-depleted cells (Fig. 6B). Similar results were obtained when analysis was performed on a large number of cells selected automatically (data not shown). When Ca^{2+} was absent only in the medium, a delay in microtubule regrowth was also observed (data not shown). When cells were activated by pervanadate, a potent protein tyrosine phosphatase inhibitor that mimics, in part, the stimulatory effect of Ag (31), microtubule regrowth was increased (Fig. 6C). The extent of microtubule regrowth could be modulated by mechanisms regulating either microtubule nucleation or microtubule dynamics. It was reported previously that microtubule dynamics is regulated at the cell periphery (32) and that a delay in microtubule regrowth is associated with defects in microtubule nucleation (13, 33). Together, these data suggest that both Ca^{2+} level and cell activation affect microtubule nucleation in BMMCLs.

Opposite regulatory roles of βPIX and GIT1 in nucleation of microtubules in BMMCLs

Because βPIX and GIT1 interact with γ-tubulin, we compared microtubule regrowth from centrosomes in BMMCLs with a re-
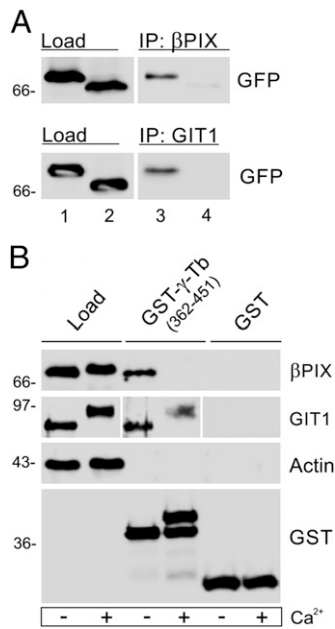
FIGURE 5. Effect of Ca^{2+} on βPIX and GIT1 binding to the C-terminal domain of γ-tubulin. (**A**) βPIX and GIT1 interact with whole-length γ-tubulin but not with its truncated form lacking a C-terminal region. Extracts from HEK cells expressing either GFP-tagged whole-length (aa 1–451; *lanes 1* and *3*) or truncated (aa 1–382; *lanes 2* and *4*) γ-tubulin were precipitated with Protein A–immobilized Abs specific to βPIX or GIT1. Blots were probed with Ab to GFP. Loads (*lanes 1* and *2*), immunoprecipitated proteins (*lanes 3* and *4*). (**B**) Binding of βPIX to the C-terminal region of γ-tubulin is affected by Ca^{2+}. Extracts from BMMCLs (Load) were incubated in the presence or absence of 0.8 mM Ca^{2+} with the GST-tagged C-terminal region of γ-tubulin (aa 362–451) or GST alone immobilized on glutathione-Sepharose beads. Blots of bound proteins were probed with Abs to βPIX, GIT1, actin, or GST. Lines on the *left* indicate the positions of molecular mass markers (in kDa).

duced level of βPIX or GIT1 in nocodazole-washout experiments. The βPIX- and GIT1-deficient cells were produced using lentiviral vectors. A typical result of immunoblotting experiments after depletion of βPIX or GIT1 is shown in Fig. 7A and Fig. 7B, respectively. At the best silencing, the amount of βPIX in βPIX-KD1 cells reached 14.7 ± 2.9% and the amount of GIT1 in GIT1-KD1 cells was 10.7 ± 2.8% (mean ± SD; $n = 5$) compared with the expression level in control cells with an empty pLKO.1 vector. Three independent experiments were performed with selected stable cells with reduced levels of βPIX, GIT1, and corresponding control cells. α-Tubulin immunofluorescence was measured at 1.5 min after washout in a 1.0-μm ROI. Control experiments revealed similar nucleation of microtubules when empty pLKO.1 vector or pLKO.1 vector with nontarget shRNA (pLKO.1-NT) was used (Supplemental Fig. 2H). Results of regrowth experiments are presented after analysis of a large number of cells selected automatically, but similar results were obtained after the analysis of a limited number of cells selected manually.

βPIX depletion resulted in an increase in microtubule regrowth (Fig. 7C). Typical staining of α-tubulin in control cells and βPIX-depleted cells is shown in Supplemental Fig. 2Ab and 2Ac, respectively. The increase in microtubule regrowth also was observed in cells with a lower level of βPIX depletion, denoted βPIX-KD2 (Supplemental Fig. 2B). For phenotypic rescue experiments, two silent point mutations were introduced into hβPIX to prevent its depletion by the shRNA. Rescue experiments revealed that the introduction of hβPIX to BMMCLs with depleted mβPIX levels led to restoration of nucleation capacity, as in control cells (Fig. 7D).

Microtubule regrowth after control βPIX depletion in rescue experiments is shown in Supplemental Fig. 2C, and an immunoblot from the rescue experiment is shown in Supplemental Fig. 2D.
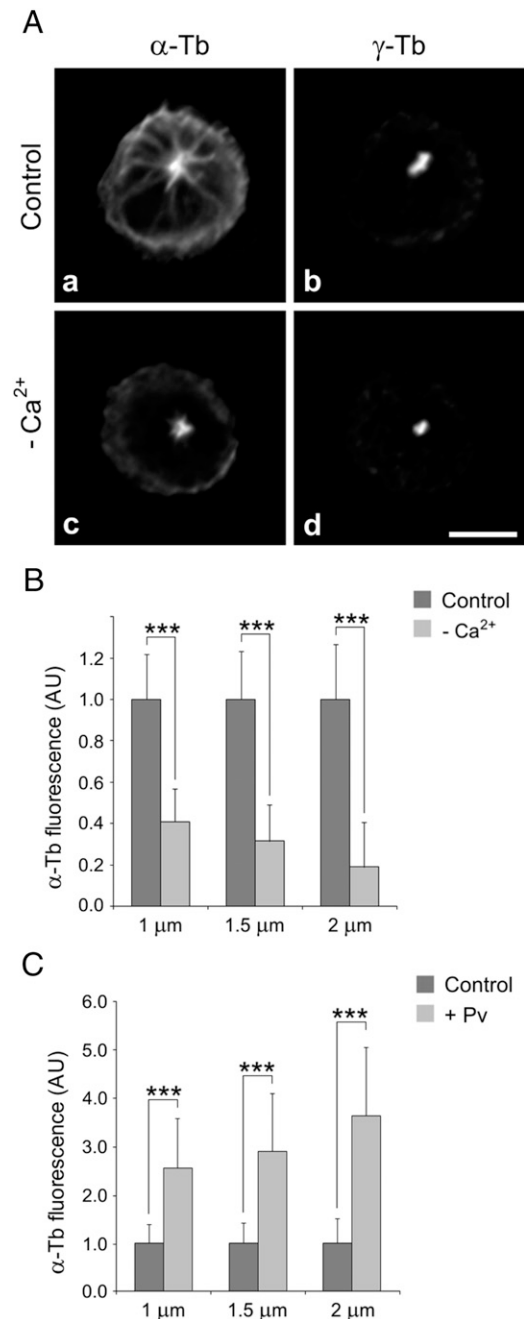
FIGURE 6. Effect of Ca^{2+} depletion and cell activation on microtubule regrowth. (**A**) Double-labeling of α-tubulin (**a** and **c**) and γ-tubulin (**b** and **d**) in a microtubule regrowth experiment in the presence or absence of Ca^{2+}. Both extracellular and intracellular Ca^{2+} were depleted, and cells were fixed at 3 min of microtubule regrowth. Scale bar, 5 μm. (**B**) Statistical analysis of α-tubulin fluorescence intensity in 1-, 1.5-, and 2-μm ROIs of BMMCLs nucleated in the absence of Ca^{2+} relative to BMMCLs nucleated in the presence of Ca^{2+}. Four independent experiments were performed, each involving 30 control cells and 30 Ca^{2+}-depleted cells (- Ca^{2+}). Data are mean ± SD ($n = 120$). (**C**) Statistical analysis of α-tubulin fluorescence intensity in 1-, 1.5-, and 2-μm ROIs of pervanadate-activated BMMCLs relative to unstimulated BMMCLs. Cells were fixed at 2.5 min of microtubule regrowth. Three independent experiments were performed, each involving 40 control cells and 40 pervanadate-activated cells (+ Pv). Data are mean ± SD ($n = 120$). ***$p < 0.001$.
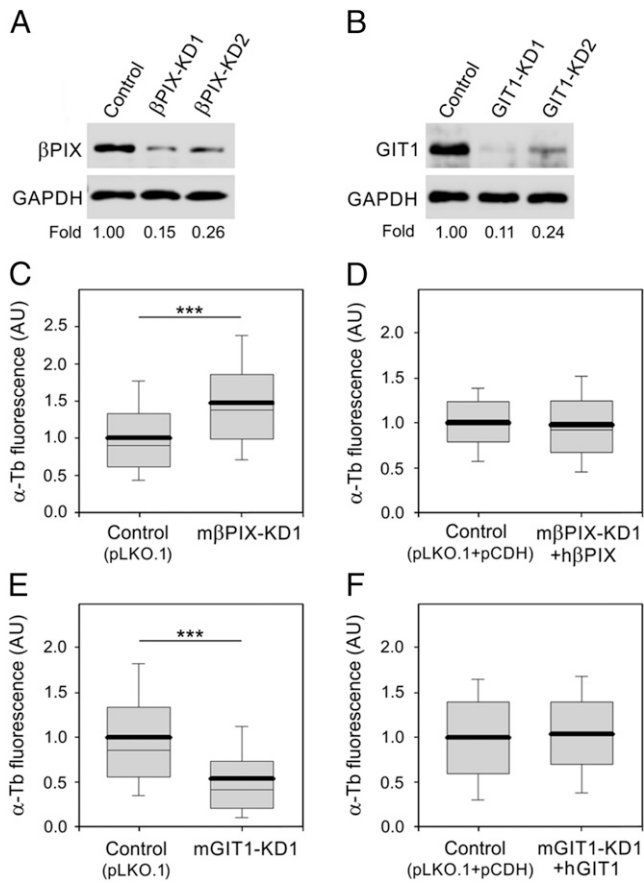
FIGURE 7. βPIX and GIT1 depletion affects microtubule regrowth. (**A**) Immunoblot analysis of cells with reduced levels of βPIX. Whole-cell lysates from cells infected with empty pLKO.1 vector (Control) or from cells selected after the knockdown of βPIX by shRNA1 (βPIX-KD1) or shRNA2 (βPIX-KD2). (**B**) Immunoblot analysis of cells with reduced levels of GIT1. Whole-cell lysates from cells infected with empty pLKO.1 vector (Control) or from cells selected after knockdown of GIT1 by shRNA1 (GIT1-KD1) or by shRNA2 (GIT1-KD2). Numbers under the blots indicate the relative amounts of βPIX (A) or GIT1 (B) normalized to control cells and to the amount of GAPDH in individual samples (Fold). (**C–F**) Distribution of α-tubulin fluorescence intensities (arbitrary units [AU]) in 1-μm ROI at 1.5 min of microtubule regrowth are shown as box plots (three independent experiments, >700 cells counted for each experimental condition). (C) Box plot of βPIX-depleted cells (mβPIX-KD1; $n = 4501$) relative to control cells (Control, pLKO.1; $n = 2788$). (D) Box plot of βPIX-depleted cells rescued by hβPIX (mβPIX-KD1 + hβPIX; $n = 2269$) relative to control cells (Control, pLKO.1 + pCDH; $n = 2645$). (E) Box plot of GIT1-depleted cells (mGIT1-KD1; $n = 3641$) relative to control cells (Control, pLKO.1, $n = 2938$). (F) Box plot of mGIT1-depleted cells rescued by hGIT1 (mGIT1-KD1 + hGIT1; $n = 4503$) relative to control cells (Control, pLKO.1 + pCDH; $n = 2,688$). In (C)–(F), bold and thin lines within the box represent the mean and median (the 50th percentile), respectively. The bottom and top of the box represent the 25th and 75th percentiles. Whiskers below and above the box indicate the 10th and 90th percentiles. ***$p < 1 \times 10^{-15}$.

The data obtained suggest that βPIX represents a negative regulator of microtubule nucleation from the centrosomes in BMMCLs.

In contrast, GIT1 depletion resulted in a decrease in microtubule regrowth (Fig. 7E). Typical staining of α-tubulin in GIT1-depleted cells is shown in Supplemental Fig. 2Ad. The decrease in microtubule nucleation also was observed in cells with a lower level of GIT1 depletion, denoted GIT1-KD2 (Supplemental Fig. 2E). Rescue experiments confirmed that the introduction of hGIT1 into BMMCLs with a reduced level of mGIT1 restored nucleation capacity to that observed in control cells (Fig. 7F). Microtubule

regrowth after control GIT1 depletion in rescue experiments is shown in Supplemental Fig. 2F, and an immunoblot from the rescue experiment is shown in Supplemental Fig. 2G. These experiments indicate that GIT1 represents a positive regulator of microtubule nucleation from the centrosomes in BMMCLs. Altogether, the results of these experiments suggest that βPIX and GIT1 differentially regulate microtubule nucleation.

*Differential effect of βPIX and GIT1 depletion on degranulation and cell motility*

We performed immunoprecipitation experiments to evaluate how the depletion of mβPIX affects the interaction of GIT1 with γ-tubulin, as well as how the depletion of GIT1 affects the interaction of βPIX with γ-tubulin. Although decreased levels of βPIX had no effect on the interaction between mGIT1 and γ-tubulin (Fig. 8A, *lanes 4, 5*, GIT1), depletion of GIT1 led to the increased association of βPIX with γ-tubulin (Fig. 8B, *lanes 4, 5*, βPIX). These results indicate that GIT1 modulates the formation of γ-tubulin/βPIX complexes.

Because microtubules are important for cell proliferation and survival, we assessed how depletion of βPIX or GIT1 affects these processes. Proliferation of βPIX-depleted cells was comparable to negative-control cells (pLKO.1 and pLKO.1-NT). In contrast, depletion of GIT1 resulted in partial inhibition of proliferation (Supplemental Fig. 3A). The viability of cells in the evaluated time interval was >99, >99, >98, and >95% for pLKO.1, pLKO.1-NT, βPIX-depleted cells, and GIT1-depleted cells, respectively. No differences between control cells (pLKO.1 and pLKO.1-NT) and βPIX- or GIT1-depleted cells were detected when genomic DNAs were analyzed for the presence of oligonucleosomal fragments characteristic of apoptotic cells (Supplemental Fig. 3B).

Finally, we measured the role of GIT1 and βPIX in Ag-induced chemotaxis and degranulation. Data in Fig. 9A show that cells with reduced GIT1 exhibited a significantly stronger Ag-mediated chemotactic response than did the control cells. In contrast, βPIX-depleted cells showed a less efficient chemotactic response. Interestingly, the general migration of GIT1-deficient cells also was enhanced, as indicated by the greater migration of cells in the absence of Ag (Fig. 9A, Control). Rescue experiments confirmed that the introduction of hGIT1 into BMMCLs with a reduced level of mGIT1 restored the chemotactic response to that observed in control cells. Similarly, the chemotactic response was rescued after the introduction of hβPIX into BMMCLs with a reduced level of mβPIX (Fig. 9A, Ag). In contrast to chemotaxis, cells with depleted GIT1 exhibited reduced degranulation, whereas βPIX-deficient cells showed significantly higher degranulation compared with control cells (Fig. 9B). Similar results were obtained when pLKO.1 or pLKO.1-NT were used as negative controls (Supplemental Fig. 3C). Two cell lines with reduced GIT1 (GIT1-KD1, GIT1-KD2) gave comparable results in the degranulation assay. Similarly, no statistically significant differences were detected in degranulation between two cell lines with reduced βPIX (βPIX-KD1, βPIX-KD2) (Supplemental Fig. 3C). Rescue experiments confirmed that introduction of hGIT1 into BMMCLs with reduced levels of mGIT1 restored degranulation to that observed in control cells. Degranulation also was recovered after the introduction of hβPIX into BMMCLs with a reduced level of mβPIX (Fig. 9B). Altogether, the results suggest that βPIX and GIT1 differentially regulate Ag-induced chemotaxis and degranulation in BMMCs.

Discussion

Ag-induced activation of mast cells leads to rapid cytoskeleton rearrangements and degranulation. Accumulating data point to the
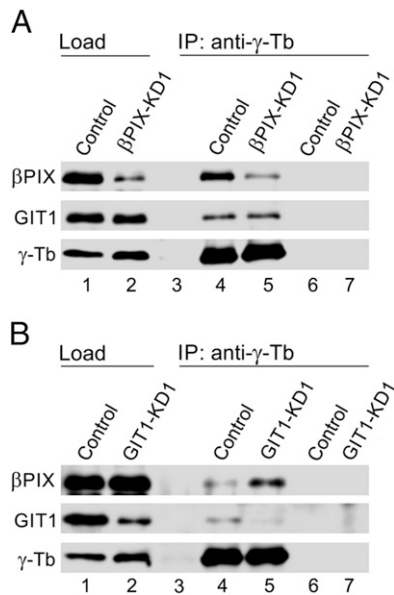
FIGURE 8. Depletion of GIT1 promotes interaction of βPIX with γ-tubulin. (**A**) Extracts from BMMCLs infected with empty pLKO.1 vector (Control) or BMMCLs with reduced levels of βPIX (βPIX-KD1) were precipitated with Protein A–immobilized Ab to γ-tubulin. Blots were probed with Abs to βPIX, GIT1, and γ-tubulin (γ-Tb). Load of control cells (*lane 1*), load of βPIX-KD1 cells (*lane 2*), immobilized Ab not incubated with cell extract (*lane 3*), precipitated proteins from control cells (*lane 4*), precipitated proteins from βPIX-KD1 cells (*lane 5*), Protein A without Ab, incubated with extract from control cells (*lane 6*), and Protein A without Ab, incubated with extract from βPIX-KD1 cells (*lane 7*). (**B**) Extracts from BMMCLs infected with empty pLKO.1 vector (Control) or BMMCLs with reduced levels of GIT1 (GIT1-KD1) were precipitated with Protein A–immobilized Ab to γ-tubulin. Blots were probed with Abs to βPIX, GIT1, and γ-tubulin (γ-Tb). Load of control cells (*lane 1*), load of GIT1-KD1 cells (*lane 2*), immobilized Ab not incubated with cell extract (*lane 3*), precipitated proteins from control cells (*lane 4*), precipitated proteins from GIT1-KD1 cells (*lane 5*), Protein A without Ab, incubated with extract from control cells (*lane 6*), and Protein A without Ab, incubated with extract from GIT1-KD1 cells (*lane 7*).

importance of microtubules in this process (3, 4, 7, 34). We showed previously that the stimulation of mast cells or basophils through FcεRI aggregation or by pervanadate exposure triggers the generation of complexes containing γ-tubulin, tyrosine-phosphorylated proteins, and tyrosine kinases (5, 35) and the reorganization of microtubules (5, 6). In this article, we report on GIT1 and βPIX as signaling proteins interacting with γ-tubulin in a Ca^{2+}-dependent manner, associating with centrosomes, and modulating microtubule nucleation from the centrosomes of BMMCLs. βPIX and GIT1 represent negative and positive regulators of microtubule nucleation, respectively. Our study provides a possible mechanism for the concerted action of tyrosine kinases, GIT1 and βPIX proteins, and Ca^{2+} in the propagation of signals leading to microtubule nucleation in activated mast cells.

Several lines of evidence indicate that the association of βPIX and GIT1 with γ-tubulin is specific. First, βPIX was repeatedly identified by MALDI/MS fingerprint analysis after immunoprecipitation of activated Lyn$^{-/-}$ BMMCLs with an anti-peptide mAb to γ-tubulin, elution of bound proteins with peptide, and concentration of tyrosine-phosphorylated proteins on an immobilized SH2 domain. Second, reciprocal precipitation experiments confirmed an interaction between βPIX or GIT1 and γ-tubulin. Third, TagRFP- or GFP-tagged γ-tubulins interacted with GIT1 and βPIX. Fourth, βPIX and GIT1 were associated with the GST-tagged C-terminal region of γ-tubulin. Finally, live-cell imaging revealed the locali-

zation of βPIX and GIT1 to centrosomes, where γ-tubulin is accumulated. Because the identification of βPIX in γ-tubulin complexes was carried out in lysates from Lyn$^{-/-}$ BMMCLs, we also analyzed GITs/βPIX–γ-tubulin complexes in BMMCLs. Although the differential expression of GIT1 and GIT2 was described in mouse tissues (36), our data document the expression of both proteins in BMMCLs and Lyn$^{-/-}$ BMMCLs. The results also demonstrate that the deletion of Lyn kinase does not affect the formation of complexes containing γ-tubulin, βPIX, and GITs.

GITs are multidomain proteins, and several signaling molecules, including βPIX, PAK, focal adhesion kinase, phospholipase Cγ, MAPK 1, and the synaptic protein Piccolo, associate with GIT1 through its Spa2 homology domain (30). Our data demonstrate that GIT1 is substrate for tyrosine kinases in pervanadate or FcεRI aggregation-activated BMMCLs. Moreover, tyrosine-phosphorylated GIT1 forms complexes with γ-tubulin. GIT1 was shown to be phosphorylated in cells in a Src kinase–dependent manner (37), and different studies pointed to the relevance of tyrosine phosphorylation in the regulation of GIT1 functions. It was shown that tyrosine phosphorylation of GIT1 is required for intramolecular
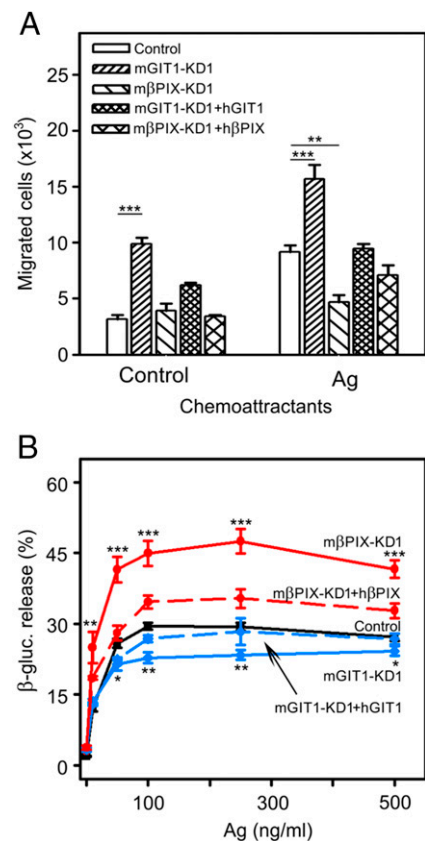
FIGURE 9. Differential effect of βPIX and GIT1 depletion on Ag-induced chemotaxis and degranulation. IgE-sensitized control cells or cells deficient in GIT1 (mGIT1-KD1) or βPIX (mβPIX-KD1) were used. hGIT1 or hβPIX was applied in rescue experiments. (**A**) The cells were analyzed in chemotactic assays with chemotaxis medium alone (Control) or supplemented with Ag (TNP-BSA, 250 ng/ml). The numbers of cells migrating into lower wells were determined after 8 h. Mean ± SE was calculated from three independent experiments performed in duplicates or triplicates. (**B**) IgE-sensitized cells were stimulated with various concentrations of Ag, and the amount of β-glucuronidase released from the cells was determined after 30 min. Mean ± SE was calculated from three independent experiments performed in duplicates or triplicates. The statistical significance of differences between control cells and βPIX-deficient cells is shown in the upper part, whereas those between control and GIT1-deficient cells are shown in the lower part. *$p < 0.05$, **$p < 0.01$, ***$p < 0.001$.

conformational changes in GIT1 and release its autoinhibitory interaction (38). Phosphorylation of GIT1 by Src family kinases is required for its association with focal adhesion kinase (39), as well as for phospholipase Cγ activation (40). In contrast, tyrosine phosphorylation of βPIX, in a Src-dependent manner, weakens its ability to bind GIT1 (41). Association of Src family kinases with γ-tubulin complexes was reported in activated RBL-2H3 (35), activated BMMCLs (5), and in differentiating P19 embryonic carcinoma cells (23, 42). Thus, tyrosine phosphorylation of GIT1 in stimulated mast cells might lead to its activation.

There are reports suggesting an important role for tyrosine kinases in the regulation of microtubule nucleation from centrosomes. Fyn kinase was found on centrosomes in myelocytic leukemia cells HL-60 (43) and in human T lymphocytes (44). Androgen and Src signaling modulated microtubule nucleation during interphase by promoting the centrosomal localization of γ-tubulin (13) via activation of the MAPK/Erk signaling pathway (45). It also was shown that Syk is catalytically active at the centrosome (46). Previous studies showed that early stages of BMMCL activation, when microtubule formation is stimulated, are characterized by the concentration of tyrosine-phosphorylated proteins in the centrosomal region (5).

Although the FcεRI proximal signaling pathways involved in mast cell activation are well defined (1), the signaling events downstream of Ca^{2+} influx are less well studied. Ca^{2+}-dependent kinases or phosphatases might participate in microtubule stability in activated mast cells (47). It was reported that STIM1-regulated Ca^{2+} influx is essential for reorganization of microtubules in activated mast cells (6). In this study, we show that the depletion of Ca^{2+} substantially delays microtubule regrowth. In contrast, elevated levels of Ca^{2+} are accompanied by increased amounts of GCP2, GCP4, and GITs in complexes with γ-tubulin. Interestingly, Ca^{2+} inhibits binding of βPIX to the C-terminal region of γ-tubulin. Direct Ca^{2+}-dependent interaction between βPIX and calmodulin was reported recently (48). Live-cell imaging with EGFP-calmodulin chimeras revealed the association of calmodulin with centrosomes after activation of RBL-2H3 (49). A truncated splice variant of the FcεRIβ binding calmodulin, Gab2, and Fyn kinase was found to accumulate in the centrosome–Golgi region and stimulate microtubule formation and degranulation in human LAD-2 mast cells. It was suggested that the truncated splice variant may act to propagate Ca^{2+} signals for microtubule nucleation (7). It also was reported that the Fyn kinase/Gab2/PI3K pathway is critical for the formation of microtubules (3, 50). Our data support the importance of Ca^{2+} for microtubule nucleation in BMMCLs.

Interestingly, elevated levels of Ca^{2+} affected γ-tubulin properties manifested by changes in the electrophoretic mobility of γ-tubulin in BMMCLs. This conclusion is supported by several findings. First, both endogenous and exogenous γ-tubulins were modified. Second, 6xHis-tagged whole-length γ-tubulin or its C-terminal part (aa 223–451) was affected. Third, EGFP-tagged whole-length γ-tubulin or its C-terminal region (aa 378–451) was modified. Fourth, experiments with EGFP-tagged C-terminal regions of γ-tubulin or α-tubulin revealed that the mobility shift is specific for γ-tubulin. Finally, the presence of EGTA inhibited the mobility shift of γ-tubulin, and elevated concentrations of Mg^{2+} or Zn^{2+} did not demonstrate this effect. It was shown that Ca^{2+} has high-affinity binding sites on the C-terminal regions of αβ-tubulin dimers (51). However, it is unlikely that only the direct binding of Ca^{2+} to the C-terminal region of γ-tubulin causes observed changes, because no mobility shift was detected when Ca^{2+} alone was added to 6xHis-tagged γ-tubulin (Fig. 4A, Control). Unique changes in γ-tubulin properties in BMMCLs warrant further in-

vestigation. Ca^{2+}-dependent modifications in the C-terminal region of γ-tubulin could affect γ-tubulin binding characteristics and, thus, modulate the nucleation of microtubules in activated cells.

Our data from live-cell imaging revealed that GIT1 and βPIX are located on centrosomes in BMMCLs, which could reflect their regulatory roles in microtubule nucleation. Although GIT1/βPIX complexes are usually connected with cell migration, the centrosomal function of the complexes has only been reported in fibroblasts. GIT1 targeting to the centrosome served as a scaffold for βPIX. Associated PAK, activated via a process not requiring Rho GTPases, phosphorylated Aurora A in mitosis (52). Our data demonstrate that GIT1 and βPIX regulate interphase microtubules of mast cells. Although GIT1 and βPIX are both associated with centrosomes in BMMCLs, they play opposite regulatory roles in microtubule nucleation from centrosomes. Depletion of βPIX led to increased nucleation, whereas depletion of GIT1 resulted in decreased nucleation. The obtained data were confirmed by rescue experiments. GIT1/βPIX could regulate the nucleation of microtubules via several mechanisms. They may directly promote the assembly of γTuRCs and/or the recruitment of γTuRCs to the centrosome. Thus, kinases associated with GIT1/βPIX may phosphorylate components of γTuRC to promote the assembly of the complex, or they may regulate the association or activity of NEDD1/GCP-WD, the attachment factor that lies most proximal to γTuRC and is required for the centrosomal recruitment of γTuRC (53). Alternatively, GIT1/βPIX may indirectly affect this process by regulating the assembly of the pericentriolar matrix or the activity of a centrosomal protein(s) required for the anchorage of γTuRCs (54).

It is generally thought that the GIT1/βPIX complex serves as a signaling cassette that elicits changes in cell shape and migration (29). Our data indicate that depletion of βPIX enhances degranulation in Ag-activated cells. This could reflect increased microtubule nucleation. In contrast, depletion of GIT1 resulted in reduced degranulation, which could be related to decreased levels of microtubule nucleation in such cells. Both proteins are also involved in chemotaxis toward Ag, where they play opposite regulatory roles: GIT1 is a negative regulator, whereas βPIX serves as a positive regulator of chemotaxis. The negative regulatory role of GIT2 in cell motility was reported in other cell types (55). In contrast, it was shown that fMLP-induced fibronectin-mediated chemotaxis was unaffected after depletion of GIT2 and was inhibited after depletion of GIT1 (56). The difference in the results presented in this study and those of another study (56) may be attributed to the different experimental cell models, different chemoattractants used, and the presence or absence of fibronectin during the chemotactic assays. Although microtubules have long been implicated in cell motility, their role in this process varies with cell types. The mechanism of their involvement in cell motility is poorly understood. It was suggested that microtubules normally act to restrain cell motility (57). This could explain the observed opposite effects in degranulation and chemotaxis after the depletion of GIT1 and βPIX proteins. Because the GIT/PIX complex affects actin-dependent processes, including cell motility (29), the observed changes in chemotaxis could reflect changes in the microtubules, as well as in the actin cytoskeleton.

In conclusion, our data suggest a novel signaling pathway for microtubule rearrangement in mast cells; tyrosine kinase–activated GIT1 and βPIX, in concert with Ca^{2+} signaling, regulate microtubule nucleation. Enhanced levels of Ca^{2+} affect γ-tubulin properties, resulting in greater binding of GCPs to γ-tubulin. Presumably, through this action, GIT1 and βPIX are involved in the regulation of such important processes in mast cells physiology as is Ag-induced degranulation and chemotaxis. Interference with the microtubular network via specific regulators of microtubule nucleation in mast

cells could open up rational new approaches to the treatment of inflammatory and allergic diseases.

Acknowledgments

Disclosures

References

1. Gilfillan, A. M., and J. Rivera. 2009. The tyrosine kinase network regulating mast cell activation. *Immunol. Rev.* 228: 149–169.
2. Smith, A. J., J. R. Pfeiffer, J. Zhang, A. M. Martinez, G. M. Griffiths, and B. S. Wilson. 2003. Microtubule-dependent transport of secretory vesicles in RBL-2H3 cells. *Traffic* 4: 302–312.
3. Nishida, K., S. Yamasaki, Y. Ito, K. Kabu, K. Hattori, T. Tezuka, H. Nishizumi, D. Kitamura, R. Goitsuka, R. S. Geha, et al. 2005. FcεRI-mediated mast cell degranulation requires calcium-independent microtubule-dependent translocation of granules to the plasma membrane. *J. Cell Biol.* 170: 115–126.
4. Martin-Verdeaux, S., I. Pombo, B. Iannascoli, M. Roa, N. Varin-Blank, J. Rivera, and U. Blank. 2003. Evidence of a role for Munc18-2 and microtubules in mast cell granule exocytosis. *J. Cell Sci.* 116: 325–334.
5. Sulimenko, V., E. Dráberová, T. Sulimenko, L. Macůrek, V. Richterová, P. Dráber, and P. Dráber. 2006. Regulation of microtubule formation in activated mast cells by complexes of γ-tubulin with Fyn and Syk kinases. *J. Immunol.* 176: 7243–7253.
6. Hájková, Z., V. Bugajev, E. Dráberová, S. Vinopal, L. Dráberová, J. Janáček, P. Dráber, and P. Dráber. 2011. STIM1-directed reorganization of microtubules in activated mast cells. *J. Immunol.* 186: 913–923.
7. Cruse, G., M. A. Beaven, I. Ashmole, P. Bradding, A. M. Gilfillan, and D. D. Metcalfe. 2013. A truncated splice-variant of the FcεRIβ receptor subunit is critical for microtubule formation and degranulation in mast cells. *Immunity* 38: 906–917.
8. Grigoriev, I., S. M. Gouveia, B. van der Vaart, J. Demmers, J. T. Smyth, S. Honnappa, D. Splinter, M. O. Steinmetz, J. W. Putney, Jr., C. C. Hoogenraad, and A. Akhmanova. 2008. STIM1 is a MT-plus-end-tracking protein involved in remodeling of the ER. *Curr. Biol.* 18: 177–182.
9. Oakley, C. E., and B. R. Oakley. 1989. Identification of γ-tubulin, a new member of the tubulin superfamily encoded by mipA gene of *Aspergillus nidulans. Nature* 338: 662–664.
10. Oegema, K., C. Wiese, O. C. Martin, R. A. Milligan, A. Iwamatsu, T. J. Mitchison, and Y. Zheng. 1999. Characterization of two related *Drosophila* γ-tubulin complexes that differ in their ability to nucleate microtubules. *J. Cell Biol.* 144: 721–733.
11. Vogel, J., B. Drapkin, J. Oomen, D. Beach, K. Bloom, and M. Snyder. 2001. Phosphorylation of γ-tubulin regulates microtubule organization in budding yeast. *Dev. Cell* 1: 621–631.
12. Keck, J. M., M. H. Jones, C. C. Wong, J. Binkley, D. Chen, S. L. Jaspersen, E. P. Holinger, T. Xu, M. Niepel, M. P. Rout, et al. 2011. A cell cycle phosphoproteome of the yeast centrosome. *Science* 332: 1557–1561.
13. Colello, D., C. G. Reverte, R. Ward, C. W. Jones, V. Magidson, A. Khodjakov, and S. E. LaFlamme. 2010. Androgen and Src signaling regulate centrosome activity. *J. Cell Sci.* 123: 2094–2102.
14. Nováková, M., E. Dráberová, W. Schürmann, G. Czihak, V. Viklický, and P. Dráber. 1996. γ-Tubulin redistribution in taxol-treated mitotic cells probed by monoclonal antibodies. *Cell Motil. Cytoskeleton* 33: 38–51.
15. Hořejší, B., S. Vinopal, V. Sládková, E. Dráberová, V. Sulimenko, T. Sulimenko, V. Vosecká, A. Philimonenko, P. Hozák, C. D. Katsetos, and P. Dráber. 2012. Nuclear γ-tubulin associates with nucleoli and interacts with tumor suppressor protein C53. *J. Cell. Physiol.* 227: 367–382.
16. Dráberová, E., V. Sulimenko, V. Kukharskyy, and P. Dráber. 1999. Monoclonal antibody NF-09 specific for neurofilament protein NF-M. *Folia Biol. (Praha)* 45: 163–165.
17. Hibbs, M. L., D. M. Tarlinton, J. Armes, D. Grail, G. Hodgson, R. Maglitto, S. A. Stacker, and A. R. R. Dunn. 1995. Multiple defects in the immune system of Lyn-deficient mice, culminating in autoimmune disease. *Cell* 83: 301–311.
18. Kovářová, M., P. Tolar, R. Arudchandran, L. Dráberová, J. Rivera, and P. Dráber. 2001. Structure-function analysis of Lyn kinase association with lipid rafts and initiation of early signaling events after Fcε receptor I aggregation. *Mol. Cell. Biol.* 21: 8318–8328.
19. Zheng, Y., M. K. Jung, and B. R. Oakley. 1991. γ-Tubulin is present in *Drosophila melanogaster* and *Homo sapiens* and is associated with the centrosome. *Cell* 65: 817–823.
20. Vinopal, S., M. Černohorská, V. Sulimenko, T. Sulimenko, V. Vosecká, M. Flemr, E. Dráberová, and P. Dráber. 2012. γ-Tubulin 2 nucleates microtubules and is downregulated in mouse early embryogenesis. *PLoS ONE* 7: e29919.
21. ten Klooster, J. P., Z. M. Jaffer, J. Chernoff, and P. L. Hordijk. 2006. Targeting and activation of Rac1 are mediated by the exchange factor β-Pix. *J. Cell Biol.* 172: 759–769.
22. Dráber, P. 1991. Quantification of proteins in sample buffer for sodium dodecyl sulfate-polyacrylamide gel electrophoresis using colloidal silver. *Electrophoresis* 12: 453–456.
23. Kukharskyy, V., V. Sulimenko, L. Macůrek, T. Sulimenko, E. Dráberová, and P. Dráber. 2004. Complexes of γ-tubulin with nonreceptor protein tyrosine kinases Src and Fyn in differentiating P19 embryonal carcinoma cells. *Exp. Cell Res.* 298: 218–228.
24. Dráber, P., L. A. Lagunowich, E. Dráberová, V. Viklický, and I. Damjanov. 1988. Heterogeneity of tubulin epitopes in mouse fetal tissues. *Histochemistry* 89: 485–492.
25. Surviladze, Z., L. Dráberová, M. Kovárová, M. Boubelík, and P. Dráber. 2001. Differential sensitivity to acute cholesterol lowering of activation mediated via the high-affinity IgE receptor and Thy-1 glycoprotein. *Eur. J. Immunol.* 31: 1–10.
26. Polakovicova, I., L. Draberova, M. Simicek, and P. Draber. 2014. Multiple regulatory roles of the mouse transmembrane adaptor protein NTAL in gene transcription and mast cell physiology. *PLoS ONE* 9: e105539.
27. Dráberová, E., and P. Dráber. 1993. A microtubule-interacting protein involved in coalignment of vimentin intermediate filaments with microtubules. *J. Cell Sci.* 106: 1263–1273.
28. Hoefen, R. J., and B. C. Berk. 2006. The multifunctional GIT family of proteins. *J. Cell Sci.* 119: 1469–1475.
29. Frank, S. R., and S. H. Hansen. 2008. The PIX-GIT complex: a G protein signaling cassette in control of cell shape. *Semin. Cell Dev. Biol.* 19: 234–244.
30. Webb, D. J., M. W. Mayhew, M. Kovalenko, M. J. Schroeder, E. D. Jeffery, L. Whitmore, J. Shabanowitz, D. F. Hunt, and A. F. Horwitz. 2006. Identification of phosphorylation sites in GIT1. *J. Cell Sci.* 119: 2847–2850.
31. Teshima, R., H. Ikebuchi, M. Nakanishi, and J. Sawada. 1994. Stimulatory effect of pervanadate on calcium signals and histamine secretion of RBL-2H3 cells. *Biochem. J.* 302: 867–874.
32. Komarova, Y. A., I. A. Vorobjev, and G. G. Borisy. 2002. Life cycle of MTs: persistent growth in the cell interior, asymmetric transition frequencies and effects of the cell boundary. *J. Cell Sci.* 115: 3527–3539.
33. Delgehyr, N., J. Sillibourne, and M. Bornens. 2005. Microtubule nucleation and anchoring at the centrosome are independent processes linked by ninein function. *J. Cell Sci.* 118: 1565–1575.
34. Tasaka, K., K. Mio, K. Fujisawa, and I. Aoki. 1991. Role of microtubules on Ca^{2+} release from the endoplasmic reticulum and associated histamine release from rat peritoneal mast cells. *Biochem. Pharmacol.* 41: 1031–1037.
35. Dráberová, L., E. Dráberová, Z. Surviladze, P. Dráber, and P. Dráber. 1999. Protein tyrosine kinase p53/p56(lyn) forms complexes with γ-tubulin in rat basophilic leukemia cells. *Int. Immunol.* 11: 1829–1839.
36. Schmalzigaug, R., H. Phee, C. E. Davidson, A. Weiss, and R. T. Premont. 2007. Differential expression of the ARF GAP genes GIT1 and GIT2 in mouse tissues. *J. Histochem. Cytochem.* 55: 1039–1048.
37. Bagrodia, S., D. Bailey, Z. Lenard, M. Hart, J. L. Guan, R. T. Premont, S. J. Taylor, and R. A. Cerione. 1999. A tyrosine-phosphorylated protein that binds to an important regulatory region on the cool family of p21-activated kinase-binding proteins. *J. Biol. Chem.* 274: 22393–22400.
38. Totaro, A., V. Astro, D. Tonoli, and I. de Curtis. 2014. Identification of two tyrosine residues required for the intramolecular mechanism implicated in GIT1 activation. *PLoS ONE* 9: e93199.
39. Ren, Y., L. Yu, J. Fan, Z. Rui, Z. Hua, Z. Zhang, N. Zhang, and G. Yin. 2012. Phosphorylation of GIT1 tyrosine 321 is required for association with FAK at focal adhesions and for PDGF-activated migration of osteoblasts. *Mol. Cell. Biochem.* 365: 109–118.
40. Wang, J., G. Yin, P. Menon, J. Pang, E. M. Smolock, C. Yan, and B. C. Berk. 2010. Phosphorylation of G protein-coupled receptor kinase 2-interacting protein 1 tyrosine 392 is required for phospholipase C-γ activation and podosome formation in vascular smooth muscle cells. *Arterioscler. Thromb. Vasc. Biol.* 30: 1976–1982.
41. Feng, Q., D. Baird, S. Yoo, M. Antonyak, and R. A. Cerione. 2010. Phosphorylation of the cool-1/β-Pix protein serves as a regulatory signal for the migration and invasive activity of Src-transformed cells. *J. Biol. Chem.* 285: 18806–18816.
42. Macurek, L., E. Dráberová, V. Richterová, V. Sulimenko, T. Sulimenko, L. Dráberová, V. Marková, and P. Dráber. 2008. Regulation of microtubule nucleation from membranes by complexes of membrane-bound γ-tubulin with Fyn kinase and phosphoinositide 3-kinase. *Biochem. J.* 416: 421–430.
43. Katagiri, K., T. Katagiri, K. Kajiyama, T. Yamamoto, and T. Yoshida. 1993. Tyrosine-phosphorylation of tubulin during monocytic differentiation of HL-60 cells. *J. Immunol.* 150: 585–593.
44. Ley, S. C., M. Marsh, C. R. Bebbington, K. Proudfoot, and P. Jordan. 1994. Distinct intracellular localization of Lck and Fyn protein tyrosine kinases in human T lymphocytes. *J. Cell Biol.* 125: 639–649.
45. Colello, D., S. Mathew, R. Ward, K. Pumiglia, and S. E. LaFlamme. 2012. Integrins regulate microtubule nucleating activity of centrosome through mitogen-activated protein kinase/extracellular signal-regulated kinase kinase/extracellular signal-regulated kinase (MEK/ERK) signaling. *J. Biol. Chem.* 287: 2520–2530.
46. Fargier, G., C. Favard, A. Parmeggiani, A. Sahuquet, F. Mérezègue, A. Morel, M. Denis, N. Molinari, P. H. Mangeat, P. J. Coopman, and P. Montcourrier. 2013. Centrosomal targeting of Syk kinase is controlled by its catalytic activity and depends on microtubules and the dynein motor. *FASEB J.* 27: 109–122.
47. Dráber, P., V. Sulimenko, and E. Dráberová. 2012. Cytoskeleton in mast cell signaling. *Front. Immunol.* 3: 130.

48. Singh, V. K., K. Munro, and Z. Jia. 2012. A novel calmodulin-β-PIX interaction and its implication in receptor tyrosine kinase regulation. *Cell. Signal.* 24: 1790–1796.

49. Psatha, M. I., M. Razi, A. Koffer, S. E. Moss, D. B. Sacks, and S. R. Bolsover. 2007. Targeting of calcium:calmodulin signals to the cytoskeleton by IQGAP1. *Cell Calcium* 41: 593–605.

50. Sibilano, R., B. Frossi, R. Suzuki, F. D'Incà, G. Gri, S. Piconese, M. P. Colombo, J. Rivera, and C. E. Pucillo. 2012. Modulation of FcεRI-dependent mast cell response by OX40L via Fyn, PI3K, and RhoA. *J. Allergy Clin. Immunol.* 130: 751–760, e2.

51. Lefèvre, J., K. G. Chernov, V. Joshi, S. Delga, F. Toma, D. Pastré, P. A. Curmi, and P. Savarin. 2011. The C terminus of tubulin, a versatile partner for cationic molecules: binding of Tau, polyamines, and calcium. *J. Biol. Chem.* 286: 3065–3078.

52. Zhao, Z. S., J. P. Lim, Y. W. Ng, L. Lim, and E. Manser. 2005. The GIT-associated kinase PAK targets to the centrosome and regulates Aurora-A. *Mol. Cell* 20: 237–249.

53. Lüders, J., U. K. Patel, and T. Stearns. 2006. GCP-WD is a γ-tubulin targeting factor required for centrosomal and chromatin-mediated microtubule nucleation. *Nat. Cell Biol.* 8: 137–147.

54. Teixidó-Travesa, N., J. Roig, and J. Lüders. 2012. The where, when and how of microtubule nucleation - one ring to rule them all. *J. Cell Sci.* 125: 4445–4456.

55. Frank, S. R., M. R. Adelstein, and S. H. Hansen. 2006. GIT2 represses Crk- and Rac1-regulated cell spreading and Cdc42-mediated focal adhesion turnover. *EMBO J.* 25: 1848–1859.

56. Gavina, M., L. Za, R. Molteni, R. Pardi, and I. de Curtis. 2010. The GIT-PIX complexes regulate the chemotactic response of rat basophilic leukaemia cells. *Biol. Cell* 102: 231–244.

57. Ganguly, A., H. Yang, R. Sharma, K. D. Patel, and F. Cabral. 2012. The role of microtubules and their dynamics in cell migration. *J. Biol. Chem.* 287: 43359–43369.

Supplement

Sulimenko V., Hájková Z., Černohorská M., Sulimenko T., Sládková V., Dráberová L., Vinopal S., Dráberová E. & Dráber, P. Microtubule nucleation in mouse bone marrow-derived mast cells is regulated by the concerted action of GIT1/βPIX proteins and calcium. *J Immunol*, **194**: 4099-4011, 2015

Supplemental Table 1

Mass spectrometry identification of the mouse Rho guanine nucleotide exchange factor 7 (mβPIX)

Measured mass	Theoretical mass	Error (ppm)	Peptide sequence	Peptide position
1225.586	1225.588	-1	TGWFPSNYVR	209 - 218
1368.632	1368.634	-1	NAFEISGSM(ox)IER	522 - 534
1452.817	1452.818	-1	ELELQILTEPIR	435 - 446
1595.837	1595.840	-2	KESAPQVLLPEEEK	774 - 787
1612.701	1612.701	0	VEEGGWWEGTHNGR	195 - 208
1832.820	1832.821	0	FNFQQTNEDELSFSK	172 - 186
1977.041	1977.041	0	SLVDTVYALKDEVQELR	805 - 821
2077.104	2077.104	0	ELQSVLSTYLRPLQTSDK	268 - 285

```
  1 MNSAEQTVTW LITLGVLESP KKTISDPEVF LQASLKDGVV LCRLLERLLP GTIEKVYPEP
 61 RNESECLSNI REFLRACGAS LRLETFDAND LYQGQNFNKV LSSLVTLNKV TADIGLGSDS
121 VCARPSSHRI KSFDSLGSQS SHSRTSKLLQ SQYRSLDMTD NTNSQLVVRA K**FNFQQTNED**
181 **ELSFSK**GDVI HVTR**VEEGGW WEGTHNGRTG WFPSNYVR**EI KPSEKPVSPK SGTLKSPPKG
241 FDTTAINKSY YNVVLQNILE TEHEYSK**ELQ SVLSTYLRPL QTSDK**LSSAN TSYLMGNLEE
301 ISSFQQVLVQ SLEECTKSPE AQQRVGGCFL SLMPQMRTLY LAYCANHPSA VSVLTEHSED
361 LGEFMETKGA SSPGILVLTT GLSKPFMRLD KYPTLLKELE RHMEDYHPDR QDIQKSMTAF
421 KNLSAQCQEV RKRK**ELELQI LTEPIR**SWEG DDIKTLGSVT YMSQVTIQCA GSEEKNERYL
481 LLFPNLLLML SASPRMSGFI YQGKLPTTGM TITKLEDSEN HR**NAFEISGS MIER**ILVSCT
541 SQQDLHEWVE HLQKQTKVTS VSNPTIKPHS VPSHTLPSHP LTPSSKHADS KPVALTPAYH
601 TLPHPSHHGT PHTTISWGPL EPPKTPKPWS LSCLRPAPPL RPSAALCYKE DLSKSPKTMK
661 KLLPKRKPER KPSDEEFAVR KSTAALEEDA QILKVIEAYC TSAKTRQTLN STWQGTDLMH
721 NHVLADDDQS SLDSLGRRSS LSRLEPSDLS EDSEYDSIWT AHSYRMGSAS RSR**KESAPQV**
781 **LLPEEEK**IIV EETKSNGQTV IEEK**SLVDTV YALKDEVQEL R**QDNKKMKKS LEEEQRARKD
841 LEKLVRKVLK NMNDPAWDET NL
```

Amino acids of the identified peptides in the mouse Rho guanine nucleotide exchange factor 7 (Arhgef7, canonical sequence of isoform B; UniProtKB/Swiss-Prot Q9ES28-1) are indicated in bold and underlined (bottom part of the table). The matched peptides cover 12.99 % of the protein sequence.
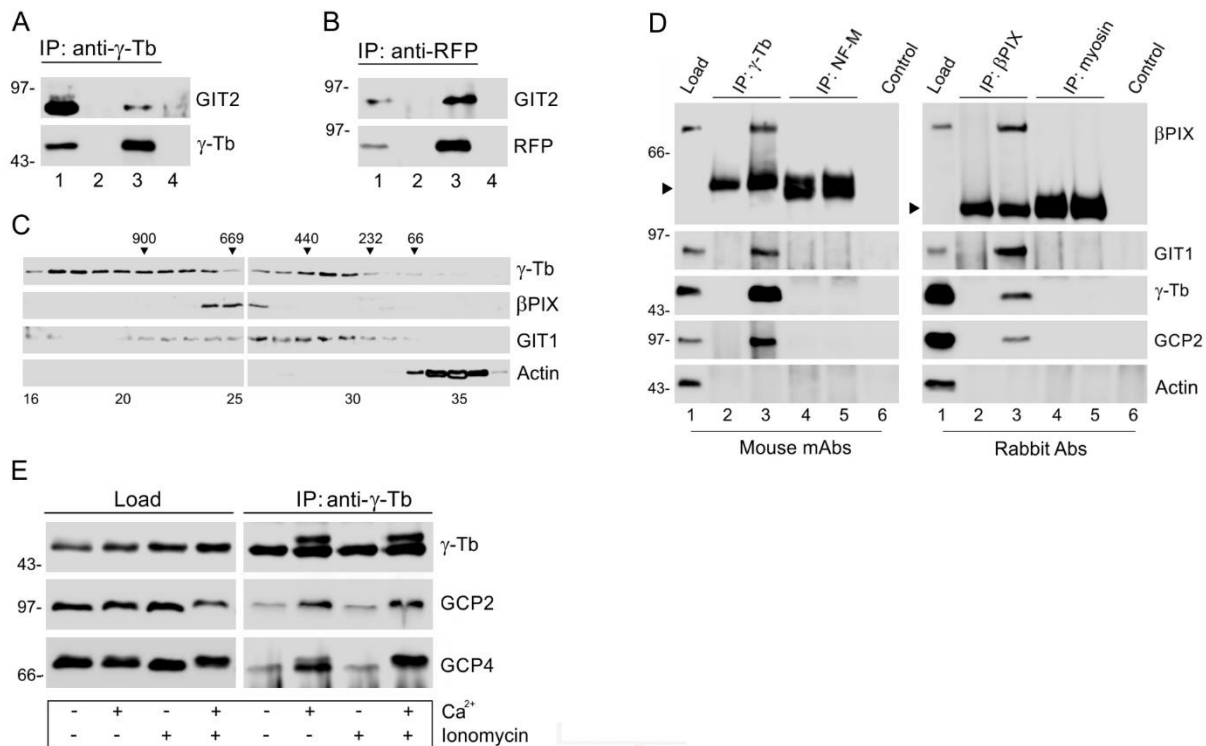
FIGURE S1. γ-Tubulin interacts with GIT2, co-distributes with βPIX and GIT1 during size fractionation of cytosolic extract of mast cells, and its interaction with GCPs is Ca^{2+}-dependent. *A*, Extract from $Lyn^{-/-}$ BMMCL was precipitated with protein A immobilized Ab to γ-tubulin. Blots were probed with Abs to GIT2 and γ-tubulin (γ-Tb). *B*, Extract from BMMCL-γTb expressing TagRFP-tagged γ-tubulin was precipitated with protein A immobilized Ab to RFP. Blots were probed with Abs to GIT2 and RFP. In *A-B*: load (*lane 1*), immobilized Ab not incubated with cell extract (*lane 2*), immunoprecipitated protein (*lane 3*), and protein A without Ab, incubated with cell extract (*lane 4*). Lines on the left indicate positions of molecular mass markers in kDa. *C*, Size fractionation of cytosolic extract. Proteins extracted from BMMCL were fractionated on Superose 6B and blots of collected fractions were probed with Abs to γ-tubulin, βPIX, GIT1 and actin. Calibration standards (in kDa) are indicated on the top. Numbers at the bottom denote individual fractions. *D*, Isotype controls for immunoprecipitation experiments. Extracts from $Lyn^{-/-}$ BMMCL were precipitated with protein A immobilized mouse mAb to γ-tubulin (IgG2b), mouse mAb to NF-M (IgG2a, control), rabbit Ab to βPIX or rabbit Ab to myosin (control). Blots were probed with Abs to βPIX, GIT1, γ-tubulin (γ-Tb), GCP2 and actin. Load (*lane 1*), immobilized Abs not incubated with cell extracts (*lanes 2 and 4*), immunoprecipitated proteins (*lanes 3 and 5*), and protein A without Ab, incubated with cell extract (*lane 6*). Lines on the left indicate positions of molecular mass markers in kDa. Arrowheads indicate position of Ab heavy chains. *E*, Effect of Ca^{2+} and ionomycin on co-immunoprecipitation of proteins with γ-tubulin. BMMCL were pre-incubated in the presence or absence of 1.8 mM Ca^{2+} and extracts were precipitated with Ab to γ-tubulin immobilized on protein A. Blots were probed with Abs to γ-tubulin (γ-Tb), GCP2 and GCP4. Note the change in electrophoretic mobility of precipitated γ-tubulin and the higher amount of co-precipitated GCP2 and GCP4 in the presence of Ca^{2+}. Lines on the left indicate positions of molecular mass markers in kDa.
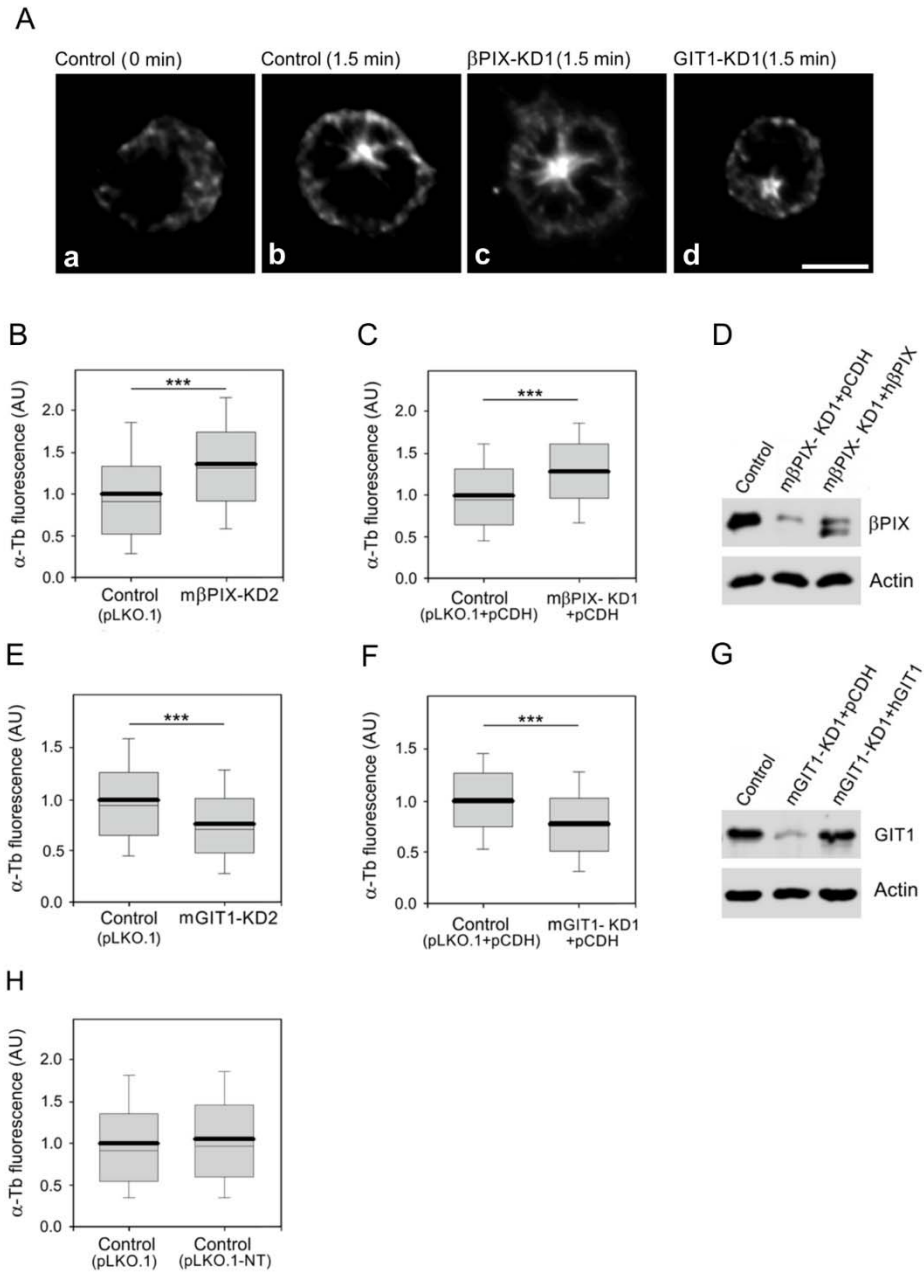
FIGURE S2. Effect of βPIX and GIT1 depletion on microtubule regrowth in BMMCL. *A*, Labeling of α-tubulin in microtubule regrowth experiment in control cells infected with empty pLKO.1 vector (*a-b*) and after depletion of βPIX (*c*; βPIX-KD1) or GIT1 (*d*; GIT1-KD1). Cells were fixed at 1.5 min of microtubule regrowth. Scale bar, 5 μm. (*B-C, E-F*) The distributions of α-tubulin fluorescence intensities (arbitrary units, AU) in 1 μm ROI at 1.5 min of microtubule regrowth are shown as box plot diagrams (three independent experiments, more than 400 cells counted for each experimental condition). *B*, Box plot of cells with a lower level of βPIX depletion (mβPIX-KD2; n = 1,894) relative to negative control cells (Control, pLKO.1; n = 1,254). *C*, Box plot of βPIX-depleted cells (mβPIX-KD1 + pCDH; n = 2,688)

relative to negative control cells (Control, pLKO.1 + pCDH; n = 1,938) in rescue experiment. *D*, Immunoblot analysis of cells in βPIX rescue experiment. Whole cell lysate from cells infected with empty pLKO.1 and pCDH vectors (Control), cells with depleted level of mβPIX containing empty pCDH vector (mβPIX-KD1 + pCDH); cells with depleted level of mβPIX rescued by hβPIX (mβPIX-KD1 + hβPIX). *E*, Box plot of cells with a lower level of GIT1 depletion (mGIT1-KD2; n = 1,590) relative to negative control cells (Control, pLKO.1; n = 1,966). *F*, Box plot of mGIT1-depleted cells (mGIT1-KD1 + pCDH; n = 2,475) relative to negative control cells (Control, pLKO.1 + pCDH; n =2,402) in rescue experiment. *G*, Immunoblot analysis of cells in the GIT1 rescue experiment. Whole cell lysate from cells infected with empty pLKO.1 and pCDH vectors (Control); cells with depleted level of mGIT1 containing empty pCDH vector (mGIT1-KD1 + pCDH); cells with depleted level of mGIT1 rescued by hGIT1 (mGIT1-KD1 + hGIT1). *H*, Box plot of cells containing non-target shRNA (pLKO.1-NT; n = 625) relative to negative control cells (pLKO.1; n = 413). In (*B-C, E-F* and *H*) bold and thin lines within the box represent mean and median (the 50th percentile), respectively. The bottom and top of the box represent the 25th and 75th percentiles. Whiskers below and above the box indicate the 10th and 90th percentiles. ***, $p < 1 \times 10^{-15}$.
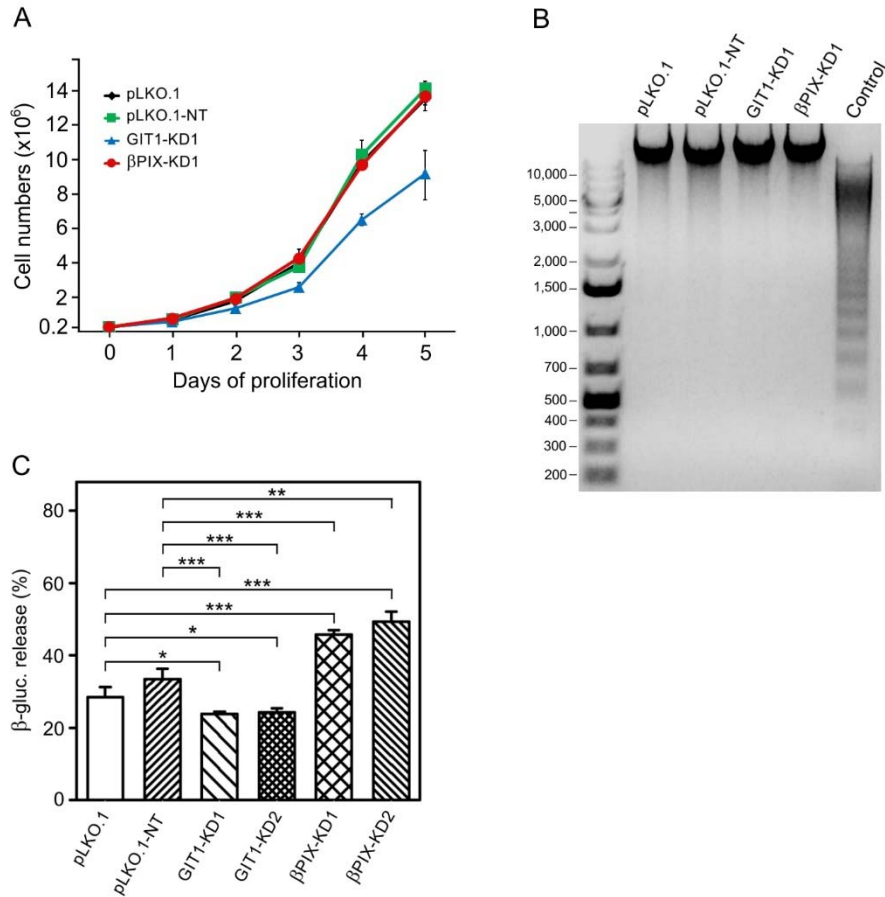
FIGURE S3. Effect of βPIX and GIT1 depletion on cell proliferation, apoptosis and degranulation in BMMCL. *A*, Growth curves of negative control cells (pLKO.1, pLKO.1-NT) and cells with depleted levels of βPIX (βPIX-KD1) or GIT1 (GIT1-KD1). A total of 2×10^5 cells were plated both in controls and βPIX- or GIT1-depleted cells. Values indicate mean $\pm$ SD; n = 3. *B*, Electrophoretic detection of apoptotic cells. DNA size marker (bp) and genomic DNA isolated from negative controls (pLKO.1, pLKO.1-NT), βPIX- (βPIX-KD1) or GIT1- (GIT1-KD1) depleted cells, and apoptotic cells (positive control) separated on 1.5 % agarose gel. *C*, Different effect of βPIX and GIT1 depletion on Ag-induced degranulation. IgE sensitized control cells (pLKO.1, pLKO.1-NT) and cells with depleted levels of βPIX (βPIX-KD1, βPIX-KD2) or GIT1 (GIT1-KD1, GIT1-KD2) were stimulated with 100 ng/ml of Ag and amount of β-glucuronidase released from the cells was determined after 30 min. Means $\pm$ SE were calculated from 3 independent experiments performed in duplicates or triplicates.

VI.3.

Černohorská, M., Sulimenko, V., Hájková, Z., Sulimenko, T., Sládková, V., Vinopal, S., Dráberová, E. & Dráber, P. GIT1/βPIX signaling proteins and PAK1 kinase regulate microtubule nucleation. Submitted 2015

GIT1/βPIX Signaling Proteins and PAK1 Kinase Regulate Microtubule Nucleation

Markéta Černohorská[*]**, Vadym Sulimenko**[*]**, Zuzana Hájková**[*]**, Tetyana Sulimenko**[*]**, Vladimíra Sládková**[*]**, Stanislav Vinopal**[*]**, Eduarda Dráberová**[*] **and Pavel Dráber**[*, 1]

[*]*Department of Biology of Cytoskeleton, Institute of Molecular Genetics, Academy of Sciences of the Czech Republic, CZ-142 20 Prague 4, Czech Republic*

Running title: GIT1/βPIX/PAK1 proteins and microtubule nucleation

[1]Address correspondence to Dr. Pavel Dráber, Department of Biology of Cytoskeleton, Institute of Molecular Genetics, Academy of Sciences of the Czech Republic, Vídeňská 1083, 142 20 Prague 4, Czech Republic. Tel.: (420) 241 062 632, Fax: (420) 241 062 758, E-mail: paveldra@img.cas.cz

Abstract

Microtubule nucleation from γ-tubulin complexes, located at centrosome, is an essential step in the formation of microtubule cytoskeleton. However, signaling mechanisms that regulate microtubule nucleation in interphase cells are largely unknown. In this study, we report that γ-tubulin is in complexes containing G protein-coupled receptor kinase-interacting protein 1 (GIT1), p21-activated kinase interacting exchange factor (βPIX) and p21 protein (Cdc42/Rac)-activated kinase 1 (PAK1) in various cell lines. Immunofluorescence microscopy on human osteogenic sarcoma cells U2OS with TagRFP-tagged GIT1 and βPIX as well as with antibodies to phosphorylated PAK1 revealed association of GIT1, βPIX and activated PAK1 with centrosomes. Microtubule regrowth experiments showed that the depletion of βPIX stimulated microtubule nucleation, while depletion of GIT1 or PAK1 resulted in decreased nucleation in interphase cells. The obtained data were confirmed in case of GIT1 and βPIX by phenotypic rescue experiments, combined knockdown and counting of new microtubules emanating from centrosomes during microtubule regrowth. Importance of PAK1 for microtubule nucleation was confirmed by inhibition its kinase activity with IPA-3 inhibitor. GIT1 with PAK1 thus represent positive and βPIX negative regulators of microtubule nucleation from the interphase centrosomes. We also demonstrated that regulatory roles of GIT1, βPIX and PAK1 in microtubule nucleation correlate with recruitment of γ-tubulin to the centrosome. Furthermore, in vitro kinase assays showed that GIT1 and βPIX, but not γ-tubulin, serve as substrates for PAK1. Finally, direct interaction of γ-tubulin with the N-terminal domain of GIT1, that targets this protein to centrosome, was determined by pull-down experiments. We propose that GIT1/βPIX signaling proteins with PAK1 kinase represent novel regulatory mechanism of microtubule nucleation in interphase cells.

Introduction

During interphase, microtubules built up from αβ-tubulin heterodimers determine the subcellular localization of organelles, promote intracellular transport and direct cell migration. The centrosome is a major site for microtubule organization in animal cells. It comprises a central pair of centrioles surrounded by pericentriolar matrix (1,2). The assembly of the microtubules is a highly regulated process initiated by nucleation. Newly nucleated microtubules become anchored at centrosome and exhibit growth, shrinkage, and stabilization in response to exterior and interior signals.

One of the key components for microtubule nucleation is γ-tubulin (3), a highly conserved member of the tubulin superfamily. It associates with other γ-tubulin complex proteins (GCPs) in the cytoplasm to form γ-tubulin ring complexes (γ-TuRCs) comprising a γ-tubulin small complexes (γTuSC, composed of two molecules of γ-tubulin, one molecule of GCP2, one molecule of GCP3) and some other proteins (4). γ-TuRCs accumulate at the centrosome to serve as templates for microtubule nucleation (1). NEDD1 and several other γ-TuRCs-associated proteins have been implicated in γ-TuRCs regulation, by mediating subcellular targeting of the complexes to centrosomes (5). It is known that recruitment of γ-TuRCs to the centrosome correlates with increased microtubule nucleation at onset of mitosis (6,7), and kinases Plk1 and Cdk1 promote enhanced centrosomal localization of γ-tubulin at mitosis (8,9). It was reported that Src signaling, that leads to activation of the MEK/ERK pathway, regulates microtubule nucleation by promoting the accumulation of γ-tubulin at interphase centrosome (10,11). We recently described that tyrosine-activated G-protein-coupled receptor kinase-interacting protein (GIT)1 and p21-activated kinase interacting exchange factor β (βPIX) interact with γ-tubulin and differentialy modulate nucleation of microtubules in mouse bone marrow-derived mast cells during interphase (12). Thus, microtubule nucleation is dynamically regulated through the cell cycle.

GIT1 and βPIX are multidomain signaling proteins that associate to provide a platform for the formation of macromolecular assemblies (13). The GIT1/βPIX1 complex serves as a signaling cassette that regulates membrane ruffling, focal adhesion turnover, polarity in motile cells, and consequently cell spreading as well as directional migration (14). While involvement of GIT1/βPIX complexes in regulation of actin cytoskeleton is well established, they role in regulation of microtubules is much less understood. GIT1/βPIX complex was found in centrosome and associated PAK1 kinase was activated by centrosome targeting.

Once activated, PAK1 dissociated from GIT1/βPIX and phosphorylated Aurora A in mitosis (15).

In this study, we identified GIT1/βPIX signaling proteins and PAK1 kinase as important regulators of microtubule nucleation in interphase cells. The GIT1 with PAK1 represent positive and βPIX negative regulators of this process. We also demonstrated that regulation is due to changes in γ-tubulin accumulation at interphase centrosome. GIT1/βPIX signaling proteins are phosphorylated by PAK1 and directly interact with γ-tubulin. Binding site for γ-tubulin on GIT1 was located in its N-terminal domain that targets GIT1 to centrosome. Our data suggest a novel regulatory mechanism of microtubule nucleation.

Material and Methods

Reagents

Nocodazole, puromycin, geneticin (G418) and GST-tagged active PAK1 were from Sigma. Protein A immobilized on Trisacryl GF-2000 and SuperSignal WestPico Chemiluminescent reagents were bought from Pierce. Protease-inhibitor mixture tablets (Complete EDTA-free) were from Roche Molecular Biochemicals. PAK1 inhibitor IPA-3 was bought from Merck-Millipore and 20 mM stock was prepared in DMSO. Purified C-terminally FLAG-tagged GIT1, βPIX and nucleophosmin were bought from Origene. Restriction enzymes were from New England Biolabs and Glutathione Sepharose 4 Fast Flow from GE Healthcare Life Sciences. Oligonucleotides were synthesized by Sigma.

Antibodies

The following anti-peptide Abs prepared to human γ-tubulin were used: mouse monoclonal Ab (mAb) TU-30 (IgG1), TU-31 (IgG2b) and mAb TU-32 (IgG1) to the sequence 434–449 (16), and mAb GTU 88 (IgG1; Sigma, Catalog No.T6657) to the sequence 38-53. α-Tubulin was detected with rabbit Ab from Genetex (GTX15246). Rabbit Abs to βPIX (HPA004744), PAK1 (HPA03565), GAPDH (G9545), FLAG (F7425) and actin (A2066) as well as mAb to Hsp70 (H5147) were from Sigma. Rabbit Abs to phosphorylated S144 of PAK1 (ab4079) and pericentrin (ab4448) were from Abcam. Rabbit Abs to GIT1 (sc-13961), PAK1 (sc-882) and phosphorylated T423 of PAK1 (sc-21903) were from Santa Cruz. mAb to ODF2 (cenexin1; H00004957-M01) was from Abnova. Rabbit Ab to tRFP (AB234) was from Evrogen and mAb to paxillin (612405) was from BD Transduction Laboratories. Rabbit Ab to non-muscle myosin heavy chain (BT-561; Biomed Tech. Inc.) and mAb NF-09 (IgG2a) to neurofilament NF-M protein (17) served as negative controls in the immunoprecipitation experiments. Rabbit Ab to GST was from Dr. Pe. Dráber (Institute of Molecular Genetics, Prague, Czech Republic). DY648-, DY549-, DY488- and AMCA-conjugated anti-mouse Abs as well as Cy3-, DY488- and AMCA-conjugated anti-rabbit Abs were from Jackson Immunoresearch Laboratories. Secondary HRP-conjugated antibodies were from Promega Biotech.

Cell cultures and transfection

Human osteogenic sarcoma cell line U-2 OS (U2OS) (Catalog No. ATCC-HTB-96) and human neuroblastoma cells SH-SY5Y (Catalog No. ATCC-CRL-2266) were obtained from

the American Type Culture Collection. Immortalized human retinal pigment epithelial cells stably expressing telomerase reverse transcriptase hTERT-RPE1 (RPE1) were obtained from Dr. M. Bonhivers (Université Bordeaux, Bordeaux, France). HEK 293-FT (HEK) cells were from Promega Biotec. U2OS cells stably expressing EB1-GFP (U2OS-EB1) were described previously (18). Cells were cultured in Dulbecco's modified Eagle's medium (DMEM) containing 10% FCS, penicillin (100 units/ml), and streptomycin (0.1 mg/ml). Cells were grown at 37°C in 5% CO_2 in air and passaged every 2d. In some cases, cells were cultivated with 10 μM nocodazole for 1 h to depolymerize microtubules. Alternatively, cells we incubated with 5 μM IPA-3 for 3 h or with 10 μM IPA-3 for 24h.

HEK cells were transfected with 17 μg DNA per 9-cm tissue culture dish using 51 μg polyethylenimine (Polysciences) and serum-free DMEM. After 12 h, the transfection mixture was replaced with fresh medium supplemented with serum, and cells were incubated for an additional 24 h. The HEK cells for lentivirus production were at passage 4-15.

To prepare U2OS cells stably expressing TagRFP-tagged proteins, cells were transfected with 2.5 μg DNA (phGIT1-TagRFP, phβPIX-TagRFP or phPAK1-TagRFP) per 3-cm tissue culture dish using Lipofectamine LTX (Invitrogen) according to manufacturer's instructions. After 12 h, the transfection mixture was replaced with fresh complete medium and cells were incubated for 48 h. Cells were thereafter incubated in fresh complete medium containing G418 at concentration 1.2 mg/ml for 7 d. Cells expressing fluorescently-tagged protein were flow sorted using the BD Influx cell sorter (BD Bioscience, USA). TagRFP emission was triggered by 561 nm lasers; fluorescence was detected with 585/20 band-pass filter. Lentiviral transduction of U2OS with phTUBG1-TagRFP-puro vector followed by selection in 2.0 μg/ml puromycin was used to prepare stable cell line expressing γ-tubulin-TagRFP. Lentiviral transduction of U2OS with phGIT1(tv1)-neo vector followed by selection in 800 μg/ml G418 was used to prepare stable cell line expressing hGIT1 (U2OS_hGIT1-neo). Cells transduced with vector pCDH-CMV-MCS- EF1-Neo (System Biosciences) were used as a negative control (U2OS_pCDH-neo). Lentiviral transduction of U2OS with pCT-Mito-GFP vector (System Biosciences, CYTO102-PB-1) followed by selection in 2.0 μg/ml puromycin was used to prepare stable cell line with labelled mitochondria.

DNA constructs

Total cellular RNA was isolated from SH-SY5Y cells using RNeasy Mini kit (QIAGEN), according to the manufacturer's directions. The quality of RNA was checked on 2100 Bioanalyzer (Agilent Technologies). Reverse transcription was performed with oligo(dT)

primers and SuperScript III Reverse Transcriptase kit (Invitrogen). The full length human GIT1 (hGIT1, gene *GIT1*) was amplified by PCR using forward 5'-GCTGAGGATGTCCCGAAAGGG-3' and reverse 5'-TGGCAGCACTAAGGGCACTTG-3'primers and SH-SY5Y cell cDNA as template. PCR product was ligated into pCR2.1 vector (Invitrogen) by TA-cloning method resulting in the plasmid pCR-hGIT1 corresponding to transcript variant 1 (tv1; Refseq ID:NM_001085454.1). To prepare C-terminally TagRFP-tagged human GIT1, the coding sequence without stop codon was amplified from the pCR-hGIT1(tv1) using forward 5'-TCCA<u>GAATTC</u>AGGATGTCCCGAAAG -3' and reverse

5'- AGT<u>GTCGAC</u>CTGCTTCTTCTCTCG -3' primers. Sites recognized by restriction endonucleases are underlined. The PCR product was digested with *EcoRI/SalI* and ligated to pCI-TagRFP (18) resulting in the plasmid phGIT1(tv1)-TagRFP. To prepare N-terminally GST-tagged human GIT1(tv1), the coding sequence with stop codon was amplified from the pCR-hGIT1(tv1) using forward 5'- TCCA<u>GAATTC</u>AGGATGTCCCGAAAG -3' and reverse

5'- AGT<u>GTCGAC</u>TCACTGCTTCTTCTCTCG -3' primers. The PCR product was digested with *EcoRI/SalI* and ligated to pGEX-6P-1 (Amersham Biosciences) resulting in the plasmid pGST-hGIT1_1-770. The N-terminal parts of GIT1 (aa 1-124), (aa 1-253) and (aa 1-376) were amplified from pCR-hGIT1(tv1) using forward primer 5'-TCCA<u>GAATTC</u>AGGATGTCCCGAAAG -3' and the following reverse primers:

5'- ATT<u>GTCGAC</u>TTAGAAGTTGGCCTGGGC-3' (aa 1-124), 5'-ATT<u>GTCGAC</u>TTAGTCAGCCATCTGTGGGAT -3' (aa 1-253) and 5'-ATT<u>GTCGAC</u>TTAGAGGTTGTCTGTGG -3' (aa 1-376), respectively. The PCR products were digested with *EcoRI/SalI* and ligated into pGEX-6P-1 (Amersham Biosciences), resulting in the plasmids pGST-hGIT1_1-124, pGST-hGIT1_1-253 and pGST-hGIT1_1-376, respectively. The C-terminal part of GIT1 (aa 377–770) was amplified from pCR-hGIT1(tv1) using forward 5'- TCCA<u>GAATTC</u>GAGCTGTCTCTGCGGAG -3' and reverse 5'- AGT<u>GTCGAC</u>TCACTGCTTCTTCTCTCG -3' primers. The PCR product was digested with *EcoRI/SalI* and ligated into pGEX-6P-1 (Amersham Biosciences), resulting in the plasmid pGST-hGIT1_377-770. The coding sequence of human GIT1, transcript variant 1 (RefSeq ID: NM_001085454.1) was excised from pGST-hGIT1(tv1) with *EcoRI/NotI* and ligated into the pCDH-CMV-MCS-EF1-neo vector (System Biosciences), resulting in the lentiviral construct phGIT1(tv1)-neo.

To prepare C-terminally TagRFP-tagged human βPIX (hβPIX; gene *ARHGEF7*; RefSeq ID: NM_003899.3), the coding sequence without stop codon was amplified from N-terminally GST-tagged hβPIX(tv1), kindly provided by Dr. P.J. Hordijk (19,20) and in this paper denoted as pGST-hβPIX(tv1)_1-646, using forward 5'-AGC<u>GCTAGC</u>GACATGACCGATAATAGC-3' and reverse 5'-TCA<u>GTCGAC</u>TAGATTGGTCTCATCCCA -3' primers. The PCR product was digested with *NheI/SalI* and ligated to pCI-TagRFP(18) resulting in the plasmid phβPIX(tv1)-TagRFP. For a phenotypic rescue experiment, three silent point mutations (a332c, a335c, c338t) were generated in this construct by site-directed mutagenesis using the QuikChange II XL Site-Directed Mutagenesis Kit (Stratagene), according to the manufacturer's protocol. The resulting construct was named phβPIX(tv1)mut-TagRFP. The N-terminal part of hβPIX(tv1) (aa 1-292) was amplified from the pGST-hβPIX(tv1)_1-646 using forward 5'-GCCA<u>GAATTC</u>ATGACCGATAATAGCAAC -3' and reverse 5'-AGT<u>GTCGAC</u>TTACTCCCAGTTCCGGAT -3' primers. The PCR product was digested with *EcoRI/SalI* and ligated to pGEX-6P-1, resulting in the plasmid pGST-hβPIX_1-292. The
C-terminal part of hβPIX(tv1) (aa 293-646) was amplified from the pGST-hβPIX(tv1) using forward 5'- TCCA<u>GAATTC</u>GGCGATGACATTAAAACTC -3' and reverse 5'-AGT<u>GTCGAC</u>TTATAGATTGGTCTCATCCCAG -3' primers. The PCR product was digested with *EcoRI/SalI* and ligated into pGEX-6P-1, resulting in the plasmid pGST-hβPIX_293-646.

To prepare C-terminally TagRFP-tagged human PAK1 (hPAK1; gene *PAK1*; RefSeq ID: NM_001128620.1), the coding sequence without stop codon was amplified from the C-terminally Myc-DDK-tagged PAK1(tv1) (Origene, Catalog No. RC225947) using forward 5'-TAA<u>GCTAGC</u>CATGTCAAATAACGGCCTAGA-3' and reverse 5'-ACA<u>GTCGAC</u>ACTGCAGCAATCAGTGGAGTG -3' primers. The PCR product was digested with *NheI/SalI* and ligated to pCI-TagRFP (18) resulting in the plasmid phPAK1(tv1)-TagRFP.

To prepare C-terminally TagRFP-tagged human γ-tubulin, the coding sequence without stop codon was digested from phTUBG1-FLAG (21) *by EcoRI/SalI* and ligated into pCI-TagRFP(18) resulting in the plasmid phTUBG1-TagRFP. Subsequently, the cassete encoding γ-tubulin-TagRFP was digested from phTUBG1-TagRFP by *Eco*RI/*Not*I and ligated into pCDH-CMV-MCS-EF1-puro vector (System Biosciences), resulting in the lentiviral construct phTUBG1-TagRFP-puro.

To prepare C terminal domain (CTD; aa 572-660) of human NEDD1 (gene *NEDD1*; RefSeq ID: NM_152905.2), corresponding sequence was amplified from the NEDD1 cDNA clone (SC100748; Origene technologies) using forward 5'-CGAATTCTAGCCGACAGCATTGGA-3' and reverse 5'-GGATCCTCAAAAGTGGGCCCGTAA-3' primers. The PCR product was ligated into pCR2.1 vector by TA-cloning method resulting in the plasmid pCR-NEDD1^{CTD}. Subsequently, the fragment corresponding to CTD was digested with *EcoRI/BamHI* and ligated into pEGFP-C3 (Clontech), resulting in the plasmid pEGFP-NEDD1^{CTD} as described previously (22).

All constructs were verified by sequencing. Construct for C-terminally FLAG-tagged human nucleophosmin was obtained from Origene (RC203344). Constructs phTUBG1-FLAG for FLAG-tagged human γ-tubulin (21) and pGST-hTUBG1 for GST-tagged human γ-tubulin (23) were described previously. Plasmid pFYSH2 encoding the GST-tagged SH2 domain of Fyn kinase was described (24).

RNA interference

U2OS cells in 6-well plates were transfected with short interfering RNAs (siRNAs) at final concentration 5 nM using LipofectamineRNAi MAX (Invitrogen) according to the manufacturer's instruction. Cells were harvested 72 h after transfection. The siRNAs that target the regions present in human GIT1 (*GIT1*, NCBI RefSeq: NM_001085454.1, NM_014030.3) were purchased from Ambion and Dharmacon. The siRNAs that target the regions present in human βPIX (*ARHGEF7*, NCBI RefSeq: NM_003899.3, NM_145735.2, NM_001113511.1, NM_001113512.1, NM_001113513.1) were bought from Ambion. The siRNAs that target the regions present in human PAK1 (*PAK1*, NCBI RefSeq: NM_001128620.1, NM_002576.4) were bought from Ambion. Immunoblotting analysis revealed that the highest reduction of GIT1 was obtained with siRNA #s26306 (Ambion); 5'-CCTTGATCATCGACATTCT-3' (GIT1-KD1) and siRNA #J-020565-07 (Dharmacon); 5'-CGAGCTGCTTGTAGTGTAT-3' (GIT1-KD2). The highest reduction of βPIX was obtained with siRNA #s16948; 5'-CAACGACAGGAATGACAAT-3' (βPIX-KD1) and siRNA #s16950; 5'-GGATATTAGTGTCGTGCAA-3' (βPIX-KD2). The highest reduction of PAK1 was obtained with siRNA #143703; 5'-CCGATTTTACCGATCCATT-3' (PAK1-KD1) and siRNA #143705; 5'-CCACTTCCTGTCACTCCAA-3' (PAK1-KD2). Selected siRNAs targeted, correspondingly, all transcript variants of GIT1, ARHGEF7 or PAK1.

To deplete human γ-tubulin 1 (*TUBG1,* NCBI RefSeq: NM_001070.4) siRNA s120194 (Ambion); 5'-CGCATCTCTTTCTCATATA-3' was used (18). Silencer GAPDH positive control siRNA (AM4624) and Silencer Negative Control #1 siRNA were from Ambion (siRNA).

Short hairpin RNAs (shRNAs), cloned into the lentiviral pLKO.1 vectors, were used for depletion of human GIT1, βPIX and PAK1 in phenotypic rescue experiments. A sets of five human GIT1 shRNA constructs, a set of five human βPIX shRNA constructs and a set of four human PAK1 shRNA constructs were purchased from Open Biosystems. Immunoblotting experiments revealed that cells with the highest reduction of GIT1 protein were obtained with vector TRCN0000008401 (GIT1-KD). Similarly, cells with the highest reduction of ARHGEF7 protein were obtained with vector TRCN0000047596 (βPIX-KD), and cells with the highest reduction of PAK1 protein were obtained with vector TRCN0000002227 (PAK1-KD). Selected vectors targeted, correspondingly, all transcript variants of GIT1, ARHGEF7 or PAK1. The stable selected cells with reduced GIT1, βPIX or PAK1 were used for additional experiments. Cells transduced with pLKO.1 vector containing non-target shRNA (Sigma) were used as negative controls.

Lentiviral infection

Lentiviral infections were done as described previously (25) using HEK 293FT packaging cells for virus preparation. Virus particles were added to cells and replaced after 3 d with fresh complete medium containing 2.5 µg/ml puromycin. Stable selection was achieved by culturing cells for 1-2 wks in the presence of puromycin. In phenotypic rescue experiments, selected cells with depleted GIT1, βPIX or PAK1 levels were transfected with phGIT1(tv1)-TagRFP, phβPIX(tv1)mut-TagRFP or phPAK1(tv1)-TagRFP, respectively, using Lipofectamine LTX (Invitrogen) according to manufacturer's protocol and analyzed 72 h after transfection.

Preparation of cell extracts

Whole-cell extracts for SDS-PAGE were prepared by washing the cells in cold HEPES buffer (50 mM HEPES pH 7.6, 75 mM NaCl, 1 mM $MgCl_2$ and 1 mM EGTA), solubilizing them in hot SDS-sample buffer without bromophenol blue and boiling for 5 min. When preparing extracts for immunoprecipitation, cells were rinsed twice in cold HEPES buffer and incubated for 10 min at 4ºC with HEPES buffer supplemented with 1% NP-40 (extraction buffer), protease inhibitor mixture and phosphatase inhibitors (1 mM Na_3VO_4, 1

mM NaF). For GST pull-down assays cells were extracted in RIPA buffer (50 mM Tris pH 8.0, 150 mM NaCl, 1% NP-40, 0.5% sodium deoxycholate, 0.1% SDS) supplemented with protease and phosphatase inhibitors. The suspensions were then spun down (20,000 x g, 15 min, 4ºC) and supernatant was collected. Protein quantification in 1% NP-40 lysates and SDS-PAGE samples was assessed with a bicinchoninic acid assay kit (Pierce) and a silver dot assay, respectively (26).

Immunoprecipitation, GST pull-down assay, kinase assay, gel electrophoresis, and immunoblotting

Immunoprecipitation was performed as previously described (27). Cell extracts were incubated with beads of protein A (Pierce, Rockford, IL) saturated with: (i) mAb TU-31 (IgG2b) to

γ-tubulin, (ii) rabbit Ab to GIT1, (iii) rabbit Ab to βPIX, (iv) rabbit Ab to PAK1 (sc-882), (v) rabbit Ab to non-muscle myosin (negative control), (vi) mAb NF-09 (IgG2a; negative control), or with (vii) immobilized protein A alone. Abs to GIT1, βPIX and PAK1 were used at Ig concentrations of 2 μg/ml. Ab to myosin was used at a dilution of 1:100. mAb TU-31 and mAb NF-09, in the form of hybridoma supernatants, were diluted 1:2. Alternatively beads with immunoprecipitated material were used for the *in vitro* kinase assay as described previously (24). The ^{32}P-labelled-immunocomplexes were separated by gel electrophoresis, blotted to membranes and ^{32}P-labeled proteins

were detected by autoradiography.

Large-scale immunoprecipitation experiments with anti-peptide monoclonal antibody to γ-tubulin TU-31 from HEK cells pretreated with pervanadate to enrich population of phosphotyrosine proteins as well as preparation of samples for MALDI/MS fingerprint analysis were performed as described previously (12). Total 50 ml of 1% NP-40 extract at concentration 1 mg/ml was used for large scale immunoprecipitation.

Preparation and purification of GST-tagged fusion proteins was described previously, as were pull-down assays with whole-cell extracts (28). Alternatively, sedimented beads with immobilized GST-γ-tubulin were incubated with FLAG-tagged GIT1, βPIX or nucleophosmin at a concentration of 0.5 μg/ml in TBS; Tris buffered saline; 10 mM Tris/HCl (pH 7.4) and 150 mM NaCl. In some experiments, 0.1 μg PAK1 kinase (specific activity 63-85 nmole/min/mg) was added to the beads with immobilized GST-fusion proteins and subjected to a kinase assay. For comparison of immunoprecipitation and pull-down assays, protein extracts were used at the same protein concentration.

Gel electrophoresis and immunoblotting were performed using standard protocols (29). For immunoblotting mAb to γ-tubulin (GTU-88) was diluted 1:10,000 and mAb to γ-tubulin (TU-32), in the form of spent culture supernatant, was diluted 1:10. Rabbit Abs to GAPDH, PAK1 (HPA03565), βPIX, actin, FLAG and GIT1 were diluted 1:50,000, 1:5,000, 1:3,000, 1:3,000, 1:2,000 and 1:1,000, respectively. MAbs to paxillin and Hsp70 were diluted 1:30,000 and 1:2,000, respectively. Rabbit Abs to GST and tRFP were diluted 1:50,000 and 1:1,000, respectively. Secondary anti-mouse and anti-rabbit Abs conjugated with HRP were diluted 1:10,000. Bound Abs were detected by SuperSignal WestPico Chemiluminescent reagents (Pierce).

Mass spectrometry

Following large-scale immunoprecipitation and concentration of peptide eluted samples on the GST-Fyn-SH2 domain, proteins dissolved in SDS sample buffer were separated on preparative 7.5% SDS-PAGE using the Multigel-Long electrophoretic system (Biometra). Gels were stained by Coomassie Brilliant Blue G-250. The bands of interest were excised from the gel, destained, and digested by trypsin. Extracted peptides were analyzed by a MALDI-FTICR mass spectrometer (APEX-Qe) equipped with a 9.4 tesla superconducting magnet (both from Bruker Daltonics, Billerica, MA) at the Core facility of the Institute of Microbiology, Academy of Sciences of the Czech Republic. The instrument was externally calibrated by using the PepMix II standart (Bruker Daltonics). The obtained data were processed by Data Analysis 4.0 software (Bruker Daltonics) and searched by the Mascot search engine against the SwissProt 2015 database of all known *Homo sapiens* proteins.

Microtubule regrowth

Microtubule regrowth from centrosomes was followed in nocodazole washout experiment. Cells growing on coverslips were treated with nocodazole at a final concentration of 10 μM for 1 h at 37°C to depolymerize microtubules. Cells were, thereafter, washed with medium precooled to 4°C (4 times 5 min each) to remove the drug, transferred to new medium tempered to 26°C and microtubule regrowth was allowed for 1-3 min at 26°C. Samples were then fixed in formaldehyde/Triton X-100 (30) and postfixed in cold methanol.

Immunofluorescence microscopy

Immunofluorescence staining was performed as described (30). Shortly, cells on coverslips were extracted with 0.1% Triton X-100 in microtubule-stabilizing buffer (MSB), fixed in 3%

formaldehyde in MSB and post-fixed in methanol (Tx/F/M). Alternatively cells were fixed with cold methanol for 20 min. In microtubule regrowth experiments microtubules were stained with rabbit Ab to α-tubulin diluted 1:200. To visualize centrosomes samples were incubated with mAb TU-30 (hybridoma spent culture supernatant) diluted 1:30. Rabbit Abs to pericentrin, PAK1(pS144) and PAK1(pT423) were diluted 1:500, 1:200 and 1:100, respectively. mAb to ODF2(cenexin 1) was diluted 1:200.

The DY549-, DY-648-, DY488- and AMCA-conjugated anti-mouse Abs were diluted 1:800, 1:500, 1:200 and 1:100, respectively. The Cy3-, DY488- and AMCA-conjugated anti-rabbit Abs were diluted 1:1,000, 1:200 and 1:100, respectively. The preparations were mounted in MOWIOL 4-88 (Calbiochem) or in MOWIOL 4-88 supplemented with 4,6-diamidino-2-phenylindole (DAPI; Sigma) and examined on an Olympus AX-70 Provis (Olympus) equipped with 60×/1.0 NA water objective. The preparations from microtubule regrowth assay were examined on the Delta Vision Core system (AppliedPrecision) equipped with 40x/0.75 NA dry objective.

Quantification of the microtubule regrowth assay was performed on a large number of cells that were after staining for α- and γ-tubulin analyzed automatically and compared with the manual analysis of smaller number of cells to confirm reliability of automatic method. In the course of automatic analysis, twenty different areas per sample were taken in both fluorescence channels, and 12 optical z-sections were acquired at 0.45 μm steps. Maximum intensity projection of γ-tubulin staining was used to identify the position of centrosomes. The sum of α-tubulin immunofluorescence intensities was generated by Sum Slices projection in ImageJ software (NIH). The α-tubulin fluorescent signal near the centrosome was measured in two separate concentric circles centered at the centrosome with radii of 1.0 and 1.5 μm (regions of interest; ROIs). Background fluorescence using circles of corresponding sizes was subtracted from each measurement. Measurements were made using ImageJ. In manually performed analysis, only images of cells with a homogenous background around the centrosomes were selected. The sum of α-tubulin immunofluorescence intensities was obtained from 9 consecutive frames (0.2 μm steps) with the middle frame chosen with respect to the highest γ-tubulin intensity. For statistical analysis, two-tailed, unpaired Student's t-test was used to compare samples and to obtain P values.

Microtubule nucleation visualized by time-lapse imaging

For time-lapse imaging, U2OS cells expressing EB1-GFP were grown on glass-bottom-dishes (InVitroScientific, D35-14-1.5-N) and transfected with different siRNAs, as specified in Result section. Cells were treated with nocodazole at a final concentration of 10 μM for 1 h at 37°C to depolymerize microtubules. Cells were thereafter 5 times quickly rinsed with medium for live-cell imaging (DMEM without phenol red, riboflavin, folic acid, pyridoxal, $Fe[NO_3]_3$) tempered to 30°C to remove the drug. Time-lapse sequences were immediately collected for 2 min at 1 sec interval on Delta Vision Core system (Applied Precision) equipped with 60x/1.42 NA oil-immersion objective and heated chamber (30°C). Time-lapse sequences were deconvolved by Hyugens Professional software (SVI, The Netherlands). Newly nucleated microtubules were detected by tracking EB1 comets emanating from centrosomes.

Results

GIT1, βPIX and PAK1 associate with γ-tubulin and locate to centrosomes in U2OS cells

We have previously identified βPIX as protein interacting with γ-tubulin in mouse bone marrow-derived mast cell line pretreated with pervanadate, a potent protein tyrosine phosphatase inhibitor (31). For this we used immunoprecipitation with anti-peptide monoclonal antibody to γ-tubulin, elution of bound proteins with peptide and concentration of eluted tyrosine-phosphorylated proteins on Fyn-SH2 domain. Proteins were then separated on SDS-PAGE and subjected to MALDI/MS fingerprint analysis. Immunoprecipitation experiments confirmed association of γ-tubulin with βPIX and its interaction protein GIT1 (12). To evaluate whether GIT1/βPIX proteins form complexes with γ-tubulin in the other cell type, we applied the same experimental setup in HEK cells. MALDI/MS fingerprint analysis revealed that of the two independent experiments, GIT1 (also known as G protein-coupled receptor kinase-interacting protein 1, ARF GTPase-activating protein GIT1, Cool-associated and tyrosine-phosphorylated Protein, CAT1; gene name *GIT1;* Swiss-Prot identifier Q9Y2X7) was identified in γ-tubulin complex two times. A typical example of MS identification is shown in Supplemental Table I.

In cells, the GIT1/βPIX proteins can form scaffold to bring together signaling molecules affecting various cellular processes, including cytoskeletal organization (14). It is well established that p21 protein (Cdc42/Rac)-activated kinase 1 (PAK1) associates with βPIX (32). To ascertain whether GIT1 and βPIX associate with γ-tubulin in well-adherent U2OS cells and whether PAK1 is part of such complexes, immunoprecipitation experiments were performed with Abs to βPIX, GIT1 and PAK1. Immunoblot analysis revealed the co-precipitation of γ-tubulin with GIT1 (Fig. 1A, lane 3), βPIX (Fig. 1B, lane 3) and PAK1 (Fig. 1C, lane 3) in U2OS cells. In addition, reciprocal precipitation with Ab to γ-tubulin confirmed an interaction of GIT1 (Fig. 1H, lane 3), βPIX (Fig. 1L, lane 3) and PAK1 (Fig. 1P, lane 3) with γ-tubulin. As expected, Ab to GIT1 co-precipitated βPIX (Fig. 1I, lane 3) and PAK1 (Fig. 1M, lane 3), Ab to βPIX co-precipitated GIT1 (Fig. 1F, lane 3) and PAK1 (Fig. 1N, lane 3), and finally Ab to PAK1 co-precipitated GIT1 (Fig. 1G, lane 3) and βPIX (Fig. 1K, lane 3). Immunoprecipitation experiments also confirmed interactions between γ-tubulin and GIT1, βPIX and PAK1 in nontransformed immortalized human retinal pigment epithelial cells RPE1, proving that the association of γ-tubulin with these proteins is not restricted to transformed cells (Supplemental Fig. 1A-P). To independently confirm the

interaction of γ-tubulin with GIT1, βPIX and PAK1, immunoprecipitation experiments were performed from HEK cells expressing C-terminally FLAG-tagged γ-tubulin or nucleophosmin. Antibodies to GIT1, βPIX and PAK1 co-immunoprecipitated exogenous γ-tubulin (Supplemental Fig. 1Q-S, lane 4) but not nucleophosmin as documented in immunoprecipitation with anti-PAK1 Ab (Supplemental Fig. 1T, lane 5). Isotype controls for immunoprecipitation experiments are shown in Supplemental Fig. 2.

The hGIT1, hβPIX and hPAK1 have 2, 5 and 2 transcription variants (tv), respectively. Transcription variants hGIT1(tv1), hβPIX (tv1) and hPAK1(tv1) were detected in U2OS cells using cDNA and specific primers (V. Sládková, unpublished observations). We have prepared cell lines stably expressing phGIT1(tv1)-TagRFP, phβPIX(tv1)-TagRFP or phPAK1(tv1)-TagRFP to evaluate localization of these proteins in U2OS cells. In interphase cells GIT1-TagRFP was associated with centrosomes. Diffuse staining of the cytoplasm and focal adhesions was also observed as demonstrated on fixed cells where centrosomes were stained by anti-γ-tubulin antibody (Fig 2, a-c). Similarly, βPIX-TagRFP was associated with interphase centrosomes and focal adhesions at cell periphery. Diffuse staining in cytoplasm was also detected (Fig 2, d-f). Both GIT1-TagRFP (Supplemental Fig 3a-d) and βPIX-TagRFP (Supplemental Fig 3e-h) were present on mitotic spindle poles. Similar results were obtained in live cells where, however, association of GIT1-TagRFP and βPIX-TagRFP with centrosomes was less obvious due to diffuse staining of cytosol. On the other hand PAK-TagRFP failed to show centrosome enrichment in interphase and mitotic cells. In control cells expressing GFP-tagged mitochondrial marker, no association of the GFP-tagged protein with the centrosome was detected (Fig. 2, g-i). It is well established that increased PAK1 activity is associated with autophosphorylation of specific sites, including S144 and S199 (33). Using Ab recognizing phospho-PAK1(pS144), clear association of autophosphorylated PAK1 with centrosomes both in interphase and mitotic cells was observed (Fig. 3). While the immunostaining was weak in interphase (Fig 3, a-d), more intensive signal was detected in prophase (Fig 3, e-h) and metaphase (Fig 3, i-l) as assessed from DNA staining with DAPI. When cells were stained with Ab to phospho-PAK1(pT423), that marks activated PAK1 (34), interphase and mitotic centrosomes were clearly labelled (Fig 3, m-p). Centrosome localization of GIT1, βPIX and PAK1 was not affected when cells were treated with nocodazole at a final concentration of 10 μM for 60 min at 37°C to depolymerize microtubules. This indicate no requirement for intact microtubules (E. Dráberová, unpublished data). Collectively taken, the data presented suggest that GIT1, βPIX, and

PAK1 form complexes with γ-tubulin in various cell types, and that GIT1, βPIX and active PAK1 associate with interphase and mitotic centrosomes in U2OS.

GIT1, βPIX and PAK1 differently regulate microtubule nucleation

Because GIT1, βPIX and PAK1 interact with γ-tubulin, we compared microtubule regrowth from interphase centrosomes in U2OS cells with a reduced level of GIT1, βPIX or PAK1 in nocodazole-washout experiments. Microtubules were depolymerized with nocodazole and allowed to grow in the absence of the drug. The α-tubulin fluorescence of microtubule asters was measured in ROIs centered at centrosomes that were marked by staining for γ-tubulin, as previously described (10,12). To verify the method we compared microtubule regrowth in cells where the levels of GAPDH (negative control) or γ-tubulin were depleted by siRNAs (Supplemental Fig. 4A). In control cells (siControl), as well as in GAPDH-depleted cells (data not shown), a clearly visible microtubule array, originating from the centrosomes, appeared after 1.5 min regrowth. In cells with knockdown of γ-tubulin only small microtubule asters were formed (Supplemental Fig. 4G, a-b). Statistical evaluation of α-tubulin fluorescence documented clear differences between regrowth in GAPDH-depleted cells (Supplemental Fig. 4B) and γ-tubulin-depleted cells (Supplemental Fig. 4C). The extent of microtubule regrowth could be modulated by mechanisms regulating either microtubule nucleation or microtubule dynamics. It was previously reported that microtubule dynamics is regulated at the cell periphery (35) and that a delay in microtubule regrowth is associated with defects in microtubule nucleation (10,12,36).

A typical results of immunoblotting experiments after depletion of GIT1, βPIX or PAK1 proteins are shown in Fig. 4A, Fig. 4C and Fig. 4E, respectively. At the best silencing, the amount of GIT1 in GIT1-KD1 cells reached $13.4 \pm 2.4\%$, the amount of βPIX in βPIX-KD1 cells $14.3 \pm 3.1\%$ and the amount of PAK1 in PAK1-KD1 cells $19.3 \pm 3.9\%$ (means $\pm$ SD; n = 3), compared with the expression level in control cells containing scrambled siRNA. Three independent experiments were performed with cells with reduced levels of GIT1, βPIX, PAK1 and corresponding control cells. α-Tubulin immunofluorescence was measured at 1.5 min after washout in a 1.0 μm ROI. Results of regrowth experiments are presented after analysis of large number of cells analyzed automatically, but similar results were also obtained after analysis of limited number of cells manually. The GIT1 depletion in both GIT1-KD1 and GIT1-KD2 cells resulted in a decrease of microtubule regrowth (Fig. 4B). On the other hand βPIX depletion led to an increase of microtubule regrowth in both βPIX-

KD1 and βPIX-KD2 cells (Fig. 4D). Finally, PAK depletion resulted in a decrease of regrowth in PAK1-KD1 and PAK1-KD2 cells (Fig. 4F).

For phenotypic rescue experiments we prepared GIT1-, βPIX- or PAK1-deficient cells using lentiviral vectors. At the best silencing, the amount of GIT1 in GIT1-deficient cells reached 11.8 ± 1.9%, the amount of βPIX in βPIX-deficient cells 16.3 ± 2.3% and the amount of PAK1 in PAK1-deficient cells 36.8 ± 3.9% (means ± SD; n = 3), compared with the expression level in control cells with nontarget shRNA (pLKO.1-NT). Depletion of PAK1 in PAK1-deficient cells was thus much less efficient when compared with siRNA. To rescue microtubule regrowth Tag-RFP-tagged GIT1 or βPIX were expressed in in GIT1- or βPIX-deficient cell lines, respectively. As used lentiviral vector targeted 3' UTR of mRNA for GIT1, we could rescue knockdown phenotype with vector producing GIT1-TagRFP. A typical result of immunoblotting experiment is shown in Fig 5A. GIT1 depletion by shRNA resulted in a decrease in microtubule regrowth. Introduction of GIT1-TagRFP into cells with reduced level of GIT1 restored microtubule regrowth as in control cells (Fig. 5B). Two silent point mutations were introduced into βPIX-TagRFP to prevent its depletion by shRNA. A typical result of immunoblotting experiment is shown in Fig 5C. βPIX depletion by shRNA led to an increase in microtubule regrowth. Introduction of βPIX-TagRFP then restored nucleation capacity to that observed in control cells (Fig. 5D).

In combined knockdown βPIX was depleted by siRNA in GIT-deficient cells produced by lentiviral vector (Supplemental Fig. 5A). Also in this case microtubule regrowth was comparable to that in control cells (Supplemental Fig. 5B).

As a second approach, we counted the numbers of new microtubules emanating from centrosomes during microtubule regrowth using the microtubule end-binding protein 1 (EB1) to label plus ends of growing microtubules (37). The number of EB1 comets leaving the centrosomes per unit time (nucleation rate) has been used to measure nucleation events in real time (7,10). For this studies we used live-cell imaging in U2OS cells stably expressing low levels of EB1-GFP (18) to demonstrate that changes in microtubule regrowth in GIT1- and βPIX-depleted cells reflect altered nucleation rates. To verify the method we compared nucleation rates in control cells and cells with depleted level of γ-tubulin. While control cells have nucleation rate 33.6 ± 2.1 comets/min (mean ± SD; n = 43), cells with depleted level of γ-tubulin 26.2 ± 1.4 comets/min (mean ± SD; n = 48). Comparison of nucleation rates in controls and γ-tubulin-depleted cells is shown in Supplemental Fig. 4D. After depletion of GIT1, nucleation rate decreased when compared to control cells (Fig. 6A). On the other hand

depletion of βPIX resulted in the increase of nucleation rate when compared to control cells (Fig. 6B). These data support the results obtained by measuring of α-tubulin signal.

As GIT1 positively regulate microtubule nucleation, we compared microtubule regrowth in cells with increased level of GIT1 (U2OS_GIT1-neo) and in negative control cells (U2OS_pCDH-neo). Only minor increase in nucleation was detected in interphase U2OS_GIT-neo when compared to control cells (Z. Hájková, unpublished data). This suggest that capacity of centrosome to harbor GIT1 or capacity of proteins essential for activation of GIT1 to promote nucleation might be limited in interphase cells.

Collectively taken, these data indicate that GIT1 and PAK1 represent positive and βPIX negative regulators of microtubule nucleation from the interphase centrosomes in U2OS.

GIT1, βPIX and PAK1 regulate requirement of γ-tubulin to the centrosome

As GIT1 and βPIX differently affect microtubule nucleation, we have evaluated the possibility that regulatory role of these proteins in microtubule nucleation is due to different accumulation of γ-tubulin at the centrosome. Firstly we quantified the immunofluorescence intensity of γ-tubulin in control regrowth experiment, secondly in cells with depleted levels of GIT1, βPIX and PAK1. We confirmed in control cells (siControl), as well as in GAPDH-depleted cells (negative control; data not shown), no changes in γ-tubulin signal at centrosomes, while depletion of γ-tubulin (positive control) resulted, as expected, in decrease of γ-tubulin signal (Supplemental Fig 4G, c-d). Statistical evaluation of γ-tubulin fluorescence documented clear differences between GAPDH-depleted (Supplemental Fig. 4E) and γ-tubulin-depleted (Supplemental Fig. 4F) cells.

After depletion of GIT1 (Fig. 7A) and PAK1 (Fig. 7C), the amount of γ-tubulin decreased, while after depletion of βPIX, the amount of γ-tubulin increased (Fig. 7B). The α-tubulin signals measured in these experiments were similar to those documented in Fig. 4, and correlated with the signals for γ-tubulin (M. Černohorská, Z. Hájková unpublished data). Altogether, these data suggest that the regulatory roles of GIT1, βPIX and PAK1 proteins in microtubule nucleation from centrosomes are conveyed by the amount of γ-tubulin nucleation complexes (γTuRCs) at centrosomes.

Centrosomal localization of GIT1, βPIX and PAK1 is independent on γ-tubulin

Since microtubule nucleation in GIT1 and βPIX-depleted cells correlated with the amount of γ-tubulin in centrosome, we wanted to know if centrosomal localization of GIT1 and βPIX in interphase cells is dependent on presence of γ-tubulin. Previously, it has been shown that

carboxy-terminal domain (CTD) of NEDD1 (aa 572-660) does not localize to the centrosome, but over-expression of this domain causes a loss of γ-tubulin from the centrosome by keeping it in cytoplasm (22). We have, therefore, evaluate the presence of GIT1 and βPIX at centrosomes in cells expressing EGFP-tagged CTD of NEDD1 (EGFP-NEDD1^{CTD}). To verify the method, we have first transfected EGFP-NEDD1^{CTD} to U2OS cells stably expressing γ-tubulin-TagRFP and after fixation stained cells with Ab to pericentrin to mark centrosomes. While γ-tubulin-TagRFP colocalized with pericentrin in nontransfected cells, γ-tubulin was not detected at centrosomes in cells expressing EGFP-NEDD1^{CTD} (Supplemental Fig. 6a-d). When EGFP-NEDD1^{CTD} was transfected to U2OS cells stably expressing GIT1-TagRFP, tagged GIT1 colocalized with pericentrin in transfected cells (Fig. 8a-d). Similarly, when EGFP-NEDD1^{CTD} was transfected to U2OS cells stably expressing βPIX-TagRFP, tagged βPIX colocalized with pericentrin in transfected cells (Fig. 8e-h). We have also evaluated the influence of EGFP-NEDD1^{CTD} on the centrosomal localization of phosphorylated PAK1 (PAK1pS144). The PAK1(pS144) was present on spindle poles, marked by ODF2(cenexin1), in cell expressing EGFP-NEDD1^{CTD} (Fig. 8i-l). Taking these findings together it is likely that centrosomal localizations of GIT1, βPIX and PAK1 are γ-tubulin independent and resemble thus the other proteins of pericentriolar matrix.

Identification of γ-tubulin binding sites on GIT1 and βPIX

Because γ-tubulin associated with GIT1 and βPIX in U2OS cells, we attempted to identify the regions on GIT1 and βPIX molecules responsible for interaction with γ-tubulin. GIT1 is a multidomain protein with specific binding sites for βPIX and paxillin (38) as schematically illustrated in Fig 9A. GST-tagged whole-length GIT1, its truncated versions (Fig. 9B) and GST alone were used in pull-down experiments. γ-Tubulin associated with whole-length molecule and all the fusion proteins containing the C-terminal GAP domain (aa 1-376, 1-253 and 1-124). No interaction was observed with fusion protein covering C-terminal half of the molecule (aa 377-770) or GST alone (Fig. 9C, γ-Tb). βPIX interacted with the full-length protein and 1-376 fragment containing Spa2 homology domain (SHD) that is responsible for the binding of βPIX to GIT1 (Fig. 9C, βPIX). We observed almost no binding of endogenous paxillin to the full-length GIT1 protein, while paxillin interacted with the truncated GIT1 (aa 377-770) containing paxillin binding domain PBD (Fig. 9C, Paxillin). Very poor binding of endogenous paxillin to the full-length inactivated GIT1 was reported previously (39). As

expected, PAK1, that associates with βPIX, interacted with the aa region 1-376 (not shown). The staining with Ab to GST was used to detect the amount of immobilized GST fusion proteins (Fig. 9C, GST). These results indicate that association of γ-tubulin with the GST-GIT1 is independent of paxillin. When lysates prepared from wild-type, βPIX- or PAK1-depleted cells were used in pull-down experiment with 1-376 fragment, the amounts of bound of γ-tubulin were comparable in all three samples (V. Sulimenko, unpublished data). γ-Tubulin binding region on GIT1 is thus the most probably in GAP (1-124) domain of GIT1.

βPIX is also multidomain protein with binding sites for GIT1 and PAK1 (40) as schematically illustrated in Fig. 9D. When the pull-down assay was performed with GST-tagged βPIX or N-terminal and C-terminal halves of βPIX molecule (Fig. 9E), γ-tubulin associated with whole-length molecule and C-terminal aa region 293-646. No interaction was observed with fusion protein covering N-terminal half of the molecule (aa 1-292) or GST alone (Fig. 9F, γ-Tb). As expected, GIT1 also interacted with the 293-646 fragment, as it contains GBD domain that is responsible for the binding of GIT1 to βPIX (Fig. 9F, GIT1). PAK1 interacted with βPIX via SH3 domain located in aa region 1-292 (Fig. 9F, PAK1). The amounts of immobilized GST fusion proteins were similar, as evidenced by staining with Ab to GST (Fig. 9F, GST). These results indicate that association of γ-tubulin with the βPIX is independent of PAK1. It is possible, however, that γ-tubulin binds to aa region 293-646 of βPIX via GIT1. When lysates prepared from wild-type or GIT1-depleted cells were used in pull-down experiment with 293-646 fragment, the amount of bound γ-tubulin was comparable (V. Sulimenko, unpublished data). This suggests that γ-tubulin binding to C-terminal half of βPIX is independent of GIT1.

To decide whether γ-tubulin interacts with GIT1 and βPIX directly, the GST pull-down assay was performed with GST-γ-tubulin and purified FLAG-tagged GIT1, βPIX or nucleophosmin (NPM1, negative control). Though both GIT1 and βPIX did bind to GST-γ-tubulin, they failed to bind to GST alone. To γ-tubulin bound more GIT1 than βPIX. FLAG-tagged nucleophosmin did not bind either to GST-γ-tubulin or GST (Fig. 10). The amounts of immobilized GST fusion proteins present in each pull-down were similar (not shown). These data indicate direct binding of GIT1 and βPIX to γ-tubulin.

PAK1 kinase phosphorylates GIT1 and βPIX and inhibits microtubule regrowth

As PAK1 is in complexes with γ-tubulin, we asked whether γ-tubulin can be phosphorylated by this kinase. Kinase assay with GST-tagged γ-tubulin, GIT1 or βPIX and purified active recombinant PAK1 revealed that while GIT1 and βPIX were phosphorylated, phosphorylation of γ-tubulin was not detected. Autophosphorylation of PAK1 was also detected (Fig. 11A).

PAK1 contains a regulatory domain that suppresses the catalytic activity of its kinase domain. IPA-3, an ATP-noncompetitive alosteric inhibitor binds to PAK1 regulatory domain and prevents binding to its upstream activator Rac/Cdc42. IPA-3 is highly specific inhibitor of PAK1 (41). Pretreatment of cells with 10 μM IPA-3 for 24 h followed by immunoprecipitation with Ab to GIT1 and in vitro kinase assay, confirmed that both GIT and co-precipitated βPIX are phosphorylated by PAK1. (Fig 11B). Phosphorylation of γ-tubulin by PAK1 kinase was not observed (V. Sulimenko unpublished data).

We next determined whether inhibition of PAK1 will affect nucleation and targeting γ-tubulin to centrosome. U2OS were preincubated in the presence of 5 μM IPA-3 or DMSO carrier (Control) for 3 h before microtubule regrowth assay. Inhibition of PAK1 activity resulted in decrease of immunofluorescence signal for α-tubulin (Fig 11C) as well as γ-tubulin (Fig. 11D). Collectively taken these results document that GIT1 and βPIX are substrates for PAK1 and that enzymatically active PAK1 modulates nucleation of microtubules in U2OS cells.

Discussion

The assembly of functional microtubules in interphase cells is a fundamental process involving microtubule nucleation, anchorage and regulated growth from centrosomes. In this study, we identified GIT1/βPIX signaling proteins and PAK1 kinase as important modulators of microtubule nucleation. The GIT1 with PAK1 represent positive and βPIX negative regulators of this process. We also demonstrated that regulation is due to changes in γ-tubulin accumulation at interphase centrosome.

Several lines of evidence indicate that the association of GIT1, βPIX and PAK1 with γ-tubulin is specific. First, GIT1 was repeatedly identified by MALDI/MS fingerprint analysis after immunoprecipitation of pervanadate-pretreated cells with an anti-peptide mAb to γ-tubulin, elution of bound proteins with peptide and concentration of tyrosine-phosphorylated proteins on an immobilized SH2 domain. Second, reciprocal precipitation experiments confirmed an interaction between γ-tubulin and GIT1, βPIX or PAK1. Third, FLAG-tagged γ-tubulins interacted with GIT1, βPIX and PAK1. Fourth, purified GIT1 and βPIX interacted with
γ-tubulin. Finally, GIT1-TagRFP and βPIX-TagRFP as well as Abs to phosphorylated PAK1 revealed the localization of GIT1, βPIX and activated PAK1 on centrosomes, where γ-tubulin is accumulated, both in interphase and mitotic cells.

Interaction of γ-tubulin with GIT1, βPIX and PAK1 was observed in human cells of different tissue origin (U2OS, osteogenic sarcoma; HEK, embryonic kidney; RPE1, nontransformed retinal epithelium) as well as on primary culture of mouse bone-marrow mast cells (BMMCs), established BMMC lines and rat basophilic leukemia cell line RBL (12)
(V. Sulimenko unpublished data). Formation of complexes containing γ-tubulin and signaling molecules is, therefore, not limited to one cell type or transformed cells.

GIT1 is multi-domain protein, and several signaling molecules, including βPIX, PAK, focal adhesion kinase (FAK), phospholipase Cγ (PLCγ) and mitogen-activated protein kinase 1 (MEK1), associate with GIT1 through its Spa2 homology domain (SHD). Paxillin binds to the paxillin-binding domain (PBD) located in the C-terminal region of GIT1 (38). Our results from pull-down assays indicate that γ-tubulin can directly interact with GIT1, and its binding site in the N-terminal ARF GTPase-activating protein (ARF-GAP) domain (aa 1-124). It was reported that centrosome targeting of GIT1 resides in this region (15). ADP ribosylation factors (ARFs) are small GTP-binding proteins that have several important

functions, including the recruitment of coat proteins that promote sorting of cargo into vesicles, the recruitment and activation of enzymes, such as the phosphoinositide kinases and interaction with cytoskeletal factors (42). Previously, we showed interaction of membrane-bound

γ-tubulin with regulatory subunit of phosphoinositide 3-kinase (23). It was also showed that γ-TuRC components are associated with recycling endosomes (43). As GIT1 interacts with endosomes (44), it is possible that association of γ-tubulin with GIT1 is not limited to centrosomes.

βPIX is also multidomain protein, that interacts with GIT1 through GIT-binding domain (GBD) and with PAK kinase through SH3 domain located in the N-terminal end of molecule (32). Our pull-down experiments revealed direct binding of γ-tubulin into C-terminal half molecule (aa 293-646), outside SH3 domain. This indicate that interaction of γ-tubulin with PAK1 is indirect. In cells expressing either GFP-tagged whole-length (aa 1-451) or truncated (aa 1-382) γ-tubulin, Abs to βPIX or GIT1 coprecipitated only whole-length γ-tubulin. This indicated that the C-terminal region of γ-tubulin is important for the interaction with GIT1 and βPIX (12).

Phosphorylation map of GIT1 revealed multiple phosphorylation sites (38) but corresponding kinases that phosphorylates these sites are largely unknown. Phosphorylation of GIT1 by PAK1 on serine 709, which is located within PBD of GIT1, increased its binding to paxillin and regulates protrusion activity in cells (45). Another PAK specific phosphorylation site on GIT1 was identified on serine 517 (15). PAK also phosphorylates βPIX with major phosphorylation sites on serine 525 and threonine 526 (46). In vitro kinase experiments with PAK1 kinase and GST-tagged γ-tubulin, GIT1 or βPIX revealed that both GIT1 and βPIX, but not γ-tubulin, serve as substrates for PAK1. The same results were obtained when in vitro kinase assay was performed after immunoprecipitation with Ab to GIT1.

Localization of GIT1, βPIX and PAK1 proteins on centrosomes in U2OS cells is independent on microtubule integrity, ruling out a passive centrosomal accumulation through microtubule transport. Centrosomal localization is also independent on γ-tubulin. In this respect GIT1, βPIX and PAK1 resemble the other proteins of pericentriolar matrix. The GIT1/βPIX complex has been most widely studied in the context of integrin-mediated cell spreading and cell motility (14). The centrosomal function of the complexes in fibroblasts has been so far reported only once. GIT1 targeting to the centrosome served as a scaffold for βPIX, and associated PAK, activated via a process not requiring Rho GTPases,

phosphorylated Aurora A in mitosis (15). Our data demonstrate that GIT1, βPIX as well as PAK1 regulate nucleation of interphase microtubules. Although GIT1, βPIX and phosphorylated PAK are associated with centrosomes in U2OS, they play different regulatory roles in microtubule nucleation. Depletion of βPIX led to increased nucleation, while depletion of GIT1 or PAK1 resulted in decreased nucleation evaluated by α-tubulin signal in close proximity of centrosome. The obtained data were confirmed in case of GIT1 and βPIX by rescue experiments, by combined knockdown, and by counting of new microtubules emanating from centrosomes during microtubule regrowth using the EB1 to label plus end of growing microtubules. Importance of PAK1 for microtubule nucleation was confirmed by inhibition its kinase activity with ATP-noncompetitive allosteric inhibitor IPA-3. GIT1 with PAK1 thus represent positive and βPIX negative regulators of microtubule nucleation from the interphase centrosomes. These findings, in case of GIT1 and βPIX, confirmed our previous results obtained on mast cells (12). Modulation of microtubule nucleation by GIT1 and βPIX is thus not limited only to specialized mast cells containing secretory granules. Exact role of PAK1 in this process is unknown and warrants further investigation.

Microtubule nucleation at the centrosome occurs from γ-TuRCs located in the pericentriolar material (5). We therefore asked whether GIT1/βPIX signaling proteins and PAK1 kinase regulate microtubule nucleation by affecting centrosomal γ-tubulin levels. Our data from measuring γ-tubulin signal in regrowth experiments suggest that while GIT1 and PAK1 promote accumulation of γ-tubulin at centrosome, βPIX inhibit such accumulation. It was reported that androgen and Src signaling, that leads to activation of the MEK/ERK pathway, regulate microtubule nucleation by promoting the accumulation of γ-tubulin at the centrosome (10,11). PAK1 could play similar role by phosphorylation of GIT1 or βPIX. Alternatively PAK1 associated with GIT1/βPIX may phosphorylate components of γTuRC to promote the assembly of the complex, or may regulate the association or activity of NEDD1/GCP-WD, the attachment factor that lies most proximal to γTuRC and which is required for the centrosomal recruitment of γTuRC (47). Additionally, PAK1 may indirectly affect this process by stimulation the assembly of the pericentriolar matrix or the activity of a centrosomal protein(s) required for the anchorage of γTuRCs (5).

In conclusion, our data suggest a novel regulatory mechanism of microtubule formation in interphase cells, in which GIT1 and βPIX signaling proteins, phosphorylated by PAK1 kinase, modulate microtubule nucleation by regulating the amount of γ-tubulin on centrosome.

References

1. Lüders, J., and T. Stearns. 2007. Microtubule-organizing centres: a re-evaluation. *Nat. Rev. Mol. Cell Biol* 8: 161-167.

2. Bornens, M. 2012. The centrosome in cells and organisms. *Science* 335: 422-426.

3. Oakley, C. E., and B. R. Oakley. 1989. Identification of γ-tubulin, a new member of the tubulin superfamily encoded by mipA gene of *Aspergillus nidulans*. *Nature* 338: 662-664.

4. Oegema, K., C. Wiese, O. C. Martin, R. A. Milligan, A. Iwamatsu, T. J. Mitchison, and Y. Zheng. 1999. Characterization of two related *Drosophila* γ-tubulin complexes that differ in their ability to nucleate microtubules. *J. Cell. Biol.* 144: 721-733.

5. Teixido-Travesa, N., J. Roig, and J. Lüders. 2012. The where, when and how of microtubule nucleation - one ring to rule them all. *J. Cell. Sci.* 125: 4445-4456.

6. Khodjakov, A., and C. L. Rieder. 1999. The sudden recruitment of γ-tubulin to the centrosome at the onset of mitosis and its dynamic exchange throughout the cell cycle, do not require microtubules. *J. Cell. Biol.* 146: 585-596.

7. Piehl, M., U. S. Tulu, P. Wadsworth, and L. Cassimeris. 2004. Centrosome maturation: Measurement of microtubule nucleation throughout the cell cycle by using GFP-tagged EB1. *Proc. Natl. Acad. Sci. USA* 101: 1584-1588.

8. Haren, L., M. H. Remy, I. Bazin, I. Callebaut, M. Wright, and A. Merdes. 2006. NEDD1-dependent recruitment of the γ-tubulin ring complex to the centrosome is necessary for centriole duplication and spindle assembly. *J. Cell Biol.* 172: 505-515.

9. Zhang, X., Q. Chen, J. Feng, J. Hou, F. Yang, J. Liu, Q. Jiang, and C. Zhang. 2009. Sequential phosphorylation of Nedd1 by Cdk1 and Plk1 is required for targeting of the gammaTuRC to the centrosome. *J. Cell Sci.* 122: 2240-2251.

10. Colello, D., C. G. Reverte, R. Ward, C. W. Jones, V. Magidson, A. Khodjakov, and S. E. LaFlamme. 2010. Androgen and Src signaling regulate centrosome activity. *J. Cell Sci.* 123: 2094-2102.

11. Colello, D., S. Mathew, R. Ward, K. Pumiglia, and S. E. LaFlamme. 2012. Integrins regulate microtubule nucleating activity of centrosome through mitogen-activated protein kinase/extracellular signal-regulated kinase kinase/extracellular signal-regulated kinase (MEK/ERK) signaling. *J. Biol. Chem.* 287: 2520-2530.

12. Sulimenko, V., Z. Hájková, M. Černohorská, T. Sulimenko, V. Sládková, L. Dráberová, S. Vinopal, E. Dráberová, and P. Dráber. 2015. Microtubule nucleation in mouse bone marrow-derived mast cells is regulated by the concerted action of GIT1/βPIX proteins and calcium. *J. Immunol.* 194: 4099-4111.

13. Schlenker, O., and K. Rittinger. 2009. Structures of dimeric GIT1 and trimeric βPIX and implications for GIT-PIX complex assembly. *J. Mol. Biol.* 386: 280-289.

14. Frank, S. R., and S. H. Hansen. 2008. The PIX-GIT complex: a G protein signaling cassette in control of cell shape. *Semin. Cell Dev. Biol.* 19: 234-244.

15. Zhao, Z. S., J. P. Lim, Y. W. Ng, L. Lim, and E. Manser. 2005. The GIT-associated kinase PAK targets to the centrosome and regulates Aurora-A. *Mo.l Cell.* 20: 237-249.

16. Nováková, M., E. Dráberová, W. Schürmann, G. Czihak, V. Viklický, and P. Dráber. 1996. γ-Tubulin redistribution in taxol-treated mitotic cells probed by monoclonal antibodies. *Cell Motil. Cytoskel.* 33: 38-51.

17. Dráberová, E., V. Sulimenko, V. Kukharskyy, and P. Dráber. 1999. Monoclonal antibody NF-09 specific for neurofilament protein NF-M. *Folia Biol. (Prague)* 45: 163-165.

18. Vinopal, S., M. Černohorská, V. Sulimenko, T. Sulimenko, V. Vosecká, M. Flemr, E. Dráberová, and P. Dráber. 2012. γ-Tubulin 2 nucleates microtubules and is downregulated in mouse early embryogenesis. *PLoS ONE* 7: e29919.

19. ten Klooster, J. P., Z. M. Jaffer, J. Chernoff, and P. L. Hordijk. 2006. Targeting and activation of Rac1 are mediated by the exchange factor beta-Pix. *J. Cell Biol.* 172: 759-769.

20. Bagrodia, S., D. Bailey, Z. Lenard, M. Hart, J. L. Guan, R. T. Premont, S. J. Taylor, and R. A. Cerione. 1999. A tyrosine-phosphorylated protein that binds to an important regulatory region on the cool family of p21-activated kinase-binding proteins. *J. Biol. Chem.* 274: 22393-22400.

21. Horejší, B., S. Vinopal, V. Sládková, E. Dráberová, V. Sulimenko, T. Sulimenko, V. Vosecká, A. Philimonenko, P. Hozák, C. D. Katsetos, and P. Dráber. 2012. Nuclear γ-tubulin associates with nucleoli and interacts with tumor suppressor protein C53. *J. Cell Physiol.* 227: 367-382.

22. Manning, J. A., S. Shalini, J. M. Risk, C. L. Day, and S. Kumar. 2010. A direct interaction with NEDD1 regulates gamma-tubulin recruitment to the centrosome. *PLoS. One.* 5: e9618.

23. Macurek, L., E. Dráberová, V. Richterová, V. Sulimenko, T. Sulimenko, L. Dráberová, V. Marková, and P. Dráber. 2008. Regulation of microtubule nucleation from membranes by complexes of membrane-bound γ-tubulin with Fyn kinase and phosphoinositide 3-kinase. *Biochem. J.* 416: 421-430.

24. Sulimenko, V., E. Dráberová, T. Sulimenko, L. Macurek, V. Richterová, Pe. Dráber, and P. Dráber. 2006. Regulation of microtubule formation in activated mast cells by complexes of γ-tubulin with Fyn and Syk kinases. *J. Immunol.* 176: 7243-7253.

25. Hájková, Z., V. Bugajev, E. Dráberová, S. Vinopal, L. Dráberová, J. Janáček, Pe. Dráber, and P. Dráber. 2011. STIM1-directed reorganization of microtubules in activated cells. *J. Immunol.* 186: 913-923.

26. Dráber, P. 1991. Quantitation of proteins in sample buffer for sodium dodecyl sulfate-polyacrylamide gel electrophoresis using colloidal silver. *Electrophoresis* 12: 453-456.

27. Sulimenko, V., T. Sulimenko, S. Poznanovic, V. Nechiporuk-Zloy, J. K. Böhm, L. Macurek, E. Unger, and P. Dráber. 2002. Association of brain γ-tubulins with αβ-tubulin dimers. *Biochem. J.* 365: 889-895.

28. Kukharskyy, V., V. Sulimenko, L. Macurek, T. Sulimenko, E. Dráberová, and P. Dráber. 2004. Complexes of γ-tubulin with non-receptor protein tyrosine kinases Src and Fyn in differentiating P19 embryonal carcinoma cells. *Exp. Cell Res.* 298: 218-228.

29. Dráber, P., L. A. Lagunowich, E. Dráberová, V. Viklický, and I. Damjanov. 1988. Heterogeneity of tubulin epitopes in mouse fetal tissues. *Histochemistry* 89: 485-492.

30. Dráberová, E., and P. Dráber. 1993. A microtubule-interacting protein involved in coalignment of vimentin intermediate filaments with microtubules. *J. Cell Sci.* 106: 1263-1273.

31. Zick, Y., and R. Sagi-Eisenberg. 1990. A combination of H_2O_2 and vanadate concomitantly stimulates protein tyrosine phosphorylation and polyphosphoinositide breakdown in different cell lines. *Biochemistry* 29: 10240-10245.

32. Manser, E., T. H. Loo, C. G. Koh, Z. S. Zhao, X. Q. Chen, L. Tan, I. Tan, T. Leung, and L. Lim. 1998. PAK kinases are directly coupled to the PIX family of nucleotide exchange factors. *Mol. Cell* 1: 183-192.

33. Chong, C., L. Tan, L. Lim, and E. Manser. 2001. The mechanism of PAK activation. Autophosphorylation events in both regulatory and kinase domains control activity. *J. Biol. Chem.* 276: 17347-17353.

34. Gatti, A., Z. Huang, P. T. Tuazon, and J. A. Traugh. 1999. Multisite autophosphorylation of p21-activated protein kinase gamma-PAK as a function of activation. *J. Biol. Chem.* 274: 8022-8028.

35. Komarova, Y. A., I. A. Vorobjev, and G. G. Borisy. 2002. Life cycle of MTs: persistent growth in the cell interior, asymmetric transition frequencies and effects of the cell boundary. *J. Cell Sci.* 115: 3527-3539.

36. Delgehyr, N., J. Sillibourne, and M. Bornens. 2005. Microtubule nucleation and anchoring at the centrosome are independent processes linked by ninein function. *J. Cell Sci.* 118: 1565-1575.

37. Akhmanova, A., and M. O. Steinmetz. 2008. Tracking the ends: a dynamic protein network controls the fate of microtubule tips. *Nat. Rev. Mol. Cell. Biol.* 9: 309-322.

38. Webb, D. J., M. W. Mayhew, M. Kovalenko, M. J. Schroeder, E. D. Jeffery, L. Whitmore, J. Shabanowitz, D. F. Hunt, and A. F. Horwitz. 2006. Identification of phosphorylation sites in GIT1. *J. Cell Sci.* 119: 2847-2850.

39. Totaro, A., V. Astro, D. Tonoli, and C. de, I. 2014. Identification of two tyrosine residues required for the intramolecular mechanism implicated in GIT1 activation. *PLoS. One.* 9: e93199.

40. Mayhew, M. W., E. D. Jeffery, N. E. Sherman, K. Nelson, J. M. Polefrone, S. J. Pratt, J. Shabanowitz, J. T. Parsons, J. W. Fox, D. F. Hunt, and A. F. Horwitz. 2007. Identification of phosphorylation sites in betaPIX and PAK1. *J. Cell Sci.* 120: 3911-3918.

41. Deacon, S. W., A. Beeser, J. A. Fukui, U. E. Rennefahrt, C. Myers, J. Chernoff, and J. R. Peterson. 2008. An isoform-selective, small-molecule inhibitor targets the autoregulatory mechanism of p21-activated kinase. *Chem. Biol.* 15: 322-331.

42. Donaldson, J. G., and C. L. Jackson. 2011. ARF family G proteins and their regulators: roles in membrane transport, development and disease. *Nat. Rev. Mol. Cell Biol.* 12: 362-375.

43. Hehnly, H., and S. Doxsey. 2014. Rab11 endosomes contribute to mitotic spindle organization and orientation. *Dev. Cell* 28: 497-507.

44. Hoefen, R. J., and B. C. Berk. 2006. The multifunctional GIT family of proteins. *J. Cell Sci.* 119: 1469-1475.

45. Webb, D. J., M. Kovalenko, L. Whitmore, and A. F. Horwitz. 2006. Phosphorylation of serine 709 in GIT1 regulates protrusive activity in cells. *Biochem. Biophys. Res. Commun.* 346: 1284-1288.

46. Koh, C. G., E. Manser, Z. S. Zhao, C. P. Ng, and L. Lim. 2001. Beta1PIX, the PAK-interacting exchange factor, requires localization via a coiled-coil region to promote microvillus-like structures and membrane ruffles. *J. Cell Sci.* 114: 4239-4251.

47. Lüders, J., U. K. Patel, and T. Stearns. 2006. GCP-WD is a γ-tubulin targeting factor required for centrosomal and chromatin-mediated microtubule nucleation. *Nat. Cell Biol* 8: 137-147.

Figure legends

Figure 1. GIT1, βPIX and PAK1 interact with γ-tubulin in U2OS cells.
Extracts from U2OS cells were precipitated with Protein A-immobilized Abs specific to GIT1 (A, E, I and M), βPIX (B, F, J and N), PAK1 (C, G, K and O), or γ-tubulin (D, H, L and P). Blots were probed with Abs to γ-tubulin (γ-Tb), GIT1, βPIX and PAK1. Load (*lane 1*), immobilized Abs not incubated with cell extracts (*lane 2*), immunoprecipitated proteins (*lane 3*), and protein A without Abs, incubated with cell extracts (*lane 4*).

Figure 2. Subcellular localization of TagRFP-tagged GIT1, βPIX in interphase U2OS cells. Cells expressing TagRFP-tagged proteins were fixed and stained for γ-tubulin. (a-c) Localization of GIT1-TagRFP (a) and γ-tubulin (b). Superposition of images (c, GIT1-TagRFP, red; γ-tubulin, green). (d-f) Localization of βPIX-TagRFP (d) and γ-tubulin (e). Superposition of images (f, βPIX, red; γ-tubulin, green). (g-i) Localization of control mitochondrial Mito-GFP (g) and γ-tubulin (h). Superposition of images (i, Mito-GFP, green; γ-tubulin, red). In (a-i), the best centrosomal plane is shown. Centrosomal regions are enlarged in the inserts. Arrow in (d) point to blown-up region. Fixation Tx/F/M. Bars, 20 μm.

Figure 3. Phosphorylated PAK1 is located on centrosome and increased in mitotic cells. U2OS cells in interphase (a-d), prophase (e-h) or metaphase (i-l) double-label stained with Abs to PAK1(pS144) (a, e, i; red) and γ-tubulin (b, f, j; green). DAPI (c, g, k; blue). Superposition of images (a-c), (e-g) and (i-k) is shown in (d), (h) and (l), respectively. Fixation by methanol. Bars, 10 μm. U2OS cells double-label stained with Ab to PAK1(pT423) (m; red) and γ-tubulin (n; green). DAPI (o; blue). Superposition of images (m-o) is shown in (p). Fixation by methanol. Bar, 10 μm.

Figure 4. GIT1, βPIX and PAK1 differently modify microtubule regrowth.
(A, C, E) Immunoblot analysis of cells with reduced levels of GIT1 (A), βPIX (C) or PAK1(E). Whole-cell lysates from cells transfected with scrambled siRNA (siControl), GIT1 (A) or βPIX (C) or PAK1 (E) siRNAs. Numbers under the blots indicate relative amount of GIT1 (A), βPIX (C) or PAK1 (C) normalized to control cells and to the amount of actin in individual samples (Fold). (B, D, F) Statistical analysis of α-tubulin fluorescence intensity in

cells with depletion of GIT1 (B), βPIX (D) or PAK1 (F) relative to the control cells. Distribution of α-tubulin fluorescence intensities (arbitrary units [AU]) in 1.0-μm ROI at 1.5 min of regrowth are shown as box plots (three independent experiments, > 96 cells counted for each experimental condition). (B) Box plot of GIT1-depleted cells (GIT-KD1, n = 1116; GIT-KD2, n = 631) relative to control cells (siControl, n = 942). (D) Box plot of βPIX-depleted cells (βPIX-KD1, n = 993; βPIX-KD2, n = 1228) relative to control cells (siControl, n = 1052). (F) Box plot of PAK1-depleted cells (PAK1-KD1, n = 304; PAK1-KD2, n = 288) relative to control cells (siControl, n = 313). In (B, D, F) bold and thin lines within the box represent mean and median (the 50th percentile), respectively. The bottom and top of the box represent the 25th and 75th percentiles. Whiskers below and above the box indicate the 10th and 90th percentiles. ***, $p < 1 \times 10^{-5}$.

Figure 5. Rescue of microtubule regrowth in cells with depleted levels of GIT1 or βPIX. (A, C) Immunoblot analysis of whole cell lysates in GIT1 (A) or βPIX (C) phenotypic rescue experiments. (B, D) Microtubule regrowth in GIT1 (B) or βPIX (D) phenotypic rescue experiments. Distribution of α-tubulin fluorescence intensities (arbitrary units [AU]) in 1.0-μm ROI at 1.5 min of regrowth are shown as box plots (three independent experiments, > 53 cells counted for each experimental condition). (A) Cells infected with non-target shRNA (pLKO.1-NT) containing pCI-TagRFP vector (pLKO.1-NT + RFP), cells selected after depletion of GIT1 by shRNA containing pCI-TagRFP vector (GIT1-KD + RFP), cells with depleted level of GIT1 rescued by pGIT1-TagRFP (GIT1-KD + GIT1-RFP). Blots probed with Abs to GIT1, RFP and actin. Black and white arrowheads point to GIT1 or GIT1-TagRFP, respectively. (B) Box plot of GIT1-depleted cells (GIT1-KD + RFP; n=171) and GIT1-depleted cells rescued by GIT1-TagRFP (GIT1-KD +GIT1-RFP; n = 190) relative to control cells (pLKO.1-NT + RFP; n = 160). (C) Cells infected with non-target shRNA (pLKO.1-NT) containing pCI-TagRFP vector (pLKO.1-NT + RFP), cells selected after depletion of βPIX by shRNA containing pCI-TagRFP vector (βPIX-KD + RFP), cells with depleted level of βPIX rescued by pβPIXmut-TagRFP (βPIX-KD + βPIX-RFP). Blots probed with Abs to βPIX, RFP and actin. Black and white arrowheads point to βPIX or βPIXmut-TagRFP, respectively. (D) Box plot of βPIX-depleted cells (βPIX-KD + RFP; n = 160) and βPIX-depleted cells rescued by βPIXmut-TagRFP (βPIX-KD + βPIX-RFP; n = 203) relative to control cells (pLKO.1-NT +

RFP; n = 190). In (B, D) bold and thin lines within the box represent mean and median (the 50th percentile), respectively. The bottom and top of the box represent the 25th and 75th percentiles. Whiskers below and above the box indicate the 10th and 90th percentiles. ***, p $< 1 \times 10^{-5}$.

Figure 6. GIT1 and βPIX differently regulate microtubule nucleation. Statistical analysis of nucleation rate in cells with depleted level of GIT1 (A) or βPIX (B) relative to the control cells (siControl). Time-lapse imaging was used to track newly nucleated microtubules in cells stably expressing EB1-GFP. The rate of nucleated microtubules (EB1 comets/min) calculated from three independent experiments, > 14 cells counted for each experimental condition. Bold line represents mean. *, p < 0.05.

Figure 7. GIT1 and βPIX differently affect accumulation of γ-tubulin to centrosome. Statistical analysis of γ-tubulin fluorescence intensity in cells with depleted level of GIT1 (A), βPIX (B) or PAK1 (C) relative to the control cells. Distribution of γ-tubulin fluorescence intensities (arbitrary units [AU]) in 1-μm ROI at 1.5 min of regrowth are shown as box plots (three independent experiments, > 75 cells counted for each experimental condition. (A) Box plot of GIT1-depleted cells (GIT-KD1, n = 612) relative to control cells (siControl, n = 816). (B) Box plot of βPIX-depleted cells (βPIX-KD1, n = 452) relative to control cells (siControl, n = 672). (C) Box plot of PAK1-depleted cells (PAK1-KD1, n = 225) relative to control cells (siControl, n = 240). Bold and thin lines within the box represent mean and median (the 50th percentile), respectively. The bottom and top of the box represent the 25th and 75th percentiles. Whiskers below and above the box indicate the 10th and 90th percentiles. ***, p $< 1 \times 10^{-5}$.

Figure 8. Centrosomal localization of GIT1, βPIX and PAK1 is not dependent on γ tubulin. (a-d) Cells expressing EGFP-tagged C-terminal domain of NEDD1 (a, EGFP-NEDD1^{CTD}) and TagRFP-tagged GIT1 (b) were fixed and stained for pericentrin (c). Superposition of images (d, EGFP-NEDD1^{CTD}, green; GIT1-TagRFP, red; pericentrin, blue). (e-h) Cells expressing EGFP-NEDD1^{CTD} (e) and TagRFP-tagged βPIX (f) were fixed and stained for pericentrin (g). Superposition of images (h, EGFP-NEDD1^{CTD}, green; βPIX-TagRFP, red; pericentrin, blue).

(**i-l**) Cells expressing EGFP-NEDD1^{CTD} (i) were fixed and double-label stained with rabbit Ab to PAK1(pS144) (j) and mouse Ab to ODF2 (k). Superposition of images (l, EGFP-NEDD1^{CTD}, green; pS144-PAK1, red; ODF2, blue). Centrosomal regions in cells expressing EGFP-NEDD1^{CTD} are enlarged in the inserts. Note presence of GIT1, βPIX and PAK1 proteins on centrosomes in cells expressing EGFP-NEDD1^{CTD}. Fixation by methanol. Bars, 20 μm (d, h);

10 μm (l).

Figure 9. Interaction of γ-tubulin with GIT1 and βPIX domains in GST pull-down assay. (A) Schematic illustration of GIT1 (isoform 3) with domains. GIT1 contains ARF-GAP domain (GAP), ankyrin repeats (ANK), Spa2 homology domain (SHD), synaptic localization domain (SLD) and paxillin-binding domain (PBD). βPIX and paxillin associate with GIT1 through SHD and PBD domain, respectively. (B) Truncated forms of GIT1 used in pull-down assay. (C) Whole-cell lysates (Load) were incubated with GST-fusion proteins or GST alone immobilized on Glutathione-Sepharose beads. Immunoblots of bound proteins were probed with Abs to γ-tubulin (γ-Tb), βPIX, paxillin and GST. Molecular-mass markers (in kDa) are indicated on the left. (D) Schematic illustration of βPIX (isoform 1) with domains. βPIX contains SH3 homology 3 domain (SH3), Dbl homology domain containing the Rho GEF activity (DH), pleckstrin homology domain (PH), prolin-rich region (PxxP), GIT binding domain (GBD) and coiled-coil region (CC). PAK1 and GIT1 associate with βPIX through SH3 and GBD domain, respectively. (E) Truncated forms of βPIX used in pull-down assay. (F) Whole-cell lysates (Load) were incubated with GST-fusion proteins or GST alone immobilized on Glutathione-Sepharose beads. Immunoblots of bound proteins were probed with Abs to γ-tubulin (γ-Tb), GIT1, PAK1 and GST. Molecular-mass markers (in kDa) are indicated on the left.

Figure 10. γ-Tubulin directly interacts with GIT1 and βPIX in pull-down assay. Purified FLAG-tagged GIT1, βPIX or nucleophosmin (NMP1; negative control) were incubated with immobilized GST-γ-tubulin (GST-γ-Tb) or GST alone. Controls were incubated without FLAG-tagged proteins. Immunoblots of bound proteins were probed with Abs to FLAG and GST. Molecular-mass markers (in kDa) are indicated on the left.

Figure 11. PAK1 phosphorylates GIT1 and βPIX, and inhibition of its enzymatic activity attenuates microtubule nucleation.

(A) PAK1 phosphorylates GIT1 and PIX in vitro. GST-fusion proteins were immobilized on Glutathione-Sepharose beads and subjected to in vitro kinase assay with active PAK1. Blots were probed with Ab to GST and phosphorylated proteins were detected by autoradiography (^{32}P). (B) PAK1 phosphorylates GIT1 and PIX in vivo. Cells pretreated for 24 h with 10 μM IPA-3, ATP-noncompetitive inhibitor of PAK1 kinase activity, or DMSO carrier alone were precipitated with Ab to GIT1, and immunocomplexes were subjected to in vitro kinase assays. Blots were probed with Abs to GIT1 or βPIX and phosphorylated proteins were detected by autoradiography (^{32}P). Black and white arrowheads in (A-B) point to GIT1-GST and βPIX-GST, respectively. (C-D) Effect of PAK1 inhibition on microtubule nucleation. U2OS were preincubated in the presence of 5 μM IPA-3 or DMSO carrier (Control) for 3 h before microtubule regrowth assay. Distributions of α-tubulin or γ-tubulin fluorescence intensities (arbitrary units [AU]) in 1.0-μm ROI at 1.5 min of regrowth are shown as box plots (three independent experiments, > 133 cells counted for each experimental condition). (C) Box plot of α-tubulin fluorescence intensities in IPA-3 preincubated cells (+IPA- 3, n = 418) relative to control cells (Control, n = 400). (D) Box plot of γ-tubulin fluorescence intensities in IPA-3 preincubated cells (+IPA-3, n = 418) relative to control cells (Control, n = 400). Bold and thin lines within the box represent mean and median (the 50th percentile), respectively. The bottom and top of the box represent the 25th and 75th percentiles. Whiskers below and above the box indicate the 10th and 90th percentiles. ***, p < 1 x 10^{-5}

FIGURES

Figure 1

IP: anti-GIT1	IP: anti-βPIX	IP: anti-PAK 1	IP: anti-γ-Tb	
A	B	C	D	γ-Tb
E	F	G	H	GIT1
I	J	K	L	βPIX
M	N	O	P	PAK1

1 2 3 4   1 2 3 4   1 2 3 4   1 2 3 4

Figure 2

a   GIT1-TagRFP
b   γ-Tb
c   Merge
d   βPIX-TagRFP
e   γ-Tb
f   Merge
g   Mito-GFP
h   γ-Tb
i   Merge

Figure 3

PAK1(pS144)   γ-Tb   DAPI   Merge

a   b   c   d

e   f   g   h

i   j   k   l

PAK1(pT423)   γ-Tb   DAPI   Merge

m   n   o   p

Figure 4

Figure 5

A

B

C

D
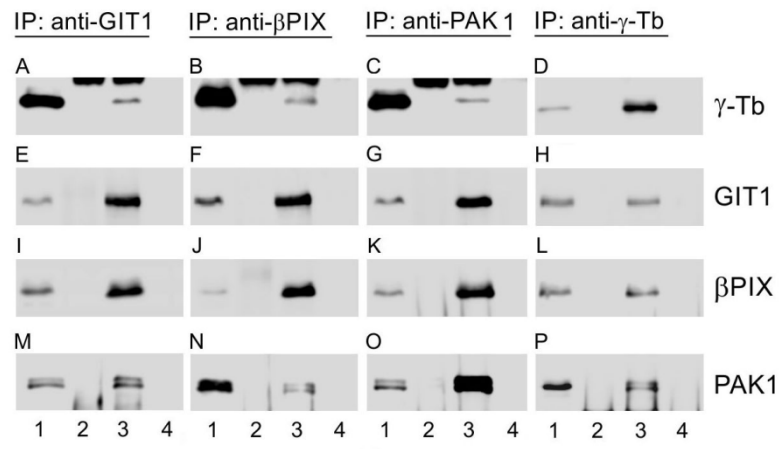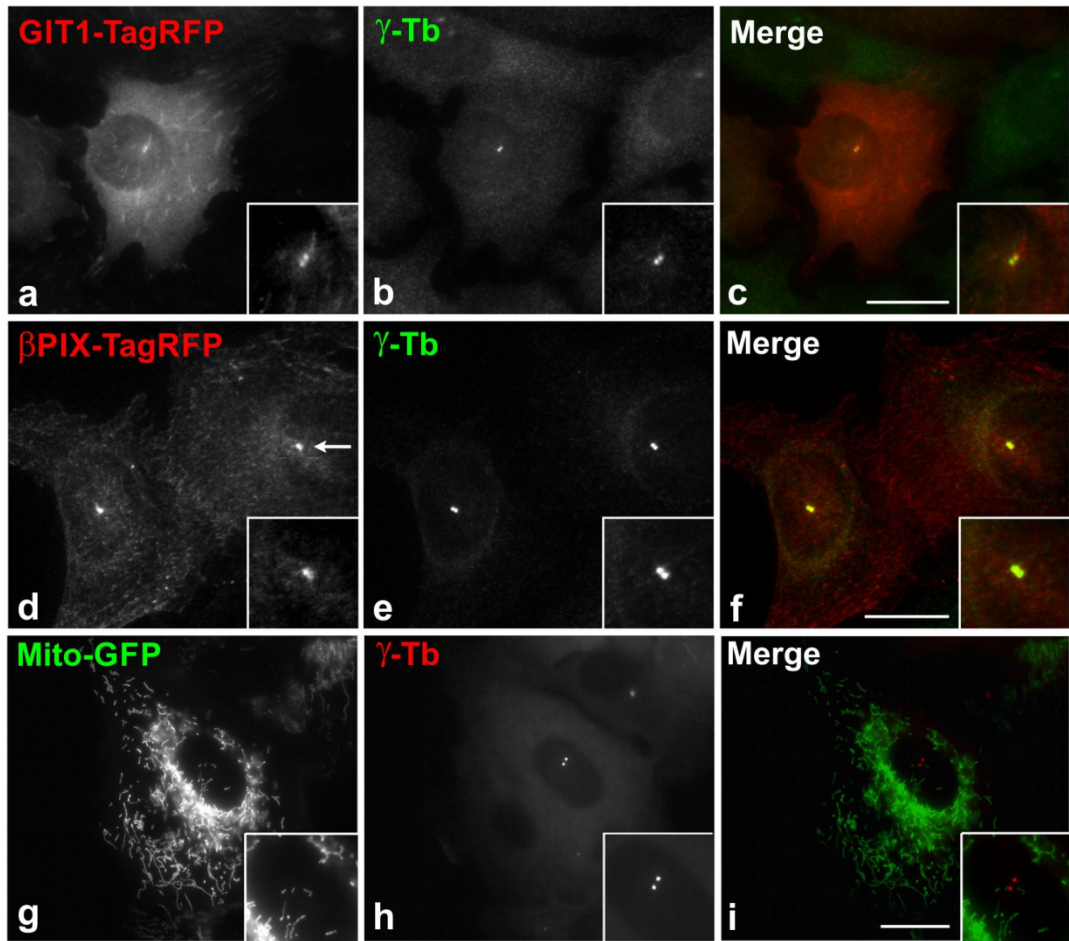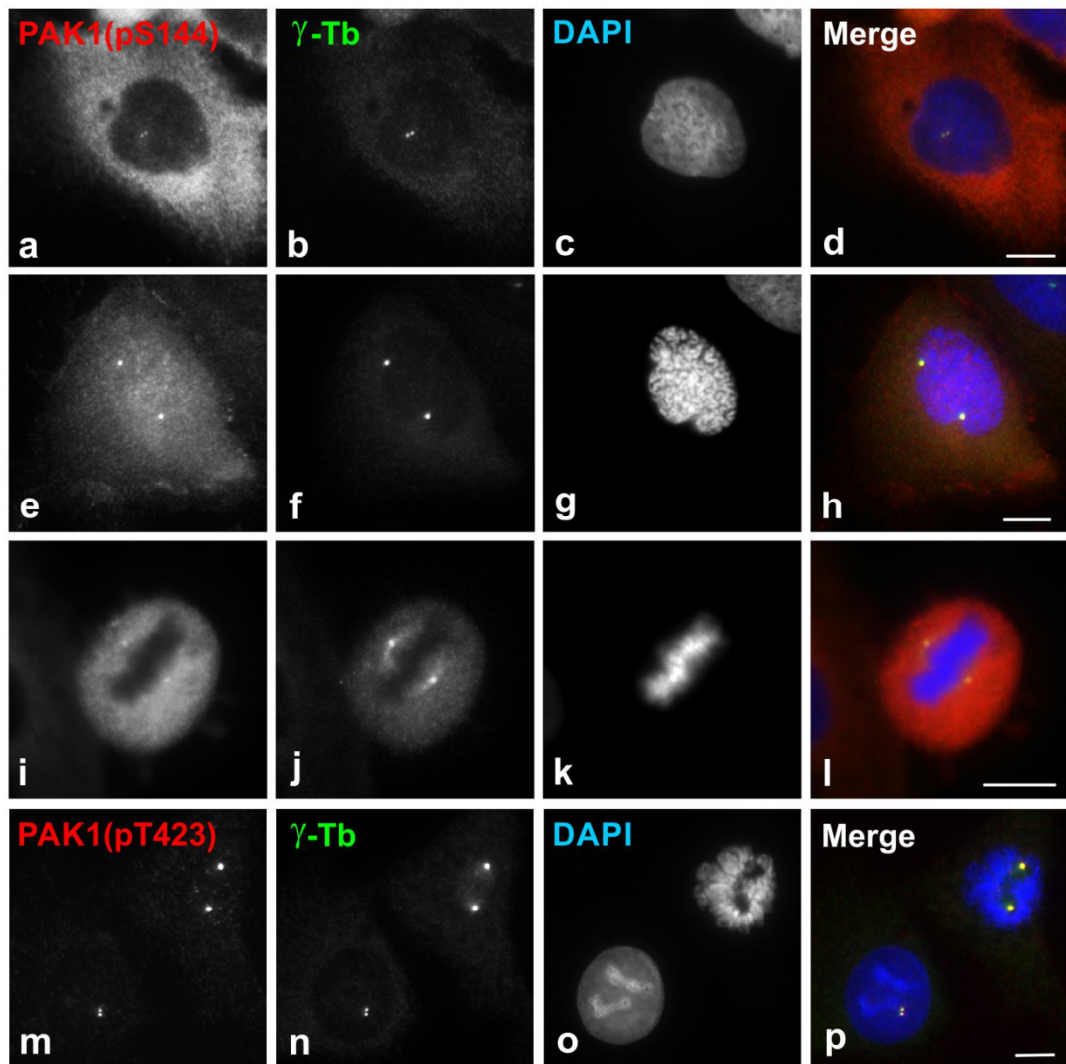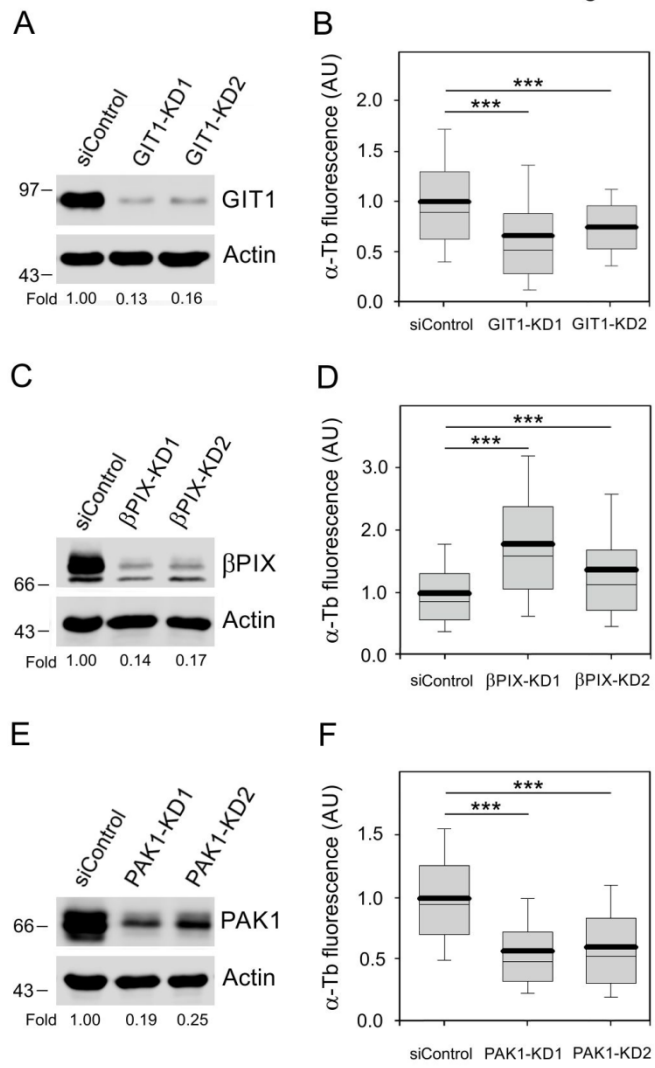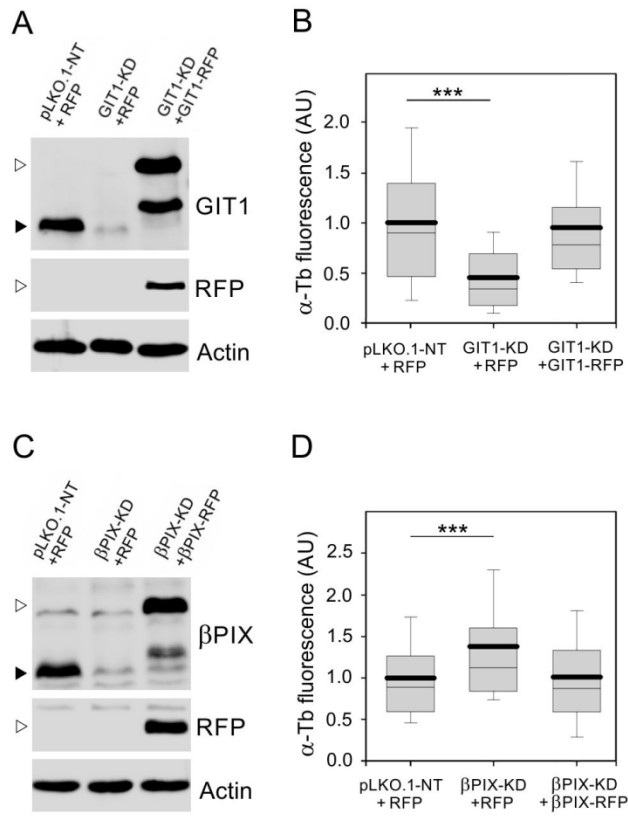
Figure 6

Figure 7

Figure 8

EGFP-NEDD1^CTD	GIT1-TagRFP	Pericentrin	Merge
a	b	c	d
EGFP-NEDD1^CTD	βPIX-TagRFP	Pericentrin	Merge
e	f	g	h
EGFP-NEDD1^CTD	PAK1(pS144)	ODF2	Merge
i	j	k	l
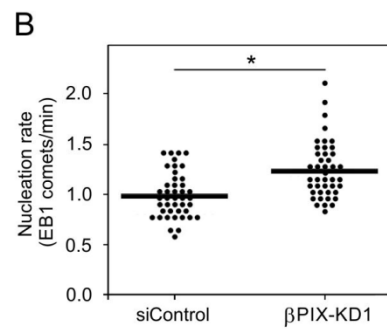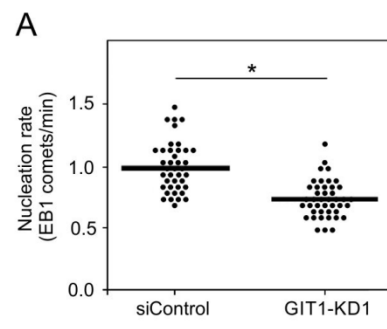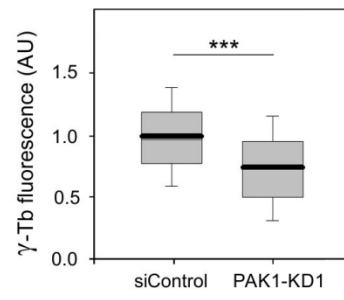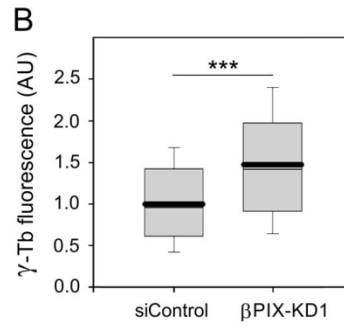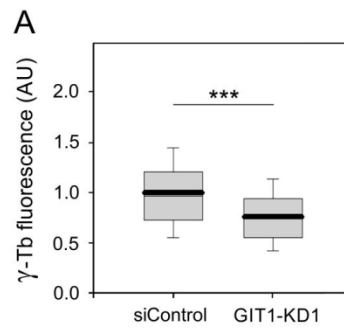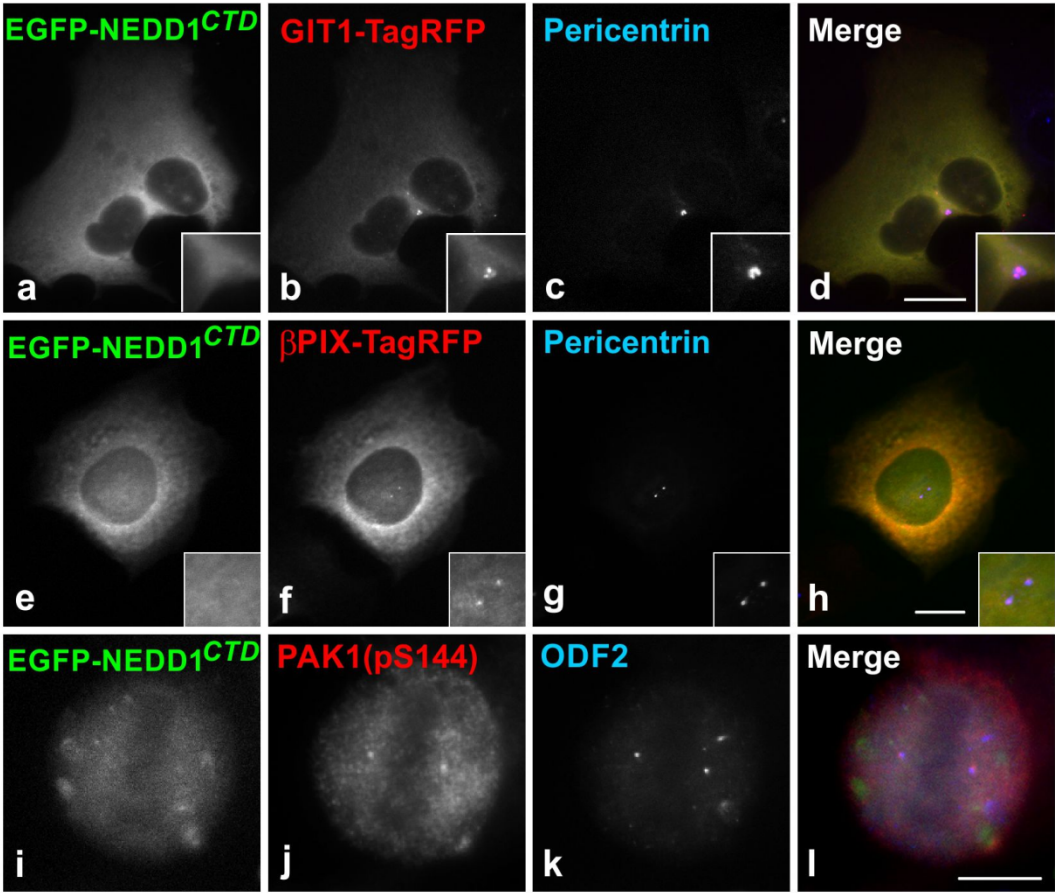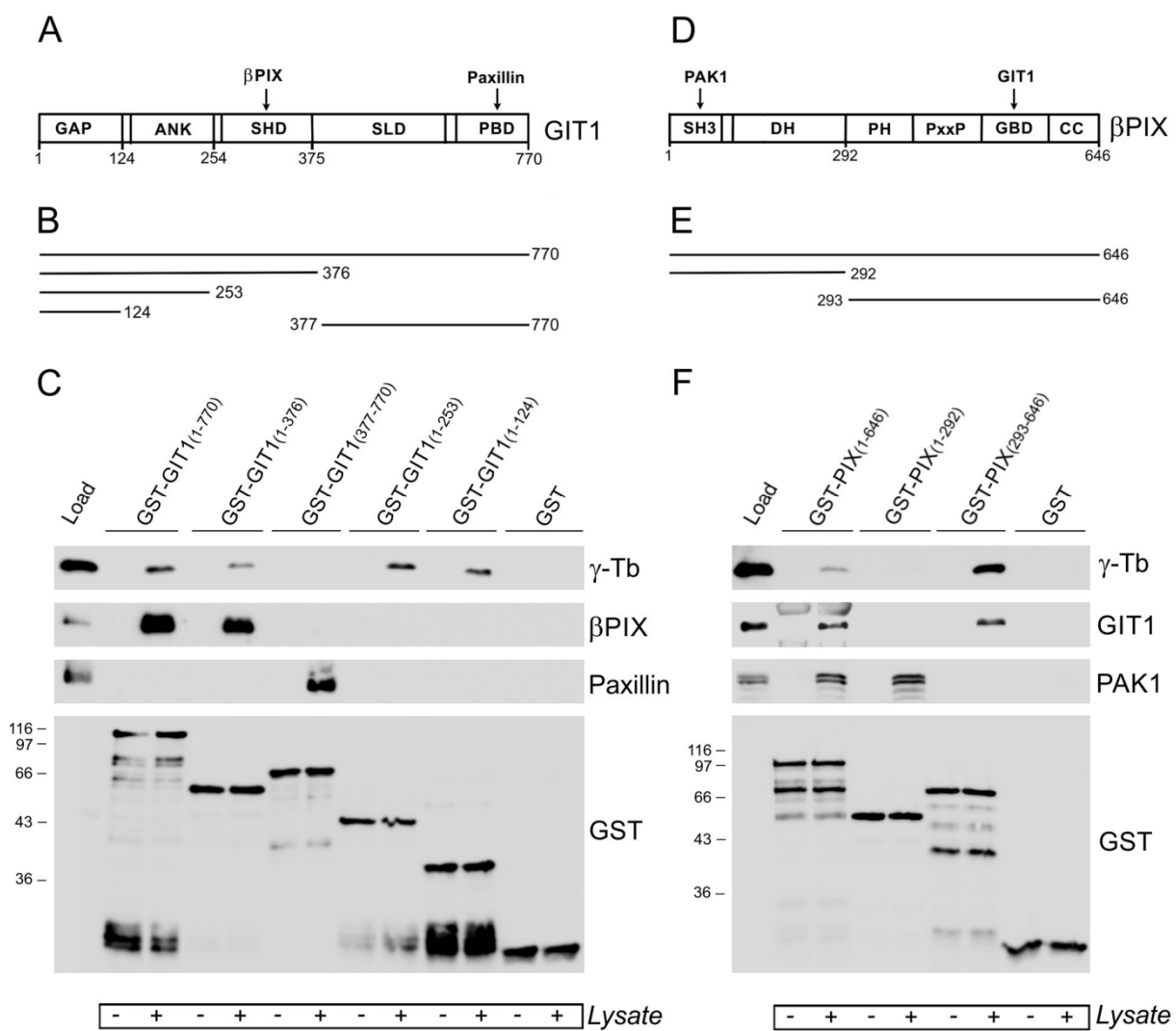
Figure 9
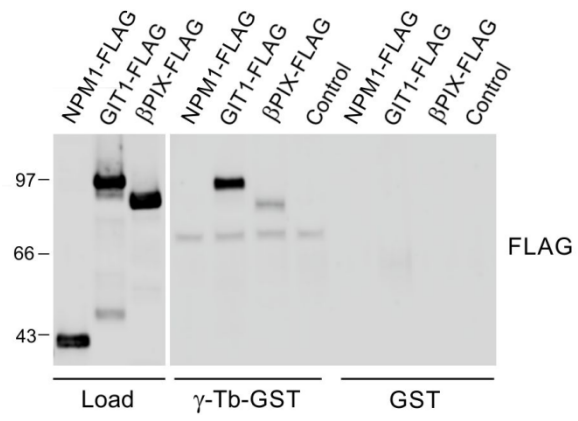
Figure 10

Figure 11

Supplement

Černohorská, M., Sulimenko, V., Hájková, Z., Sulimenko, T., Sládková, V., Vinopal, S., Dráberová, E. & Dráber, P. GIT1/βPIX signaling proteins and PAK1 kinase regulate microtubule nucleation. Submitted 2015

Figure S1. GIT1, βPIX and PAK1 interact with γ-tubulin in nontransformed RPE1 cells and with exogenous γ-tubulin.

(*I*) Extracts from RPE1 cells were precipitated with Protein A-immobilized Abs specific to GIT1 (A, E, I and M), βPIX (B, F, J and N), PAK1 (C, G, K and O), or γ-tubulin (D, H, L and P). Blots were probed with Abs to γ-tubulin (γ-Tb), GIT1, βPIX and PAK1. Load (*lane 1*), immobilized Abs not incubated with cell extracts (*lane 2*), immunoprecipitated proteins (*lane 3*), and protein A without Abs, incubated with cell extracts (*lane 4*). (*II*) Extracts from HEK cells expressing FLAG-tagged γ-tubulin or FLAG-tagged nucleophosmin were precipitated with Protein A-immobilized Abs specific to GIT1 (Q), βPIX (R) or PAK1 (S, T). Blots were probed with Abs to γ-tubulin (γ-Tb) or FLAG. Load with γ-tubulin-FLAG (*lane 1*), load with nucleophosmin-FLAG (*lane 2*), immobilized Abs not incubated with cell extract (*lane 3*), immunoprecipitated proteins from extract containing γ-tubulin-FLAG (*lane 4*), immunoprecipitated proteins from extract containing nucleophosmin-FLAG (*lane*

5), protein A without Abs, incubated with cell extract containing γ-tubulin-FLAG (*lane 6*) and protein

A without Abs, incubated with cell extract containing nucleophosmin-FLAG (*lane 7*).

Black arrowheads and white arrowhead point to γ-tubulin-FLAG or nucleophosmin-FLAG, respectively.
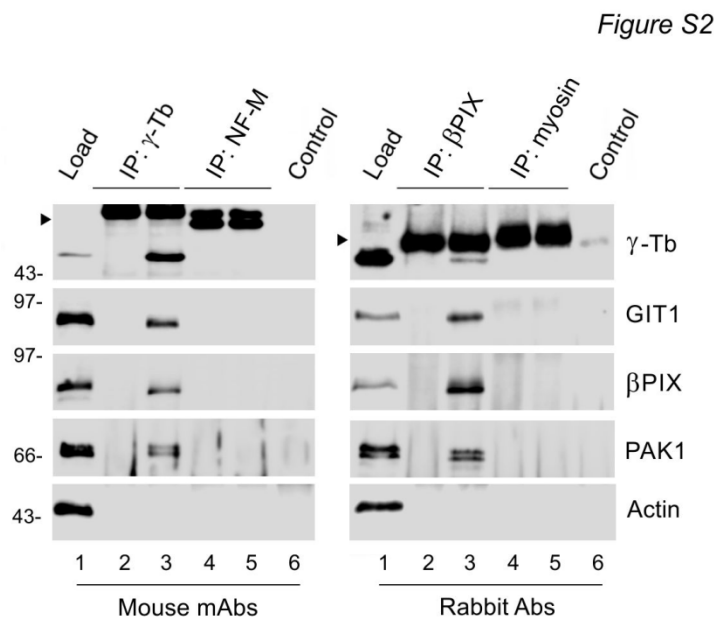
Figure S2. Isotype controls for immunoprecipitation experiments.

Extracts from U2OS cells were precipitated with Protein A-immobilized mAb to γ-tubulin (IgG2b), mAb to NF-M (IgG2a), rabbit Ab to βPIX or rabbit Ab to myosin. Blots were probed with Abs to γ-tubulin (γ-Tb), GIT1, βPIX, PAK1 and actin. Load (*lane 1*), immobilized Abs not incubated with cell extracts (*lanes 2 and 4*), immunoprecipitated proteins (*lanes 3 and 5*), and Protein A without Ab, incubated with cell extract (*lane 6*, Control). Molecular-mass markers (in kDa) are indicated on the left. Black arrowheads indicate positions of Ab heavy chains.
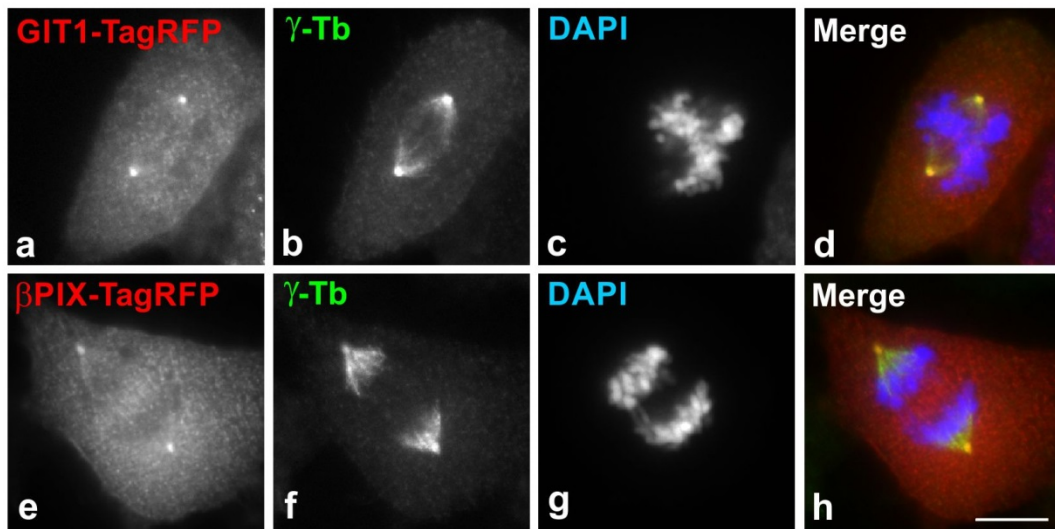
Figure S3. Subcellular localization of TagRFP-tagged GIT1 and βPIX in mitotic U2OS cells. Cells expressing TagRFP-tagged proteins were fixed and stained for γ-tubulin. (a-d) Localization of GIT1-TagRFP (a), γ-tubulin (b) and DAPI (c). Superposition of images (d, GIT1-TagRFP, red; γ-tubulin, green; DAPI, blue). (e-h) Localization of βPIX-TagRFP (e), γ-tubulin (f) and DAPI (g). Superposition of images (h, βPIX-TagRFP, red; γ-tubulin, green; DAPI, blue). Fixation Tx/F/M. Bar, 10 μm.
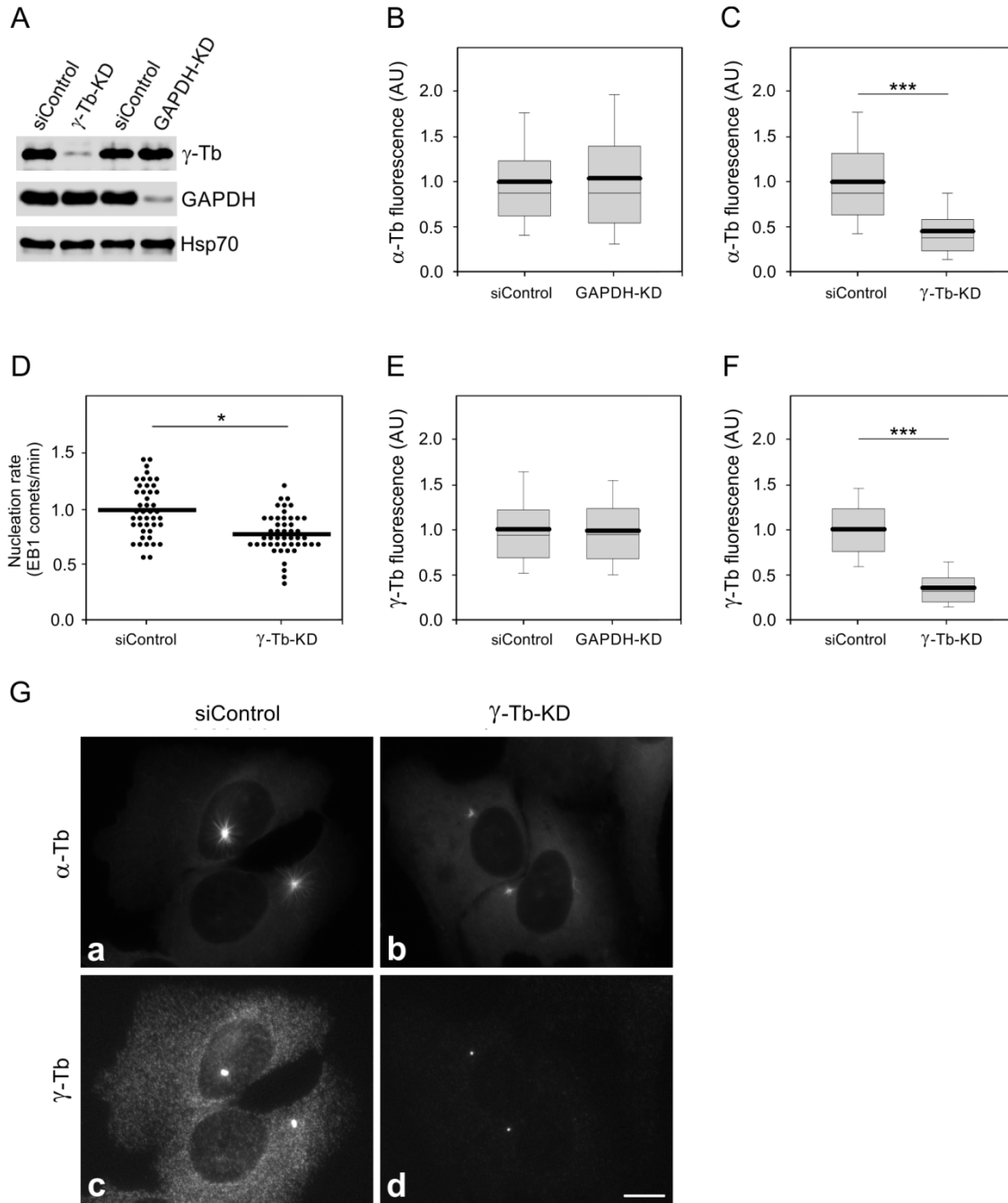
Figure S4. Depletion of γ-tubulin affects microtubule regrowth.

(A) Immunoblot analysis of cells with reduced levels of γ-tubulin and GAPDH. Whole-cell lysates from cells transfected with scrambled siRNA (siControl), γ-tubulin (γ-Tb-KD) or GAPDH (GAPDH-KD) siRNAs. Blots were probed with Abs to γ-tubulin (γ-Tb), GAPDH or Hsp70 (loading control). (B-C) Statistical analysis of α-tubulin fluorescence intensity in cells with depleted GAPDH (B) or γ-tubulin (C) relative to the control cells. Distribution of

α-tubulin fluorescence intensities (arbitrary units [AU]) in 1.0-µm ROI at 1.5 min of regrowth are shown

as box plots (three independent experiments, > 115 cells counted for each experimental condition). (B) Box plot of GAPDH-depleted cells (GAPDH-KD; n = 846) relative to control cells (siControl; n = 775). (C) Box plot of γ-tubulin-depleted cells (γ-Tb-KD; n = 347) relative to control cells (siControl; n = 446). (D) Statistical analysis of nucleation rate in cells with depleted γ-tubulin (γ-Tb-KD) relative to the control cells (siControl). Time-lapse imaging was used to track newly nucleated microtubules during microtubule regrowth in cells stably expressing EB1-GFP. The rate of nucleated microtubules (EB1 comets/min) calculated from three independent experiments, > 14 cells counted for each experimental condition. Bold line represents mean. *, $p < 0.05$. (E-F) Statistical analysis of γ-tubulin fluorescence intensity in cells with depleted GAPDH or γ-tubulin relative to the control cells. Distribution of γ-tubulin fluorescence intensities (arbitrary units [AU]) in 1.0-µm ROI at 1.5 min of regrowth are shown as box plots (three independent experiments, > 110 cells counted for each experimental condition). (E) Box plot of GAPDH-depleted cells (GAPDH-KD; n = 641) relative to control cells (siControl; n = 607). (F) Box plot of γ-tubulin-depleted cells (γ-Tb-KD; n = 331) relative to control cells (siControl; n = 469). In (B-C) and (E-F) bold and thin lines within the box represent mean and median (the 50th percentile), respectively. The bottom and top of the box represent the 25th and 75th percentiles. Whiskers below and above the box indicate the 10th and 90th percentiles. ***, $p < 1 \times 10^{-5}$. (G) Double-label staining for α-tubulin (a-b) and γ-tubulin

(c-d) in control (siControl) and γ-tubulin-depleted (γ-Tb-KD) cells at 1.5 min of microtubule regrowth. Fixation Tx/F/M. Images (a-b) and (c-d) were collected and processed in exactly the same manner. Bar, 10 µm.
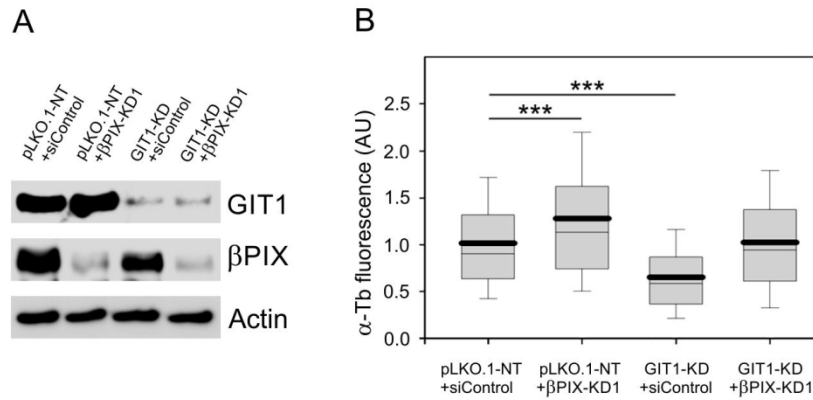
Figure S5. Effect of combined depletion of GIT1 and βPIX on microtubule nucleation. (A) Immunoblot analysis of cells with reduced levels of GIT1 and βPIX. Whole-cell lysates from cells infected with non-target shRNA (pLKO.1-NT) containing scrambled siRNA (pLKO.1-NT + siControl), cells infected with non-target shRNA after knockdown of βPIX by siRNA (pLKO.1-NT + βPIX-KD1), GIT1-deficient cells produced by lentiviral vector containing scrambled siRNA (GIT1-KD + siControl) and GIT1-deficient cells after knockdown of βPIX (GIT1-KD + βPIX-KD1). Blots probed with Abs to GIT1, βPIX and actin. (B) Distribution of α-tubulin fluorescence intensities (arbitrary units [AU]) in 1.0-μm ROI at 1.5 min of regrowth are shown as box plots (three independent experiments, > 233 cells counted for each experimental condition). Box plot of βPIX-depleted cells (pLKO.1-NT + βPIX-KD1; n = 770), GIT1-deficient cells (GIT1-KD + siControl; n = 881) and GIT1-deficient cells with depleted level of βPIX (GIT1-KD + βPIX-KD1; n = 864) relative to control cells (pLKO.1-NT + siControl; n = 815). Bold and thin lines within the box represent mean and median (the 50th percentile), respectively. The bottom and top of the box represent the 25th and 75th percentiles. Whiskers below and above the box indicate the 10th and 90th percentiles. ***, $p < 1 \times 10^{-5}$.
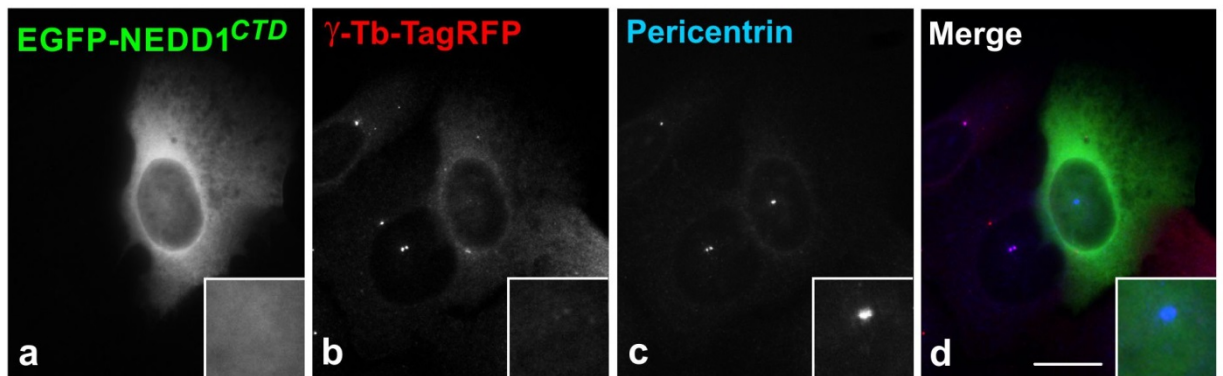
Figure S6. Stripping of γ-tubulin from centrosome by C-terminal domain of NEDD1. Cells expressing EGFP-tagged carboxyl-terminal domain (CTD) of NEDD1 (a, EGFP-NEDD1^{CTD}) and TagRFP-tagged γ-tubulin (b) were fixed by methanol and stained with anti-rabbit antibody for pericentrin (c). Superposition of images (d, EGFP-NEDD1^{CTD}, greeen;

γ-tubulin, red; pericentrin, blue). Centrosomal region in the cell expressing EGFP-NEDD1^{CTD}

is enlarged in the inserts. Note centrosomal depletion of γ-tubulin in cell expressing EGFP-NEDD1^{CTD}. Fixation by methanol. Bar, 20 μm.

VI.4.

Jurášek, M., Džubák, P., Sedlák, D., **Černohorská, M.**, Darmostuk, M., Ruml, T., Sulimenko, T., Dráberová, E., Dráber, P., Hajdůch, M., Bartůněk, P. & Drašar, P. Estradiol Dimer Blocks Microtubule Polymerization. Submitted 2015

Estradiol Dimer Blocks Microtubule Polymerization

Michal Jurášek,[†] Petr Džubák,[‡,*] David Sedlák,[§] Markéta Černohorská,[*,] Maria Darmostuk,[†] Tomáš Ruml,[†] Tetyana Sulimenko,[*] Eduarda Dráberová,[*] Pavel Dráber,[*] Marián Hajdůch,[‡] Petr Bartůněk[§] and Pavel Drašar[†,*]**

[†] *Institute of Chemical Technology, CZ-166 28 Prague, Czech Republic*

[‡] *Institute of Molecular and Translational Medicine, CZ-775 15 Olomouc, Czech Republic*

[§] *CZ-OPENSCREEN, Institute of Molecular Genetics of the ASCR, v.v.i., CZ-142 20 Prague, Czech Republic*

[*] *Laboratory of Biology of Cytoskeleton, Institute of Molecular Genetics, Academy of Sciences of the Czech Republic, CZ-142 20 Prague 4, Czech Republic*

[**] *Department of Cell Biology, Faculty of Science, Charles University, Prague, CZ-128 43 Prague 2, Czech Republic*

Abbreviations: DMF, N,N-dimethylformamide; DMSO, dimethylsulfoxide; DAPI, 4′,6-diamidino-2-phenylindole; ER, estrogen receptor; AR, androgen receptor; pH3[Ser10], phospho-Histon (Ser10); BrDU, 5-bromo-2-deoxyuridin; BrU, 5-bromouridin; BRB80, 80 mM PIPES pH 6.8 buffer containing 1 mM EGTA and 1 mM $MgCl_2$;

Address correspondence to Petr Džubák (Phone: +420 604 851 158, E-mail: dzubakp@gmail.com); to Pavel Drašar (Phone: +420 220 443 698, E-mail: pavel.drasar@vscht.cz)

Abstract

Microtubules represents targets for chemotherapeutic agents as they are essential for cell division and cell movement of cancer cells. As cells can get resistance to used tubulin drugs, it is necessary to identify new compounds that could interfere with microtubules. Here we report on synthesis and biological profiling of new steroidal dimers that exhibit cytotoxic activity based on the interference with microtubules. Steroidal dimers were generated from estradiol, testosterone and pregnenolone by bridging with by 2,6-bis(azidomethyl)pyridine between D rings. Steroidal dimers exhibited minor induction of the transactivation by steroid receptors when compared to the parental monomeric molecules. Cytotoxicity was examined on 11 different human cell lines including multidrug resistant variants. Estradiol dimer exerted cytotoxicity at micromolar concentrations and cells were arrested in G2/M phase of the cell cycle. Thorough investigation precluded genomic mechanism and revealed that estradiol dimer inhibited tubulin polymerization in vitro and reversibly disrupted microtubules in cells similarly to nocodazole. Moreover, it affected (+) end microtubule dynamics at nanomolar concentrations. Molecular dynamic simulation revealed that estradiol dimer partially binds to colchicine binding site on tubulin molecule. Estradiol dimer thus represents first steroid compound causing microtubule destabilization associated with cytotoxicity.

Introduction

Steroids and their synthetic analogs belong to a class of compounds exhibiting diverse biological activities in living organisms. Synthetically prepared dimeric steroids are special entities which offer unique features applicable in various fields (1,2). In medicinal chemistry, multivalent ligands coupled via sundry links were synthesized and investigated as molecular tools to target HIV protease, opioid, muscarinic or glycosidase receptors (3). Steroids are used as anti-inflammatory, anti-cancer, anabolic, anti-androgenic, progestational and contraceptive agents (4). Generally, these molecules are less inclinable to multi-drug-resistance and highly bioavailable due to their lipophilic properties (5). To date, large number of steroidal dimers and ribbons were synthetized (6). Recently, biological properties of dimers of estradiol (7-10), testosterone (11-13) and pregnenolone (14) dimers were reported.

Steroid hormones exert their biological function by diverse mechanisms, but the modulation of the transcription activity of different steroid receptors represents a principal way of their function. Steroid receptor cell lines were used to evaluate how dimerization of the parental steroid molecule affects the transactivation by corresponding steroid receptor (19).

Microtubules, built up from α/β-tubulin heterodimers, are essential for basic physiological functions in a cell, and represent targets for cancer therapy. Microtubules have intrinsic polarity and are highly dynamic. They stochastically switch between phases of growth and shortening. Precise regulation of microtubule dynamics is important for many biological processes ranging from proper attachment and segregation of chromosomes during mitosis (16) to local stabilization of microtubule toward the front of migrating cells (17). Pathologic changes affecting microtubule dynamics can cause changes in cell invasivity and cell division. Although resistance to microtubule stabilizing drugs is well characterized, molecular mechanisms still remain poorly understood and uncontrolled. Therefore, it is necessary to find out new bioorganic principles that could be applicable to personalized treatment of cancer (18).

We have described previously synthesis and biological profiles of steroidal dimers derived from non-hormonal steroids (cholic and etienic acid) and 3-*O*-bridged estradiol dimer (15). In the present work we investigated dimers derived from steroid hormones estradiol, 3-*O*-methyl estradiol, testosterone and pregnenolone. These steroids structurally differ in the shape of A-ring, presence of functional groups and position of double bonds.

To keep the A-ring untouched, we used corresponding ethynylated steroids at C-17 position in the case of estradiol, 3-*O*-methyl estradiol and testosterone and C-20 in the case of pregnenolone. Dimers were synthesized using copper catalyzed azide-alkyne click chemistry approach (CuAAC), occurring between corresponding ethynylated steroids and 2,6-bis(azidomethyl)pyridine (15). Synthesized dimers were subjected to different assays in order to determine their steroid receptor activities, cytotoxic potency on cancer cell lines of different histogenic origin, multidrug resistance and p53 gene status. To determine the mechanism of toxicity of dimers, we investigated their effect on cell-cycle progression and microtubule organization.

Material and Methods

Steroid compounds

All chemicals, reagents and solvents were used without further purification as purchased from commercial sources. Coupling unit 2,6-bis(azidomethyl)pyridine and 24-norchol-5-en-22-yn-3β-ol were synthesized according to established protocols. Plates coated by silica gel bound with starch for detection in UV light (TLC Silica gel 60 $F_{254,}$ Merck) were used for thin-layer chromatograms (TLC). For visualization, ~ 50 % solution of sulphuric acid in MeOH was used and plates were successively heated. For column chromatography, silica gel (30-60 μm, SiliTech, MP Biomedicals) was used. The final products were run with Bruker 600 Avance, working at 600 MHz for proton and 151 MHz for carbon-13 (APT technique). For the complete characterization of steroidal cyclic systems 2D techniques (COSY, HMQC, HMBC) were performed and successfully resolved. ^{1}H and ^{13}C NMR chemical shifts were referenced to the signal of internal standard TMS or towards the used solvent. HRMS were measured by Q-TOF (Micromass) with ESI ionization. FTIR spectra were measured on Nicolet iS10 models by ATR technique using KBr crystal. Specific rotations were measured on Autopol VI polarimeter (Rudolph Research Analytical).

Cell cultures

All cells were purchased from the American Tissue Culture Collection (ATCC). The highly chemosensitive CCRF-CEM cell line is derived from T lymphoblastic leukemia, K562 represent cells from an acute myeloid leukemia patient sample with bcr-abl translocation, HCT116 is colorectal tumor cell line and its p53 gene knock-down counterpart (HCT116p53-/-, Horizon Discovery, UK) is a model of human cancers with p53 mutation frequently associated with poor prognosis, A549 line is lung adenocarcinoma. The daunorubicine resistant subline of CCRF-CEM cells (CEM-DNR bulk) and paclitaxel resistant subline K562-TAX were selected in our laboratory by the cultivation of maternal cell lines in increasing concentrations of daunorubicine or paclitaxel, respectively. The CEM-DNR bulk cells overexpress MRP-1 and P-glycoprotein protein, while K562-TAX cells overexpress P-glycoprotein only. Both proteins belong to the family of ABC transporters and are involved in the primary and/or acquired multidrug resistance phenomenon (20). MRC-5 cell line was used as a non-tumor control, and represent human fibroblasts. The cells were maintained in Nunc/Corning 80 cm^2 plastic tissue culture flasks and cultured in DMEM/RPMI 1640 media supplemented with 5 g/L glucose, 2 mM

glutamine, 100U/mL penicillin, 100 μg/mL streptomycin, 10% fetal calf serum, and NaHCO$_3$). Human osteogenic sarcoma cells U2OS stably expressing GFP-tagged end binding protein 1 (U2OS-EB1) were described previously {Vinopal, 2012 1076 /id}. Cells were cultured in DMEM media containing 10% foetal bovine serum, penicillin (100 units/ml), and streptomycin (0.1 mg/ml). Cells were grown at 37°C in 5% CO$_2$ in air, and passaged every 2 or 3 days using 0.25% trypsin/0.01% EDTA in PBS. In some cases cells were incubated in the presence of estradiol, 2-ME, estradiol dimer or nocodazole (all in concentration 2.5 μM) for 20 h before cell fixation and immunofluorescence examination. In microtubule regrowth experiments pre-treated cells were washed (3 times 5 min each) with medium to remove tested compounds, microtubule regrowth was allowed for 30 min at 37°C, and fixed samples were thereafter used for immunofluorescence. Controls contained equivalent amount of carrier (DMSO).

Steroid reporter assay

Development of panel of steroid receptor reporter cell lines and the luciferase reporter assay were described recently (21). Transcriptional response of steroid receptors to tested compounds was evaluated in the panel of the U2OS stable reporter cell lines stably expressing human full-length steroid receptors. In the ERα and ERβ reporter cell lines the luciferase expression is driven by the 3 repeats of estrogen response elements (ERE) in the promoter of the reporter vector, while viral promoter (derived from MMTV LTR) controls the expression of luciferase in the AR reporter cell line. Reporter assays were carried out in white 1536-well plates (Corning Costar, USA). Each well contained 2000 cells. Compounds were transferred to cells using contact-free acoustic transfer by ECHO 520 (Labcyte, Inc., USA). In the agonist mode, cells were incubated with compounds for 24 h and then the luciferase activity was measured with Oneglo compound (Promega, USA). Values are reported as mean ± standard error of the mean (SEM) from quadruplicate measurements. Estradiol was used as a control ligand in the ERα and ERβ reporter assay and dihydrotestosterone in the AR reporter assay. In the antagonist mode, 30 minutes incubation of cells with compounds was followed by addition of estradiol to final concentration of 1 nM for ERα, 2 nM E2 for ERβ and 0.2 nM dihydrotestosterone for AR reporter assay. ICI 182780 was used as a control ligand in the ERα and ERβ reporter assay, nilutamide in the AR reporter assay. Luciferase activity was measured 24h after compound addition. LogEC$_{50}$ values were generated by fitting data from the luciferase reporter assay by nonlinear regression function in GraphPad Prism (GraphPad Software, Inc., USA).

MTT assay

Cell suspensions were prepared and diluted according to the particular cell type and the expected target cell density (25,000–30,000 cells/well based on cell growth characteristics). Cells were added by pipette (80 µL) into 96-well microtiter plates. Inoculates were allowed a pre-incubation period of 24 h at 37°C and 5% CO_2 for stabilization. Four-fold dilutions, in 20-µL aliquots, of the intended test concentration were added to the microtiter plate wells at time zero. All test compound concentrations were examined in duplicate. Cells were incubated with test compounds for 72 h at 37°C. At the end of the incubation period, the cells were assayed using MTT. Aliquots (10 µL) of the MTT stock solution were added into each well and incubated for further 1–4 h. After this incubation period the produced formazan was dissolved by the addition of 100 µL/well of 10% SDS (pH 5.5), followed by a further incubation at 37 °C overnight. The optical density (OD) was measured at 540 nm with a Labsystem iEMS Reader MF. Tumor cell survival (IC_{50}) was calculated using the following equation: IC = (OD of drug-exposed cells/mean OD of control cells) x 100%. The IC_{50} value, the drug concentration lethal to 50% of the tumor cells, was calculated from appropriate dose-response curves (22).

Cell cycle and apoptosis analysis

Suspension of CCRF-CEM cells, seeded at a density of 10^6 cells/ml in 6-well panels, were cultivated with the 1 or 5x IC50 of tested compound in a humidified CO2 incubator at 37°C in RPMI 1640 cell culture medium containing 10% fetal calf serum, 10 mM glutamine, 100 U/mL penicillin, and 100 µg/ mL streptomycin. Together with the treated cells, control sample containing vehicle was harvested at the same time point after 24 h. After another 24 hours, cells were washed with cold 1x PBS and fixed in 70% ethanol added dropwise and stored overnight at -20°C. Afterwards, cells were washed in hypotonic citrate buffer, treated with RNase (50 µg/mL) and stained with propidium iodide. Flow cytometer using a 488 nm single beam laser (Becton Dickinson) was used for measurement. Cell cycle was analyzed in the program ModFitLT (Verity), and apoptosis was measured in logarithmic model expressing percentage of the particles with propidium content lower than cells in G0/G1 phase (<G1) of the cell cycle. Half of the sample was used for pH3^{Ser10} antibody (Sigma) labeling and subsequent flow cytometry analysis of mitotic cells (22).

BrDU incorporation analysis

Marker of DNA synthesis, 10 µM 5-bromo-2-deoxyuridine (BrDU), was added to the cells for puls-labeling for 30 min. The cells were fixed with ice-cold 70% ethanol and stored overnight. Before analysis, they were incubated on ice for 30 min, washed once with PBS and re-suspended in 2 M HCl for 30 min at room temperature to denature their DNA. Following neutralization with 0.1 M $Na_2B_4O_7$, the cells were washed with PBS containing 0.5% Tween-20 and 1% BSA, and stained with primary anti-BrdU antibody (Exbio) for 30 min at room temperature in the dark. Cells were washed with PBS and stained with secondary anti-mouse antibody conjugated with FITC (Sigma). After washing (PBS) cell were incubated with propidium iodide (0.1 mg/mL) and RNase A (0.5 mg/mL) for 1 h at room temperature in the dark and afterwards analyzed by flow cytometry using a 488 nm single beam laser (FACS Calibur, Becton Dickinson) (22).

Tubulin preparation

Microtubule protein was purified from porcine brain by two temperature-dependent cycles of assembly and disassembly (23). Subsequent purification of tubulin was performed by phosphocellulose chromatography (24). The eluted tubulin was immediately subjected to another cycle of assembly and disassembly as described (25). Tubulin was stored in BRB80 buffer (80 mM PIPES pH 6.8, 1 mM EGTA, 1 mM $MgCl_2$) supplemented with 0.1 mM GTP. Tubulin concentration was determined by measuring the absorbance at 280 nm using an extinction coefficient at 280 nm of 115,000 $M^{-1}cm^{-1}$. Recycled tubulin was more than 98% pure and it was stored in liquid nitrogen. For tubulin polymerization assay taxol was used (a gift from National Cancer Institute, Bethesda, MD) and nocodazole (Sigma-Aldrich).

Turbidimetric measurement

The microtubule assembly was monitored by turbidimetry (26) at 350 nm and 37°C using recording spectrophotometer (UV-1800, Shimadzu) with temperature-controlled cuvette holder. The resulting assembly mixture contained 15 µM tubulin in BRB80 buffer supplemented with GTP and glycerol at final concentrations 1 mM and 3.0 M, respectively. Polymerization was also performed in the presence of ethynylated steroids (1a, 2a, 3a, 4a), steroid dimers (1, 2, 3, 4) or taxol (NIH, Bethesda), all in concentration of 10 µM. In some cases polymerization was performed at presence of nocodazole (Sigma-Aldrich) or estradiol dimer (1) at concentrations varying from 0.5 to 6 µM. Tested compound were incubated with

tubulin for 4 min at 4°C before monitoring of assembly. In controls an equivalent volume of DMSO (carrier) was applied.

Immunofluorescence

Immunofluorescence microscopy on formaldehyde-fixed, Triton X-100 extracted cells was performed as previously described (27). Mouse monoclonal antibody TU-01 (IgG1) directed to α-tubulin (28) in the form of hybridoma spent culture medium was diluted 1:10. The DY488-conjugated anti-mouse antibody (Jackson Immunoresearch Laboratories) was diluted 1:200.

Time-lapse imaging

Time-lapse imaging was performed as described (29). For time-lapse imaging, U2OS-EB1 cells were grown on glass-bottom-dishes (InVitroscience). Before imaging DMEM was replaced with medium for live-cell imaging (DMEM without phenol red, riboflavin, folic acid, pyridoxal, Fe[NO_3]$_3$). Cells were treated with 50 nM 2-ME, estradiol dimer or nocodazole for 3 hours at 37°C. Controls contained equivalent volume of DMSO carrier. Time-lapse sequences of EB1-GFP dynamics were collected for 2 min at 1 sec interval (exposure time 0.3 sec) on Delta Vision Core system (Applied Precission) equipped with 60x/1.42 NA oil-immersion objective and incubator with controlled temperature and CO_2. The focus plane was near the coverslip where the best resolution of EB1 comets was observed.

Image analysis

Microtubule growth dynamics was analyzed from EB1 time-lapse movies using plusTipTracker software, version 1.1.3 (30, 31) based on Matlab (MathWorks). The following parameter set for all movies in the dataset was used: maximum gap length, 5 frames; minimum track length, 3 frames; search radius range, 2-9 pixels; maximum forward angle, 30°; maximum backward angle, 10°; maximum shrinkage factor, 1.5; fluctuation radius, 1 pixels; pixel size, 106.2 nm.

To categorize EB1 tracks based on growth speed and growth excursion lifetime, "Quadrant Scatter Plot" (within plusTipTracker software) was applied. Briefly, the function generates a scatter plot of speed versus lifetime with each point representing a single microtubule growth excursion defined by a single continuous EB1 track. The points on the graph are divided into four subpopulations based on whether they were above or below the

average growth speed (16.5 µm/min) and average growth lifetime (7 sec) of all EB1 tracks from all control cells analyzed in the study. The four subpopulations are coded by color, and a percentage bar showing the relative proportion of the subpopulations is generated. Colored tracks are overlaid on an inverted image of U2OS using the same color scheme to show how each subpopulation is distributed across the cell (32).

For statistical analyses, the "plusTipGroupAnalyse" (within plusTipTracker software) was applied. For most of the dynamic parameters, the program collects and analyzes all the data from all the cell for each treatment. For parameters for which the program performs analysis per cell (dynamicity of microtubule, calculated as the combined length of all gap-containing tracks [growth plus shrinkage] over their combined lifetime), the cells´ values were analyzed by t-test for significant differences between the treatments (33).

Results and Discussion

Synthesis of steroid dimers

The pharmacological effect of modified steroids depends heavily upon structural features of the steroid multi-cyclic system and side chain. Here we used ethynylated steroids (Figure 1) modified on D-ring of the cyclic system, namely 17α-ethynylestradiol, 3-*O*-methyl 17α-ethynylestradiol and 17α-ethynyltestosterone. 24-Norchol-5-en-22-yn-3β-ol was synthesized from pregnenolone by ethynylation of its side chain with the yield and physical behavior consentaneous to the literature (34). Ethynylated steroids were tethered to dimers using bis(azidomethyl)pyridine building block[15]. CuAAC reactions were carried out under deep-rooted conditions using catalytic amounts of copper(II) sulphate and sodium ascorbate with the addition of tris((1-benzyl-1*H*-1,2,3-triazolyl)-methyl)amine (TBTA) accelerator (35) (Figure 2 & Supplement figure S1-4.). All the dimers were successfully analytically characterized by NMR, HRMS-ESI, IR and optical rotations data. Prior to biological testing, the samples were re-purified by column chromatography and their purity checked by HPLC analysis (Supplement figure S5.). In further text compounds in figure 1 and figure 2 are presented in bold.

Steroid dimers have agonistic activities in steroid receptor reporter assays

First we tested the activity of compounds using reporter assay for estrogen receptor α (ERα), estrogen receptor β (ERβ) and androgen receptor (AR) in the concentration range starting from 10 μM to 1 nM. We performed the experiment in both agonist and antagonist modes but we have detected activity in the agonist mode only. The agonistic properties of the steroid dimers are summarized in the table (Table I.). The dimerization of **1** maintained its activity on both ERα and ERβ but reduced the potency on ERs by more than 3 orders compared to the parental molecule. The methoxy group in the C-3 position of dimer **2** resulted in further potency and efficacy reduction on ERα while it improved activity on ERβ to some extent. Overall, both estradiol derived dimers (**1** and **2**) exhibit only weak estrogenic activity, detectable at micromolar concentrations on both ERs. Dimerization of testosterone dimer **3** abolished completely its ability to activate AR in the entire concentration range. Finally and similarly to dimer **3,** dimer **4** was not active in any of the reporter assays.

Steroid dimers exhibit cytotoxic activity

The cytotoxic activity was analyzed on the human cancer cell lines, their resistant variants and two unrelated human cell lines (Table II.). The over-expression of *MDR1* gene encoding P-glycoprotein (P-gp) and *ABCC2* gene encoding multidrug resistance-associated protein 1 (MRP-1) are pumps responsible for the most common forms of clinical resistance. High levels of P-gp decrease the cellular up-take of drugs which is associated with response to microtubule-targeted drugs and poor prognosis for the patients. The structure-activity relationship ought to be evaluated for individual cell lines independently, because it may vary due to different tissue origin and potential molecular targets in particular cell lines. The cytotoxic activity of dimer **4** is low on the threshold to the maximum tested concentration (100 μM). Nevertheless, estradiol **1**, 3-*O*-methyl estradiol **2** and testosterone **3** dimers exhibit promising cytotoxic activity (the lowest in case of dimer **1**, IC_{50} = 0.49 μM on CCRF-CEM). Estradiol dimer **1** is showing low cytotoxicity to resistant cell line CEM-DNR bulk (IC_{50} = 94.65 μM) which is expressing both the P-gp and MRP-1 proteins. On the other hand, the cytotoxic activity to resistant K562-Tax and HeLa cell lines expressing only P-gp protein is rather low (IC_{50} = 3.65 μM and 0.78 μM, respectively) suggesting preferential transport by MRP-1 protein (36). Strengthening this hypothesis, physiologically occurring metabolites of 17β-estradiol (17β-estradiol-17β-glucuronide and estrone-3-sulphate) are eliminated from the cell by mechanism including MRP-1 transport (37) but there is no evidence of such transportation of 3-*O*-methylated estrans. From our results it is evident that the 3-*O*-methyl estradiol dimer **2** retained the cytotoxicity when compared to CEM-CCRF and its resistant variant (see Figure 3.). We observed similar trend in the case of testosterone dimer **3**, which may suggest similar mechanism of the resistance and action, however, the difference in cytotoxicity is not as huge as in the case of dimer **1**. We did not notice significant differences in the case of colorectal carcinoma HCT116 cell line and its p53-/- knock-down counterpart, suggesting p53 independent mechanism of the cytotoxicity. Generally, the therapeutic index (based on the ratio between the IC_{50} for normal human cells and cancer cell lines) of the compounds is rather low and varies in the range of 0.01 - 22.98.

Cytotoxic activity of steroid dimers regulates cell cycle, DNA synthesis and apoptosis

The cell cycle investigation of the most active dimers **1, 2** and **3** has been performed on CCRF-CEM lymphoblasts at 1× and 5×IC_{50} concentrations within 24 hours treatment. In the case of dimers **1** and **3**, we observed accumulation of cells arrested in G2/M phase of the cell

cycle, positivity for pH3^{Ser10} and decrease of the DNA/RNA synthetic activity. Suppression of the DNA/RNA synthetic activity by the dimer **3** in 5×IC$_{50}$ concentrations is probably due to general cytotoxic activity of this compound (Table III).

Estradiol dimer interferes with tubulin polymerization in vitro

To shed the light on mechanism of action and to find the reason for M phase inhibition, we focused on the major cytoskeletal protein tubulin, which is involved in formation of mitotic spindle and is crucial for successful cell division. Although, there are reports, that major metabolite of 17β-estradiol-2-methoxyestradiol acts as competitive inhibitor of colchicine binding to tubulin (37-40), we found no evidence of "testosterone-like" tubulin destabilizers in the literature. Variety of compounds derived from estrane skeleton were synthesized (e.g. ENMD-1198, estramustine, 2-ethoxyestradiol) in order to increase the cytotoxicity and tubulin polymerization inhibition. In the context, the hydroxy-group at C-17 position contributes substantially to the anticancer and pharmacokinetic profile of estradiol derivatives, since its oxidation leads to its deactivation and steroid clearance. Deactivating metabolic processes could be inhibited by replacement of this moiety or by chemical modification of C-17 position to quaternary atom (like in case of dimers **1** and **2**). In anti-cancer therapy, drugs inhibiting polymerization (e.g. vincristine) or stabilizing the microtubules (e.g. taxol) are used. For the mentioned reasons, we performed *in vitro* tubulin assembly assay to test dimers **1** and **3**.

Turbidimetric measurements revealed that ethynylated steroids (**1**a, **2**a, **3**a, **4**a) (Figure 1) at concentration 10 μM had basically no effect on tubulin assembly (Figure 4A). When turbidimetric measurements were performed in the presence of steroid dimers (**1**, **2**, **3**, **4**) at concentration 10 μM, estradiol dimer profoundly inhibited tubulin assembly, while the other steroid dimers had no or only minor effect on tubulin assembly (Figure 4B). When the effect of estradiol dimer (10 μM) on tubulin assembly was compared with known anti-mitotic drugs, namely taxol, 2-ME and nocodazole (methyl [5-(thiophen-2-ylcarbonyl)-1*H*-benzimidazol-2-yl]carbamate]), estradiol dimer was stronger inhibitor than 2-ME but did not reach the inhibitory activity of nocodazole (Figure 4C). To define the concentration of estradiol dimer that inhibited microtubule assembly by 50% (IC$_{50}$), tubulin assembly was carried out in the presence of estradiol dimer at different concentrations. As control was used nocodazole. Typical example is shown in Figure 4D. The IC$_{50}$ for estradiol dimer and nocodazole were, respectively, 3.6 and 1.50 μM.

Estradiol dimer causes reversible microtubule depolymerization in vivo

To compare the effect of estradiol, estradiol dimer, 2-ME and nocodazole on microtubule arrangement in interphase osteosarcoma U2OS cells, cells were incubated in the presence of these compounds (all in concentration 2.5 μM) for 20 h before cell fixation and immunofluorescence staining for α-tubulin. Both in estradiol-treated cells and control cells no changes in microtubule distribution were detected (Figure 5A, a-b). On the other hand pre-treatment with 2-ME led to bundling of microtubules and microtubules were less prominent in cell periphery (Figure 5B, a). Microtubules disassembled after treatment with estradiol dimer (Figure 5B, c), similarly as in the case of nocodazole (Figure 5B, e). To evaluate if the observed changes in microtubule organization are reversible, tested compounds were wash out and microtubule regrowth was allowed for 30 min. Removing of 2-ME (Figure 5B, b) as well as estradiol dimer (Figure 5B, d) and nocodazole (Figure 5B, f) resulted in complete restoration of microtubule network.

These data indicate that estradiol dimer at concentration 2.5 μM resembles nocodazole in respect of its mechanism of action in cells. This data show that estradiol dimer not only inhibits the tubulin polymerization *in vitro*, but also disrupts microtubules in cell. The data from *in vitro* and cellular experiments suggest that, similarly to nocodazole, estradiol dimer causes mitotic arrest of CCRF-CEM cells.

Estradiol dimer affects microtubule plus end dynamics

As nocodazole at low concentrations inhibits microtubule dynamics (44), we examined the possibility that estradiol dimer also affects microtubule plus ends. For these experiments we have used U2OS cells stably expressing GFP-tagged end binding protein 1 (U2OS-EB1), that marks ends of growing microtubules. The EB1 comets were visualized using time-lapse microscopy in cells pre-treated with estradiol dimer, 2-ME or nocodazole (all in concentration 50 nM) for 3 h. As a control served cells containing the equivalent volume of carrier (DMSO). Typical examples of time-lapse sequences from control and estradiol dimer-treated cells are shown in the Supplemental Material (Supplemental movie S1). The plusTipTracker automated tracking system (30) allows simultaneous chasing of microtubule tracks and discrimination of four microtubule subpopulations according to their comparative speed and growth lifetime (Figure 6A). As can be seen in Figure 6B the percentages of fast speed sub-tracts (both short and long lived; yellow and blue, respectively) were substantially reduced in estradiol dimer (1) or nocodazole-treated cells compared to the control or 2-ME-

treated cells. Typical examples of differences in microtubule subpopulations in control and estradiol dimer-treated cells are shown in Supplemental Figure 6. Dynamicity is a general measure of the amount of dynamic instability occurring in microtubule population. Higher dynamicity enables faster adjustment of microtubules to their surrounding microenvironment. The dynamicity of nocodazole- or estradiol dimer-treated cells was reduced, respectively, by about 37% and 25%. On the other hand no substantial changes in dynamicity were observed in 2-ME-treated cells (Figure 6C).

Estradiol dimer binds to colchicine site in α/β-tubulin dimer

Tubulin molecule has at least two binding sites for nocodazole differing in affinity (41). Nocodazole has the highest affinity for α/β_{IV} and lowest for α/β_{III} subunit. The α/β_{IV} subunits seem to have the least rigid conformation among the tubulin isotypes which have been studied. This lack of rigidity can facilitate the interaction of the molecule, moreover, binding of drugs which favor binding to colchicine site prefer α/β_{IV} but the other do not (e.g. taxol).

Since the interference of estradiol dimer with microtubules was observed both in the cellular and *in vitro* biochemical experiment, we hypothesize that estradiol dimer interacts directly with tubulin rather than with microtubules associated proteins. In order to predict how estradiol dimer binds to tubulin, the structure of tubulin dimer was extracted for experimental structure (4O2B) (42), missing residues were added by homology modelling in Modeller (43) and estradiol dimer was manually docked. Then the system was equilibrated by several rounds of geometry optimization, restrained molecular dynamics simulations and gradual tempering. This was followed by 10 ns unrestrained molecular dynamics simulations. The system contained tubulin dimer, one molecule of estradiol dimer, 213 sodium, 181 chloride ions and 60322 water molecules. The predicted binding mode was stable in 10 ns molecular dynamics simulation with only minor structural changes, which supports its prediction. In the predicted mode, the first steroid moiety is bound in the colchicine binding site. This rationalizes similar properties of the tested compound with the colchicine-site agonist nocodazole. The second moiety was predicted to bind to a hydrophobic patch on the second tubulin monomer. Molecular modelling indicated that estradiol dimer was bound to tubulin molecule in its colchicine binding site between α- and β-tubulin monomers (Figure 7). This binding site is responsible for tubulin interactions in both lateral and proximal directions.

Conclusion

Newly synthesized dimers derived from estradiol, testosterone and pregnenolone show only marginal potency in steroid receptor reporter assays, nevertheless, both estradiol derivatives estradiol dimer and 3-O-methyl estradiol dimer and testosterone dimer exerted general cytotoxicity in units of micromoles. The estradiol dimer, which showed the highest potency in the cytotoxic profiling, caused accumulation of cells within G2/M phase.

Moreover, we have found that estradiol dimer but not testosterone dimer inhibits tubulin polymerization, reversibly affects microtubule distribution in interphase cells and suppresses microtubule dynamics. Estradiol dimer is more effective than 2-ME and its effect on microtubules resembles that of nocodazole. Finally, we predicted the binding site of estradiol dimer on tubulin molecule by molecular dynamics simulations. We propose that the estradiol dimer binds to the colchicine site on the first tubulin monomer and second steroid moiety of the dimer interacts particularly via hydrophobic residues with the other tubulin monomer.

ASSOCIATED CONTENT

Supporting Information. Experimental procedures of synthetic experiments, details including analytical characteristics, biological assays and calculation method. This material is available free of charge via the Internet http://pubs.acs.org.

Author contributions

[†]M.J. and [‡]P.D. contributed equally to this work.

Notes

The authors declare no competing financial interest.

REFERENCES

(1) Ramirez-Lopez, P., de la Torre, M. C., Montenegro, H. E., Asenjo, M., Sierra, M. A. A straightforward synthesis of tetrameric estrone-based macrocycles. *Org. Lett.* **2008**, *10*, 3555-3558.

(2) Montenegro, H. E., Ramirez-Lopez, P., de la Torre, M. C., Asenjo, M., Sierra, M. A. Two versatile and parallel approaches to highly symmetrical open and closed natural product-based structures. *Chem. - Eur. J.* **2010**, *16*, 3798-3814.

(3) Gestwicki, J. E., Cairo, C. W., Strong, L. E., Oetjen, K. A., Kiessling, L. L. Influencing receptor-ligand binding mechanisms with multivalent ligand architecture. *J. Am. Chem. Soc.* **2002**, *124*, 14922-14933.

(4) Shan, L. H., Liu, H. M., Huang, K. X., Dai, G. F., Cao, C., Dong, R. J. Synthesis of 3 beta, 7 alpha, 11 alpha-trihydroxy-pregn-21-benzylidene-5-en-20-one derivatives and their cytotoxic activities. *Bioorg. Med. Chem. Lett.* **2009**, *19*, 6637-6639.

(5) Banday, A. H., Mir, B. P., Lone, I. H., Suri, K. A., Kumar, H. M. S. Studies on novel D-ring substituted steroidal pyrazolines as potential anticancer agents. *Steroids* **2010**, *75*, 805-809.

(6) Drašar, P., Buděšínsky, M., Reschel, M., Pouzar, V., Černý, I. Etienic etienate as synthon for the synthesis of steroid oligoester gelators. *Steroids* **2005**, *70*, 615-625.

(7) Lee, A. J., Sowell, J. W., Cotham, W. E., Zhu, B. T. Chemical synthesis of two novel diaryl ether dimers of estradiol-17β. *Steroids* **2004**, *69*, 61-65.

(8) Fournier, D., Poirier, D. Estradiol dimers as a new class of steroid sulfatase reversible inhibitors. *Bioorg. Med. Chem. Lett.* **2009**, *19*, 693-696.

(9) Rabouin, D., Perron, V., N'Zemba, B., C.-Gaudreault, R., Berube, G. A facile synthesis of C2-symmetric 17β-estradiol dimers. *Bioorg. Med. Chem. Lett.* **2003**, *13*, 557-560.

(10) LaFrate, A. L., Carlson, K. E., Katzenellenbogen, J. A. Steroidal bivalent ligands for the estrogen receptor: Design, synthesis, characterization and binding affinities. *Bioorg. Med. Chem.* **2009**, *17*, 3528-3535.

(11) Bastien, D., Leblanc, V., Asselin, É., Bérubé, G. First synthesis of separable isomeric testosterone dimers showing differential activities on prostate cancer cells. *Bioorg. Med. Chem.* **2010**, *20*, 2078-2081.

(12) Rodriguez-Molina, B., Pozos, A., Cruz, R., Romero, M., Flores, B., Farfan, N., Santillan, R., Garcia-Garibay, M. A. Synthesis and solid state characterization of molecular rotors with steroidal stators: ethisterone and norethisterone. *Org. Biomol. Chem.* **2010**, *8*, 2993-3000.

(13) Manbeck, G. F., Brennessel, W. W., Stockland, R. A., Jr., Eisenberg, R. Luminescent Au(I)/Cu(I) alkynyl clusters with an ethynyl steroid and related aliphatic ligands: An octanuclear Au_4Cu_4 cluster and luminescence polymorphism in Au_3Cu_2 clusters. *J. Am. Chem. Soc.* **2010**, *132*, 12307-12318.

(14) Nahar, L., Sarker, S. D., Turner, A. B. Convenient synthesis of new pregnenolone oximinyl oxalate dimers. *Chem. Nat. Compd.* **2008**, *44*, 315-318.

(15) Jurášek, M., Džubák, P., Sedlák, D., Dvořáková, H., Hajdůch, M., Bartůněk, P., Drašar, P. Preparation, preliminary screening of new types of steroid conjugates and their activities on steroid receptors. *Steroids* **2013**, *78*, 356-361.

(16) Gierke, S., Wittman, T. EB1-recruited microtubule +TIP complexes coordinate protrusion dynamics during 3D epithelial reodeling. *Curr. Biol.* **2012**, *22*, 753-762.

(17) Wittman, T., Waterman-Storer, C.M. Cell motility: can Rho GTPases and microtubules point the way? *J. Cell. Sci.* **2001**, *114*, 3795-3803.

(18) Das, V., Štěpánková, J., Hajdúch, M., Miller, J.H. Role of tumor hypoxia in acquisition of resistance to microtubule-stabilizing drugs. *Biochim. Biophys. Acta.* **2015**, *1885*, 172-182.

(19) Sedlák, D., Paguio, A., Bartůněk, P. Two panels of steroid receptor luciferase reporter cell lines for compound profiling. *Comb. Chem. High T. Scr.* **2011**, *14*, 248-266.

(20) Lorendeau, D., Dury, Lk, Genoux-Bastide, E., Lecerf-Schmidt, F., Simoes-Pires, C., Carrupt, P.A., Terreux, R., Magnard, S., Di Pietro, A., Boumendjel, A., Baubichon-Cortay, H. Collorectal sensitivity of resistant MRP1-overexpressing cell to falvonoids and derivatives through GSH efflux. *Biochem. Pharm.* **2014**, *90*, 235-345.

(21) Jurášek, M., Džubák, Pl., Sedlák, D., Dvořáková, H., Hajdúch, M., Bartůněk, P. Drašar, P. Preparation, preliminary screening of new types of steroid conjugates and their activities on steroid receptors. *Steroids.* **2013**, *78*, 356-361.

(22) NoskovaV., Dzubak, P., Kuzmirova, G., Ludkova, A., Stehlik, D., Trojanec, R. Janostakova, A., Korinkova, G., Mihal, V., Hajduch, M. In vitro chemoresistance profile and expression/function of MDR associated proteins in resistant cell lines derived from CCRF-CEM, K562 and MDA-MB-231 parental cells. *Neoplasma.* **2002**, *49*, 418-425.

(23) Schelanski, M.L. Chemistry of the filaments and tubules of brain. *J. Histochem. Cytochem.* **1973**, *21*, 529-539.

(24) Weingarten, M.D., Lockwood, A.H., Hwo, S.Y. Kirschner, M.W. A protein factor essential for microtubule assembly. *Proc. Natl. Acad. Sci. USA.* **1975**, *72*, 1858-1862.

(25) Dráberová, E., Sulimenko, V., Sulimenko, T., Böhm, K.J., Dráber, P. Recovery of tubulin functions after freeze-drying in the presence of trehalose. *Analyt. Biochem.* **2010**, *397*, 67-72.

(26) Gaskin, F., Cantor, C.R., Shelanski, M.L. Turbidimetric studies of the in vitro assembly and disassembly of porcine neurotubules. *J. Mol. Biol.* **1974**, *89*, 737-755.

(27) Nováková, M., Dráberová, E., Schürmann, W., Czihak, G., Viklický, V., Dráber, P. gamma-Tubulin redistribution in taxol-treated mitotic cells probed by monoclonal antibodies. *Cell. Motil. Cytoskeleton.* **1996**, *33*, 38-51.

(28) Viklický, V., Dráber, P., Hasek, J, Bártek, J. Production and characterization of a monoclonal antitubulin antibody. *Cell. Biol. Int. Rep.* **1982**, *6*, 725-731.

(29) Vinopal, S., Černohorská, M., Sulimenko, V., Sulimenko, T., Vosecká, V., Flemr, M., Dráberová, E., Dráber, P. γ-Tubulin 2 nucleates microtubules and is downregulated in mouse early embryogenesis. *Plos One.* **2012**, *7*, e29919.

(30) Applegate, K.T., Besson, S., Matov, A., Bagonis, M.H., Jaqaman, K., Danuser, G. PlusTipTracker: Quantitative image analysis software for the measurement of microtubule dynamics. *J. Struct. Biol.* **2011**, *176*, 168-84.

(31) Matov, A., Applegate, K., Kumar, P., Thoma, C., Krek, W., Danuser, G., Wittmann, T. Analysis of microtubule dynamic instability using a plus-end growth marker. *Nat Mathods.* **2010**, *7*, 761-768.

(32) Nishimura, Y., Applegate, K., Davidson, M.W., Danuser, G., Waterman, C.M. Automated screening of microtubule growth dynamics identifies MARK2 as a regulator of leading edge microtubules downstream of rac1 in migrating cells. *Plos One.* **2012**, *7*, e41413.

(33) Cohen, S., Aizer, A., Shav-Tal, Y., Yanai, A., Motro, B. Nek7 kinase accelerates microtubule dynamic instability. *Biochim. Biophys. Acta.* **2013**, *1833*, 1104-1113.

(34) Wong, F. F., Chuang, S. H., Yang, S.-c., Lin, Y.-H., Tseng, W.-C., Lin, S.-K., Huang, J.-J. One-pot ethynylation and catalytic desilylation in synthesis of mestranol and levonorgestrel. *Tetrahedron.* **2010**, *66*, 4068-4072.

(35) Hein, J. E., Tripp, J. C., Krasnova, L. B., Sharpless, K. B., Fokin, V. V. Copper(I)-catalyzed cycloaddition of organic azides and 1-iodoalkynes. *Angew.Chem., Int. Ed.* **2009**, *48*, 8018-8021.

(36) Munoz, M., Henderson, M., Haber, M., Norris, M. Role of the MRP1/ABCC1 multidrug transporter protein in cancer. *Iubmb. Life.* **2007**, *59*, 752-757.

(37) Cushman, M., Mohanakrishnan, A. K., Hollingshead, M., Hamel, E. The effect of exchanging various substituents at the 2-position of 2-methoxyestradiol on cytotoxicity in human cancer cell cultures and inhibition of tubulin polymerization. *J. Med. Chem.* **2002**, *45*, 4748-4754.

(38) Lu, Y., Chen, J. J., Xiao, M., Li, W., Miller, D. D. An overview of tubulin inhibitors that interact with the colchicine binding site. *Pharm. Res.* **2012**, *29*, 2943-2971.

(39) Cushman, M., He, H. M., Katzenellenbogen, J. A., Varma, R. K., Hamel, E., Lin, C. M., Ram, S., Sachdeva, Y. P. Synthesis of analogs of 2-methoxyestradiol with enhanced inhibitory effects on tubulin polymerization and cancer cell growth. *J. Med. Chem.* **1997**, *40*, 2323-2334.

(40) Edsall, A. B., Agoston, G. E., Treston, A. M., Plum, S. M., McClanahan, R. H., Lu, T. S., Song, W., Cushman, M. Synthesis and in vivo antitumor evaluation of 2-methoxyestradiol 3-phosphate, 17- phosphate, and 3,17-diphosphate. *J. Med. Chem.* **2007**, *50*, 6700-6705.

(41) Xu, K., Schwarz, P. M., Luduena, R. F. Interaction of nocodazole with tubulin isotypes. *Drug Develop. Res.* **2002**, *55*, 91-96.

(42) Prota, A. E., Danel, F., Bachmann, F., Bargsten, K., Buey, R. M., Pohlmann, J., Reinelt, S., Lane, H., Steinmetz, M. O. The novel microtubule-destabilizing drug BAL27862 binds to the colchicine site of tubulin with distinct effects on microtubule organization. *J. Mol. Biol.* **2014**, *426*, 1848-1860.

(43) Sali, A., Blundell, T. L. Comparative protein modelling by satisfaction of spatial restraints. *J. Mol. Biol.* **1993**, *234*, 779-815.

(44) Vasquez, R.J., Howell, B., Yvon, A.M., Wadsworth, P., Cassimeris, L. Nanomolar concentrations of nocodazole alter microtubule dynamics instability in vivo and in vitro. *Mol. Biol. Cell.* **1997**, *8*, 973-985.

Figure legends

Figure 1. Structures of ethynylated steroids.

Figure 2. Structures of steroidal dimers prepared by dimerization of ethynylated steroids by click chemistry (CuAAc).

Figure 3. Comparison of toxicities of dimers on leukemia cancer cell lines, their resistant variants and normal cycling fibroblasts.

Figure 4. Effect of ethynylated steroids and steroid dimers on tubulin assembly. (A) Tubulin assembly in the presence of ethynylated steroids (**1**a, **2**a, **3**a, **4**a) in concentration of 10 μM or equivalent volume of carrier DMSO (Control). (B) Tubulin assembly in the presence of steroid dimers (**1**, **2**, **3**, **4**) in concentration of 10 μM or equivalent volume of carrier DMSO (Control). (C) Comparison of tubulin assembly in the presence of taxol, 2-ME, estradiol dimer (**1**) or nocodazole (all in concentration 10 μM) or equivalent volume of carrier DMSO (Control). (D) Effect of increasing concentration of nocodazole and estradiol dimer **1** on tubulin assembly. Maximum absorbance was recorded after 30 min polymerization. Assembly was carried out at 37°C at a tubulin concentration of 15 μM in the presence of 3.0 M glycerol.

Figure 5. Comparison of microtubule arrangements in cells pre-treated with estradiol, 2-ME, estradiol dimer or nocodazole. U2OS cells were incubated for 20 h at 37°C with studied compounds at concentration 2.5 μM. Preparations were directly fixed and microtubules were immunostained with antibody to α-tubulin. Alternatively, pre-treated cells were washed with medium and microtubule regrowth was allowed for 30 min at 37°C. Preparations were thereafter fixed and microtubules were immunostained for α-tubulin. (A) Distribution of microtubules in cells treated with estradiol (a) or in control cells (b; Con.). Scale bar for a-b, 20 μm. (B) Distribution of microtubules in cells treated with 2-ME (a, b), estradiol dimer (c, d; 1) and nocodazole (e, f; Noc.). Staining for α-tubulin directly after the treatment (left column; a, c, e) and staining after removing of tested compounds (right column; b, d, f). Scale bar for a-f, 20 μm.

Figure 6. Effect of 2-ME, estradiol dimer and nocodazole on microtubule dynamics. (A) Scatter plot of speed versus lifetime with each point representing a single microtubule growth excursion defined by a single continuous EB1 track. The points on the graph are divided into subpopulations based on whether they were above or below the average growth speed (16.5 µm/min) and average growth lifetime (7 sec) of all EB1 tracks from control cells with DMSO carrier. The four subpopulations of microtubules are coded by color: slow and short-lived (red), fast and short-lived (yellow), slow and long-lived (green) and fast and long-lived (blue). The same colors serve to represent subpopulations in B. (B) Proportions of the four sub-tracks populations in the indicated experiments. Cells were treated with 2-ME, estradiol dimer or nocodazole (Noc.), all in concentration of 50 nM for 3 h. Control cells (Con.) contained equivalent volume of DMSO carrier. Numbers of evaluated cells are shown on the left. (C) Histogram showing the calculated dynamicity of the microtubules in different treatments. In total more than 30 different cells were tracked in three independent experiments. Values indicate mean ± SD, n = 31 for control; n = 33 for 2-ME; n = 37 for estradiol dimer; n = 33 for nocodazole (Noc.); ***, $p < 0.0001$.

Figure 7. Putative binding site of estradiol dimer bound to tubulin dimer after 10 ns molecular dynamics simulation.

Table I. Activities of steroidal dimers in the steroid receptor reporter assays.

Dimer	Potency[a] ERα	Potency ERβ	Potency AR	Efficacy[b] ERα	Efficacy ERβ	Efficacy AR
Control	5.6×10^{-5}	1.5×10^{-5}	2.6×10^{-6}	100	100	100
1	0.11	3.55	>10	102	>120	n.a.
2	4.27	0.49	>10	74.4	115	n.a.
3	>10	>10	>10	n.a.[c]	n.a.	n.a.
4	>10	>10	>10	n.a.	n.a.	n.a.

[a]Potency (EC_{50}, μM) was calculated from dose response experiment comprising 9 concentration points in quadruplicates. 17β-estradiol was used as a control compound for ERα and ERβ and dihydrotestosterone for AR. [b]Efficacy (%) was calculated as a percentage of maximal response level achieved with control compound. [c]Not active. **1-4** refer to compounds depicted in Figure 2.

Table II. Summary of cytotoxic activities (IC$_{50}$, µM).

Dimer	CCRF-CEM	CEM-DNR bulk	K562	K562-Tax	A549	HCT116	HCT116p53-/-	HeLa	U2OS	MRC-5	HEK 293T
1	0.49	94.65	0.57	3.65	1.11	0.95	0.90	0.78	3.65	1.16	0.92
2	4.26	2.32	7.26	4.38	4.24	3.41	4.69	31.44	29.57	53.32	16.99
3	3.43	15.07	4.63	6.85	14.20	5.09	7.02	8.59	7.05	13.54	8.77
4	>100.00	93.23	>100.00	81.22	91.98	51.90	51.10	>100	>100	89.14	85.16

Cytotoxic activity was determined by MTT or WST assay following 3 day incubation. Values represent means of IC$_{50}$ from 3 independent experiments with SD ranging from 10-25% of the average values. Tested cell lines: CCRF-CEM (acute T-lymphocytic leukemia), CEM-DNR (T-lymphoblastic leukemia daunorubicin resistant), K562 (erythromyeloblastoid leukemia), K562-Tax (K562 paclitaxel resistant), A549 (lung adenocarcinoma), HCT116 (colorectal cancer), HCT116p53-/- (null p53 gene), HeLa (cervical cancer), U2OS (osteosarcoma). Normal human cell lines: MRC-5 cells (normal cycling fibroblasts) and HEK 293T (human embryonic cells). **1-4** refer to compounds depicted in Figure 2.

Table III. Effect of dimers on cell cycle, apoptosis and DNA/RNA synthesis in CCRF-CEM lymphoblasts (% of positive cells).

Dimer	<G1	G0/G1	S	G2/M	pH3^{Ser10}	BrDU	BrU
control	4.58	36.52	37.46	26.03	1.10	43.84	50.76
1 1× IC$_{50}$	11.51	33.48	40.93	25.59	8.08	19.54	34.33
1 5× IC$_{50}$	22.78	2.50	38.39	59.11	48.71	15.94	15.43
2 1× IC$_{50}$	5.2	42.66	44.49	12.85	1.37	49.05	29.66
2 5× IC$_{50}$	24.15	51.95	37.64	10.41	0.41	40.85	39.98
3 1× IC$_{50}$	13.40	40.25	36.97	22.78	2.32	42.06	32.43
3 5× IC$_{50}$	40.19	24.43	42.18	33.39	3.34	1.73	0.25

1-3 refer to compounds depicted in Figure 2.

Table III. Effect of dimers on cell cycle, apoptosis and DNA/RNA synthesis in CCRF-CEM lymphoblasts (% of positive cells).

Dimer	<G1	G0/G1	S	G2/M	pH3^{Ser10}	BrDU	BrU
control	4.58	36.52	37.46	26.03	1.10	43.84	50.76
1 1× IC$_{50}$	11.51	33.48	40.93	25.59	8.08	19.54	34.33
1 5× IC$_{50}$	22.78	2.50	38.39	59.11	48.71	15.94	15.43
2 1× IC$_{50}$	5.2	42.66	44.49	12.85	1.37	49.05	29.66
2 5× IC$_{50}$	24.15	51.95	37.64	10.41	0.41	40.85	39.98
3 1× IC$_{50}$	13.40	40.25	36.97	22.78	2.32	42.06	32.43
3 5× IC$_{50}$	40.19	24.43	42.18	33.39	3.34	1.73	0.25

1-3 refer to compounds depicted in Figure 2.

Figure 1

1a   2a   3a   4a

Figure 2

1
Estradiol dimer

2
3-O-Methyl estradiol dimer

3
Testosterone dimer

4
Pregnene dimer
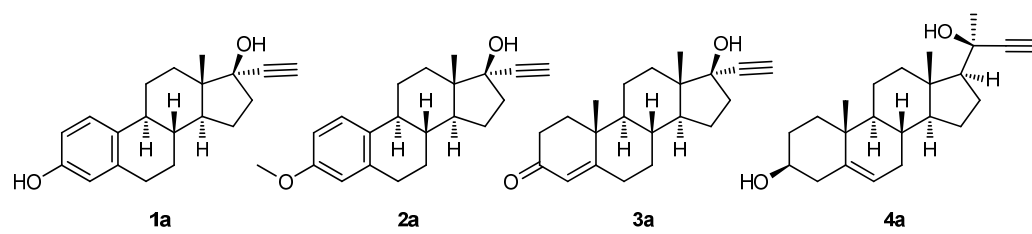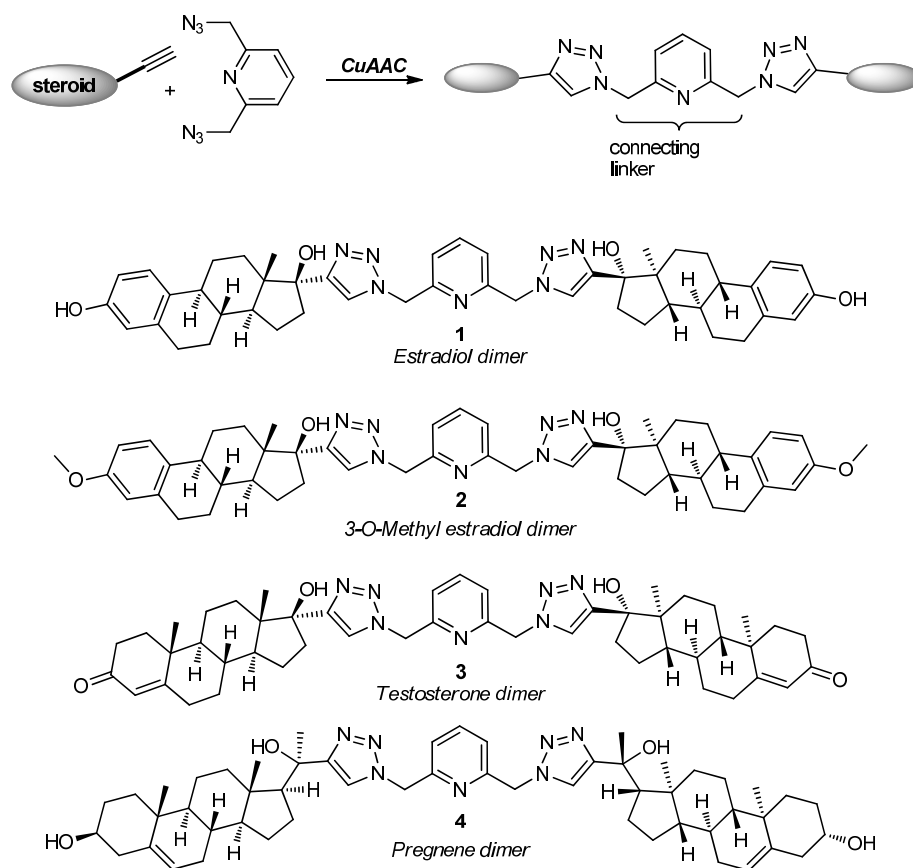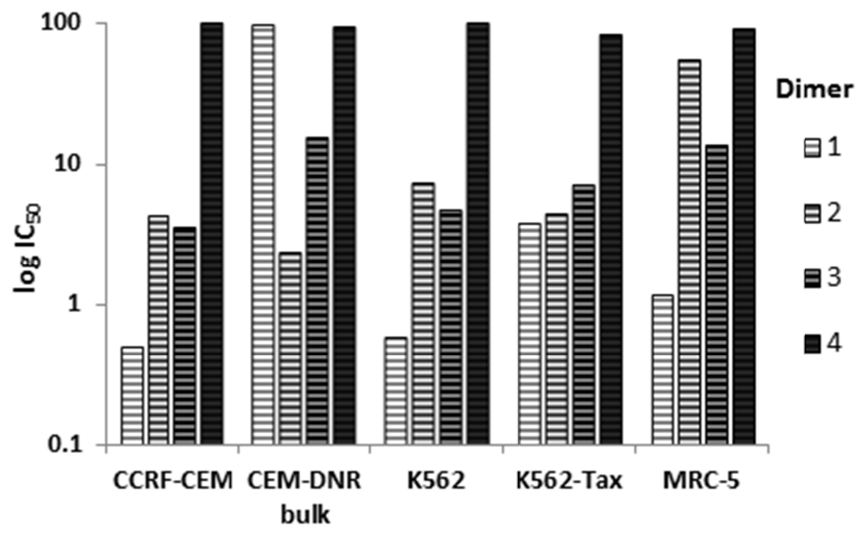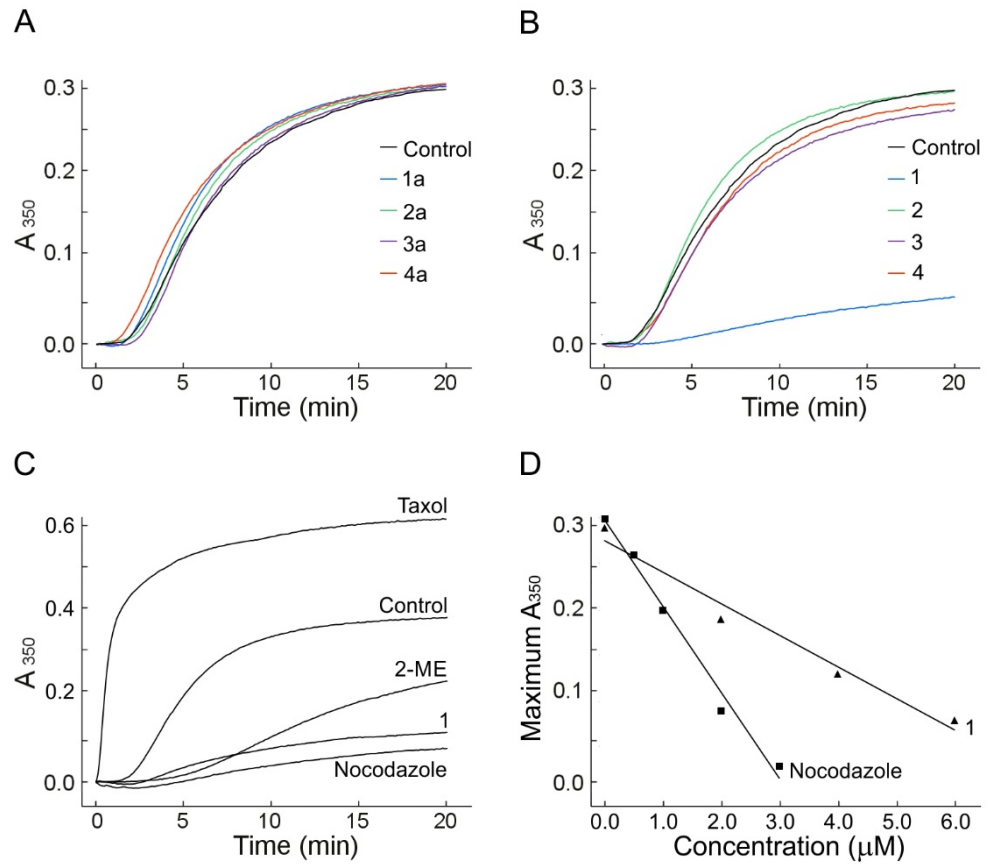
Figure 3

Figure 4

Figure 5
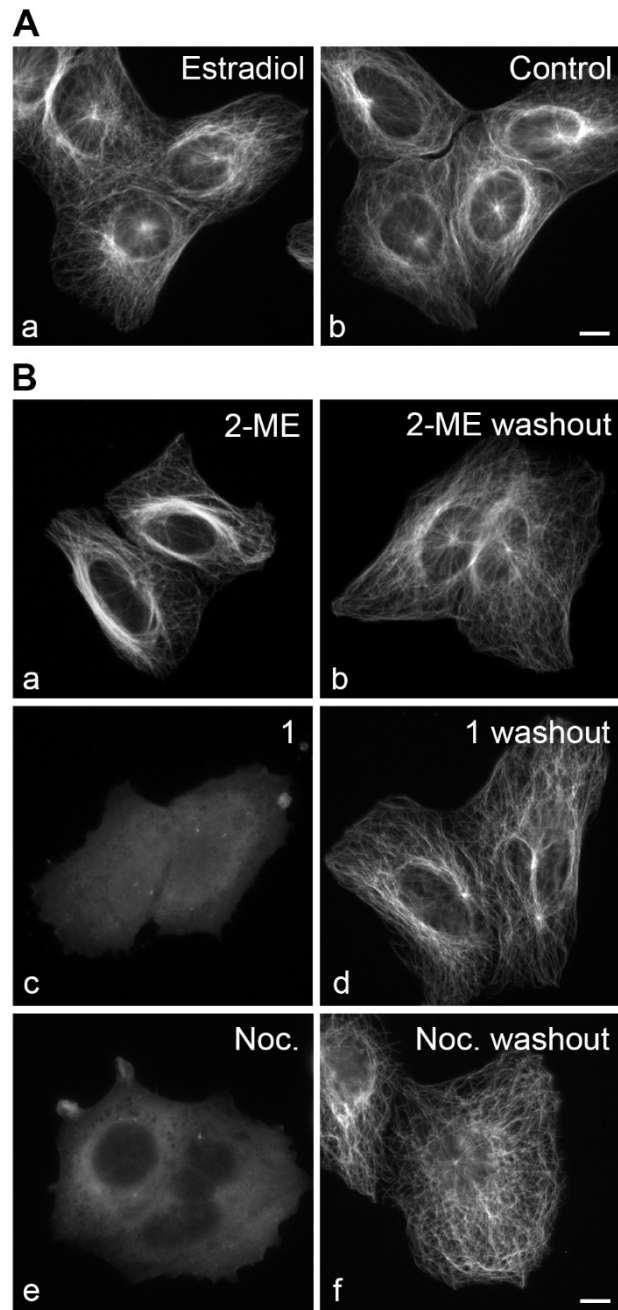
Figure 6
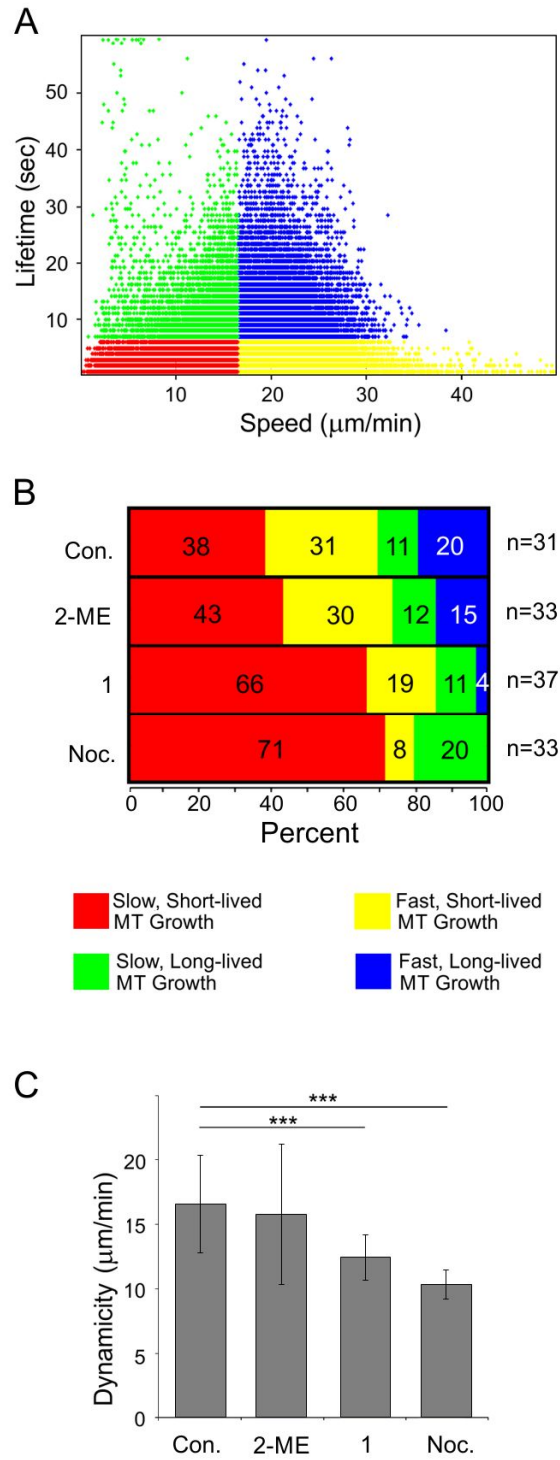
Figure 7
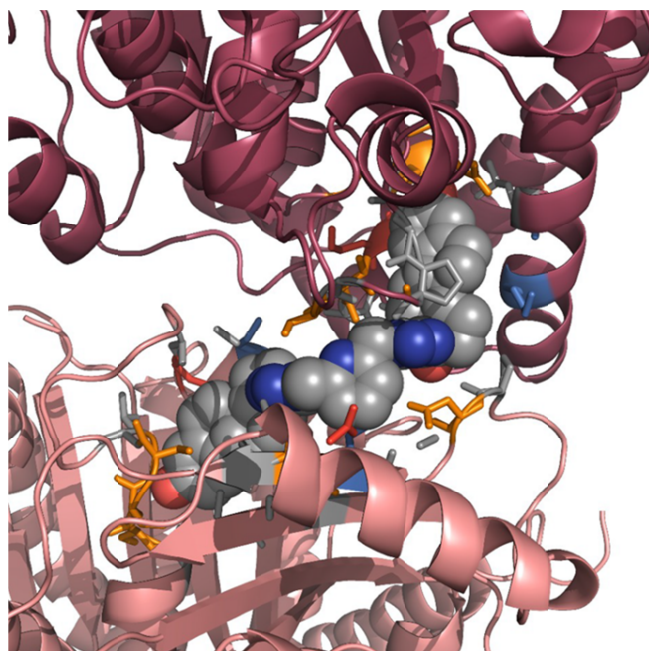
Supplement

Jurášek, M., Džubák, P., Sedlák, D., **<u>Černohorská, M.</u>**, Darmostuk, M., Ruml, T., Sulimenko, T., Dráberová, E., Dráber, P., Hajdůch, M., Bartůněk, P. & Drašar, P. Estradiol Dimer Blocks Microtubule Polymerization. Submitted 2015
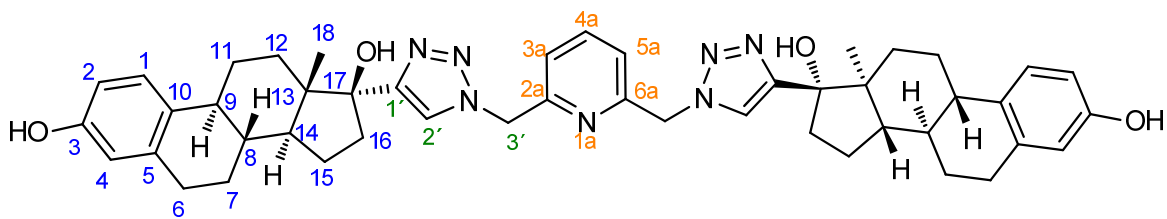
Figure S1. (17β,17'β)-17,17'-[Pyridine-2,6-diylbis(methanediyl-1*H*-1,2,3-triazole-1,4-diyl)]bisestra-1,3,5(10)-triene-3,17-diol as estradiol dimer **1**

Diazide (91 mg, 0.48 mmol) and 17-ethynylestradiol (330 mg, 1.01 mmol) were dissolved in DMF (6 mL) and CuSO$_4$·5H$_2$O (38 mg, 0.15 mmol, 15 mol%), sodium ascorbate (59 mg, 0.3 mmol, 30 mol%) and TBTA (79 mg, 0.15 mmol, 15 mol%) were added. Temperature was gradually increased to 70°C and the mixture was stirred overnight (14 hrs). Solvent was removed under reduced pressure and purification (silica, CH$_2$Cl$_2$-MeOH; grad 100:1→20:1) gave desired product **1** (296 mg, 0.38 mmol) in 79% yield (calculated from diazide). R_f=0.22 (CH$_2$Cl$_2$-MeOH, 20:1), yellow spot. ^{1}H NMR (600 MHz, DMSO-d_6) δ ppm: 0.66 (td, *J*=12.79, 3.58 Hz, 2 H, H-12α), 0.94 (s, 6 H, 2×C*H*$_3$, H-18), 1.18 - 1.30 (m, 4 H, H-11β,7α), 1.31 - 1.39 (m, 2 H, C*H*, H-8β), 1.44 (qd, *J*=11.92, 6.05 Hz, 2 H, H-15β), 1.49 - 1.55 (m, 2 H, H-12β), 1.66 (td, *J*=11.14, 7.98 Hz, 2 H, H-14α), 1.76 - 1.88 (m, 6 H, H-7β, 9α,15α), 1.93 - 2.00 (m, 2 H, H-16α), 2.07 - 2.15 (m, 2 H, H-11α), 2.37 - 2.42 (m, 2 H, H-16β), 2.66 - 2.73 (m, 4 H, H-6α,6β), 5.15 (s, 2 H, 17βO*H*), 5.70 (s, 4 H, PyC*H*$_2$, H-3′), 6.42 (d, *J*=2.20 Hz, 2 H, Ar*H*, H-4), 6.47 (dd, *J*=8.53, 2.48 Hz, 2 H, Ar*H*, H-2), 6.96 (d, *J*=8.80 Hz, 2 H, Ar*H*, H-1), 7.10 (d, *J*=7.70 Hz, 2 H, PyC*H*,H-3a,5a), 7.86 (t, *J*=7.70 Hz, 1 H, PyC*H*, H-4a), 7.95 (s, 2 H, triazole*H*, H-2′), 8.95 (s, 2 H, ArO*H*). ^{13}C NMR (151 MHz, DMSO-d_6) δ ppm: 14.86 (*C*H$_3$, C-18), 24.06 (*C*H$_2$, C-15), 26.59 (*C*H$_2$, C-11), 27.68 (*C*H$_2$, C-7), 29.75 (*C*H$_2$, C-6), 33.14 (*C*H$_2$, C-12), 37.63 (*C*H$_2$, C-16), 39.79 (*C*H$_2$, C-8), 43.68 (*C*H, C-9), 47.24 (*C*, C-13), 48.08 (*C*H, C-14), 54.60 (*C*H$_2$, C-3′), 81.61 (*C*, C-17), 113.12 (Ar*C*H, C-2), 115.35 (Ar*C*H, C-4), 121.48 (Py*C*H, C-3a,5a), 124.04 (triazole*C*H, C-2′), 126.49 (Ar*C*H, C-1), 130.91 (*C*, C-10), 137.63 (Ar*C*, C-5), 139.09 (Py*C*H, C-4a), 154.85 (triazole*C*, C-1′), 155.35 (Ar*C*OH, C-3), 155.87 (Py*C*, C-2a,6a). IR (ATR, KBr): 3377 (vs), 2930 (s), 2900 (s), 1729 (m), 1661 (m), 1597 (m), 1454 (m), 1433 (m), 1383 (m), 1369 (m), 1336 (w), 1271 (w), 1218 (m), 1191 (m), 1137 (s), 1095 (s), 1056 (vs). α_D^{25}=+49.6 in DMF, *c*=0.25. HRMS-ESI: *monoisotopic mass* 781.43155 Da, found (*m/z*) 804.42043 (clcd

804.42077) corresponds to [M+Na]+ and 820.39375 (clcd 820.39471) corresponds to [M+K]+.
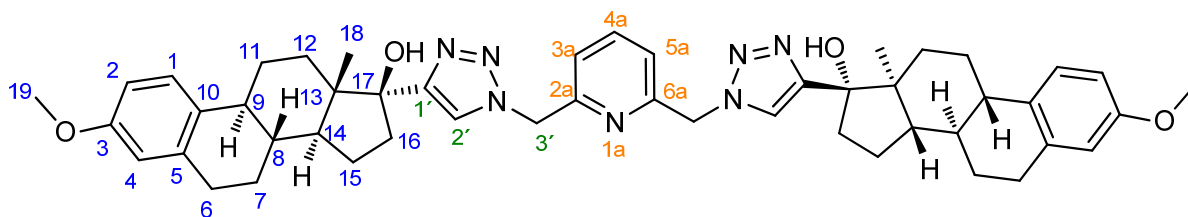
Figure S2. (17β,17'β)-17,17'-[Pyridine-2,6-diylbis(methanediyl-1*H*-1,2,3-triazole-1,4-diyl)]bis[3-methoxyestra-1,3,5(10)-trien-17-ol] as estradiol dimer **2**

Diazide (43 mg, 0.23 mmol) and mestranol (0.52 mmol, 162 mg) were dissolved in DMF (4 mL) and CuSO$_4$·5H$_2$O (19.5 mg, 0.78 μmol, 15 mol%), sodium ascorbate (31 mg, 1.56 μmol, 30 mol%) and TBTA (83 mg, 1.56 μmol, 15 mol%) were added. The mixture was stirred overnight (13 hrs) at 70°C after which the solvents were removed under reduced pressure and purification (silica, CH$_2$Cl$_2$-MeOH; grad 100:1→20:1) gave desired product **2** (149 mg, 0.18 mmol) in 80% yield (calculated from diazide). Rf=XX ^{1}H NMR (600 MHz, CDCl$_3$) δ ppm: 0.71 (td, *J*=12.79, 4.13 Hz, 2 H, H-12α), 1.05 (s, 6H, C*H*$_3$, H-18), 1.30 - 1.64 (m, 12 H, H-15β, 14, 12β, 11β, 8, 7α), 1.89 - 1.98 (m, 6 H, H-15α,9,7β), 2.08 - 2.17 (m, 4 H, H-11α,16α), 2.41 - 2.48 (m, 2 H, H-16β), 2.78 - 2.90 (m, 4 H, C*H*$_2$, H-16), 3.15 (br. s., 2 H, O*H*), 3.75 (s, 6 H, C*H*$_3$, H-19), 5.58 - 5.65 (m, 4 H, C*H*$_2$, H-3′), 6.61 (d, *J*=2.75 Hz, Ar*H*, 2 H, H-4), 6.66 (dd, *J*=8.80, 2.75 Hz, Ar*H*, 2 H, H-2), 7.10 (d, *J*=8.80 Hz, Ar*H*, 2 H, H-1), 7.16 (d, *J*=7.70 Hz, Py*H*, 2 H, H-3a,5a), 7.57 (s, triazoleC*H*, 2H, H-2′), 7.69 (t, *J*=7.70 Hz, t, *J*=7.70 Hz, Py*H*, 1 H, H-4a). ^{13}C NMR (151 MHz, CDCl$_3$) δ ppm: 14.32 (*C*H$_3$, C-18), 23.55 (*C*H$_2$, C-15), 26.32 (*C*H$_2$, C-11), 27.41 (*C*H$_2$, C-7), 29.88 (*C*H$_2$, C-6), 33.01 (*C*H$_2$, C-12), 37.96 (*C*H$_2$, C-16), 39.50 (*C*H, C-8), 43.42 (*C*H, C-9), 47.39 (*C*, C-13), 48.46 (*C*H, C-14), 55.09 (*C*H$_2$, C-3′), 55.22 (*C*H$_3$, C-19), 82.45 (*C*, C-17), 111.46 (Ar*C*H, C-2), 113.79 (Ar*C*H, C-4), 121.77 (Py*C*H, C-3a,5a), 122.32 (triazole*C*H, C-2′), 126.25 (Ar*C*H, C-1), 132.58 (Ar*C*, C-10), 138.01 (Ar*C*, C-5), 138.63 (Py*C*H, C-4a), 154.18 (triazole*C*, C-1′), 154.64 (Ar*C*, C-3), 157.43 (Py*C*, C-2a,6a). IR: 3420, 3143, 3060, 2930, 2867, 2028, 1958, 1607, 1499, 1459, 1280, 1253, 1235, 1045, 755.). α_D^{20}=+ 18.6 (*c*=0.26, CHCl$_3$). HRMS-ESI: *monoisotopic mass* 809.46285 Da, found (*m/z*) 832.45196 (clcd 832.45207) corresponds to [M+Na]+.
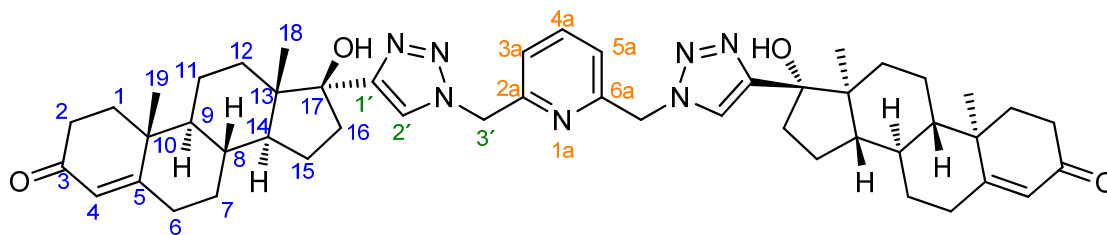
Figure S3. (17β,17'β)-17,17'-[Pyridine-2,6-diylbis(methanediyl-1*H*-1,2,3-triazole-1,4-diyl)]bis(17-hydroxyandrost-4-en-3-one) as estradiol dimer **3**

Diazide (90 mg, 0.48 mmol) was dissolved in DMF (6 mL) and ethisterone (300 mg, 0.96 mmol), CuSO$_4$·5H$_2$O (12 mg, 0.048 mmol, 10 mol%), sodium ascorbate (19 mg, 0.096 mmol, 20 mol%) and TBTA (25 mg, 0.048 mg, 10 mol%) were added. The mixture was stirred overnight (13 hrs) at 70°C after which the solvent was removed under reduced pressure and purification (silica, CH$_2$Cl$_2$-MeOH; grad 25:1→18:1) gave desired product **3** (340 mg, 0.42 mmol) in 87% yield (calculated from diazide). (R_f=0.48, CH$_2$Cl$_2$-MeOH, 10:1, brown spot. ^{1}H NMR (600 MHz, CDCl$_3$) δ ppm: 0.49 - 0.55 (m, 2 H, H-12α), 0.71 - 0.77 (m, 2 H, H-9α), 1.02 - 1.08 (m, 2 H, H-7α), 1.09 (s, 6 H, C*H*$_3$, H-18), 1.19 (s, 6 H, C*H*$_3$, H-19), 1.35 - 1.61 (m, 10 H, H-16β,14α,11β,11α,15β), 1.65 (qd, *J*=11.06, 3.25 Hz, 2 H, 8β), 1.88 - 1.94 (m, 4 H, H-7β,15α), 1.95 - 1.99 (m, 2 H, H-16α), 2.13 (ddd, *J*=14.25, 12.08, 3.61 Hz, 2 H, H-1α), 2.25 - 2.28 (m, 2 H, H-2α), 2.29 (br. s., 2 H, H-6α,6β), 2.32 (t, *J*=3.61 Hz, 1 H, H-2β), 2.36 - 2.47 (m, 4 H, H-1β,12β), 5.56 - 5.65 (m, 4 H, triazoleC*H*$_2$Py, H-3′), 5.70 (s, 2 H, C=C*H*, H-6), 7.19 (d, *J*=7.94 Hz, 2 H, PyC*H*, H-3a,5a) 7.54 (s, 2 H, triazoleC*H*, H-2′), 7.73 (t, *J*=7.76 Hz, 1 H, PyC*H*, H-4a). ^{13}C NMR (151 MHz, CDCl$_3$) δ ppm: 14.37 (*C*H$_3$, C-18), 17.44 (*C*H$_3$, C-19), 20.67 (*C*H$_2$, C-11), 23.85 (*C*H$_2$, C-15), 31.63 (*C*H$_2$, C-6), 32.72 (*C*H$_2$, C-7), 32.86 (*C*H$_2$, C-2), 33.96 (*C*H$_2$, C-12), 35.68 (*C*H$_2$, C-16), 36.27 (*C*H, C-8), 37.84 (*C*H$_2$, C-1) 38.62 (*C*, C-10), 46.92 (*C*,C-13), 48.88 (*C*H, C-14), 53.34 (*C*H, C-9), 54.98 (triazole*C*H$_2$Py, C-3′), 82.19 (*C*, C-17), 121.76 (Py*C*H, C-3a,5a), 122.45 (triazole*C*H, C-21), 123.79 (C=*C*H, C-4), 138.61 (Py*C*H, C-4a), 153.97 (triazole*C*, C-2a), 154.45 (Py*C*, C-2a,6a), 171.44 (-*C*=, C-5) 199.70 (*C*=O, C-3). IR: 3417 (m), 3143 (w), 3052 (w), 2943 (s), 2868 (m), 1664 (vs), 1613 (m), 1577 (w), 1456 (m), 1433 (m), 1380 (w), 1357 (w), 1331 (w), 1271 (m), 1231 (m), 1187 (w), 1127 (m), 1048 (m), 1017 (w). α_D^{25}=+93.4 (*c*=1, MeOH). HRMS-ESI: *monoisotopic mass* 813.49415 Da, found (*m/z*) 836.48352 (clcd 836.48337) corresponds to [M+Na]$^+$ and 852.45545 (clcd 852.45731) corresponds to [M+K]$^+$.
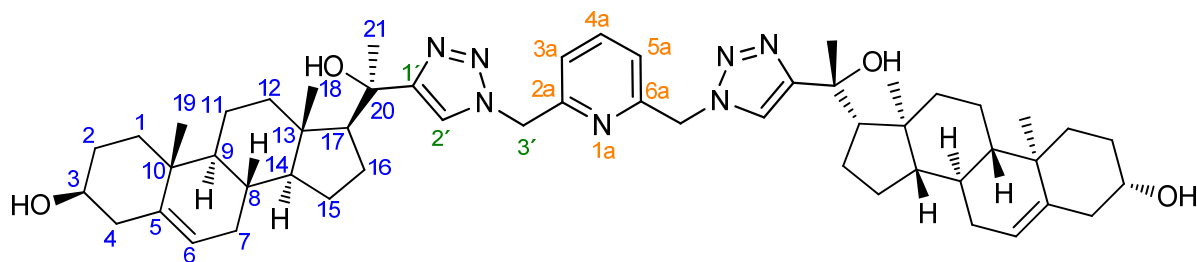
Figure S4. (3β,3'β)-20,20'-[Pyridine-2,6-diylbis(methanediyl-1*H*-1,2,3-triazole-1,4-diyl)]bispregn-5-ene-3,20-diol as estradiol dimer **4**

Diazide (50 mg, 0.26 mmol) and 24-norchol-5-en-22-yn-3β-ol (200 mg, 0.58 mmol) were dissolved in DMF (4 mL) and $CuSO_4 \cdot 5H_2O$ (14 mg, 0.058 mmol, 10 mol%), sodium ascorbate (23 mg, 0.12 mmol, 20 mol%) and TBTA (31 mg ,0.058 mmol, 10 mol%), were added. The mixture was stirred overnight at 70°C after which the solvent was removed under reduced pressure and purification (silica, CH_2Cl_2-MeOH; grad 35:1→15:1) gave desired product **4** (177 mg, 0.48 mmol) in 78% yield (calculated from diazide). R_f=0.52 (CH_2Cl_2-MeOH, 10:1), dark brown spot. ^{1}H NMR (600 MHz, CDCl$_3$) δ ppm: 1.01 (s, 6 H, C*H*$_3$, H-18), 1.11 (td, *J*=11.55, 4.95 Hz, 2 H, H-9α), 1.18 (s, 6 H, C*H*$_3$, H-19), 1.20 - 1.32 (m, 6 H, H-14α,1α,15α), 1.40 - 1.56 (m, 4 H, H-16β,12α), 1.58 - 1.78 (m, 12 H, H-2β,7α,8β,11α,11β,15β), 1.84 (s, 6 H, C*H*$_3$, H-21), 2.06 - 2.27 (m, 8 H, H-7β, 12β,16α,17α), 2.32 - 2.45 (m, 4 H, H-4α,4β), 3.51 - 3.59 (m, 2 H, H-3), 3.66 (s, 2 H, O*H*), 4.80 (d, *J*=4.40 Hz, 2 H, O*H*), 5.49 (d, *J*=4.95 Hz, 2 H, C=C*H*, H-6), 5.90 - 5.97 (m, 4 H, C*H*$_2$Py, H-3′), 7.35 (d, *J*=7.70 Hz, 2 H, PyC*H*, H-3a,5a), 8.06 (t, *J*=7.70 Hz, 1 H, PyC*H*, H-4a), 8.12 (s, 2 H, triazoleC*H*, H-23). ^{13}C NMR (151 MHz, DMF-*d$_7$*) δ ppm: 13.39 (*C*H$_3$, C-18), 19.29 (*C*H$_3$, C-19), 21.08 (*C*H$_2$, C-11), 23.03 (*C*H$_2$, C-16), 23.85 (*C*H$_2$, C-15), 29.21 (*C*H$_3$, C-21), 31.63 (*C*H, C-8), 31.87 (*C*H$_2$, C-7), 31.97 (*C*H$_2$, C-2), 36.69 (*C*, C-10), 37.62 (*C*H$_2$, C-1), 40.20 (*C*H$_2$, C-12), 42.79 (*C*H$_2$, C-4), 42.80 (*C*, C-13), 50.51 (*C*H, C-9), 54.69 (*C*H$_2$Py, C-3′), 57.17 (*C*H, C-14), 60.41 (*C*H, C-17), 70.92 (*C*HOH, C-3), 72.65 (*C*, C-20), 120.81 (Py*C*H, C-3a,5a), 121.14 (C=*C*H, C-6), 122.20 (triazole*C*H, C-23), 138.71 (Py*C*H, C-4a), 141.93 (-*C*=, C-5), 156.13 (triazole*C*, C-2a), 157.88 (Py*C*, C-2a,6a). IR: 3390 (s), 2930 (s), 2899 (s), 1645 (m), 1596 (m), 1454 (m), 1433 (m), 1383 (m), 1336 (w), 1271 (w), 1218 (m), 1191 (w), 1136 (m), 1094 (s), 1056 (s), 1029 (m), 1006 (m). α_D^{25}=-61.6 (*c*=0.25, MeOH-CHCl$_3$). HRMS-ESI: *monoisotopic mass* 873.58805 Da, found (*m/z*) 896.57700 (clcd 896.57727) corresponds to [M+Na]$^+$.
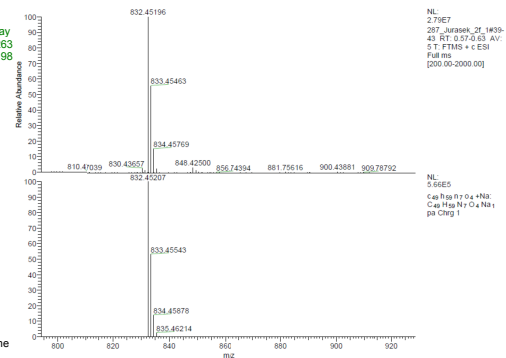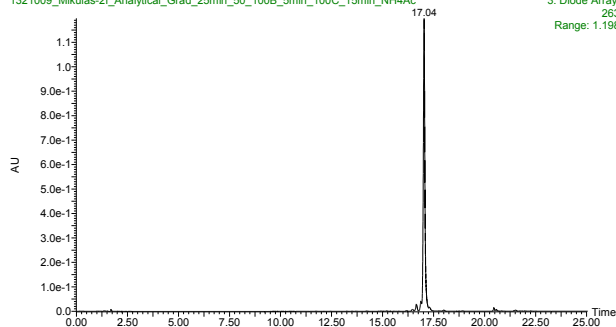
Compound 1
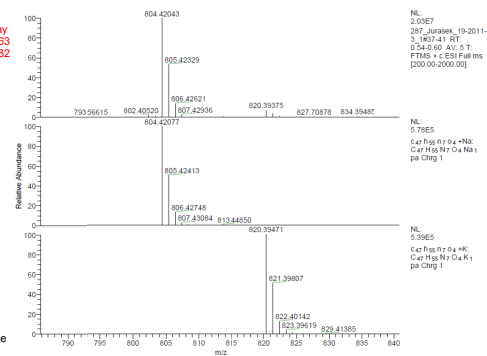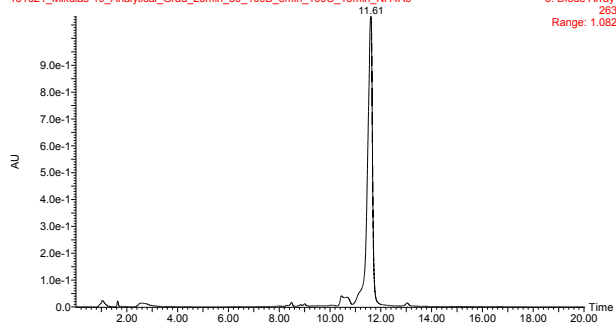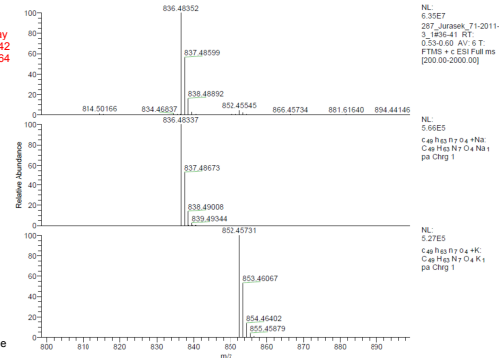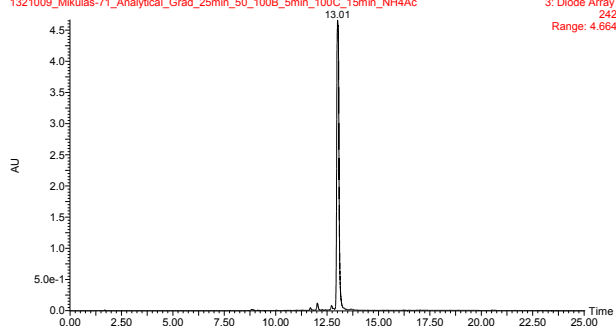
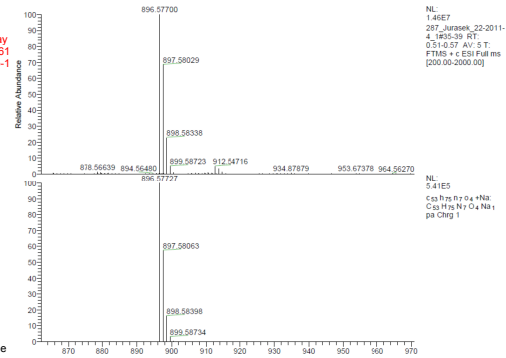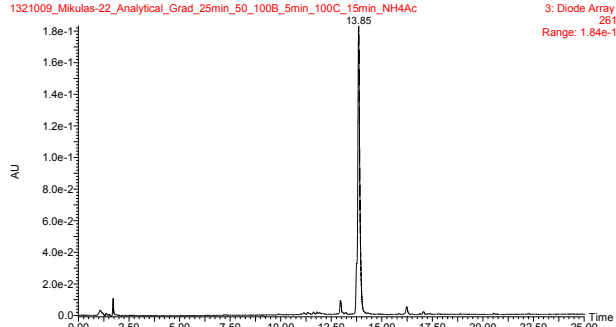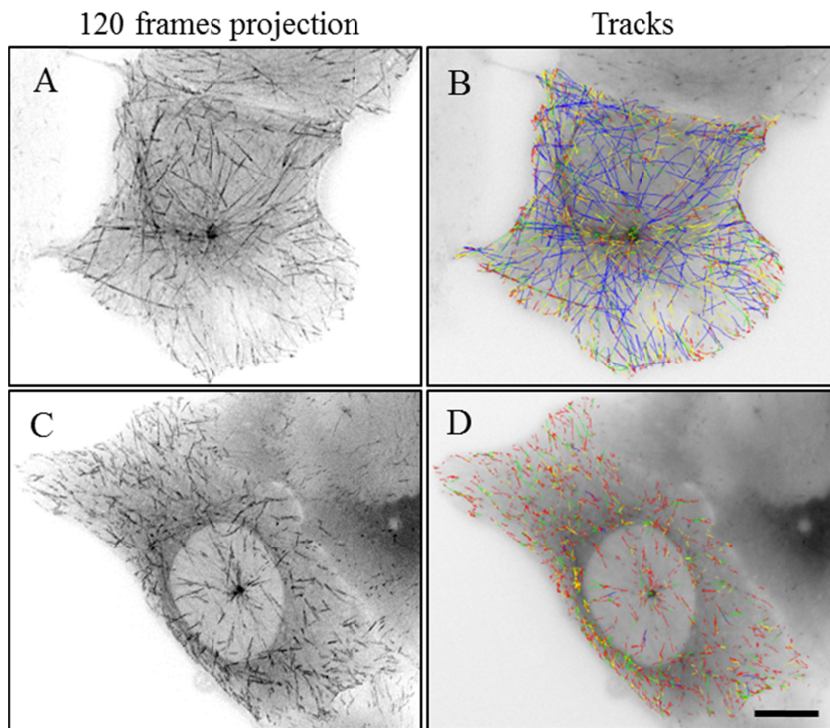# Compound 2

Compound 3

Compound 4

Figure S5. HRMS and HPLC analyses of tested compounds.

Figure S6. Comparison of microtubule subpopulations in control and estradiol dimer-treated cells. Time-lapse sequences were collected for 2 min (frame rate = 1 sec) from control U2OS-EB1 cells (A, B) or U2OS-EB1 cells treated with 50 nM estradiol dimer for 3 h (C, D). Maximum intensity projections of the 120 consecutive frames (A, C) and colored tracks overlaid on inverted image (B, D). Microtubule subpopulations are colored as described in Figure 6. Scale bar for A-D, 10 μm.
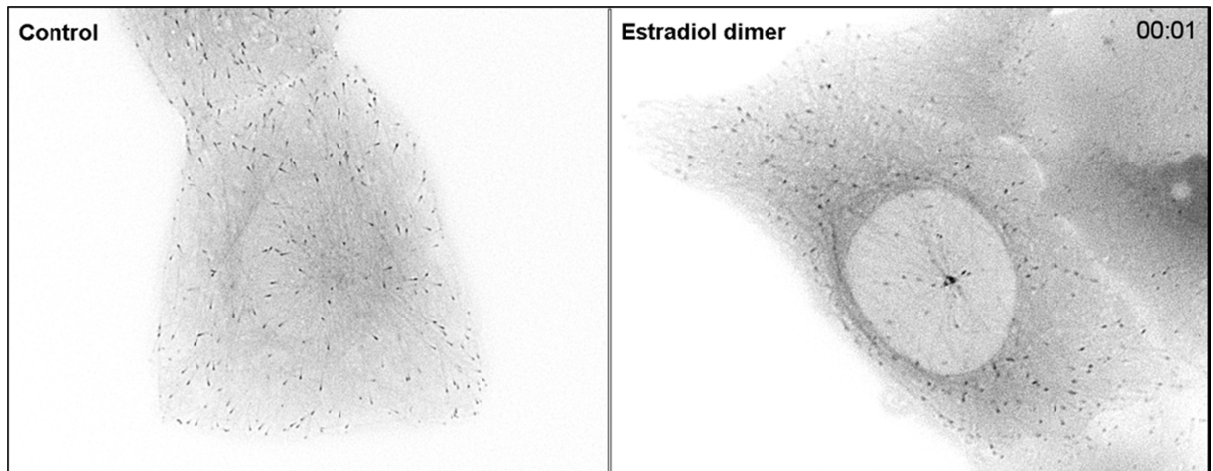
Suppl. movie 1. Example of time-lapse imaging of control and estradiol dimer-treated cells. U2OS-EB1 cells were treated with DMSO carrier (Control) or 50 nM estradiol dimer for 3 h, and time-lapse sequences were collected for 2 min at 1 sec interval (exposure time 0.3 sec) on Delta Vision Core system. Note shorter lifetime of EB1 comets in estradiol dimer-treated cells when compared to control cells. Elapsed time in sec is depicted in the upper right.